Institut National de la Recherche Scientifique (INRS)
Armand-Frappier Santé Biotechnologie Research Centre

THE ROLE OF CLN3 AND CLN5 IN ENDOSOMAL FUNCTION

by

Seda Yasa

A thesis submitted for the degree of
Doctor of Philosophy, Ph.D.
in Biology

Evaluation Committee Members

Committee Chair and Internal Examiner	Prof. Daniel G. Cyr INRS-Centre Armand-Frappier Santé Biotechnologie
External Examiner	Prof. Emyr Lloyd-Evans Cardiff University
External Examiner	Prof. John Presley McGill University
Supervisor	Prof. Stéphane Lefrançois INRS-Centre Armand-Frappier Santé Biotechnologie

To my mother
—to whom I share the same mitochondria;
providing me all of her astonishing energy of life, creativity, and enthusiasm

To my father
—to whom I promised to do my best to become aware of everything around me;
so as to understand the great life

Acknowledgments

First and foremost, I would like to express my most heartfelt gratitude to my academic supervisor, Prof. Stéphane Lefrançois, for his invaluable guidance and support throughout my Ph.D. years. I thank him for offering many opportunities and for sharing his scientific and personal experiences. He is a science father to me leading my way to becoming a true scientist!

I would like to thank Prof. Daniel Cyr for following up on my Ph.D. progress. Thanks to his questions, I realized the importance of the story out of scientific discovery. Furthermore, I am grateful to my external committee members, Prof. Emyr Lloyd-Evans and Prof. John Presley, for devoting their time to evaluate my thesis. I am proud to be evaluated by these three respected scientists.

I deeply thank all current and former lab members, for a truly fruitful working environment and their important contributions to endocytic trafficking. The fundamentals of this thesis are based on their previous findings. Especially, I would like to thank Graziana Modica for the scientific discussions and her sincere friendship that will last for many more years. I extend my thanks to Etienne Sauvageau for his support and help, especially throughout the crazy paper revision intervals. And, thanks to Olga Skorabogata, I adapted to the lab environment pretty quickly. Also, special thanks to Juliette Maes for her friendly help in correcting the French part of the thesis.

I respectfully acknowledge NCL Stiftung Foundation for financially supporting me to participate in the international scientific meetings each year. Meeting with the leading scientist of the NCL field and listening to their discoveries together with the constructive discussions on my project paved the way for me to produce this thesis. My earnest thanks also go to Fondation Armand-Frappier and Fond de recherche du Quebec - Santé for providing me the scholarship and making this work possible.

My beloved family, although beyond the ocean, motivated me to be strong, resilient, grateful, happy, healthy, and much more... Sevgi (mom), Selim (dad), Feyza (sis), Reyyan (sis), love you all! Many thanks to WhatsApp for making possible all these every day (literally every day) calls. Moreover, many thanks to my Ercan family; Hulya (mom), Omer (dad), Betul (sis), and Talha (bro). Together, everything is possible, meaningful, and much more beautiful.

And the magical city Montreal, thanks a lot for bringing me the love of my life; Furkan Ercan! He inspired me to work hard, dream big. Cleared out all my complaints with his big smile and courage. He gives my motivations and accomplishments a meaning that cannot be formed otherwise. Also, I certainly need to mention his great help in correcting the Latex codes of the whole thesis. Thank you so much my best friend, husband, and partner in crime!

There are no incurable diseases — only the lack of will.
There are no worthless herbs — only the lack of knowledge.

—Ibn Sina

Abstract

Recessive inheritance of *CLN3* and *CLN5* monogenic gene mutations are the cause of CLN3 and CLN5 diseases, respectively. They are rare neurodegenerative diseases grouped under the Neuronal Ceroid Lipofuscinosis (NCL) disorder. Being the most common cause of childhood dementia, NCL significantly reduces the patient lifespan resulting in inevitable death at a young age. The principal characteristics of NCL are aberrant lysosomal function and excess accumulation of autofluorescent ceroid lipopigments in neurons and peripheral tissues. CLN5 is a soluble endolysosomal protein, while CLN3 is an integral membrane protein localized to the same compartment. Although they have been implicated in lysosomal homeostasis and intracellular trafficking, none of their exact cellular functions have been demonstrated. The work presented in this thesis elucidates some of the functional roles of CLN3 and CLN5 proteins at endosomes, which provides a molecular explanation behind phenotypes observed in CLN3 and CLN5 disorders and gives an indication of the pathogenic mechanism behind Batten disease.

Lysosomal sorting receptor (LSR) retrieval from endosomes back to the trans Golgi Network (TGN) is crucial for lysosomal homeostasis by preventing their lysosomal degradation, and maintaining transport of soluble lysosomal proteins needed for normal lysosomal function. We have shown that CLN3 is required for the efficient endosome-to-TGN trafficking of the LSRs by regulating the RAB7A/retromer interaction. GTP bound RAB7A is localized to late endosomes and regulates the spatiotemporal recruitment of retromer, which subsequently interacts with the LSRs and is required for retrieval. In cells lacking CLN3 or expressing CLN3 harboring a disease-causing mutation, retromer did not bind the LSRs, which were degraded. We also demonstrated that CLN3 is required for the Rab7A–PLEKHM1 interaction, which is required for the fusion of autophagosomes to lysosomes.

We previously found that depletion of CLN5 also leads to dysfunctional retromer, resulting in the degradation of the LSRs. However, how a soluble lysosomal protein can modulate the function of a cytosolic protein, retromer, is not known. In this work, we show that CLN5 is required for the palmitoylation of Rab7A, which is required for retromer membrane recruitment. Furthermore, we demonstrate that CLN5 regulates retromer function by modulating key interactions between CLN3, RAB7A, retromer, and sortilin. Moreover, we observed impaired endolysosome fusion events in CLN5 deficient cells. This results in delayed degradation of endocytic proteins and defective autophagy.

Overall, this work demonstrates that CLN3 and CLN5 are required for downstream interactions of Rab7A. Their cooperative work at endosomes acts as an endosomal switch to coordinate endosome-to-TGN retrieval of the LSRs. Taken together, our findings provide a molecular explanation for the reported abnormal lysosomal function in CLN3 disease and CLN5 disease patients.

Keywords: endosomes, CLN5, CLN3, retromer, sortilin, palmitoylation, Rab7A

Résumé

L'hérédité récessive des mutations génétiques monogéniques *CLN3* et *CLN5* est la cause d'une maladie neurodégénérative rare appelée lipofuscinose neuronale des céroïdes (NCL), ou maladie de Batten. Étant la cause la plus fréquente de démence infantile, la NCL réduit considérablement la durée de vie des patients, entraînant leur décès inévitable au cours des premières années. Les principales caractéristiques de la NCL sont une fonction lysosomale aberrante et une accumulation excessive de lipopigments céroïdes auto-fluorescents dans les neurones et les tissus périphériques. CLN5 est une protéine endolysosomale soluble, tandis que CLN3 est une protéine membranaire intégrale localisée dans le même compartiment. Bien que leur rôle soit impliqué dans l'homéostasie lysosomale et le trafic intracellulaire, aucune de leur fonction cellulaire exacte n'a été démontrée. Avec mon projet de doctorat, j'ai élucidé certains des rôles fonctionnels des protéines CLN3 et CLN5 au niveau des endosomes, ce qui fournit une explication moléculaire des phénotypes observés dans les troubles CLN3 et CLN5 et donne une indication du mécanisme pathogène derrière la maladie de Batten.

Le recyclage du récepteur de tri lysosomal (LSR) vers Golgi est crucial pour l'homéostasie lysosomale. Ainsi, les LSR ne seront pas dégradés dans l'environnement acide, mais continueront à transporter les enzymes vers les lysosomes nécessaires à la fonction lysosomale normale. Dans mon premier article, nous avons montré que CLN3 est nécessaire pour le trafic endosome-TGN efficace des LSR car il régule l'interaction de Rab7A avec le rétromère. GTP lié Rab7 est localisé aux endosomes tardifs et régule le recrutement spatio-temporel du rétromère pour le trafic rétrograde des LSR. Dans les cellules dépourvues de CLN3 ou exprimant CLN3 portant une mutation pathogène, les LSR étaient dégradés. Nous avons également démontré que CLN3 est nécessaire pour l'interaction Rab7A – PLEKHM1, qui est nécessaire pour la fusion des autophagosomes aux lysosomes.

Nous avons précédemment constaté que l'épuisement du CLN5 conduit également à un rétomère dysfonctionnel, entraînant la dégradation du LSR, la sortiline. Cependant, la façon dont une protéine lysosomale soluble peut moduler la fonction d'une protéine cytosolique, le rétomère, n'est pas connue. Dans mon deuxième travail, nous montrons que CLN5 est nécessaire pour la palmitoylation de Rab7A, qui est nécessaire pour le recrutement de la membrane rétromère. Et par son interaction CLN3, CLN5 régule la fonction du rétomère en modulant les interactions clés entre CLN3, Rab7A, rétomère et sortiline. De plus, nous avons observé des événements de fusion d'endolysosomes altérés dans les cellules déficientes en CLN5. Cela entraîne une dégradation retardée des protéines endocytaires et une autophagie défectueuse.

Dans l'ensemble, mes travaux ont démontré que CLN3 et CLN5 régulent le tri rétrograde de la sortiline au niveau des endosomes. Leur travail coopératif au niveau de l'endosome agit comme un commutateur endosomal pour coordonner le trafic endosome-TGN et diverses fonctions de Rab7A.

Mots-clés: endosomes, CLN5, CLN3, retromer, sortilin, palmitoylation, Rab7A

Sommaire Récapitulatif

Le lysosome

En 1949, alors qu'il étudie l'activité de la glucose 6-phosphatase, le biologiste belge Christian Duve découvre des «structures en forme de sac». C'est en 1955, après avoir découvert d'autres hydrolases qu'ils portent, que Duve nomme ces nouveaux organites des "lysosomes". Les lysosomes contiennent plus de 60 hydrolases acides dans leur lumière, tels que des phosphatases, des lipases, des nucléases, des glycosidases et autres, qui sont nécessaires pour dégrader les macromolécules biologiques de déchets cellulaires, de vieilles cellules, d'agents pathogènes, de nutriments consommés et d'autres débris. Les hydrolases lysosomales opèrent à un pH acide inférieur à 5. Le maintien du pH interne du lysosome, plus acide que celui du reste de la cellule, est assuré par les protéines transmembranaires.

Grâce à plusieurs autres découvertes, il a été démontré que cet organite, en plus de sa fonction de système d'élimination des déchets, est au centre d'un réseau de regulation complexe. En effet, les lysosomes contrôlent l'homéostasie cellulaire en régulant la signalisation métabolique, la transcription génique, l'immunité, la réparation de la membrane plasmique, l'adhésion cellulaire et les mécanismes de migration. Ils le font en se déplaçant dans le cytosol et en interagissant avec d'autres structures cellulaires pour avoir des informations sur le besoin cellulaire. En conséquence, les lysosomes peuvent modulerleur composition, leur taille et leur nombre par des mécanismes de fusion et fission afin deréguler les voies et montrer leurs diverses fonctions.

Autophagie

Les cellules eucaryotes ont évolué de manière à résister à la faim pendant de longues périodes de temps par un mécanisme d'autolyseappelé autophagie. La digestion d'une partie de leurs propres composants cytoplasmiques fournit aux cellules des molécules à recycler afin de construire les métabolites nécessaires à leur survie. Les lysosomes détectent la disponibilité des nutriments dans la cellule par le biais du complexe protéique LYNUS (détection des nutriments lysosomaux). Dans des conditions normales, la cible mammifère de la rapamycine (mTOR) se trouve à l'état actif sur la membrane lysosomale, associée à LYNUS et stimule la croissance cellulaire. Dans le même temps, mTOR bloque l'autophagie en inhibant le facteur de transcription EB (TFEB), dont les complexes activateurs d'autophagie, par un mécanisme de phosphorylation. Si les niveaux de nutriments sont faibles, LYNUS se dissocie de mTOR et le TFEB est acheminée vers le noyau pour la synthèse de protéines liées à l'autophagie. Dans le même temps, une vésicule à double membrane appelée phagophore commence à se former. Le complexe ULK est d'abord activé pour phosphoryler AMBRA1, étape nécessaire à l'activation du complexe PI3K. Ensuite, le système de type ubiquitine est activé pour induire la conjugaison de la protéine de chaîne légère 3b (LC3) associée aux microtubules avec la phosphatidyléthanolamine (PE), induisant alors la lipidation de LC3-I pour former LC3-II. L'extension et l'achèvement du phagophore sont assurés par des protéines LC3-II situées sur les deux surfaces de la membrane. Le phagophore en croissance engloutit les matériaux

cytosoliques de manière sélective ou non sélective pour former des vésicules appelées autophagosomes. Lorsqu'un autophagosomes complet est formé, un complexe protéique transmembranaire est activé pour former des vésicules intraluminales avant l'acidification. Ensuite, l'autophagosome fusionne avec le lysosome pour décomposer les matériaux ou les organites à l'intérieur de ces autolysosomes. Ce processus nécessite le complexe HOPS pour faciliter l'attache et PLEKHM1 pour établir une forte interaction des deux membranes. Ceci est suivi d'interactions autophagosomiques SNARE (Syntaxin-17, Atg14, synaptosomal associated protein 29 (SNAP-29)) avec les SNARE endosomiques / lysosomaux tardifs (Vamp8 / Vamp7) pour la fusion des bicouches lipidiques. Plus tard, les molécules sont dégradées et recyclées pour la synthèse des molécules nécessaires.

Les protéines lysosomales et leur tri

Les glycolipides complexes comme les esters de cholestéryle et les triglycérides sont décomposés en acides gras libres et en cholestérol par les lipases acides lysosomales (LAL). Les *beta* -galactosidases et les hexosaminidases sont quelques-unes des enzymes dégradant les lipides contenant des molécules comme les gangliosides. De même, les cathepsines sont un groupe de protéases lysosomales ayant un rôle dans de nombreuses fonctions cellulaires. Ils sont classés en trois groupes en fonction de leur rôle et de leur site catalytique actif; sérine, aspartique et cystéine. Il a été démontré que les mutations liées aux enzymes lysosomales provoquent des troubles génétiques rares. Par exemple, une mutation dans le gène de la palmitoyl protéine thioestérase 1 (*PPT1*), codant pour une sérine lipase, conduit à une maladie neuronale de la lipofuscinose céroïde (NCL) de type 1 (CLN1). De plus, les mutations des cathepsines D et F, de la tripeptidyl-peptidase 1 (TPP1) provoquent respectivement des troubles CLN10, CLN13, CLN2. Un autre trouble NCL est causé par des mutations *CLN5*, dont la protéine soluble mature est localisée dans la lumière lysosomale lors du clivage. Bien que la fonction de CLN5 ne soit pas connue, son rôle dans le trafic de l'endosome vers le réseau trans-Golgi (TGN) par le biais de la régulation de rétomère a été démontré par notre laboratoire.

Afin de prévenir les dommages de la membrane lysosomale causés par le pH acide de la lumière, la plupart des protéines de la membrane lysosomale (LMP) sont glycosylées, formant ainsi une couche de glycoprotéine sur la surface interne de la membrane lysosomale. On dénombre plus de 100 LMP, les plus abondantes étant les protéines membranaires associées au lysosome (LAMP-1 et LAMP-2), suivies par la protéine membranaire intégrale du lysosome 2 (LIMP2; également connue sous le nom de SCARB2) et la tétraspanine CD63. En plus d'être une simple barrière, ils jouent un rôle important dans les événements de phagocytose, d'autophagie, de mort cellulaire, d'infection et de réparation membranaire. Deux LMP liées à la maladie sont CLN3 et CLN7, dont les fonctions n'ont pas bien élucidées. Les mutations de ces protéines provoquent des NCL qui sont des troubles rares du stockage lysosomal.

Les hydrolases acides sécrétées et les protéines membranaires plasmatiques du lysosome sont traduites par des polyribosomes à la surface du réticulum endoplasmique rugueux (RER). Au cours de leur synthèse, les enzymes lysosomales sont glycosylées pour leur transport de Golgi dans des vésicules recouvertes de COPII. A leur arrivée dans le Golgi, les résidus M6P des protéines lysosomales sont modifiés par phosphorylation. Cela permet aux glycoprotéines d'être reconnues par le récepteur du mannose-6-phosphate cation-dépendant (CD-MPR) et MPR cations-indépendant (CI-MPR) pour leur transport lysosomal. Il convient de garder à l'esprit que l'adressage des protéines au lysosome n'implique pas toujours la reconnaissance des résidus M6P. En effet, la voie de tri des protéines grâce au récepteur de la sortiline est l'un des mécanismes de trafic lysosomal indépendants du M6P.

Trafic du TGN vers l'endosome

La liaison du récepteur lysosomal aux protéines adaptatrices des clathrines dans le cytosol est suivie de la formation de vésicules pour la libération de la cargaison à l'endosome. L'activation de la GTPase Arf1 initie le bourgeonnement des vésicules, suivie du recrutement des GGA et du complexe AP-1 à la membrane du TGN. Ils reconnaissent les séquences d'acides aminés des récepteurs de tri. Les vésicules chargées de protéines destinées au lysosome iront ensuite dans l'endosome. Étant donné que le pH des endosomes est plus acide que celui de l'appareil de Golgi, les enzymes dédiées au lysosome seront dissociés des récepteurs de tri, de sorte que les récepteurs soient recyclés vers le TGN pendant que la cargaison se déplace vers le lysosome.

Récupération d'endosome à Golgi

Une fois que les récepteurs ont libéré leur cargaison, ils peuvent être recyclés vers l'appareil d Golgi pour continuer le transport d'enzymes lysosomales. Le processus de recyclage est effectué par un complexe protéique appelé rétromère. La première partie du complexe est composée des protéines de tri des protéines vacuoliques (Vps) Vps26, Vps29 et Vps35, responsables de la reconnaissance des récepteurs et d'autres cargaisons contenant des protéines transmembranaires (telles que la sortiline et le récepteur au mannose-6-phosphate cation-indépendant CI-MPR). Par conséquent, il est également appelé complexe sélectif de cargaison (CSC). Le deuxième sous-complexe consiste à trier les nexines (SNX), responsables de la liaison avec les membranes. La petite GTPase Rab7 régule le recrutement spatio-temporel de rétomère vers les membranes endolysosomales pour le trafic endosome-TGN.

Rab7A GTPase

Les ras-like dans les protéines cérébrales (Rabs) sont de petites GTPases appartenant à la superfamille Ras. Depuis leur découverte en 1987, environ 70 d'entre elles ont été retrouvées chez l'homme. Les rabs sont spécifiquement localisées sur certaines membranes intracellulaires pour fonctionner. Rab7A est une petite GTPase de la famille Rab, associée aux endosomes tardifs et aux lysosomes . Cette GTPase est le principal régulateur du trafic endocytaire avec de nombreuses fonctions vitales. Son rôle est impliqué dans le trafic de l'endosome au lysosome et de l'endosome au réseau trans-Golgi. Comme toutes les autres Rab GTPases, Rab7A varie entre un état actif et inactif. Sous sa forme active, Rab7A est lié au GTP et est localisé sur les membranes endolysosomales, alors que sous sa forme inactive, Rab7A est lié au GDP et reste cytosolique. Des GEF et des GAP spécifiques catalysent respectivement le GDP en GTP et les événements d'hydrolyse inverse.

Rab7 est impliqué dans de nombreux processus cellulaires, y compris le transport des lipides et le positionnement desautophagosomes. Au niveau des endosomes tardifs, Rab7 régule leur formation, leur maturation etla composition membranaire des lysosomes. Cette GTPase est impliquée dans la biogenèse des lysosomes par son rôle dans la maturation des vésicules endocytaires, la phagocytose et l'autophagocytose. En outre, il joue un rôle clé dans la régulation de la dégradation de protéines endocytées telles que le récepteur au facteur de croissance épidermique (EGFR). Et enfin, il intervient dans la fusion des lysosomes avec les autophagosomes, régulant ainsi l'autophagie. Rab7 remplit ces différentes fonctions en recrutant une grande variété d'effecteurs (tels que le retromer, FYCO1 (FYVE and Coiled-Coil- (CC) -domain containing 1), RILP (Rab7 lysosomal interacting protein), PLEKHM1 (Pleckstrin homology domain contains protein family membre 1), HOPS (fusion homotypique et tri des protéines vacuolaires)) sur les membranes endolysosomales. Retromer régule le trafic endosome-TGN des récepteurs de tri. FYCO1 et RILP régulent le positionnement périphérique et périnucléaire des vésicules acides nécessaires aux événements de fusion. Ensuite,

HOPS et PLEKHM1 attachent et stabilisent deux membranes vésiculaires pour leur fusion avec l'action de la protéine SNARE.

L'activité et les fonctions de Rab7 sont étroitement régulées par différentes modifications post-traductionnelles (PTM). Première PTM identifiée, la prénylation de Rab7A s'est avérée importante pour son ancrage membranaire. Son ubiquitination a été liée à sa stabilité, à l'ancrage à membrane et son interaction avec RILP. Il a été démontré que les phosphorylations de Rab7A sont importantes pour la dégradation de l'EGFR et la mitophagie. Le rôle de la palmitoylation Rab7A sur le recrutement de rétromère au niveau des membranes a été récemment démontré par notre laboratoire. Le moment et la sélection d'effecteurs particuliers pour des fonctions cellulaires spécifiques sont très importants pour la fonction de Rab7, dont les problèmes sont associés à de nombreux troubles neurodégénératifs. Il est donc indispensable d'étudier et de découvrir les mécanismes de régulation en amont, les GEF et les PTM de Rab7. La combinaison d'événements complexes doit être sous le contrôle de molécules inconnues en amont pour son cycle d'activation et la régulation de son activité.

Lipofuscinose neuronale céroïde (NCL)

Les troubles métaboliques héréditaires affectant la fonction lysosomale sont connus sous le nom de troubles lysosomaux. Ils sont 70 d'entre eux connus à ce jour, tous avec une prévalence rare. Des mutations dans les gènes exprimant les protéines lysosomales empêchent le catabolisme lysosomal et conduisent à une accumulation de matière dans la cellule suivie de la mort cellulaire. Presque tous les LSD se manifestent par une neurodégénérescence. Etant la maladie neurodégénérative pédiatrique la plus courante, la NCL est une sous-famille de maladies lysosomales rares avec une incidence de 1: 12 500 dans la population mondiale. La rétinopathie, les troubles moteurs, l'épilepsie, la régression cognitive et une durée de vie considérablement réduite sont les symptômes retrouvés chez les patients souffrant de maladies NCL.

CLN3

Les mutations du gène *CLN3* altèrent la protéine codée et conduisent à l'apparition de la maladie neurodégénérative la plus courante chez les enfants. Les symptômes commencent par une perte de vision entre 4 et 7 ans et la durée de vie du patient est d'environ 30 ans. CLN3 contient six domaines transmembranaires avec des terminaisons N et C cytosoliques. La mutation CLN3 la plus courante a une délétion des exons 7 et 8; provoquant une troncature de 1 kb (CLN3 $^{Delta\ ex7\ /\ 8}$, (c.462-677del)). Les autres patients ont une variété de maladies différentes provoquées par des mutations par substitution, telles que CLN3^{R334H}, CLN3^{V330F}, CLN3^{E295K} et CLN3^{L101P}. Hormis la version tronquée, aucun de ces mutants CLN3 n'est associé à une mauvaise localisation cellulaire.

Bien que la localisation de CLN3 ait été démontrée sur les membranes lysosomales en tant que protéine membranaire intégrale hautement glycosylée, sa fonction est encore mal comprise. Auparavant, le rôle du CLN3 dans les voies d'autophagie et du trafic lysosomal a été proposé. De multiples déficiences enzymatiques ont été observées dans des cellules ayant une protéine CLN3 mutée. De plus, son interaction avec Rab7, RILP et les protéines motrices (tubuline, dynactine, dynéine, kinésine-2) a été montrée, régulant la localisation des compartiments endocytaires tardifs. Cependant, ni la fonction de ces interactions ni la maladie provoquant des mutations sur les fonctions en aval du CLN3 et la cause du déficit enzymatique n'ont été déterminées.

CLN5

Les mutations dans *CLN5* provoquent des défauts dans la protéine CLN5. CLN5 est également une protéine lysosomale soluble, bien qu'elle ne semble pas avoir d'activité enzymatique. Les symp-

tômes commencent entre 3 et 7 ans et les patients peuvent vivre jusqu'à l'adolescence. CLN5 n'a d'homologie avec aucune autre protéine connue. Le gène code en une protéine membranaire intégrale de 407 aa. Elle est ensuite clivée à l'extrémité N-terminal pour former une protéine mature soluble de 93 à 407 aa pour son transport endolysosomal. La mutation la plus courante de CLN5 causant la maladie est $CLN5^{Y392X}$. Elle induit l'apparition d'un codon stop prématuré, conduisant à une délétion de 2 pb. D'autres mutations germinales causant des mutations faux-sens dommageables incluent $CLN5^{D279N}$, $CLN5^{N192S}$ et $CLN5^{R112P}$.

Récemment, la fonction de CLN5 en tant que glycoside hydrolase potentielle dans Dictyostelium discoideum a été proposée. Cependant, aucune cible n'a été identifiée et cette fonction n'a pas été démontrée pour CLN5 chez les mammifères. D'autres études ont montré un rôle du CLN5 dans la régulation du pH lysosomal et de la mitophagie. Notre groupe a montré une diminution du recrutement de Rab7 et rétromère au niveau des membranes dans les cellules HeLa knockdown ($CLN5^{KD}$) CLN5. Par co-immunoprécipitation, il a été démontré que le CLN5 interagit avec CLN3. Cependant, ni la fonction de son interaction avec CLN3, ni les mutations induisant la maladie et perturbant les fonctions en aval de Rab7, nila cause des problèmes d'acidité lysosomale n'ont été déterminées.

Premier article: CLN3 régule la fonction endosomale en modulant les interactions Rab7-effecteurs

La lipofuscinose céroïde neuronale juvénile (JNCL) est causée par des mutations germinales dans la lipofuscinose céroïde neuronale-3 (CLN3). Plus souvent appelée maladie de Batten, c'est la maladie neurodégénérative pédiatrique la plus courante. CLN3 est une protéine membranaire intégrale hautement glycosylée qui se localise dans la membrane endosomale / lysosomale parmi d'autres emplacements intracellulaires et est impliquée dans le trafic lysosomal et l'autophagie. CLN3 interagit avec et a été impliqué dans le recrutement de Rab7A au niveau des membranes endosomales; cependant, la fonction de cette interaction est inconnue. En outre, la façon dont les mutations de CLN3 causant la maladie affectent cette interaction ou les fonctions en aval de Rab7A, n'a pas été élucidée.

Les Rabs fonctionnent en interagissant avec des effecteurs en aval et un processus clé régulant ces interactions est le chargement de GTP ou «l'activation» des Rab GTPases sur des sites membranaires spécifiques. Rab7A actif chargé de GTP se localise sur les membranes endosomales et recrute de nombreux effecteurs pour exécuter diverses fonctions telles que le trafic endosome-reseau trans-Golgi (TGN), la fusion autophagosome-lysosome, le positionnement lysosomal et la dégradation de la cargaison endocytaire, comme le récepteur du facteur de croissance épidermique (EGF) (EGFR).

Dans cette étude, nous avons analysé plusieurs de ces voies médiées par Rab7A pour déterminer laquelle était sous le contrôle de CLN3. Pour commencer, nous voulions comprendre le rôle de l'interaction CLN3 / Rab7A et l'effet des mutations pathogènes sur cette interaction. Pour les études d'interactions, nous avons utilisé le transfert d'énergie de résonance par bioluminescence (BRET). Par rapport à la co-immunoprécipitation, le BRET est réalisé dans des cellules vivantes, avec des protéines localisées dans leur environnement naturel. À partir des courbes de titrage BRET, il est possible de calculer le $BRET_{50}$ qui est la valeur à laquelle la concentration de l'accepteur est nécessaire pour obtenir 50 % du signal BRET maximal ($BRET_{MAX}$) et indique la propension du couple de protéines à interagir. Plus le $BRET_{50}$ est petit, plus l'interaction est forte. Le donneur d'énergie renilla luciférase II (RlucII) a été fusionné à l'extrémité N-terminale à Rab7A de type sauvage (RlucII-Rab7A). La protéine fluorescente verte accepteur d'énergie 10 (GFP10) a

été fusionnée à l'extrémité N-terminale de mutants de type sauvage et divers CLN3 (GFP10-CLN3, GFP10-CLN3^{R334H}, GFP10-CLN3^{V330F}, GFP10-CLN3^{E295K}, GFP10-CLN3^{L101P}). Ces mutations ont déjà été étudiées et se sont révélées localisées dans les endosomes / lysosomes tardifs de manière similaire au CLN3 de type sauvage. Les cellules HeLa ont été co-transfectées avec une quantité constante de RlucII-Rab7A et des quantités croissantes de GFP10-CLN3 pour générer des courbes de titrage BRET. Le signal BRET entre RlucII-Rab7A et GFP10-CLN3 augmente rapidement avec des quantités croissantes de GFP10-CLN3 exprimées jusqu'à ce qu'il atteigne la saturation, suggérant une interaction spécifique (Fig. 2.1 A, courbe bleue). Nous avons également testé une autre Rab GTPase, Rab1a (Fig. 2.1 A, courbe rouge), qui est localisée au Golgi, pour confirmer la spécificité de l'interaction CLN3 – Rab7A. Nous avons extrapolé le BRET $_{50}$ pour l'interaction entre CLN3 et les deux GTPases Rab et constaté que l'interaction Rab7A – CLN3 avait un BRET $_{50}$ beaucoup plus petit par rapport à la valeur de l'interaction Rab1a – CLN3, indiquant que Rab7A a une plus grande propension à interagir avec CLN3 par rapport à Rab1a (Fig. 2.1 B). Une petite fraction de CLN3 se localise sur le Golgi, nous n'avons donc pas été surpris de détecter une interaction entre CLN3 et Rab1a. Ensuite, nous avons testé l'interaction entre CLN3 et Rab7A^{C205,207S} qui est une forme mutante de Rab7A qui ne peut pas être recrutée sur les membranes en raison de son absence de prénylation. Nous n'avons trouvé aucune interaction entre Rab7A^{C205,207S} et CLN3 (Fig. 2.1 A, ligne verte). Enfin, nous avons testé si la petite GTPase Arf6 pouvait interagir avec CLN3 (Fig. 2.1 A, ligne orange) et n'avons trouvé aucune interaction. Cela indique que le signal mesurobservé entre Rab7a et CLN3 est bien spécifique. Nous avons ensuite réalisé une expérience de BRET pour déterminer l'impact des mutations causant la maladie CLN3 sur l'interaction CLN3 – Rab7A (Fig. 2.1 C). Par rapport au CLN3 de type sauvage, nous avons trouvé une interaction significativement plus forte (BRET$_{50}$) entre Rab7A et CLN3^{R334H} ou CLN3^{V330F} (Fig. 2.1 D), alors que les mutations CLN3^{E295K} et CLN3^{L101P} avaient des effets négligeables sur l'interaction CLN3 – Rab7A (Fig. 2.1 D). Pour confirmer nos données BRET, nous avons testé ces interactions par co-immunoprécipitation (co-IP) (Fig. 2.8 A).

Les mutations dans CLN5, qui interagit avec CLN3, provoquent une forme de NCL avec des symptômes qui sont aussi retrouvés dans la maladie CLN3. Dans nos travaux précédents, nous avons montré que CLN5 interagit avec la sortiline (également appelée SORT1). Par conséquent, nous avons rationalisé que CLN3 pourrait également interagir avec ce récepteur de tri lysosomal. Pour tester cette hypothèse, nous avons réalisé une expérience de BRET et trouvé une interaction entre CLN3 et la sortiline (Fig. 2.1 E, courbe bleue). Nous avons ensuite déterminé l'impact que les mutations causant la maladie CLN3 pourraient avoir sur cette interaction. Par rapport au CLN3 de type sauvage, nous avons trouvé des interactions plus faibles pour la sortiline – CLN3^{E295K} et la sortiline – CLN3^{L101P} (Fig. 2.1 F). Fait intéressant, nous n'avons trouvé aucun changement dans les interactions sortiline – CLN3^{R334H} et sortiline – CLN3^{V330F} par rapport à l'interaction sortiline – CLN3 (Fig. 2.1 F). Pour confirmer nos données BRET, nous avons testé ces interactions par co-immunoprécipitation (co-IP) (Fig. 2.8 A).

Une étude précédente avait montré que la coloration par immunofluorescence de Rab7A était diminuée dans les cellules exprimant la mutation homozygote (CLN3 $^{Delta\ ex7\ /\ 8}$ / CLN3 $^{Delta\ ex7\ /\ 8}$) par rapport aux cellules de type sauvage . Sur cette base, nous avons étudié si CLN3 est nécessaire pour le recrutement membranaire de Rab7A en générant des cellules HeLa CLN3-KO en utilisant la technologie CRISPR / Cas9 (Fig. 2.9 A). Nous avons également généré des cellules Rab7A-KO en utilisant la même souche parentale HeLa pour servir de contrôle dans nos expériences (Fig. 2.9 B). Des travaux antérieurs ont démontré que les cellules porteuses de mutations de CLN3 accumulent des autophagosomes positifs pour LC3II, suggérant une activité autophagique défectueuse. Pour tester les cellules CLN3-KO présentaient le même phénotype en ce qui concerne l'autophagie, nous

avons induit l'autophagie par privation de nutriments en incubant des cellules de type sauvage, CLN3-KO et Rab7A-KO en présence ou en l'absence de BafA1. Les résultats obtenus dans les cellules HeLa CLN3-KO soutiennent les résultats précédemment publiés, suggérant que les cellules dépourvues de CLN3 sont défectueuses aux derniers stades de l'autophagie. Combiné avec nos données de séquençage, cela confirme la perte de fonction de CLN3 dans cette lignée cellulaire.

En utilisant la lignée cellulaire HeLa CLN3-KO, nous avons réalisé une technique d'isolation membranaire pour déterminer si CLN3 est nécessaire pour le recrutement membranaire de Rab7A dans des cellules HeLa de type sauvage, CLN3-KO et CLN3-KO exprimant FLAG-CLN3 (Fig. 2.2 A). La quantification de 5 expériences indépendantes a montré que le recrutement membranaire de Rab7A n'était pas altéré dans les cellules CLN3-KO (Fig. 2.2 B). La petite GTPase Rab7A régule le recrutement spatio-temporel de rétomère, un complexe protéique nécessaire pour un trafic endosome-TGN efficace du récepteur au mannose 6-phosphate cation-indépendant (CI-MPR) et de la sortiline. Dans les cellules dépourvues de rétomère, ces récepteurs ne sont pas efficacement recyclés vers le TGN, s'accumulent au niveau des endosomes tardifs et sont ensuite dégradés dans les lysosomes. Cependant, dans les cellules n'exprimant pas Rab7A, CI-MPR n'est pas recyclé efficacement vers le TGN, sans pourtant être dégradé. Nous avons répété le test d'isolation de membrane et inclus des cellules HeLa Rab7A-KO comme contrôle. En effet, nous avons démontré précédemment une réduction du recrutement de rétromère au niveau des membranesdans les cellules HEK293 Rab7A-KO. Par rapport aux cellules HeLa de type sauvage, nous avons observé une diminution significative du recrutement de rétromère (tel que détecté par coloration avec la sous-unité de retromère Vps26A) dans les cellules HeLa Rab7A-KO,.Néanmoins, nous n'avons observé aucun changement significatif en ce qui concerne les cellules CLN3-KO (Fig. 2.2 C).

Bien que la distribution membranaire de rétomère ne soit pas modifiée dans les cellules CLN3-KO, nous nous sommes demandé si nous pouvions observer d'autres changements. Rab7A interagit avec rétromère, ce qui est nécessaire pour le recrutement spatio-temporel de ce dernier. Nous avons déterminé si l'interaction entre Rab7A et rétromère est affectée dans les cellules CLN3-KO. Par rapport aux cellules HeLa de type sauvage, nous avons trouvé une interaction plus faible entre Rab7A à Vps26A dans les cellules CLN3-KO (Fig. 2.3 B). Nous avons précédemment démontré Rab7A doit d'être palmitoylé pour pouvoir interagir efficacement avec rétromère. Nous avons testé si le niveau de palmitoylation de Rab7A était plus faible dans les cellules CLN3-KO par rapport aux cellules HeLa de type sauvage, en utilisant la technique Acyl-RAC (Fig. 2.3 C). La quantification de trois dosages Acyl-RAC indépendants n'a pas permis de trouver de changements significatifs dans le niveau de palmitoylation de Rab7A dans les cellules CLN3-KO, par rapport aux cellules HeLa de type sauvage (Fig. 2.3 D). Nous avons ensuite voulu testé si la charge GTP que porte Rab7A était affectée dans les cellules CLN3-KO, grâce à l'utilisation d'un biocapteur de FRET bien caractérisé. Nous n'avons trouvé aucune différence dans la charge GTP de Rab7A entre les cellules HeLa de type sauvage et CLN3-KO (Fig. 2.3 E), suggérant que CLN3 ne modifie pas la charge GTP de Rab7A.

Nous nous sommes ensuite demandé si CLN3 pouvait interagir avec rétromère. En utilisant la technique de BRET, nous avons pu mettre en évidence une interaction entre ces deux partenaires (Fig. 2.4 A, courbe bleue). Les mutations $CLN3^{R334H}$ (Fig. 2.4 A, courbe rouge) et $CLN3^{E295K}$ (Fig. 2.4 A, courbe noire) n'ont aucun impact sur cette interaction (Fig. 2.4 B). Il est intéressant de noter que le $CLN3^{V330F}$ (Fig. 2.4 A, courbe verte) augmente la propension CLN3 à interagir avec rétromère, tandis que la mutation $CLN3^{L101P}$ (Fig. 2.4 A, courbe violette), affaiblit significativement l'interaction (Fig. 2.4 B). Nous avons à nouveau utilisé la co-immunoprécipitation pour confirmer ces résultats de BRET (Fig. 2.8 A). CI-MPR et la sortiline sont connus pour interagir avec rétomère,

ce qui est nécessaire pour leur trafic endosome-TGN. En utilisant la technique de BRET, nous avons étudié l'interaction dans les cellules HeLa CLN3-KO pour déterminer si CLN3 joue un rôle dans cette interaction (Fig. 2.4 E, courbe bleue). Nous avons trouvé une interaction significativement affaiblie entre rétomère et la sortiline dans les cellules CLN3-KO par rapport aux cellules HeLa de type sauvage (Fig. 2.4 F). Ces résultats ont une nouvelle fois été confirmés par co-immunoprécipitation (Fig. 2.10 B).

Puisque nous avons observé une plus faible interaction entre rétromère et la sortiline dans les cellules CLN3-KO et que rétomère est nécessaire pour le trafic endosome-TGN efficace de CI-MPR et de la sortiline, nous voulions déterminer si le recyclage des récepteurs de tri lysosomal était régulé par CLN3. Nous avons effectué une expérience de chasse au cycloheximide pour déterminer la stabilité du récepteur. Nous avons observé une diminution des niveaux de sortiline et de CI-MPR dans les cellules HeLa CLN3-KO par rapport aux cellules Rab7A-KO et HeLa de type sauvage (Fig. 2.11 A). La complémentation de la lignée CLN3-KO par la protéine CLN3 fusionnée à l'épitoge FLAG (FLAG-CLN3) a permis de rétablir le phénotype (Fig. 2.11 A). Lorsque nous avons voulu déterminé les effets des mutations pathogènes de CLN3 sur la stabilité de ces deux récepteurs cargo, nous avons observé que l'expression de $CLN3^{V330F}$, $CLN3^{E295K}$, $CLN3^{L101P}$ et $CLN3^{R334H}$ dans les cellules CLN3-KO ne rétablissent que partiellement la dégradation de la sortiline et du CI-MPR. Cela suggère que ces mutants conservent tout de même une certaine activité, bien qu'inférieure à celle de CLN3 de type sauvage.

La cathepsine D (également connue sous le nom de CTSD) est une hydrolase lysosomale dont le trafic vers les lysosomes est médié par CI-MPR. La perturbation du trafic de CI-MPR induit par l'inhibition post-transcriptionnelledes sous-unités de rétromère ou de Rab7A conduit au bloquage de la maturation de la cathepsine D, entraînant l'accumulation de formes pro et intermédiaires de la protéine, et une réduction de la forme lysosomale mature. Puisque nous avons observé la dégradation du CI-MPR et de la sortiline dans les cellules HeLa CLN3-KO, nous avons cherché à déterminer si cela avait un impact sur le traitement de la cathepsine D (Fig. 2.5 C). Par rapport aux cellules HeLa de type sauvage, les cellules HeLa CLN3-KO et Rab7A-KO présentaient une augmentation des formes pro et intermédiaires, mais une réduction de la cathepsine D mature par rapport aux cellules HeLa de type sauvage (Fig. 2.5 D).

Lors de la stimulation de l'EGF, le récepteur de l'EGF (EGFR) est internalisé et peut être soit recyclé vers la membrane plasmique, soit dégradé dans les lysosomes. Rab7A est un régulateur clé de la voie de dégradation qui intervient dans les étapes ultérieures de ce processus. Au moins deux effecteurs Rab7A sont impliqués dans la dégradation de l'EGFR : RILP et PLEKHM1. En effet, l'inhibition de l'une ou l'autre de ces protéines entraîne des retards significatifs dans la cinétique de dégradation de l'EGFR. Afin de déterminer si CLN3 module cette voie qui implique Rab7A, nous avons étudié la cinétique de dégradation de l'EGFR dans les cellules HeLa de type sauvage, CLN3-KO et Rab7A-KO. Lors d'une stimulation des cellules avec de l'EGF et cycloheximide, le niveau d'EGFR endogène a été déterminé par Western blot (Fig. 2.6 A). Lorsque nous avons comparé la cinétique de dégradation de l'EGFR dans les cellules CLN3-KO, nous avons trouvé des retards significatifs à 10, 15 et 30 min par rapport aux cellules de type sauvage. Ensuite, nous avons étudié la cinétique de dégradation de l'EGF couplé à la sonde Alexa Fluor 488 (EGF-488) en utilisant les mêmes lignées cellulaires pour confirmer notre résultat de dégradation de l'EGFR. Après 30 min de chasse, les cellules CLN3-KO HeLa présentaient presque deux fois plus d'EGF que les cellules de type sauvage (Fig. 2.6 D). La cinétique de dégradation retardée observée dans les cellules CLN3-KO peut être expliquée par une fonction lysosomale diminuée en raison d'un trafic endosome-TGN défectueux. Il est aussi envisageable que l'EGF et l'EGFR ne soient pas dégradés

car ils n'atteigneraient pas les lysosomes efficacement en raison de problèmes de fusion entre les membranes des endosmoses tardifs et les lysosomes les empêcheraient .

Afin de comprendre le mécanisme impliqué dans la dégradation retardée de l'EGFR, nous avons utilisé le BRET pour déterminer si les interactions Rab7A – RILP, Rab7A – PLEKHM1 et / ou Rab7A – FYCO1 étaient affectées (Fig. 2.7 A – F). FYCO1 est un effecteur Rab7A requis pour le trafic antérograde des vésicules, tandis que RILP et PLEKHM1 sont impliqués dans la fusion et la dégradation de la membrane. Nous n'avons trouvé aucun changement significatif dans l'interaction entre RILP et Rab7A (Fig. 2.7 A, B) ou FYCO1 et Rab7A (Fig. 2.7 C, D) dans la nature -type par rapport aux cellules CLN3-KO HeLa. Nous avons trouvé un changement dans l'interaction entre PLEKHM1 et Rab7A, donnant moins d'interaction dans les cellules CLN3-KO par rapport aux cellules de type sauvage (Fig. 2.7 E, F).

Discussion & Conclusion

Nous avons confirmé l'interaction CLN3-Rab7A en utilisant la technique de BRET dans des cellules vivantes. De plus, nous avons montré que deux mutations de CLN3, $CLN3^{R334H}$ et $CLN3^{V330F}$, augmentaient la force de cette interaction. Cela suggère que ces deux mutations pourraient retenir Rab7A sur les membranes plus longtemps ou empêcher son cycle efficace, un processus nécessaire pour un fonctionnement optimal. Fait intéressant, deux autres mutations ponctuelles, $CLN3^{E295K}$ et $CLN3^{L101P}$, n'ont eu aucun effet sur cette interaction. Cependant, ces deux mutations ont affaibli l'interaction CLN3-sortiline. Combiné avec le fait que CLN3 est nécessaire à la fois pour les interactions Rab7A-rétromère et rétromère-sortiline, nos données révèlent un rôle pour CLN3 dans la modulation de la fonction de rétromère. Il est bien établi que des défauts de la fonction de rétromère ou de la sortiline affectent le tri et la maturation de la cathepsine D. Une publication précédente a mis en évidence des défauts dans le trafic et la maturation de l'enzyme lysosomale cathepsine D dans des cellules $CLN3^{\,Delta\ ex7\ /\ 8}$ / $CLN3^{\,Delta\ ex7\ /\ 8}$. L'ablation de CLN3 entraîne la dégradation lysosomale de la sortiline et du CI-MPR, phénomène très probablement due à un trafic endosome-TGN déficient de sortiline et de CI-MPR. En outre, une étude protéomique récemment publiée étudiant l'impact des mutations CLN3 sur le contenu lysosomal a révélé une diminution de 28 protéines lysosomales, dont la cathepsine D et la prosaposine. Alors que le trafic de la cathepsine D vers les lysosomes est médié par CI-MPR, la prosaposine nécessite la sortiline. Considérés dans leur ensemble, ces résultats indiquent que CLN3 jouerait un rôle crucial dans la régulation du tri et du trafic lysosomal. En tant que tels, nos résultats fournissent une explication moléculaire à ces observations précédentes.

Rab7A joue également un rôle crucial dans la dégradation des cargaisons endocytaires telle que l'EGFR. Nous avons trouvé des retards significatifs dans la dégradation de l'EGFR et de l'EGF dans les cellules CLN3-KO. Cela pourrait s'expliquer de deux manières. Premièrement, CLN3 est impliqué dans le trafic de la sortiline,récepteur de tri lysosomal. Il a été démontré que des défauts dans le trafic de cette protéine ou des défauts de la fonction de rétromère ont un impact significatif sur la fonction des lysosomes. Deuxièmement, Rab7A est nécessaire pour la fusion des endosomes et des lysosomes, un processus nécessitant la présence des protéines RILP et PLEKHM1. Bien que nous n'ayons trouvé aucun changement dans l'interaction Rab7A – RILP dans les cellules CLN3-KO, nous avons trouvé une réduction significative de l'interaction Rab7A – PLEKHM1. Cela suggère des événements de fusion défectueux. Combiné à une fonction lysosomale diminuée, cela pourrait expliquer le retard significatif de la dégradation de l'EGF et de l'EGFR. La voie Akt – mTOR est régulée à la hausse dans les fibroblastes de patients JNCL. EGFR est connu pour activer plusieurs voies de signalisation, y compris Akt. Le trafic dérégulé et la dégradation de l'EGFR peuvent conduire à une signalisation accrue. Nos résultats pourraient au moins partiellement expliquer la

régulation à la hausse de la voie Akt-mTOR trouvée dans les fibroblastes de patients atteints de JNCL.

L'autophagie est affectée dans les cellules n'exprimant pas CLN3. Les cellules HeLa CLN3-KO présentent également une altération de autophagie, similaire à celle observée dans le Rab7A-KO. Cela suggère des défauts aux étapes avancée de la voie de l'autophagie, probablement à l'étape de fusion avec les lysosomes. PLEKHM1 est l'un des facteurs jouant un rôle essentiel dans la modulation de la fusion des autophagosomes avec les lysosomes. Des défauts dans cette machinerie de fusion conduisent à un dérèglement de l'autophagie, mais également à une diminution de la cinétique de dégradation de l'EGFR. Nous proposons l'hypothèse que ce phénotype observéchez les patients atteints de JNCL est du à des défauts de la fonction de PLEKHM1 et de la fonction du lysosome induit par un mauvais adressage de la sortiline et du CI-MPR.

En conclusion, nos résultats indiquent que CLN3 joue un rôle majeur dans la régulation d'un sous-ensemble de fonctions Rab7A. Nous avons précédemment montré un rôle similaire pour CLN5, une protéine soluble trouvée dans la lumière des endosomes et des lysosomes. Comme CLN3 et CLN5 sont connus pour interagir, nous posons l'hypothèse que les deux protéines pourraient fonctionner comme un complexe régulant Rab7A et rétromère. La découverte de ces mécanismes moléculaires permettrait d'expliquer au moins partiellement, le phénotype observé chez les patients atteints de la JNCL.

Deuxième article: CLN5 et CLN3 fonctionnent comme un complexerégulateur de la fonction de l'endolysosome

Des mutations de la lignée germinale dans le gène *CLN5* sont des causes de la maladie CLN5. On trouve notamment des mutations par substitutions substitutions d'acides aminés (R112H, N192S, D279N) mais des mutations non-sens conduisant à la production de protéines tronquées suite à l'apparition de codons stop prématurés (W75X et Y392X), La mutation non-sens , $CLN5^{Y392X}$, est la mutation la plus courante chez les patients. Les patients atteint de cette forme de NCL ont des symptômes qui apparaissent précocement, entre 3 à 7 ans, et et ont une durée de vie qui ne dépasse pas l'adolescence. Des travaux récents ont suggéré que le CLN5 pourrait fonctionner comme une glycoside hydrolase, mais ses cibles endogènes n'ont pas été identifiées. De plus, CLN5 serait lié à la régulation du pH lysosomal et de la mitophagie. Pour approfondir notre compréhension de cette protéine, en utilisant de petits ARN interférents (siRNA), notre laboratoire a généré des cellules HeLa knockdown CLN5 ($CLN5^{KD}$). Dans ces cellules, nous avons précédemment démontré une diminution du recrutement de Rab7A au niveau des membranes. Rab7A est une petite GTPases qui peut se lier et recruter rétomère, un complexe protéique qui régule le trafic endosome-trans Golgi (TGN). Une fois recruté,rétromère interagit avec les extrémités cytosoliques des récepteurs de tri lysosomal, le récepteur du mannose 6-phosphate cation-indépendant (CI-MPR) et la sortiline pour permettre leur recyclage. Dans les cellules HeLa CLN5-KD, la diminution du recrutement de Rab7A et de rétrocède au niveau des membranes a entraîné la dégradation lysosomale de CI-MPR et de la sortiline, et un mauvais adressage de lacathepsine D. Au-delà du recrutement de rétromère, Rab7A régule également la dégradation de la cargaison endocytique telle que l 'EGFR via son interaction t avec PLEKHM1, régule le mouvement des organites en interagissant avec RILP et régule les derniers stades de l'autophagie en médiant la fusion entre les autophagosomes et les lysosomes grâce au complexe HOPS et d'autres facteurs d'attache.

Dans mon premier article déjà mentionné, nous avons montré que CLN3 est également nécessaire pour le recyclage des récepteurs de tri lysosomal vers le réseau endosome-TGN. Cette protéine CLN3 glycosylée se localise dans les membranes endolysosomales parmi d'autres emplacements

intracellulaires, et peut interagir avec d'autres protéines CLN, y compris CLN5. Cependant, les fonctions de ces interactions ne sont pas connues. L'inhibition de CLN3, au contraire de CLN5, n'a pas affecté la localisation ou l'activation de Rab7A ou de son effecteur rétomère. , CLN3 est nécessaire pour l'interaction efficace de Rab7A avec rétomère, et pour l'interaction rétomère / sortiline, agissant très probablement comme une protéine d'échafaudage.

Dans cette étude, nous avons généré des cellules HeLa knockout CLN5 ($CLN5^{KO}$) sur la même lignée cellulaire parentale utilisée pour générer des cellules knockout CLN3 ($CLN3^{KO}$) et Rab7A ($Rab7A^{KO}$). Ce système knock-out nous a permis d'étudier les effets d'une mutation causant la maladie CLN5. Nous avons étendu nos études pour tenter d'identifier les mécanismes responsables des défauts de dégradation endocytaire et d'autophagie.

Dans nos travaux antérieurs menés sur des cellules HeLa $CLN5^{KD}$, nous avons montré une diminution du recrutement membranaire de Rab7A conduisant à une diminution significative du recrutement membranaire de son effecteur, rétromère. Afin d'étudier le rôle des mutations causant la maladie CLN5, nous avons généré des cellules HeLa $CLN5^{KO}$ en utilisant la technologie d'édition de génome CRISPR / Cas9. Pour confirmer nos résultats précédents obtenus dans les cellules $CLN5^{KD}$, nous avons réalisé une expérience d'isolation membranaire dans les cellules HeLa $CLN5^{KO}$ et montré que la inactivation totale de CLN5 ou l'expression de mutation $CLN5^{Y392X}$ -HA n'avait pas d' effet significatif sur la distribution membranaire de Rab7A (Fig. 3.1 B). La petite GTPase Rab7A régule le recrutement spatio-temporel de rétromère. Par conséquent, nous avons répété le test de membrane comme ci-dessus pour tester si CLN5 est nécessaire pour le recrutement membranaire de rétomère. Par rapport aux cellules HeLa de type sauvage, nous avons observé une diminution significative du recrutement de rétromère dans les cellules $CLN5^{KO}$ (Fig. 3.1 A). Le phénotype de type sauvage a pourtant pu être rétabli lorsque les cellules les cellules $CLN5^{KO}$ ont été complémentées avec CLN5-HA., Cela indique que l'effet observé sur le recrutement de Vps26A est spécifique à la suppression de CLN5, et probablement pas un effet « off-target"(Fig. 3.1 A et C). L'expression de CLN5 ^{Y392X} -HA dans les cellules CLN5 ^{KO} a partiellement restauré le recrutement desrétromère, mais pas à des niveaux comparables à celui de CLN5 de type sauvage (Fig. 3.1 C) .

La question restait de savoir comment Rab7A était lié à la membrane, mais incapable de recruter rétromère. Ces dernières années, il a été démontré que Rab7A était phosphorylé, ubiquitiné et palmitoylé. Il a été démontré que ces modifications post-traductionnelles régulent diverses fonctions de cette petite GTPase, souvent en modulant l'interaction avec ses effecteurs. En particulier, nous avons précédemment montré que la palmitoylation de Rab7A est nécessaire pour le recrutement de rétomère sur les membranes endosomales. Puisque Rab7A est toujours lié à la membrane dans les cellules CLN5 ^{KO} HeLa, mais que rétromère ne l'est pas, nous avons utilisé la technique Acyl-RAC pour tester si la palmitoylation de Rab7A est affectée dans ces cellules (Fig. 3.1 D) . Nous avons constaté que la palmitoylation Rab7A était significativement diminuée dans les cellules HeLa CLN5 ^{KO} par rapport aux cellules de type sauvage (Fig. 3.1 E).

Rab7A coordonne le recrutement spatio-temporel de rétomère sur les membranes endosomales. Étant donné que nous avons observé une diminution du recrutement membranaire de rétomère ainsi qu'une diminution de la palmitoylation de Rab7A, nous nous attendions à observer une interaction plus faible entre Rab7A et rétomère dans les cellules HeLa CLN5 ^{KO}. Pour tester notre hypothèse, nous avons utilisé le transfert d'énergie de résonance de bioluminescence (BRET), comme nous l'avons expliqué précédemment pour le premier article. Par rapport aux cellules HeLa de type sauvage, nous avons trouvé une interaction plus faible entre Rab7A à Vps26A dans les cellules CLN5 ^{KO} (Fig. 3.2 B). Pour tester si la mutation causant la maladie dans CLN5 affectait l'interaction Rab7A / rétromère, nous avons exprimé HA-CLN5 de type sauvage (figure 2A, courbe verte) ou

HA-CLN5 ^{Y392X} (figure 2A, courbe violette) dans les cellules CLN5 ^{KO}. Alors que l'expression de HA-CLN5 a permis de rétablir l'interaction Rab7 / étromère (Fig. 3.2 B), l'expression de HA-CLN5 ^{Y392X} ne l'a pas fait (Fig. 3.2 B). Nos travaux précédents suggèrent que la palmitoylation favorise l'association de Rab7A à un domaine endosomal spécifique pour optimiser son interaction avec rétromère, sans affecter la capacité globale de la petite GTPase à interagir avec cet effecteur. En tant que tel, lorsque l'interaction Rab7A / retromère a été analysée par la technique de BRET, préservant ainsi les membranes cellulaires, nous avons observé une diminution de l'interaction, alors qu'aucun changement n'a été observé par co-immunoprécipitation, cette méthode ne permettant pas de conserver la compartmentation cellulaire. Pour confirmer si tel était le cas dans les cellules HeLa CLN5 ^{KO}, nous avons effectué une co-immunoprécipitation entre Rab7A et rétomère dans des cellules HeLa de type sauvage et CLN5 ^{KO} (Fig. S1C). Nous n'avons trouvé aucun changement dans l'interaction Rab7A / rétomère en utilisant cette méthode.

Le CI-MPR et la sortiline sont connus pour interagir avec rétomère, ce qui est nécessaire pour leur trafic endosome-TGN. En utilisant la technique de BRET, dans mon premier article, nous avons montré que la sortiline et la sous-unité Vps26A interagissent, et que cette interaction est significativement plus faible dans les cellules CLN3 ^{KO} par rapport aux cellules HeLa de type sauvage. Nous avons testé l'interaction sortiline / rétomère dans les cellules CLN5 ^{KO} HeLa pour déterminer si cette protéine joue un rôle dans cette interaction. Nous avons trouvé une interaction significativement affaiblie entre rétomère et la sortiline dans les cellules CLN5 ^{KO} par rapport aux cellules HeLa de type sauvage (Fig. 3.2 D). L'interaction entre rétromère et la sortiline dans les cellules CLN5 ^{KO} HeLa pourrait être rétablie en exprimant HA-CLN5 (Fig. 3.2 C, courbe verte). En revanche, l'expression de HA-CLN5 ^{Y392X} dans des cellules HeLa CLN5 ^{KO} (Fig. 3.2 C, courbe violette) n'a pas permis de rétablir l'interaction (Fig. 3.2 D). Pour confirmer nos données de BRET, nous avons immunoprécipité la sous-unité Vps26A endogène avec un anticorps anti-Vps26A et réalisé un western blot suivi d'un marquage de sortiline endogène (Fig. S1C). Par co-immunoprécipitation, nous n'avons observé aucun changement dans l'interaction Vps26A / sortiline dans les cellules CLN5 ^{KO}, suggérant que les protéines peuvent interagir lorsque leur localisation intracellulaire membranaire n'est pas prise en compte.

Dans les cellules n'exprimant pas rétomère, la sortiline n'est pas efficacement recyclée vers le TGN, s'accumule dans les endosomes tardifs et est ensuite dégradée dans les lysosomes. Nous avons précédemment démontré que les cellules CLN5-KO présentent le même phénotype . En utilisant les cellules HeLa CLN5 ^{KO}, nous avons effectué une expérience de chasse de cycloheximide afin de déterminer la stabilité du récepteur sortiline. Une analyse par Western blot (Wb) montre une diminution des niveaux de sortiline dans les cellules HeLa CLN5 ^{KO} à 3 et 6 heures par rapport aux cellules HeLa de type sauvage (Fig. 3.3 A). La complémentation de la lignée CLN5-KO par une la protéine CLN5 fusionnée à l'épitoge HA (CLN5-HA) a permis de rétablir le phénotype de type sauvage (Fig. 3.3 A). Au contraire, la complémentation des cellules CLN5-KO avec le mutant CLN5 ^{Y392X} -HA d n'a pas réduit la dégradation de la sortiline (Fig. 3.3 A).

Puisque nous avons observé la dégradation de la sortiline dans les cellules HeLa CLN5 ^{KO}, nous avons cherché à déterminer si cela avait un impact sur la fonction lysosomale. La cathepsine D est d'abord produite sous forme de pro-cathepsine D de 53 kDa (proCatD), qui est ensuite clivée en une forme intermédiaire de 47 kDa (iCatD), avant de devenir la cathepsine D mature de 31 kDa (mCatD), une fois localisée dans le lysosome. Par rapport aux cellules HeLa de type sauvage, les cellules CLN5 ^{KO} présentent une fraction d'iCatD significativement plus grande et une fraction de mCatD significativement réduite (Fig. 3.3 D).

Récemment, nous avons montré que CLN3 fonctionne comme une protéine d'échafaudage pour assurer les interactions Rab7A / rétomère et rétomère / sortiline, qui sont séquentiellement nécessaires pour réguler le recyclage de la sortiline vers le réseau endosome-TGN. Dans cette étude, nous avons démontré un rôle de CLN5 dans la régulation de la stabilité de la sortiline. Cependant, la question demeure de savoir comment une protéine lysosomale soluble, CLN5, peut réguler les interactions Rab7A / rétomère et rétomère / sortiline, qui ont lieu dans le cytosol. Afin de mieux comprendre la relation entre CLN5 et CLN3 et leurs fonctions dans cette voie, nous avons voulu déterminer si CLN5 pouvait jouer un rôle dans la modulation des interactions impliquant CLN3 et ses effecteurs. Des études antérieures ont montré que CLN3 et CLN5 interagissent. Nous avons confirmé ces données par co-immunoprécipitation puis étudié l'effet de la mutation de CLN5 ^{Y392X} sur la force de l'interaction (Fig. S2A). Il apparait que ^{Y392X} n'affecte pas l'interaction de CLN5 et CLN3 (Fig. S2A). L'interaction CLN3 / Rab7A a été précédemment mise en évidence en utilisant des expériences de co-immunoprécipitation et de BRET. Pour déterminer si CLN5 joue un rôle dans cette interaction, nous avons utilisé la technique de BRET, qui nous a permis d'observer que l'interaction CLN3 / Rab7A est plus faible dans les cellules n'exprimant pas de CLN5 (Fig.3.4 B). Le phénotype de type sauvage a pu être complètement rétabli lorsque les cellules CLN5-KO ont été complémentées avec HA-CLN5 (Fig. 3.4 A, courbe verte) (Fig. 3.4 B); alors que la complémentation réalisée avec HA-CLN5 ^{Y392X} n'a conduit qu'à un rétablissement partiel du phénotype (Fig. 3.4 A, courbe violette) (Fig. 3.4 B).

Nous avons précédemment démontré l'interaction entre CLN3 et rétromère. Nous avons utilisé la technique de BRET afin de tester si CLN5 joue un rôle dans la modulation de cette interaction. Nous avons trouvé que l'interaction CLN3 / retromer était significativement plus faible dans les cellules CLN5 ^{KO} que dans les cellules HeLa de type sauvage (Fig. 3.4RÉ). Comme attendu, la complémentation des cellules CLN5 ^{KO} avec HA-CLN5 a permis de rétablir l'interaction CLN3 / retromer (Fig. 3.4 B, courbe verte); alors que la complémentation réalisée avec HA-CLN5 ^{Y392X} n'a que partiellement rétabli l'interaction (Fig. 3.4 C, courbe violette) (Fig. 3.4 D).

Nous avons également montré les interactions entre CLN3 et la sortiline et entre CLN5 et la sortiline. Pour tester si la mutation pathogène de CLN5, CLN5 ^{Y392X}, affectait sa capacité à interagir avec la sortiline, nous avons effectué un test de co-immunoprécipitation (Fig. S2C). CLN5 de type sauvage et CLN5 ^{Y392X} ont pu interagir avec la sortiline. Nous avons ensuite utilisé le BRET pour comparer l'interaction CLN3 / sortiline dans les cellules HeLa de type sauvage (Fig. 3.4 E, courbe bleue) ou CLN5 ^{KO} (Fig. 3.4 E, courbe rouge). Nous avons trouvé une interaction significativement diminuée dans les cellules CLN5 ^{KO} (Fig. 3.4 F). L'expression de HA-CLN5 dans les cellules CLN5 ^{KO} HeLa a permis de restaurer le phénotype (Fig. 3.4 F, courbe verte), au contraire du mutant HA-CLN5 ^{Y392X} (Fig. 3.4 F, courbe violette). Pour confirmer nos résultats de BRET, nous avons effectué une expérience de co-immunoprécipitation pour déterminer le rôle de CLN5 dans la modulation des interactions CLN3 / Rab7A, CLN3 / rétomère et sortiline / CLN3 (Fig. S2B). Nous avons constaté que le rétromère (Vps26A), Rab7A et la sortiline pouvaient co-immunoprécipiter avec Flag-CLN3 dans les cellules HeLa de type sauvage, mais pas dans les cellules HeLa CLN5 ^{KO}.

Une autre fonction de Rab7A est la médiation des étapes clés de la dégradation de la cargaison endocytaire. Lors de la stimulation avec le facteur de croissance épidermique (EGF), le récepteur EGF (EGFR) est internalisé et peut être soit recyclé à la surface cellulaire, soit dégradé dans les lysosomes. Au moins deux effecteurs Rab7A ont été impliqués dans la dégradation de l'EGFR, RILP et PLEKHM1. L'inhibition de l'une ou l'autre de ces protéines entraîne des retards significatifs dans la cinétique de dégradation de l'EGFR. Pour déterminer si le CLN5 est impliqué dans cette voie,

nous avons étudié la cinétique de dégradation de l'EGFR dans les cellules HeLa de type sauvage et CLN5 ^{KO}. Lorsque nous avons comparé la cinétique de dégradation de l'EGFR dans les cellules CLN5 ^{KO}, nous avons trouvé un retard significatif 15 minutes après stimulation à l'EGF par rapport aux cellules de type sauvage, sans différence significative après 120 minutes (Fig. 3.5 B). Ensuite, nous avons testé la cinétique de dégradation de l'EGF couplé à la sonde Alexa-488 (EGF-488) en utilisant les mêmes lignées cellulaires, pour confirmer nos résultats de dégradation de l'EGFR par miscorpscopie. Après 15 minutes de poursuite, les cellules HeLa CLN5 ^{KO} ont montré une dégradation retardée par rapport aux cellules de type sauvage (Fig. 3.5 I).

Afin de comprendre le mécanisme responsable du retard de dégradation de l'EGF et de l'EGFR, nous avons utilisé le BRET pour déterminer si les interactions Rab7A / PLEKHM1 ou Rab7A / RILP étaient affectées (Fig. 3.6 A - D). RILP et PLEKHM1 sont impliquées dans la dégradation de cargaisons protéiques internalisées telles que l'EGFR soit en participant à la fixation des vésicules, comme c'est le cas de PLEKHM1, soit en régulant le mouvement des vésicules, comme c'est le cas de RILP. Nous n'avons trouvé aucun changement significatif dans l'interaction entre PLEKHM1 et Rab7A dans les cellules HeLa CLN5 ^{KO} par rapport aux cellules de type sauvage (Fig. 3.6 B). D'autre part, l'interaction entre RILP et Rab7A a été significativement réduite dans les cellules CLN5 ^{KO} (Fig. 3.6 D). Rab7A peut interagir avec RILP pour ensuite engager des moteurs à dynéine pour le transport des lysosomes versl'extrémité négative des microtubules . Si ce système de transport est affecté en raison de la diminution de l'interaction Rab7A / RILP, nous nous attendrions à observer une diminution du mouvement des lysosomes après l'induction de l'autophagie et la privation de nutriments. Nous avons comparé le positionnement des lysosomes, par coloration avec la protéine de membrane lysosomale CD63, dans des cellules de type sauvage et CLN5 ^{KO} qui ont été privées de nutriments afin d'activer le processus d'autophagie (Fig. 3.6 E - H). Bien que nous ayons observé le mouvement des lysosomes dans les cellules CLN5 ^{KO}, ces derniers étaient beaucoup moins importants que dans les cellules HeLa de type sauvage (Fig. 3.6 H et H '). En effet, le nombre de lysosomes périnucléaires étaient significativement inférieurs pour les cellules CLN5 ^{KO} que pour cellules HeLa de type sauvage (Fig. 3.6 I).

En se déplaçant vers l'extrémité négative des microtubules, les lysosomes peuvent fusionner de manière efficace avec les autophagosomes. Cette étape est nécessaire pour garantir une dégradation autophagique efficace. Des études antérieures ont rapporté des anomalies autophagiques dans des cellules dans lesquelles l'expression de CLN5 était inhibée ou éteinte. Par conséquent, dans les cellules HeLa CLN5 ^{KO}, on s'attendrait à moins de fusions autophagosome / lysosome et à un flux autophagique défectueux. Pour tester la capacité des lysosomes à fusionner avec les autophagosomes, nous avons exprimé mCherry-LC3 et Lamp1-GFP de type sauvage (Fig. 3.7 A - C) et CLN5 ^{KO} (Fig. 3.7 D - F). LC3 est un marqueur des autophagosomes, tandis que Lamp1 est un marqueur des lysosomes. Au début de l'autophagie induite par privation de nutriments , les autophagosomes LC3-positifs fusionnent avec les lysosomes Lamp1-positifs, formant des autolysosomes afin de dégrader le matériel. Les cellules ont été privées de nutriments pendant 3 heures dans du EBSS et la colocalisation de mCherry-LC3 et Lamp1-GFP a été déterminée. Par rapport aux cellules de type sauvage, la colocalisation de LC3 et Lamp1 était significativement réduite dans les cellules HeLa CLN5 ^{KO} (Fig. 3.7 J), suggérant que le mouvement rétrograde déficient des lysosomes empêchait la fusion entre les autophagosomes et les lysosomes.

Ensuite, nous avons utilisé une sonde LC3 en tandem (mTagRFP-mWasabi-LC3) pour étudier leflux autophagique. mWasabi est sensible au pH (plus sensible que l'EGFP), alors que mTagRFP ne l'est pas. Lorsque l'autophagie a lieu de manière normale, la fusion des autophagosomes avec des lysosomes entraine la dégradation du mWasabi, on observe alors du rouge. Au contraire, des

blockage des derniers stades de l'autophagie (pas de fusion autophagosome avec les lysosomes) se traduisent par une augmentation dejaune, avec une diminution correspondante du signal rouge, car mWasabi n'a pas été désactivé. Nous avons exprimé mTagRFP-mWasabi-LC3 dans les cellules de type sauvage (Fig. 3.7 K) et CLN5 ^{KO} (Fig. 3.7 L), puis nous avons induit une carence en nutriment avec duEBSS pendant 3 heures. Dans les cellules HeLa CLN5 ^{KO}, la fusion est altérée, par conséquent, mWasabi n'est pas exposé au pH acide de la lumière du lysosome et aucune extinction ne se produit. Par conséquent, le signal rouge est significativement diminué (Fig. 3.7 L et N).

Discussion & Conclusion

Dans les cellules HeLa CLN5 ^{KD}, nous avons précédemment observé que moins de Rab7A et de rétromère étaient liés à la membrane. Nous avons retrouvé le même phénotype dans les cellules HeLa CLN5 ^{KO}, lorsqu'elles sont complémentées avec CLN5 de type sauvage, mais pas lorsqu'elles sont complémentées avec le mutant pathogène CLN5 ^{Y392X}. Bien que le recrutement de rétromère soit altéré dans les cellules HeLa CLN5 ^{KO}, Rab7A, lui, était toujours lié à la membrane. Cela a soulevé deux interrogations. Comment expliquer l'écart de phénotypes entre les modèles KD et KO, et comment Rab7A pourrait-il être lié à la membrane sans pourtant être capable de recruter rétromère? Nous avons émis l'hypothèse que l'extinction totale de l'expression de CLN5 dans le modèle KO a conduit la cellule à compenser l'effet, tandis que l'inhibition à court terme de CLN5 par siRNA était trop transitoire pour permettre à la cellule de mettre en place ces mécanismes . Nous avons précédemment montré que la palmitoylation Rab7A était nécessaire au le recrutement efficace de rétomère sur les membranes endosomales, mais n'était pas nécessaire à la localisation membranaire de Rab7A. Nous avons constaté que la palmitoylation de Rab7A était significativement diminuée dans les cellules HeLa CLN5 ^{KO}, ce qui explique la diminution de l'interaction Rab7A / rétomère mesurée d par BRET, ainsi que la diminution subséquente du recrutement de rétromère. La palmitoylation de Rab7A n'est pas nécessaire pour moduler l'interaction Rab7A / rétomère en soi, mais sert à localiser Rab7A dans des domaines spécifiques de la membrane endosomale pour favoriser l'interaction. Lorsque la compartimentation cellulaire n'est pas conservée, comme lors de la réalisation d'une co-immunoprécipitation, la forme non palmitoylée de Rab7A interagit s avec rétomère. En tant que tel, il n'est donc pas surprenant qu'avoir observé l'interaction de Rab7A avec retromère par co-immunoprécipitation dans des cellules HeLa CLN5 ^{KO}.

Le recrutement de rétomère sur les membranes endosomales permet le recyclage du récepteur lysosomal de tri sortiline vers le réseau endosome-TGN. L'interaction sortiline / rétomère a été perturbée dans les cellules HeLa CLN5 ^{KO} par rapport aux cellules HeLa de type sauvage. Alors que l'expression de CLN5 de type sauvage dans les cellules HeLa CLN5 ^{KO} a permis de rétablir l'interaction sortiline / rétomère, l'expression CLN5 ^{Y392X} ne l'a pas fait. Cela suggère que les résidus à l'extrémité C-terminale de CLN5 sont nécessaires pour l'interaction sortiline / rétomère. Cependant, le mécanisme par le biais duquel ces résidus modulent cette interaction reste à déterminer. La diminution de l'interaction sortiline / rétomère observée dans les cellules HeLa CLN5 ^{KO} devrait conduire à la dégradation de la sortiline . Comme dans les cellules HeLa CLN5 ^{KD}, la sortiline est dégradée dans les cellules HeLa CLN5 ^{KO}. Ce phénotype reste inchangé lorsque les cellules sont complémentées avec le mutant pathogène CLN5 ^{Y392X} . Seule lexpression de CLN5 de type sauvage a permis de prévenir la dégradation de la sortiline,. Prises ensemble, ces observations soulignent le rôle crucial de CLN5 dans la modulation du recrutement Rab7A-dépendant de rétromère et de sa fonction . En effet, en modulant le niveau de palmitoylation de la petite GTPase, CLN5 établit les conditions d'une interaction Rab7 / rétomère optimale, assurant une liaison rétomère / sortiline efficace et le recyclage de cette dernière vers le TGN; qui à son tour se traduit par un fonctionnement normal du lysosome .

Dans mon premier travail publié, nous avons démontré que CLN3 fonctionne comme une protéine d'échafaudage assurant des interactions protéine-protéine efficaces. Dans cette étude, nous avons démontré la diminution des interactions Rab7A / retromère et rétomère / sortiline dans les cellules HeLa CLN3 ^{KO}, ce qui conduit par conséquent à la dégradation anormale de la sortiline. Nous avons trouvé des résultats similaires dans les cellules HeLa CLN5 ^{KO}. En outre, nous avons constaté que CLN5 est nécessaire pour les interactions CLN3 / rétomère et CLN3 / sortiline. La complémentation des cellules HeLa CLN5 ^{KO} avec la protéine CLN5 de type sauvage a conduit à la restauration du phénotype sauvage, alors que la complémentation avec le mutant pathogène ne l'a pas permis . Sur la base de ces données, nous proposons un modèle dans lequel CLN3 et CLN5 fonctionnent comme un complexe endosomal requis pour le trafic endosome-TGN efficace de la sortiline. Un recyclage inefficace entraîne un désordre lysosomal caractéristique de la maladie CLN5. Dans cette étude, nous proposons donc un mécanisme potentiel de la pathogénèse pour la maladie CLN5.

Nous nous sommes ensuite demandé si d'autres voies médiées par Rab7A sont affectées dans les cellules HeLa CLN5 ^{KO}. Nous avons trouvé des retards significatifs dans la dégradation de l'EGFR et de l'EGF. Ce phénomène pourrait être due à une altération de la fonction lysosomale, ou bien à une diminution des évènement de fusion de la cargaison endocytaire avec les lysosomes, mécanisme également modulé par Rab7A. La protéine RILP, effectrice de Rab7A, est impliquée dans la dégradation de cargaisons internalisées telles que l'EGFR, en médiant le mouvement des vésicules. L'effecteur de Rab7A PLEKHM1, quant à lui, est un facteur d'arrimage nécessaire à la fusion des endosmoses à la fois pour les processus de dégradation et d'autophagie. Dans les cellules HeLa CLN5 ^{KO}, nous n'avons trouvé aucun changement au niveau de l'interaction Rab7A / PLEKMH1, mais avons trouvé une diminution de l'interaction Rab7A / RILP. Cela a entraîné une diminution du mouvement des lysosomes CD63 positifs vers la région périnucléaire, étape importante dans le processus autophagique. En effet, nous avons observé moins de colocalisation des autophagosomes contenant la protéine LC3II avec les lysosomes Lamp1-positifs , lorsque la carence en nutriments est induite dans les cellules HeLa CLN5 ^{KO}.En outre, l'utilisation de la sonde LC3 en tandem (mTagRFP mWasabi-LC3) a également permis de mettre en évidence une réduction du flux autophagique . Alors que la diminution de la fonction lysosomale joue un rôle dans la pathogénicité de la maladie CLN5, les troubles de l'autophagie et de la dégradation des cargaisons endocytaires sont très probablement dus à la dérégulation des mouvements des lysosomes donc à une diminution des événements de fusion.

En conclusion, dans cette étude, nous démontrons que CLN5et CLN3fonctionnent comme un complexe de régulation du trafic endosome-TGN. Alors que CLN3 se comporte comme une plate-forme d'interaction, CLN5 garantit que les interactions de CLN3 avec ses effecteurs, qui sont vitales pour le bon fonctionnement lysosomal, sont maintenues et régulées. Ces découvertes éclairent les mécanismes moléculaires responsables de la pathogenèse des NCL causées par des mutations des protéines CLN5 et CLN3.

Contents

List of Figures

Part I

General Introduction

Chapter 1

Introduction

Can dementia be diagnosed in children? Although not being heard much, there are over 70 rare disorders causing dementia in children, collectively affecting 1 in 2,800 newborns worldwide. In 1903, Dr. Frederick Eustace Batten described the most common cause of childhood dementia as neuronal ceroid lipofuscinoses (NCL). The mutations in the genes coding for 13 different CLN proteins lead to this deadly neurodegenerative disease. As the name indicates, NCL causes toxic lipofuscin accumulation inside the lysosomal compartments. Unfortunately, there are no treatment options for this inherited disorder because the function of most CLN proteins is still not known. The goal of this thesis is to gain fundamental insights into the functional role of CLN3 and CLN5. Understanding the pathways these lysosomal proteins regulate holds the key to identify biomarkers and/or therapeutic targets to treat children suffering from NCL.

Lysosomes are the acidic organelles regulating the digestive functions of cells while also serving as a signaling hub to modulate cellular needs. The lysosomal homeostasis strictly relies on endocytic trafficking. RAB7A is the master regulator of this pathway. It modulates the biogenesis, formation, maturation, and membrane composition of lysosomes. Interestingly, RAB7A interacts with both CLN3 and CLN5. We hypothesize that soluble lysosomal CLN5 protein functions through endolysosomal transmembrane CLN3 protein to regulate various RAB7A functions. This principle might explain the toxic auto-fluorescent lipopigment accumulation within the lysosomal compartment of NCL patient cells.

1.1 Lysosome

In 1949, Belgian biologist Christian de Duve discovered the lysosome while studying glucose 6-phosphatase activity. Compared to whole cellular extracts, they obtained very low acid phosphatase activity using differential centrifugation. By chance, they observed the expected activity when they left the fractionated cells to rest for a few days before the measurement. Through these observations, he hypothesized that this enzyme is sealed in an enclosed compartment, limiting its access to the substrate. Over time, diffusion enabled it to show its enzymatic activity. They described these spherical compartments as "saclike structures". In 1955, upon additional discovery of some other hydrolases, Duve named these new organelles as "lysosomes"(de Duve, 2005; Castro-Obregon, 2010).

1.1.1 Structure and function of lysosomes

Micrometre diameter-sized (0.2 to 1.2 μm) spherical structures originate from the Golgi apparatus, by their tiny vesicular pinching out of Golgi, to generate these membrane-enclosed lysosomal organelles (Trivedi *et al.*, 2020). The biogenesis of lysosomes are decribed by four different models. While "maturation" model describes their formation from plasma membrane followed by their maturation into acidic vesicles, "vesicular transport" model indicates the need of multivesicular bodies (MVBs) for vesicular cargo mobilization to lysosomes. "Kiss and run" model, on the other hand, describes the cargo transfer between lysosomes and endosomes by contact site formation. The last model, "fusion and fission", defines a hybrid organelle formation to rebuilt the lysosomes (Trivedi *et al.*, 2020). A mammalian cell contains around 50 to 1000 lysosomes dispersed throughout the cytoplasm (Meyers, 2006). Lysosomes contain more than 60 acid hydrolases in their lumen. They include phosphatases, lipases, nucleases, glycosidases, and others (Lubke *et al.*, 2009) to degrade biological macromolecules of cellular waste, old cells, pathogens, consumed nutrients, and other debris. A single outer lysosomal membrane protects the rest of the cell from this degradation process. Lysosomal hydrolases operate at an acidic pH of mostly less than 5. This internal pH of the lysosome, which is more acidic than the rest of the cell, is provided by transmembrane proteins. An H^+ pump in the lysosomal membrane uses the energy of ATP hydrolysis to pump H^+ into the lysosome to maintain its acidity (Forgac, 2007). Other than the vacuolar H^+-ATPase (V-ATPase), there are Na^+ and Cl^- transporters involved in maintaining lysosomal H^+ ion content by translocating the ions in and out of lysosomes. Acidification mechanisms must be offset by either the influx

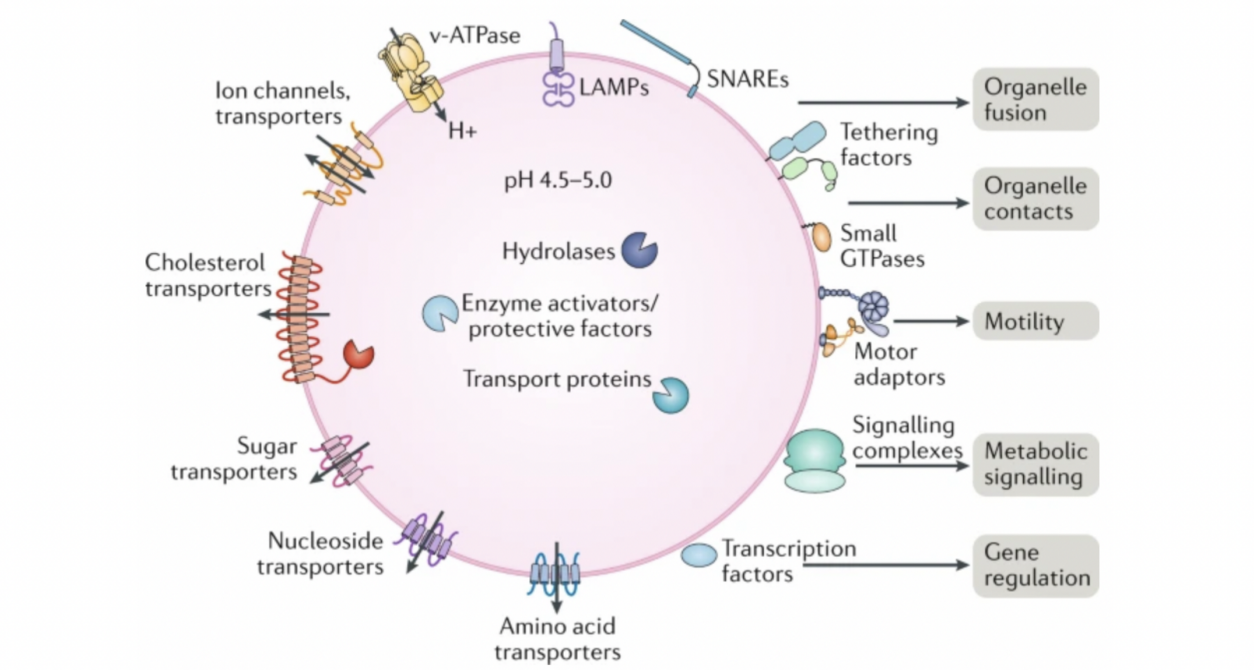

Figure 1.1: Properties of lysosome (Ballabio & Bonifacino, 2020)

The lysosome comprises a specific set of luminal (hydrolases, transport proteins, and enzyme activators), integral-membrane (Transporters, ion channels, LAMPs, v-ATPase), and peripherally associated proteins (Small GTPases, motor adaptors, tethering factors). The luminal proteins are required to degrade various substrates, integral membrane proteins serve as gateways into and out of the lumen, protect the membrane from degradation and serve to regulate lysosome biogenesis, while peripheral proteins are necessary for motility and fusion.

of cytosolic anions into the organelle or the efflux of luminal cations to the cytoplasm to operate (Steinberg *et al.*, 2010).

The very first endocytosis experiments, using labeled proteins and bacterias, demonstrated the digestive function of lysosomes. Fragments of internalized molecules were observed within the lysosomal compartments (Straus, 1954; Cohn, 1963). Because of their role in terminal degradation, lysosomes have often been considered as a waste disposal system of the cell. Thanks to several discoveries (such as the localization of the master growth regulator (mTORC1) on lysosomal membranes), it has been shown that lysosomes are at the center of a complex regulatory network. Today, we know that lysosomes control cellular homeostasis by regulating metabolic signaling, gene transcription, immunity, plasma membrane repair, cell adhesion, and migration mechanisms. They do so by moving around the cytosol to interact with other cellular structures (such as the cholesterol sensor ORP1L (oxysterol-binding protein)) to communicate with other organelles (such as ER (Endoplasmic reticulum)) (Rocha *et al.*, 2009). Accordingly, lysosomes can change their composition,

size, and number via fusion and fission to regulate pathways and to show their diverse functions to maintain cellular homeostasis.

1.1.2 Autophagy

Eukaryotic cells evolved in a way to resist hunger for long periods by a self-eating mechanism called autophagy. Digesting their cytoplasmic components allows a cell to recycle its molecules to build up the necessary metabolites for their survival. Just like starvation, some other stimuli like hypoxia, oxidative stress, infection, and ER stress can also induce autophagy (Khandia *et al.*, 2019).

Under normal conditions, the mammalian target of rapamycin (mTOR) is found in an active state on the lysosomal membrane to stimulate cellular growth. At the same time, mTOR blocks autophagy by inhibiting autophagy activator complexes via phosphorylation. Unc-51-like kinase (ULK), phosphatidylinositol 3-kinase (PI3K) complex, transmembrane protein complex (Atg9 and WIPI), and two ubiquitin-like protein conjugation systems (Atg12 and LC3) are the 4 complexes for autophagy activation. ULK complex is composed of ULK-1, Atg13, Atg101, and FAK-family interacting protein (FIP200). The PI3K complex is composed of Atg15, vacuolar protein sorting (VPS)15, VPS34, Beclin 1, and Beclin 1-regulated autophagy protein 1 (AMBRA1) (Hansen *et al.*, 2018).

Lysosome-to-nucleus signaling is regulated by transcription factor EB (TFEB), which is under the control of mTOR. TFEB induces the expression of lysosomal genes upon cellular need by regulating the expression of the Coordinated Lysosomal Expression and Regulation (CLEAR) group of genes. Palindromic CLEAR elements (with GTCACGTGAC motif) were found in the promoter region of 96 lysosomal genes. TFEB was shown to bind this CLEAR elements to code for soluble lysosomal enzymes, membrane proteins, and all of the accessory proteins that regulate lysosome physiology. Under normal conditions, mTOR phosphorylates TFEB for its cytosolic localization. When autophagy is induced, inactive mTOR can no longer phosphorylate TFEB. So, TFEB relocates to the nucleus for lysosomal gene transcription. Thus, the nuclear activity of TFEB increases lysosomal function and trafficking needed for autophagy (Sardiello, 2016).

The autophagic activity starts with the formation of a double-membrane vesicle called a phagophore. The ULK complex is activated first to phosphorylate AMBRA1, required for PI3K complex acti-

vation. Then, the ubiquitin-like system gets activated to induce microtubule-associated light chain protein 3b (LC3)/ phosphatidylethanolamine (PE) conjugation. Then, LC3-I starts to become lipidated to form LC3-II. LC3-II proteins locate on both surfaces of the membrane to extend and complete the phagophore. The growing phagophore engulfs cytosolic materials either in a selective or a non-selective way to form vesicles called autophagosomes. When a complete autophagosome is formed, transmembrane protein complexes get activated to form intraluminal vesicles before acidification takes place. Then, the autophagosome fuses with the lysosome to break down the materials or organelles inside these autolysosomes. This process requires the HOPS (homotypic fusion and protein sorting) complex to aid tethering, and PLEKHM1 (pleckstrin homology domain-containing family M member 1) to establish a strong interaction of the two membranes (van der Kant *et al.*, 2013; McEwan *et al.*, 2014), two of which are regulated by Rab7 GTPase. This is followed by autophagosomal SNARE (Syntaxin-17, Atg14, synaptosomal associated protein 29 (SNAP-29)) interactions with the late endosomal /lysosomal SNAREs (Vamp8 / Vamp7) (Seranova *et al.*, 2017) for the fusion of the lipid bilayers (Parlati *et al.*, 2002; Zhao & Zhang, 2018). The fusion is also regulated by the lysosomal membrane proteins like lysosome-associated membrane proteins 1 and 2 (LAMP1-2). At the same time, they are important for autophagosomal maturation. Later, the molecules are degraded and recycled for the synthesis of needed molecules (Khandia *et al.*, 2019).

Concerning the mechanism of cargo sequestration, autophagic processes are divided into 3 different groups. Direct engulfment of cytoplasmic components into the lysosome is called microautophagy. On the other hand, if the cargo contains a unique (pentapeptide (KFERQ)) motif for lysosomal degradation, chaperone-mediated autophagy (CMA) takes over. In CMA, proteins are recognized by HSC70 (Heat Shock Cognate 70 kDa protein) chaperone complex, bringing them to the lysosomal surface for Lamp2A favored lysosomal translocation (Kumsal & Maria, 2017). The third and the best-characterized group is macroautophagy. If not indicated, the autophagic process refers to this group. Double-membrane autophagosomal vesicles fusion with lysosomes is called macroautophagy. The autophagy of selective targets can be named with respect to the degraded cargo; such as mitophagy for mitochondrial, ribophagy for ribosomes, and xenophagy for pathogen degradation (Hansen *et al.*, 2018). Poly-ubiquitination of the cargo allows cargo receptors to specifically localize on the cargo with high affinity. Autophagic machinery is then recruitted on the cargo through their interaction with the cargo receptors. Autophagosome forms around the cargo with high avidity to avoid other cytoplasmic material enclosure (Zaffagnini & Martens, 2016).

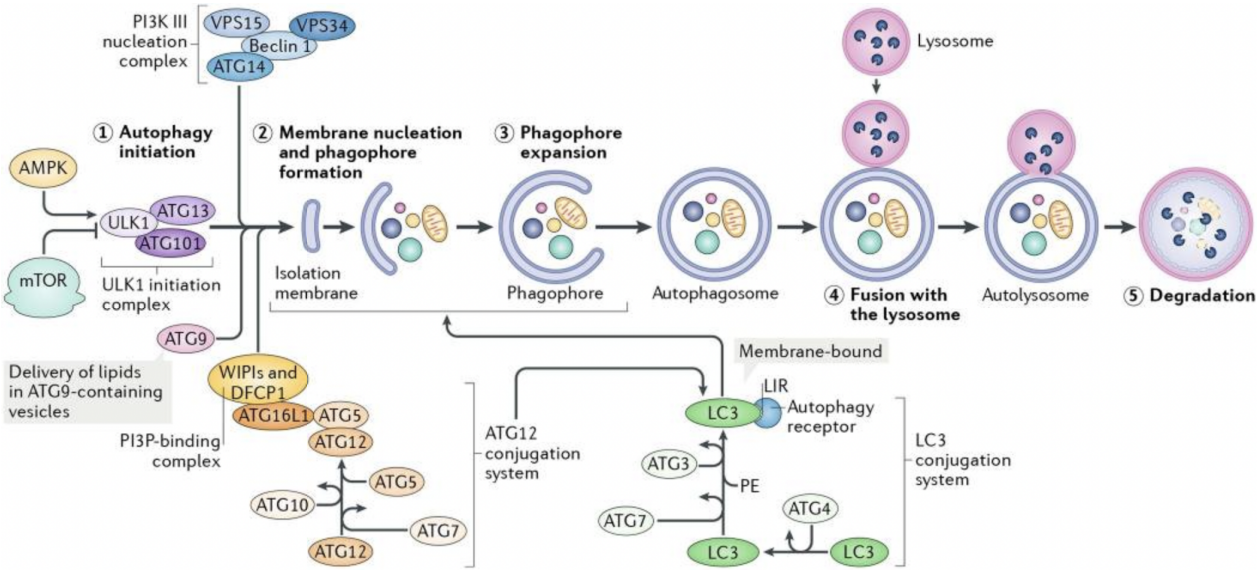

Figure 1.2: The macroautophagy process (Hansen *et al.*, 2018)

mTOR and AMP-activated kinase (AMPK) are the two sensors for cellular metabolism and growth. While mTOR activity blocks autophagy, AMPK activates it. Upon autophagy induction, the cargo to be degraded is engulfed in a double-membrane phagophore structure. When the sequestration of the cargo is completed, these autophagosome structures become ready to fuse with acidic vesicles. Autophagosome/lysosome fusion creates the autolysosomes to degrade the autophagic cargo. Unc-51-like kinase (ULK), phosphatidylinositol 3-kinase (PI3K) complex, transmembrane protein complex (Atg9 and WIPI), and two ubiquitin-like protein conjugation systems (Atg12 and LC3) are the 4 complexes for autophagy activation. ULK complex is composed of ULK-1, Atg13, Atg101, and FAK-family interacting protein (FIP200). The PI3K complex is composed of Atg15, vacuolar protein sorting (VPS)15, VPS34, Beclin 1, and Beclin 1-regulated autophagy protein 1 (AMBRA1). For the initiation, ULK1 is activated (1) to start membrane nucleation (2) by activating the PI3K complex. PI3K together with the Atg9 and WIPI starts the phagophore formation (2). Then, the two ubiquitin-like protein conjugation systems get activated to lipidate the LC3 proteins. The formation of LC3-II provides phagophore extension (3). Cytosolic materials are included inside the autophagosomes upon complete phagophore formation. Autophagosome/lysosome fusion (4) results in the degradation of the autophagic materials (5).

1.2 Lysosomal proteins and their synthesis

Lysosomes are filled with various forms of hydrolytic enzymes (acid hydrolases) to degrade complex macromolecules. Proteases, sulfatases, nucleases, lipases, phosphatases, and glycosidases reside in the acidic lumen of this organelle to degrade proteins, sulfate esters, nucleic acids, lipids, phosphoric acid monoesters, and glycosidic bonds, respectively. The acidity and the various functions of lysosomes are secured by lysosomal membrane proteins which include integral membrane proteins and ion channels.

1.2.1 Soluble lysosomal proteins

Complex lipoproteins containing cholesteryl esters and triglycerides are broken down into fatty acids (FA) and free cholesterol (FC) by lysosomal acid lipase (LAL). Re-esterification of FA and

FC in ER form lipid droplets, which can be stored for later use. Lysosomal hydrolysis of lipid droplets by LAL provides energy supply to cells by fatty acid oxidation (FAO) (Li & Zhang, 2019). α- and β-galactosidases, hexosaminidases, sialidases, arylsulfatase A, β-galactosyl-ceramidase, β-glucocerebrosidase (β-GC), ceramidases and sphingomyelinases are enzymes degrading lipids like sphingolipids (Gieselmann, 1995). Likewise, cathepsins are a group of lysosomal proteases having a role in many other cellular functions. They are classified into three groups concerning their function and catalytic active site; serine, aspartic, and cysteine. The most well-characterized group is the cysteine proteases, which is composed of cathepsin B, C, F, H, K, L, O, S, V, X, and W. Cathepsin A and G are in the serine group, while D and E are in the aspartic group. Within all, cathepsin B, L, D are the most abundant ones within a cell. Mutations related to lysosomal enzymes are shown to cause rare genetic disorders. For instance, mutation in palmitoyl protein thioesterase 1 (*PPT1*) gene, coding for a serine lipase, leads to neuronal ceroid lipofuscinosis (NCL) type 1 (CLN1) disease. Moreover, cathepsin D, cathepsin F, tripeptidyl-peptidase 1 (TPP1) mutations cause CLN10, CLN13, CLN2 disorders, respectively. Another NCL disorder is caused by *CLN5* mutations, whose mature soluble protein is located in the lysosomal lumen upon cleavage (Jules *et al.*, 2017). Although the function of CLN5 is not known (Mole & Cotman, 2015), its role in endosome-to-TGN trafficking through retromer regulation has been shown by our lab (Mamo *et al.*, 2012).

Since hydrolytic enzymes have digestive action on proteins, their activity is tightly controlled. Upon their synthesis in an inactive state, they are glycosylated for their endolysosomal translocation. When they reach an acidic pH, they become active (Stoka *et al.*, 2016). The acidity is mostly regulated by presenilin 1 (PS1), a transmembrane protein, through its action on the proton pump vacuolar-type ATPase (V-ATPases). PS1 glycosylates v-ATPases for their stability and function (Lee *et al.*, 2015). Being the importance of proton pumps in the acidification process is mentioned, it is essential to introduce the lysosomal ions regulating lysosomal biogenesis, motility, membrane contact site formation, and homeostasis. Ca^{2+}, Na^{+}, K^{+}, Zn^{2+}, H^{+}, Fe^{2+}, and Cl^{-} are the well known lysosomal ions. Cl^{-} is the most abundant anion in the lysosome. The most abundant cation is Na^{+}, regulating lysosomal membrane potential. Ca^{2+} is, on the other hand, known to have a very important role in signal transduction, lysosomal mobilization, trafficking, nutrient sensing, and lysosomal biogenesis (Trivedi *et al.*, 2020; Li *et al.*, 2019). The H^{+} ion content of the lysosome (which is modulated by v-ATPase activity) depends on the location of the lysosome and

the metabolic state of the cell. While peripheral lysosomes are more alkaline, perinuclear ones are shown to be more acidic (Johnson *et al.*, 2016). Lysosomal acidification is known to be important for cellular proliferation and growth. And recently, it was shown that lysosomal Fe^{2+} is the limiting ion for cell survival (Weber *et al.*, 2020).

1.2.2 Lysosomal membrane proteins

To prevent lysosomal membrane damage from the acidic lumen, most of the lysosomal membrane proteins (LMPs) are glycosylated to form a glycoprotein layer, called glycocalyx, in the inner surface of the lysosomal membrane. There are over 100 LMPs, with the most abundant ones being lysosomal associated membrane proteins (LAMP-1 and LAMP-2), followed by lysosome integral membrane protein 2 (LIMP2; also known as SCARB2), and the tetraspanin CD63. Other than being a simple barrier, LMPs have important roles in phagocytosis, autophagy, cell death, infection, and membrane repair events (Schwake *et al.*, 2013). LAMP-2A has important roles in chaperone-mediated autophagy, β-GC trafficking, and the export of low-density lipoproteins (LDL) derived cholesterol. Mutations in this protein have been shown to cause Danon disease. Patients experience cardiomyopathy, muscle weakness, and intellectual disability(Schwake *et al.*, 2013). Two other disease-related LMPs are CLN3 and CLN7, whose functions are not well defined. Mutations in these CLN proteins cause rare lysosomal storage disorders (LSDs) (Mole & Cotman, 2015).

Other than LMPs, there are ion channels and transporters located on lysosomal membranes. One of which is V-ATPase, which promotes acidification of the lumen, as already mentioned. Another transporter is Niemann-Pick C 1 (NPC1) that exports lysosomal cholesterols. Mutation in this protein leads to lysosomal accumulation of cholesterol and sphingolipids causing Niemann-Pick C (NPC) syndrome (Pfeffer, 2019). The ion channels are transient receptor potential mucolipin proteins (TRPMLs), two-pore channels (TPCs), big potassium channels (BK), human transmembrane protein 175 (TMEM175), purinoceptor (P2X4), and chloride channels (CLCs). TRPML proteins are non-selective ion channels permeable to mostly Ca^{2+} and also to Na^{+}, K^{+}, Fe^{2+}, Zn^{2+} ions. Their activity causes Ca^{2+} export regulates various functions of the lysosome. Lysosomal pH and membrane potential are important factors regulating their activity. An increase in reactive oxygen species (ROS) is known to activate TRPML1 followed by TFEB nuclear translocation. TRPML1 is mostly lysosomal while TRPML2 is mostly endosomal. On the other hand, the TRPML3 amount

is quite similar on both membranes. TRPML1 is ubiquitously expressed, more in the brain, kidney, spleen, liver, and heart. However, TRPML2 expression is limited to the thymus, liver, kidney, heart, and spleen. Likewise, TRPML3 is expressed just in the cochlea, thymus, kidney, lung, eye, spleen, melanocytes, and somatosensory neurons. Mutation in the encoding *MCOLN1* gene (coding for TRPML1 channel) is related to Mucolipidosis type IV (MLIV) (a neurodegenerative disorder) and many other LSDs (Trivedi *et al.*, 2020). The stability of the lysosomal pH and the fusion events are related to TMEM175 activity, which is regulating the majority of lysosomal K^+ homeostasis. In addition to TMEM175, BK channels (which belongs to the voltage-gated K^+ channel superfamily) mediates K^+ levels depending on the Ca^{2+} flux for their activation. By forming a complex with TRPML1, it has been proposed that the released Ca^{2+} from TRPML1 activates BK channels to start lysosomal K^+ influx to regulate lysosomal acidity (Feng *et al.*, 2018). Next, there are the TPCs. TPC1 and TPC2 are the two mammalian forms having selective impermeability to K^+ ions. On the other hand, they are impermeable to Ca^{2+}, Na^+ and H^+ ions. Lastly, there is the P2X4, which is permeable to Ca^{2+}. Interestingly, this channel is inactive in acidic but active in alkaline environments. Also, its activity is shown to depend on luminal ATP. P2X4 plays a role in membrane fusion events by activating calmodulin, an intracellular calcium-binding messenger protein (Cao *et al.*, 2015; Halling *et al.*, 2016).

1.2.3 Synthesis of lysosomal proteins

Acid hydrolases, plasma membrane and secreted proteins of the lysosome are translated by polyribosomes on the surface of the rough endoplasmic reticulum (RER). Their N-terminal region contains a hydrophobic signal peptide of 20 to 25 amino acids to secure their location at the beginning of translation. Otherwise, they would be released into the cytosol (Moremen *et al.*, 2012). The signal peptide is recognized by the peptide-signal recognition particle (SRP) which transports the nascent protein to the translocon (protein-conducting channel) in the ER membrane (Walter & Blobel, 1981). After the synthesis of the protein, the signal peptide is cleaved by a signal peptidase, which causes the release of the enzyme into the RER (Fig. 1.3a).

During their synthesis, lysosomal enzymes are glycosylated by oligosaccharide transferase (OST). OST adds preformed molecules of oligosaccharides, Glc3Man9GlcNAc2, to a certain asparagine residue from a lipid intermediate. Glucosidase I (GlsI) then removes the terminal glucose residue. It

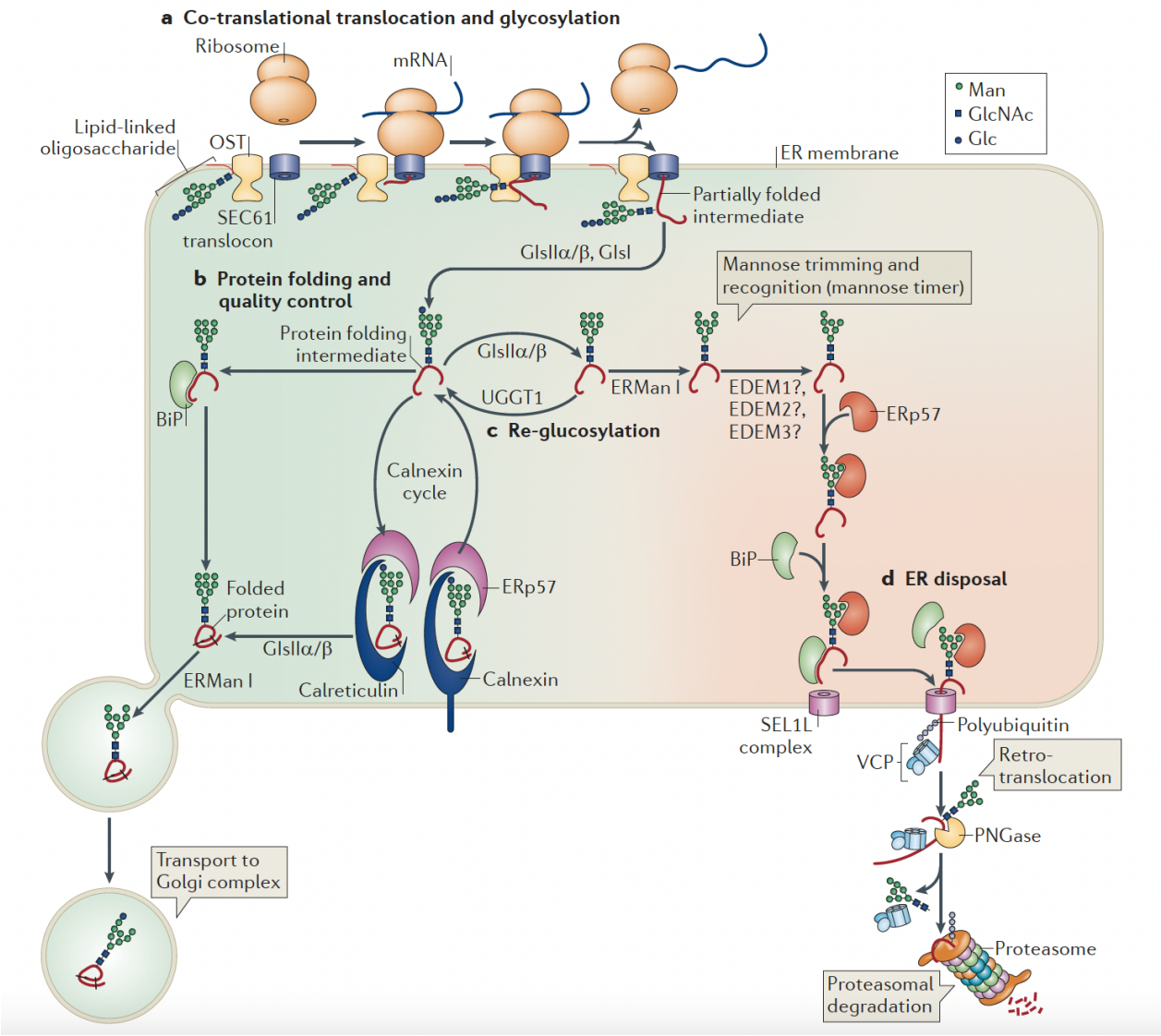

Figure 1.3: Protein N-glycosylation and quality control of protein folding (Moremen *et al.*, 2012)

(a) Synthesized glycoproteins are tagged with a lipid-linked intermediate by the oligosaccharyltransferase (OST). (b) The partially formed intermediate undergoes the glycan trimming process by the activity of α-glucosidase I (GIsI) and α-glucosidase II α–β heterodimer (GIsII α/β). Protein folding and quality control are performed by the function of ERp57 complex activity together with calnexin/ calreticulin function. (c) The folding sensor (UDP-Glc: glycoprotein glucosyltransferase (UGGT1)) recognizes and re-glucosylates the incompletely folded glycoproteins to reintegrate them into the calnexin cycle. The correctly folded proteins leave the ER for their Golgi localization. (d) On the other hand, the ER disposal system trims the misfolded proteins by ER α-mannosidase I (ERManI) for proteasomal degradation.

is followed by glucosidase II (GlsII) maturation which removes two central glucose molecules. The lysosomal enzymes now containing monoglucose are then folded by chaperones such as calnexin, calreticulin, and BiP, which ensure the quality of protein folding (Moremen *et al.*, 2012) (Fig. 1.3b). After correct folding of the enzyme, chaperones cleaves the last glucose residue. The free glycoproteins then interact with mannosidase I (ERMan I) to produce octamannosyl intermediates. Now, they are free to be transported to the Golgi in COPII coated vesicles (Fig. 1.3b). On the other

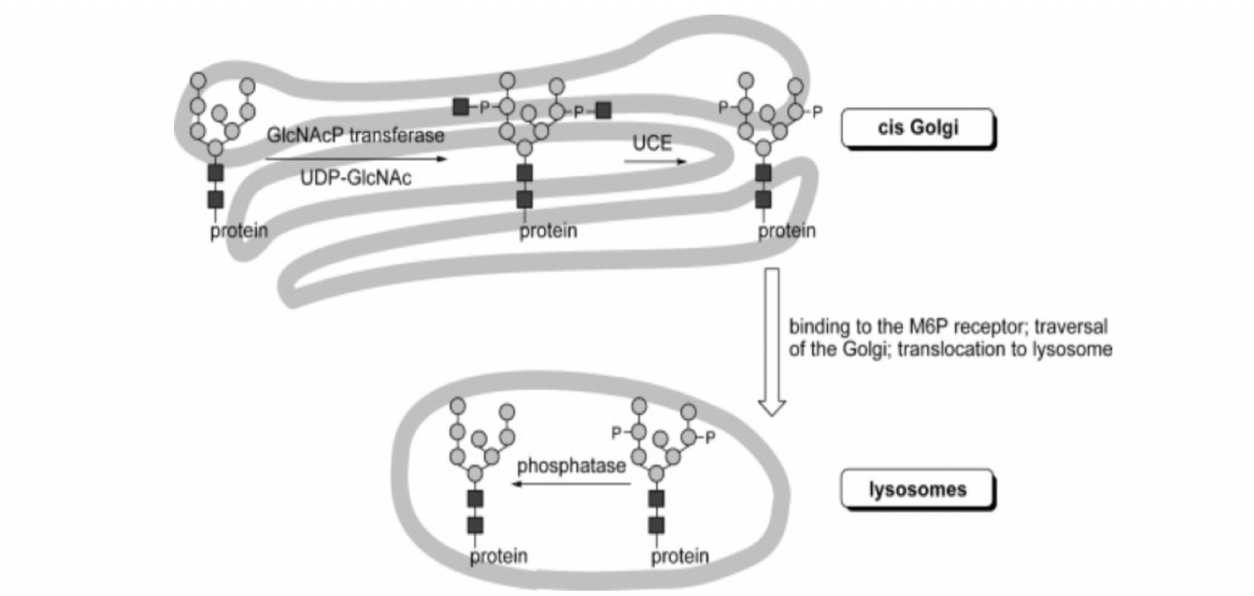

Figure 1.4: Protein modification for lysosomal targeting (Stick & Williams, 2009)

Lysosomal proteins are modified by UDP-N-acetylglucosamine:lysosomal-enzyme N-acetylglucosamine-1-phosphotransferase (N-acetylglucosamine-phosphotransferase) and a glycoside hydrolase (N-acetylglucosamine-1-phosphodiester α-N-acetylglucosaminidase (uncovering enzyme, UCE)) to transfer N-acetylglucosamine 1-phosphate to a mannose residue and to cleave the glycosidic bond to free the phosphate group for M6P generation. M6P signals for lysosomal targeting, which then is cleaved by phosphatases inside the lysosome.

hand, poorly folded glycoproteins are recognized by UGGT1 and reglucosylated for reintegration to the chaperone cycle (Fig. 1.3c). Only the enzymes that have been correctly folded can leave the RER for the Golgi. The others are degraded in the proteasome after withdrawal of their mannose residues by ERMan I. This is followed by the intervention of mannosidases by EDEM family members (Fig. 1.3d).

Upon arrival in the Golgi, lysosomal proteins are modified with a complex set of sorting signals and recognition proteins for their vesicular transportation. This modification can either be a removal/addition of complex sugar residues or phosphorylation to their oligosaccharide chains. The most important modification of lysosomal enzymes is the phosphorylation of their mannose residues to form mannose 6-phosphate (M6P) molecules. This enables the glycoproteins can to be distinguished for lysosomal transportation. UDP-N-acetylglucosamine (UDP-GlcNAc) and the uncovering enzyme (UCE) N-acetylglucosamine- Phosphodiester α-N-acetylglucosaminidase works one after another to generate M6P. While UDP-GlcNAc makes the phosphodiester intermediate, UCE then trims an N-acetylglucosamine to reveal the phosphate residue. Finally, the lysosomal sorting receptors recognize M6P containing proteins for their destination to the endosomal/lysosomal system (Fig. 1.4) (Stick & Williams, 2009). It should be kept in mind that not all lysosomal cargo

works with M6P residue recognition for lysosomal sorting. Upon M6P route blockage, lysosomal localization of some hydrolyses has been shown to be normal. The cargo sorting routh that uses sortilin is one of the M6P independent lysosomal trafficking mechanism (Glickman & Kornfeld., 1993).

1.3 Lysosomal sorting receptors

1.3.1 Mannose 6-phosphate receptor

When the lysosomal enzymes are marked by the M6P, they are recognized by specific receptors in the Golgi. These mannose 6-phosphate (MPR) receptors form the two members of the " P-Type lectin" family; the cation-dependent mannose 6-phosphate (CD-MPR) and the cation-independent mannose 6-phosphate receptor (CI-MPR) (Fig. 1.5) (Ghosh *et al.*, 2003).

CI-MPR is a type-1 integral membrane glycoprotein of 274 kDa. Its broad extracellular region has a domain of 15 repeat units with up to 38% similarity with CD-MPR. Also, the extracytoplasmic region of CI-MPR has two M6P recognition sites in addition to the site that recognizes insulin-like growth factor II (IGF II) on the cell surface. These sites provide the dual function of transporting enzymes to the lysosome and a role in embryonic development (Morgan *et al.*, 1987). CI-MPR is also involved in immune function by being responsible for the endocytosis of granzymes A and B (Motyka *et al.*, 2000).

CD-MPR is a 31 kDa type-I transmembrane protein. The extracellular portion of this receptor has only one site that can bind M6P and no recognition site for other signals. CD-MPR was observed in dimeric and tetrameric forms although the dimeric form was the most observed form. CI-MPR, on the other hand, is mainly found as a monomer, but *in vitro* studies have shown that this receptor can also form dimers in certain conditions (pH, temperature, and presence of mannose 6-phosphate residues). This observation led to the hypothesis that the formation of dimers enables the receptors to be more specific for their different ligands (York *et al.*, 1999). Despite the similarity of their extracellular sites to bind M6P, the two MPRs are not always interchangeable. This difference is due to binding of the closest domain of the C-terminal end of CI-MPR to M6P when pH is between 6.4 and 6.5, which is similar to the optimum pH of CD-MPR binding which is between 6.0 and 6.5

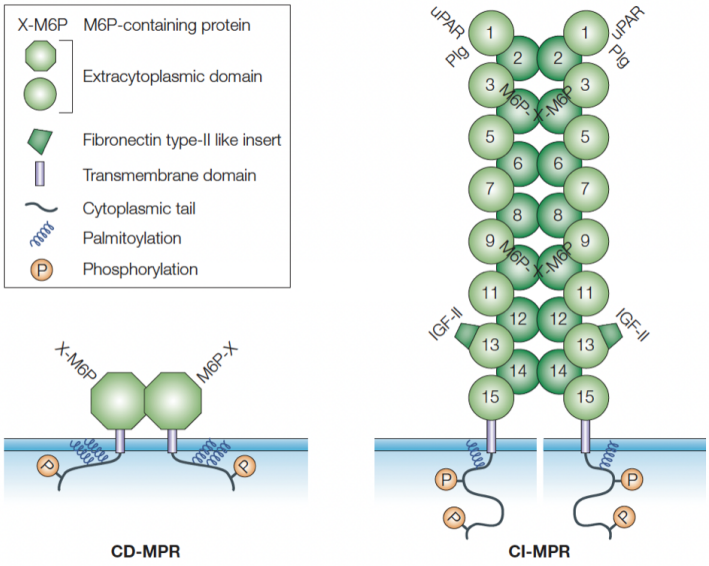

Figure 1.5: Mannose 6-phosphate receptor (Ghosh *et al.*, 2003)

While the cation-dependent mannose 6-phosphate (M6P) receptor (CD-MPR) mostly forms homodimers with a single polypeptide binding site, the cation-independent (CI)-MPR forms dimers on the membranes and monomers in chelating solutions. Palmitoylations, phosphorylations, and many other post-translational modifications are present in these receptors. uPAR, urokinase (plasminogen activator) receptor; IGF-II, insulin-like growth factor; Plg, plasminogen.

(Tong & Kornfeld, 1989; Dahms & L. J. Olson, 2008). The second CI-MPR recognition site, on the other hand, binds M6P at an optimal pH between 6.9 and 7.0. This difference also allows CI-MPR to function at the plasma membrane even if the pH of the extracellular medium is more alkaline. The number of M6P residues and their localization on lysosomal enzymes also explain the difference in specificity between the two MPRs. Deletion experiments of only CI-, only CD-, and double deletion of CI-CD- MPRs resulted in different groups of soluble lysosomal enzyme secretion. This observation allowed classification of enzymes interacting with M6P receptors into three subgroups. Group I contains the enzymes (E1A stimulated genes (Creg1), RNAse t2, and heparanase) that are secreted in the absence of CD-MPR which means they are unable to perfectly interact with CI-MPR. In contrast, group II is composed of enzymes (α-mannosidase B1 and cathepsin D) secreted in the absence of CI-MPR, and finally, group III enzymes are secreted in the absence of both receptors (Qian *et al.*, 2007; Dahms & L. J. Olson, 2008; Braulke & S.Bonifacino, 2009).

1.3.2 Sortilin

Most of the tissues of MPR-deficient mice did not show abnormal levels of lysosomal content. This suggested an M6PR- independent transport of lysosomal enzymes. Research in this area identified

alternative receptors. One of which is the 95 kDa protein sortilin, also named neurotensin receptor 3, because of its ability to bind neurotensin on the cell surface. It is one of the five structurally related receptors. The others include sorting protein-related receptor with A-type repeat (SorLA, known also as SorL1 or LR11), SorCS1, SorCS2, SorCS3 (Fig. 1.6). They all contain a short cytoplasmic tail (10–78 amino acids) for adaptor protein interactions need in trafficking and also the evolutionary conserved vacuolar protein sorting 10 (VPS10) domain for cargo binding (Malik & Willnow, 2020). Upon their synthesis, furin protease in Golgi removes their pro-peptides for receptor activation (Petersen *et al.*, 1999).

Sortilin is mostly located in neurons of the mammalian nervous system and metabolic tissues, including the liver (Nykjaer & Willnow, 2012). It has been shown that many lysosomal proteins; prosaposin, GM2 activator protein (Coutinho *et al.*, 2012), acid sphingomyelinase (Ni & Morales, 2006; Lefrancois *et al.*, 2003), cathepsin D, cathepsin H (Canuel *et al.*, 2008), and the β-amyloid precursor protein-cleaving enzyme (BACE)-1 (Finan *et al.*, 2011) are transported by sortilin receptors. Apart from those, sortilin is shown to bind the pro-form of nerve growth factor (NGF;proNGF) and neurotrophin (NT) precursors (proNTs), resulting in cellular death. Other than lysosomal targeting, further functions of sortilin are demonstrated in secretion, cell surface exposure, endocytic uptake, anterograde/retrograde sorting of different proteins (Nykjaer & Willnow, 2012). Thus, it should not be surprising that mutations altering sortilin functions give rise to a diverse group of complex disorders. For instance, sortilin knockout mice show an accumulation of apolipoprotein E and amyloid β. That implies a link between this receptor and Alzheimer's disease (Carlo, 2013).

So far some other receptors have been identified which also allow the transport of enzymes to the lysosome. For example, low-density lipoprotein receptor-related protein (LRP) is responsible for the internalization of prosaposin (Hiesberger *et al.*, 1998). Another receptor, lysosomal integral membrane protein type 2 (LIMP-2) is capable of transporting β -glucocerebrosidase to the lysosome (Reczek *et al.*, 2007). Some enzymes also appear to use co-receptors to get to the lysosome. A recently identified co-receptor that could have this function is serglycin. This protein is responsible for the packaging of proteins dedicated to secretory lysosomes such as defensins, elastases, and lysozyme. Serglycine can also act as an intermediate for the transport of lysosomal enzymes by acting as a bridge between them and the MPRs (Kolset *et al.*, 1996).

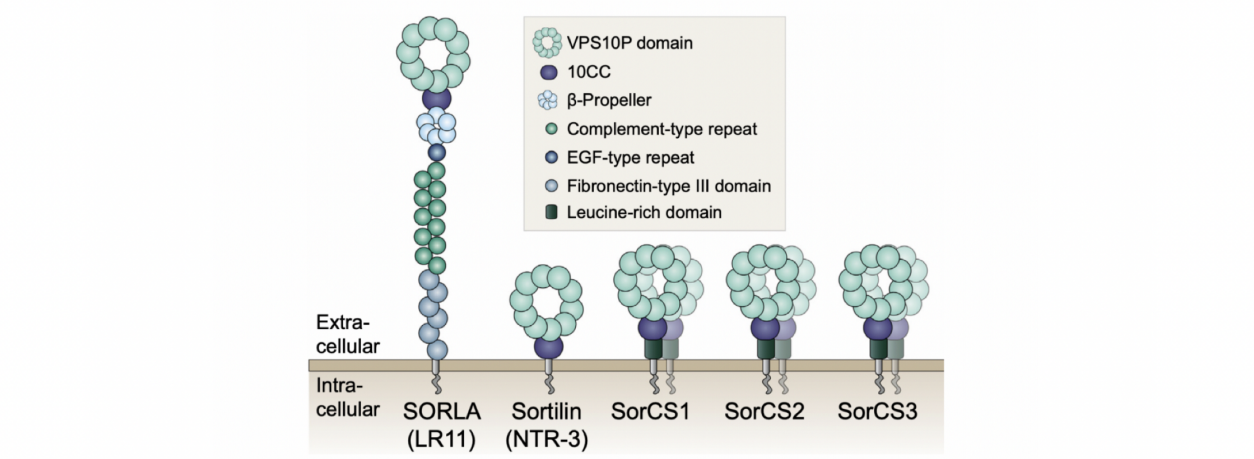

Figure 1.6: Vps10 domain receptors (Malik & Willnow, 2020)

Abbreviations: EGF, epidermal growth factor; LR11, LDLR-related receptor with 11 ligand binding type repeats; NTR-3, neurotensin receptor 3; SorCS, sortilin-related receptor CNS expressed; SORLA, sorting protein-related receptor containing LDLR class A repeats; VPS10P, vacuolar protein sorting 10 protein.

1.4 Cytosolic sorting proteins

Cargo-loaded receptor localization from the Golgi exit-site to the lysosome is a complex process and requires multiple specific protein interactions. First, they should be recognized for their sorting within an intermediate transporting vesicle. Second, its transportation should be successful between the compartments. Lastly, the fusion of the carrier vesicle with the target membrane must be achieved. *Trans*-Golgi network (TGN) is formed from Golgi by its fragmentation into smaller vesicles and tubules. Since the TGN has different functions and morphology from Golgi, it is considered a specialized organelle. Its trafficking function is very important for cellular homeostasis. It mainly traffics proteins for secretion or to lysosomes and plasma membranes. To do so, the TGN contains a distinct set of proteins, such as AP1, AP4 adaptor proteins, and adaptor-related GGAs (Golgi-localized, γ-ear-containing, Arf (ADP-ribosylation factor)-binding proteins) (Vlieta *et al.*, 2003).

1.4.1 Trafficking from TGN-to-endosome

The lysosomal sorting receptors contain specific signals within their cytosolic tails for efficient sorting. Within these signals, the dileucine moiety generally consists of the amino acid sequence (DER)XXXL(LVI) or (DE)XL(LI) where the amino acids between () are interchangeable. The

dileucine motif is recognized by the GGAs which allow the formation of vesicles coated with clathrin. A second motif, located on the cytosolic tail of the receptors, is the tyrosine motif consisting of the amino acid sequence YXXϕ (where ϕ is a big bulky hydrophobic amino acid) or NPXY. This motif is, on the other hand, recognized by the heterotetrameric AP-1 which is associated with clathrin. These motifs are not only present on the sorting receptors that are directed towards the lysosome but also on several transmembrane proteins circulating through the different intracellular compartments (Bonifacino & Traub, 2003).

Lysosomal receptor binding to clathrin adaptor proteins in the cytosol is followed by vesicle formation for endosomal delivery of the cargo. This process is carried out in three stages: the recruitment of the scaffold proteins, the budding of the membrane, and the scission of the vesicles. The activation of the adenosine diphosphate (ADP)-ribosylation factor (Arf) GTPases initiates the budding of vesicles. When Arf1 is activated, the GGAs are recruited to the TGN membrane thanks to their GAT (GGA and TOM) domain. Mammalian cells are known to have GGA1, GGA2, GGA3. VHS (Vps27, Hrs, STAM), GAT, hinge, EAR of GGAs are the shared domains in all. While the VHS domain recognizes the dileucine signal of the cargo receptors, the hinge and EAR domains regulate clathrin and coat protein recruitment. Subsequently, the GGAs in combination with Arf1 and phosphatidylinositol-4-phosphate (PI4P) on the TGN membrane recruits the AP-1 complex, which participates in the formation of the vesicles (Bonifacino, 2004).

There are five AP complexes known so far. AP-1 and AP-2 are important for clathrin-coated vesicle (CCV) formation. While AP-1 participates in TGN-to-endosome trafficking, AP-2 functions on the plasma membrane for endocytosis. On the other hand, AP-3 regulates endosome to lysosome transport, while AP-4 is important for basolateral cargo trafficking. And the last one is AP-5 known to localize on late endosomal membranes (Fig. 1.8). AP-1,2,3,4 are heterotetramers composed of two large, a medium, and a small subunit with 100, 50, and 20 kDa molecular size, respectively. Within those, the medium (μ), the small (σ), and one of the large (β) subunits are present in all. The second large subunits are divergent as γ, α, δ, ε for AP-1, AP-2, AP-3, AP-4, respectively (Fig.1.7). The core of AP is composed of heterotetramers that are attached to flexible linkers having different appendages (Sanger *et al.*, 2019).

While membrane budding begins, the AP-1 complex is hypothesized to replace the GGAs to recruit enthoprotine and clathrin. These proteins bend the membrane and concentrate the receptors

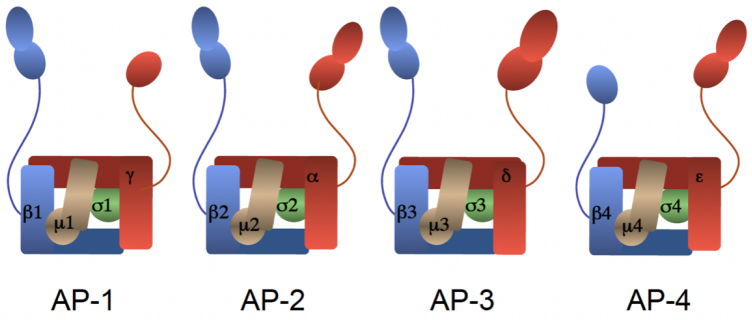

Figure 1.7: Adaptor protein complexes

All of them contain two large, one medium, and one small subunit. One of the large subunits is variable. They contain flexible linkers attached to their heterotetramer cores. AP-1 is found on trans-Golgi network (TGN) and it mediates TGN-to-endosome trafficking (Fig. 1.8). AP-2 associates with the plasma membrane and it mediates endocytosis. They are important for clathrin-coated vesicle (CCV) formation. AP-3 is localized to endosomes and it mediates endosome to lysosome transport. AP-4 is located to Golgi and it mediates basolateral cargo trafficking.

in the forming vesicle. The Rabaptin5 / Rabex5 complex is also recruited to allow the recruitment of Rab5 which allows the targeting of the vesicles towards the endosome. P56 and γ-synergin are then recruited to allow interaction with the cytoskeleton. Finally, dynamin, a large GTPase, leads the scission of the transport vesicle (Bonifacino, 2004). The vesicles loaded with proteins destined for the lysosome will then go to the endosome. Since the pH in endosomes is more acidic than Golgi, the enzymes targeted to the lysosome will be released from the sorting receptors, so that the receptors can be recycled back to the TGN while cargo moves on to the lysosome.

1.4.2 Endosome-to-Golgi retrieval

Once the receptors have released their cargo, they can follow two distinct pathways. 1) Follow their cargo to the lysosome where they will be degraded, or 2) They can be recycled back to the Golgi apparatus in order to continue the transport of lysosomal enzymes. The mechanism that determines the fate of receptors is still not completely understood yet, but we know that their recycling is carried out by a protein complex called retromer (Seaman, 2009).

The retromer complex was first discovered in yeast during the study of the mechanism of recycling of Vps10p, the homolog of sortilin. Retromer can be subdivided into two subcomplexes that assemble separately and interact transiently. The first part of the complex is conserved from yeast to mammals and is composed of the vacuole protein sorting proteins (Vps) Vps26, Vps29, and Vps35 (Seaman *et al.*, 1997). The trimer Vsp26:Vps29:Vps35 is responsible for the recognition of

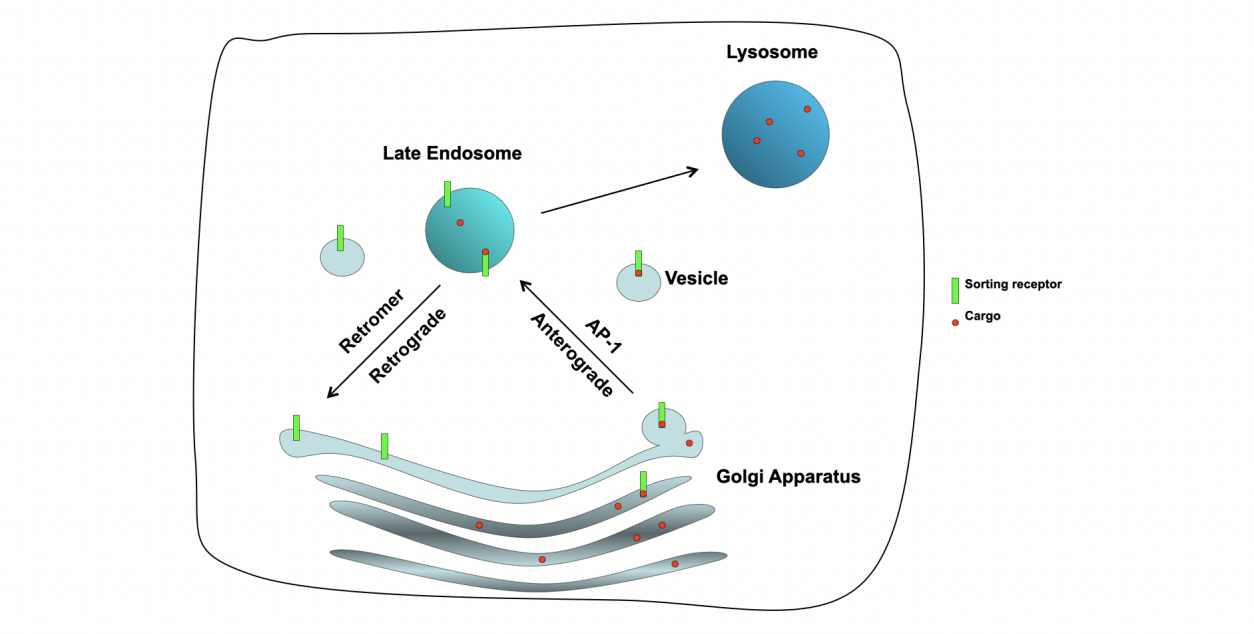

Figure 1.8: Endosomal sorting

The cargo-loaded sorting receptor binds to clathrin adaptor proteins in the cytosol. That is followed by vesicle formation for endosomal delivery of the cargo inside a transportation vesicle. AP-1 adaptor protein mediates the anterograde trafficking of the intermediate vesicles. Upon their arrival into a more acidic environment, cargo detaches from the receptor. While cargo goes to the lysosome, the cargo-free receptor is trafficked back to Golgi for another round of sorting. That retrograde trafficking is mediated by the retromer complex.

the receptors and other cargo containing transmembrane proteins, such as sortilin and CI-MPR. Therefore, it is also called as cargo-selective complex (CSC) (Fig. 1.10).

The second subcomplex consists of PX-domain containing sorting nexin (SNX) dimers. There are twelve SNX-BAR family in mammals; SNX1, SNX2, SNX4, SNX5, SNX6, SNX7, SNX8, SNX9, SNX18, SNX30, SNX32 and SNX33. Within those, SNX1:SNX5, SNX1:SNX6, SNX2:SNX5 or SNX2:SNX6 heterodimers are included in the retromer complex. The SNX part of the retromer is responsible for binding to the membrane by its Bin/Amphiphysin/Rvs (BAR) domain. Being called SNX-BAR, it distinguishes itself from other nexins (van Weering *et al.*, 2012). The PX (phox-homology) domain of SNX-BAR important for PI3P (phosphatidylinositol 3-phosphate) recognition to stabilize its membrane attachment (Fig. 1.10). The small GTPase Rab7 regulates the spatiotemporal recruitment of retromer to endolysosomal membranes for endosome-to-TGN trafficking. Endosome-to-plasma membrane trafficking is also regulated by retromer. Yet, this trafficking is under the control of SNX27, independent from Rab7 (Tu *et al.*, 2020).

1.5 Ras-like GTPases

The ras-like in brain proteins (Rabs) are small GTPases belonging to the Ras superfamily. Since their discovery in 1987, around 70 of them have been found in humans. Rabs are specifically localized to certain intracellular membranes to function. This makes them a perfect marker to differentiate distinct parts of a cell. Through recruiting their effector proteins, Rabs crosstalk to regulate almost all intracellular trafficking pathways in eukaryotes. Most Rabs are ubiquitously expressed, but some have specific expression profiles for some cell types (Stenmark, 2009).

The newly synthesized GDP-bound Rab protein in the cytosol associates with Rab escort protein (REP) to be delivered to its target membrane. REP does so by providing geranylgeranyltransferase (RabGGTase) to prenylate Rab proteins (Rak *et al.*, 2004). This irreversible post-translational modification provides a lipid group for membrane anchoring. Otherwise, Rab would always be a cytosolic protein (Modica *et al.*, 2017). In an inactive form, Rabs are mostly found in the cytosol. A guanine nucleotide exchange factor (GEF) catalyzes the exchange of GDP to GTP for Rab activation. Interaction with its associated GTPase activating protein (GAP), on the other hand, catalyzes the hydrolysis of GTP back to GDP. It is followed by the dissociation of Rab from the membrane by guanine nucleotide dissociation inhibitor (GDI), which masks the prenyl group to prepare the GTPase for another cycle (Fig. 1.9). The association of Rab to the target membrane is mediated by a GDI dissociation factor (GDF) by releasing the Rab from GDI (Homma *et al.*, 2020).

1.5.1 Rab7 and its effectors

Rab7 is a late endosome/lysosome-associated small GTPase of the Rab family. This GTPase is the master regulator of endocytic trafficking with many vital functions (Feng *et al.*, 1995). Its function is involved in the trafficking from endosome to lysosome and endosome to trans-Golgi network. As with all other Rab GTPases, Rab7 has its specific GAPs and GEFs to get de/activated. And Rab7 crosstalks with Rab5 for its time of action.

Early endosomal (EE) membrane-bound active Rab5 recruits its Rabaptin-5 effector to call its GEF (Rabex-5) onto the membrane. When the amount of active Rab5 on EE reaches saturation, another effector of Rab5 is recruited (Zerial & McBride, 2001). This effector of Rab5 is the Mo-

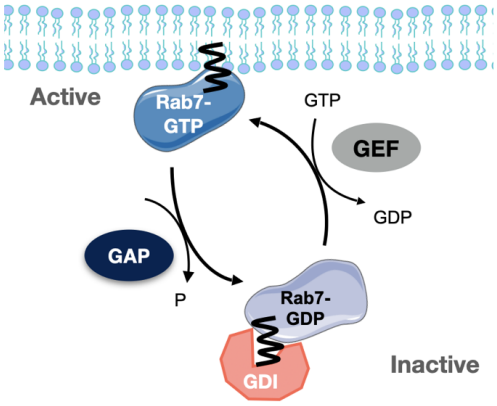

Figure 1.9: The Rab cycle

Rab7 is a small GTPase that regulates the endocytic trafficking pathways. Upon Rab7 synthesis, it is prenylated (irreversible post-translational modification) for its membrane attachment. For the cytosolic localization of Rab7, guanine nucleotide dissociation inhibitor (GDI) masks the prenyl group. A guanine nucleotide exchange factor (GEF) provides GTP loading of Rab7 for its activity and membrane attachment. On the other hand, GTP hydrolysis of Rab7 by its GTPase activating protein (GAP) detaches Rab7 from the membrane.

nensin sensitivity (Mon)1/Calcium caffeine zinc sensitivity (Ccz)1 complex. While Mon1-Ccz1 is detaching Rab5 GEF from the membrane (Poteryaev *et al.*, 2010), it also functions as a Rab7 GEF (Nordmann *et al.*, 2010). For Rab5 complete deactivation, another Rab5 effector (Vps34) brings Rab5 GAP (Armus/TBC1D2A) to the EE membrane (Law & Rocheleau, 2017), so that, late endosomal maturation can take place. There is relatively little information about the proteins acting upstream of Rab7. Rab7 GEF is identified as Mon1-Ccz1 in yeast and arabidopsis and its role for phagosome maturation in mammals has also been demonstrated (Kinchen & Ravichandran, 2010). Two inactivating Rab7 GAP proteins, on the other hand, have been identified as TBC1D15 and TBC1D5 (Seaman *et al.*, 2009).

Rab7 works in many cellular processes including lipid transportation and autophagosome positioning. At the level of late endosomes, Rab7 regulates the formation, maturation, and membrane composition of lysosomes. This GTPase is involved in the biogenesis of lysosomes by its role in endocytic vesicle maturation, phagocytosis, and autophagocytosis (Feng *et al.*, 1995). Also, it plays a key role in regulating the degradation of endocytosed cargo such as the epidermal growth factor receptor (EGFR). Finally, it mediates the fusion of lysosomes to autophagosomes thereby regulating autophagy. Rab7 performs these various functions by recruiting a wide variety of effectors on endolysosomal membranes (Fig. 1.10)(Fig. 1.11)(Zerial & McBride, 2001; Nordmann *et al.*, 2012).

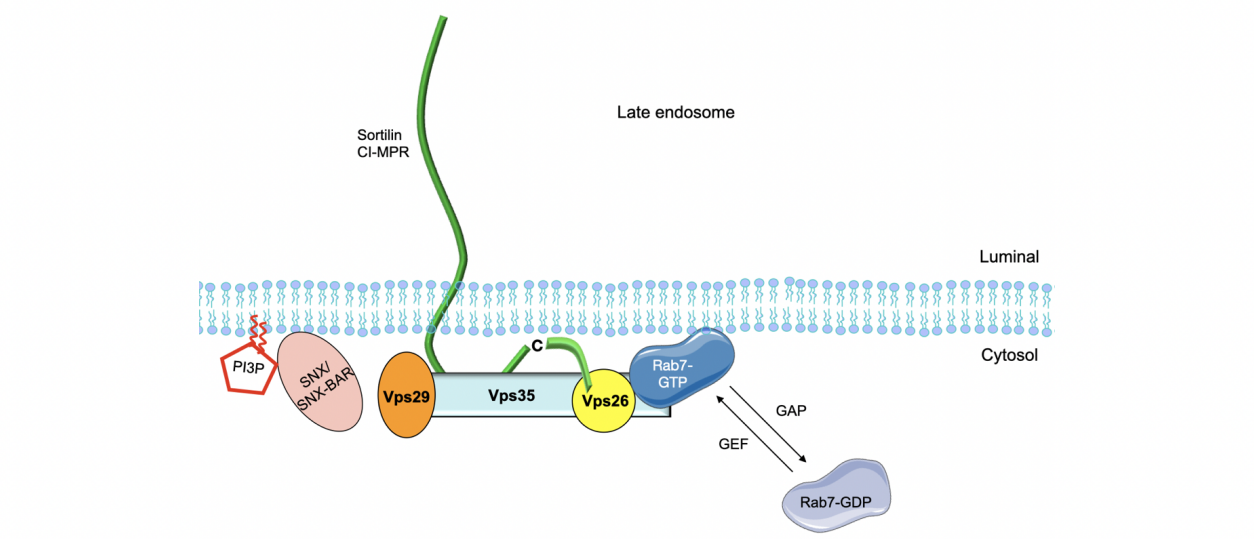

Figure 1.10: Proposed model for retromer recruitment to late endosomes

The membrane-bound active Rab7 recruits retromer to endosomal membranes. SNX/BAR domain provides a retromer to attach the membranes. The cargo-selective complex portion of retromer can then interact with sortilin by its Vps26 and Vps35 subunits for sortilin retrograde trafficking.

Retromer effector function

We have already explained the leading role of the evolutionarily conserved retromer (Vps26:Vps29:Vps35) heterodimer complex in endosome-to-Golgi retrieval. Membrane-bound active Rab7 recruits retromer and directly binds to its Vps26 and Vps35 subunits (Fig. 1.10), so that, this retromer can bind to receptors (like sortilin, CI-MPR, and phagocytic receptors) for their recycling back to TGN. Retromer dysfunction was firstly linked to Alzheimer's disease in 2005. β-amyloid precursor protein (APP) is a known cargo of SORLA, which is trafficked by retromer (Small & Petsko, 2015). Also, a recent GWAS study demonstrated the risk factor genes for late-onset AD. APOE4, ABCA7, BIN1, CD2AP, PICALM, SORL1, and EPH1A are the ones related to intracellular trafficking (Perdigao *et al.*, 2020). Since then there have been dozens of papers published about retromer protein complex, linking its role to other neurodegenerative disorders.

FYCO1 and RILP effector functions

Lysosomes are mostly in the perinuclear area. Thus, minus-end movement of autophagosomes is important for their interaction and fusion with lysosomes. In the autophagy section, we have previously mentioned that LC3 and PI3P are the autophagic vesicle membrane components. In 2010,

it was shown that FYCO1 (FYVE and Coiled-Coil-(CC)-domain containing 1) protein interacts with LC3, PI3P, Rab7, and kinesin1 by its LIR, FYVE, coiled-coil, and CC domains, respectively. Together, movement of late endosomal vesicles is provided along microtubules to the periphery (Pankiv *et al.*, 2010). Because late endosomal membranes mostly have PI3,5P, it is speculated that its dephosphorylation might be the regulatory mechanism for FYCO1 membrane recruitment for its Rab7 interaction.

Contrary to FYCO1, GTP-loaded Rab7 recruits cytosolic RILP (Rab-interacting lysosomal protein) molecules for retrograde positioning of endocytic vesicles. RILP regulates phagosome maturation and late endosomes/lysosome fusion. Upon RILP membrane recruitment, they make homodimers to interact with two Rab7 proteins, forming Rab7-RILP2–Rab7 (Wu *et al.*, 2005). Formation of this complex then recruits another Rab7 effector ORP1L (oxysterol-binding protein) to link them onto dynein motors. At the same time, RILP recruits the $p150^{Glued}$ subunit of the dynein motor complex. This can drive minus-end transportation of the late endosomes/lysosomes via microtubule cytoskeleton (Nordmann *et al.*, 2012). Besides, low-density lipoprotein (LDL) trafficking to lysosomes is also provided by RILP function. When the cellular cholesterol levels are in the normal range, the RILP-Rab7 complex is stabilized on the late endosomes and promotes their perinuclear movement. ORP1L is responsible for detecting cholesterol levels. By doing so, it changes its conformation; remains attached to RILP-Rab7 complex with one arm and to the endosomal membrane with another. On the contrary, when the cholesterol levels drop, ORP1L sticks on VAP (VAMP [vesicle-associated membrane protein]-associated ER protein) on ER membrane. So that, VAP can interact with RILP and prevents its connection with motor proteins. A newly formed ER contact site provides the required cholesterol exchange on the cell periphery (Rocha *et al.*, 2009). Other than ORP1L, Rab7-RILP dimer recruits another Rab7 effector; HOPS complex. By interacting with Vps41 subunit of HOPS, endolysosomal membrane tethering is provided for membrane fusion (Fig. 1.11) (Lin *et al.*, 2014).

HOPS and PLEKHM1 effector functions

The process of fusion of vesicles of late endosomes with lysosomes are also under the control of Rab7. HOPS complex acts as an anchoring complex in this process. It is a hetero-hexamer consisting of Vps11, Vps16, Vps18, Vps33, and HOPS-specific Vps41 and Vps39 subunits. We have mentioned the

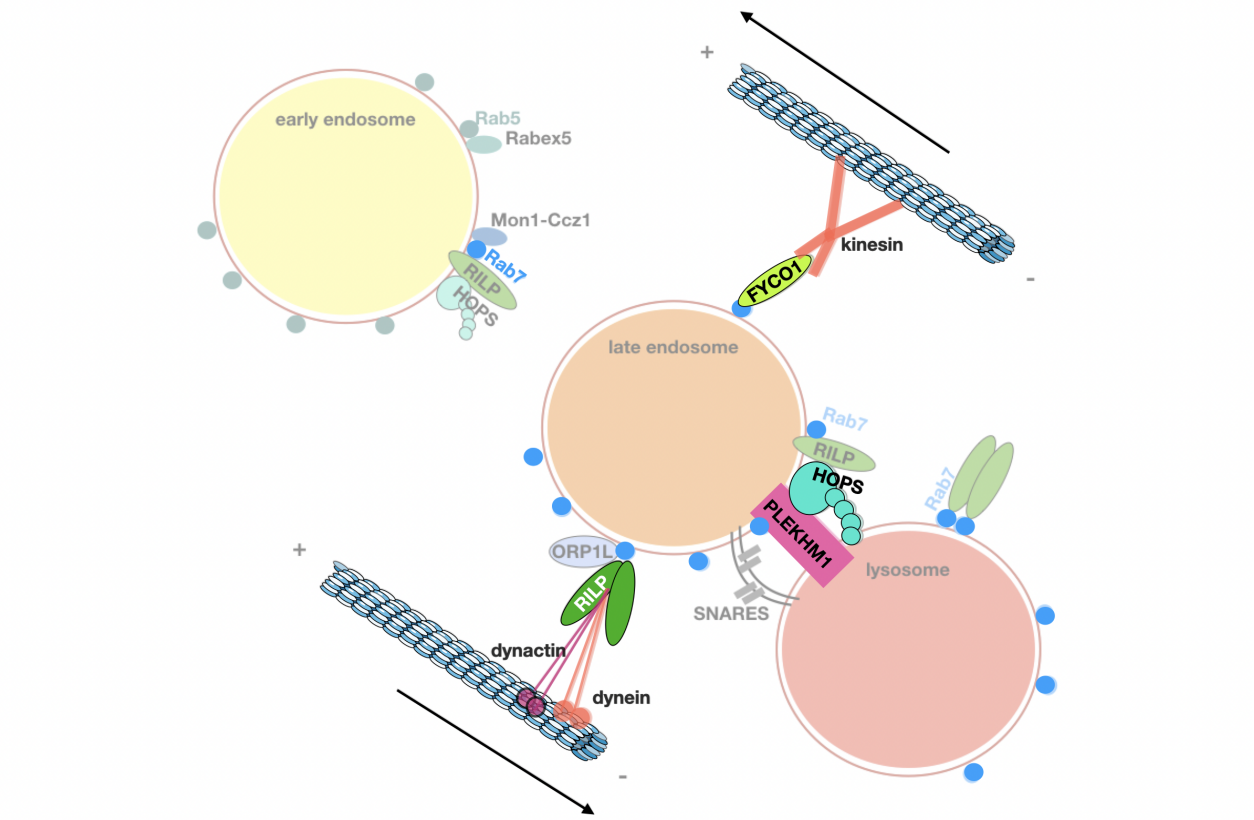

Figure 1.11: Interactions of Rab7 at the late endosome

While early endosomes (EEs) contain Rab5, late endosomes (LEs) contain Rab7. Rab7 recruits RILP (Rab-interacting lysosomal protein) to LE membranes, so that, RILP interacts with the motor proteins (dynein/dynactin) to connect LEs with the microtubules. In this way, RILP provides vesicular retrograde positioning of the LEs. Rab7 recruits FYCO1 (FYVE and Coiled-Coil-(CC)-domain containing 1) for the vesicular peripheral positioning of the LEs. FYCO1 attachment to motor proteins (kinesin) provides the anterograde trafficking of the LEs. Rab7 recruits PLEKHM1 (Pleckstrin homology domain-containing protein family member 1) to the LE membranes for vesicular membrane tethering to promote LE fusion with the lysosome.

function of Rab7-RILP dimer on vesicular movement. When the positioning is achieved, this complex recruits HOPS from its Vps41 and Vps39 subunits. From the same sites, HOPS interacts with SNAREs to actually fuse by mixing the membrane lipid bilayers. Yet, HOPS tethering is not sufficient for stabilization of two vesicular membrane associations (van der Kant *et al.*, 2013). Pleckstrin homology domain-containing protein family member 1 (PLEKHM1) is the protein strengthening the membrane connections for SNARE action. PLEKHM1 is another Rab7 effector, binds to the GTP-loaded Rab7 and Vps39 subunit of HOPS complex. Its membrane dissociation depends on PI4P to PI(4,5)P2 conversion (Baba *et al.*, 2019). Also, PLEKHM1 contains an LIR domain for its autophagosomal membrane recognition. It has been shown that its deficiency blocks epidermal growth factor receptor (EGFR) degradation and autophagy (McEwan *et al.*, 2014). When the final step for membrane tethering is provided by PLEKHM1, SNARE proteins take over the function.

Soluble N-ethylmaleimide-sensitive factor attachment protein receptors (SNAREs) are mostly transmembrane proteins attached to the membrane by PTMs; prenylation and palmitoylation. Amino acid in the central position of a SNARE protein classifies their type. One R-SNARE should come together with three Q-SNAREs to start a fusion event. Vesicular and target membrane SNAREs recognize each other to form trans-SNARE to generate enough energy for the fusion. When the process is complete, cis-SNARE forms to enable its detachment from the membrane to be used for another fusion event (Fig. 1.11) (Parlati *et al.*, 2002; Zhao & Zhang, 2018). For homotypic late-endosome fusion, Syntaxin (Stx) 7, Stx8 and Vt1b and Vamp8 (Vesicle associated membrane protein) 8 proteins are included in the SNARE complex. For endolysosomal fusion, Vamp7 protein is included (instead of Vamp8) in the SNARE complex (Mullock *et al.*, 2000).

1.5.2 Rab7 post-translational modifications (PTMs)

Rab7 activity is tightly regulated by different PTMs for its variety of different cellular functions. We have already mentioned the irreversible prenylation modification of Rab7 on their C-terminal cysteines (C205, C207). Being the first identified PTM, prenylation of Rab7 has been shown to be important for its membrane anchoring. Then, phosphoproteomic analysis conducted in 2014 demonstrated two phosphorylation sites of Rab7; serine 72 (S72) and tyrosine 183 (Y183). Serine, threonine, and tyrosine residue phosphorylations are known as key modulators in signal transduction events by acting on the protein structures to alter their activity (Sharma *et al.*, 2014). LRRK1 (leucine-rich repeat kinase 1) has been shown to be responsible for S72 phosphorylation, promoting Rab7-RILP effector interaction and Rab7 function on EGFR degradation (Hanafusa *et al.*, 2019). Moreover, another kinase TBK1 (TANK Binding Kinase 1) is demonstrated to phosphorylate the same S72 region of Rab7. TBK1 modification of S72, on the other hand, is shown to be important for mitophagy (Heo *et al.*, 2018). Problems in both Rab7, LRRK1, and TBK1 are related with Parkinson's disease (Singh & Muqit, 2020). Src (Proto-oncogene tyrosine-protein) is a kinase that phosphorylates the Y183 site of Rab7 and is demonstrated to inhibit Rab7-RILP interaction (Lin *et al.*, 2017a). Dephosphorylation of Y183 region of Rab7 has been shown to promote EGFR degradation (Shinde & Maddika, 2016). While Lin *et al.* (2017b) demonstrated that Y183-phosphorylation of Rab7 blocks EGFR degradation, Francavilla *et al.* (2016) showed that it ubiquitinates EGFR for its degradation. Therefore, all these findings indicate a highly regulated cycle of Y183 de/phosphorylation for Rab7 function. For removal of those phosphorylations, PTEN

(Phosphatase and tensin homolog deleted on chromosome 10) has been demonstrated as a Rab7 phosphatase (Shinde & Maddika, 2016).

Another PTM of Rab7 is its palmitoylation. It is a reversible modification that covalently adds fatty acids to cysteine residues of proteins, thus also called S-acylation. Hydrophobicity gained by lipidation affects the protein structure, assembly, maturation, trafficking, and function. It regulates modified protein function by regulating its stability and interactions with other proteins and membranes (Chamberlain & Shipston, 2015). Our lab has shown the cysteine 83 and 84 regions are the Rab7 palmitoylation sites, required for efficient retromer membrane recruitment (Modica *et al.*, 2017), followed by retromer interaction with palmitoylated sortilin for receptor retrograde transportation (McCormick *et al.*, 2008). Yet, the mechanism of palmitoylation of Rab7 has not been established so far. Until now, 24 palmitoyltransferases (PATs) reported to mediate palmitoylation. Being a transmembrane protein containing tetrapeptide of Aspartic Acid, Histidine, Histidine, and Cysteine, they are also called as DHHCs (Mitchell *et al.*, 2006). Upon their activity, palmitoylation can promote a protein to anchor and localize to a specific membrane, and interact with some other proteins (Linder & Deschenes, 2007) for cellular trafficking (J.Bonangelino *et al.*, 2002).

Finally, there is ubiquitination; another reversible PTM of Rab7. A small ubiquitin-protein attachment to (K38, K191, and K194) lysine residues of Rab7 is controlled by Parkin, an E3 ubiquitin ligase (Song *et al.*, 2016). Rab7 stability and its membrane anchor together with its RILP interaction have been shown to be related to its ubiquitination. Importantly, K38 region mutation, preventing its Parkin modification has been related to Parkinson's disease (Mertins *et al.*, 2013; Wagner *et al.*, 2011). On the other hand, deubiquitination is provided by deubiquitinating (DUBs) enzymes. In humans, there are around 100 DUBs and one of them is USP32, which is membrane-associated. In 2019, Rab7 was been found to be a substrate of USP32. While ubiquitinated Rab7 favors the interaction with the Vps35 subunit of retromer for endosome-to-TGN trafficking, deubiquitinated Rab7 by UPS32 has been shown to be important for its interaction with RILP for EGFR degradation. Other than the GTP-loaded state of Rab7, its ubiquitination also serves as an important regulator for its membrane/cytosol cycle; providing a multifaceted control over membrane dynamics (Sapmaz *et al.*, 2019).

Timing and selection of particular effectors for specific cellular functions are highly important for Rab7 function, whose problems are associated with many neurodegenerative disorders. So, it

is indispensable to study and discover the upstream regulatory mechanisms, GEFs, and PTMs of Rab7. A combination of complex events must be under the control of unknown upstream molecules for its punctual cycle and precise activity.

1.6 Lysosomal disorders

Metabolic inherited disorders affecting lysosomal function are known as lysosomal disorders. They are 70 of them known so far, all with a rare prevalence. Although most of them are monogenic disorders with autosomal recessive inheritance, 3 of them are X-linked. Mutations in the genes expressing lysosomal proteins prevent lysosomal catabolism and lead to material accumulation in the cell followed by cell death. Most of the lysosomal disorders are named with respect to the product accumulated. Mucopolysaccharidoses, mucolipidoses, oligosaccharidoses, sphingolipidoses, glycoproteinoses, and neuronal ceroid lipofuscinoses are some of them (Platt *et al.*, 2018). On the other hand, some other lipid storage disorders are named by the scientist who described the disease, such as Gaucher, Sandhoff, Tay-Sachs, and Fabry disorders. Depending on the location and the amount of the storage material within the cell, signs, and symptoms can vary between patients, even sometimes within the same disease. The common symptoms include intellectual physical disability, behavioral problems, and seizures (Greiner-Tollersrud & Berg, 2013).

1.6.1 Neuronal Ceroid Lipofuscinosis (NCL)

Almost all LSDs manifest as neurodegeneration. Being the most common pediatric neurodegenerative disorder, NCL is a subfamily of rare lysosomal diseases (Jalankoa *et al.*, 2006). To date, this inherited disease is linked to over 430 mutations in 13 genetically distinct genes (CLN1-8 and CLN10-14) (Mole & Cotman, 2015). Despite the diversity of NCL-encoded proteins, patients exhibit similar symptoms and physiological characteristics. Retinopathy, motor disorders, epilepsy, cognitive regression, and a significantly reduced lifespan are the symptoms found in patients suffering from NCL diseases (Andersona *et al.*, 2013). At the cellular level, NCL displays abnormal lysosomal function, extreme accumulation of autofluorescent ceroid lipopigments in neurons and peripheral tissues, and neurodegeneration. Thalamus, cerebellum, cortex, retina, optic nerve have been shown to be affected the most in NCL patients with common cardiac and bowel problems

SUMMARY OF NEW CLASSIFICATION NOMENCLATURE OF THE NCLS

Gene	Disease Name	Also Known As	Gene Product (Protein)	Protein Description
CLN1	CLN1 disease, infantile CLN1 disease, late infantile CLN1 disease, juvenile CLN1 disease, adult	Infantile	Palmitoyl protein thioesterase 1, PPT1	soluble lysosomal enzyme deficiency
CLN2	CLN2 disease, late infantile CLN2 disease, juvenile	Late-Infantile	Tripeptidyl peptidase 1, TPP1	soluble lysosomal enzyme deficiency
CLN3	CLN3 disease	Juvenile	CLN3 transmembrane protein	transmembrane protein
CLN4/DNAJC5	CLN4 disease	Adult autosomal dominant Batten Kuf's disease Ceroid Lipofuscinosis Parry type	Cysteine string proteinα	secretory vesicle protein
CLN5	CLN5 disease, late infantile CLN5 disease, juvenile CLN5 disease, adult	Finnish variant late-infantile	Ceroid-lipofuscinosis neuronal protein 5	soluble lysosomal enzyme deficiency
CLN6	CLN6 disease, late infantile CLN6 disease, juvenile CLN6 disease, adult	Early juvenile variant or late-infantile variant	Ceroid-lipofuscinosis neuronal protein 6	transmembrane protein, endoplasmic reticulum
CLN7	CLN7 disease, late infantile	Late-infantile variant	Major facilitator superfamily domain-containing protein 8	transmembrane protein, endolysosomal transporter
CLN8	CLN8 disease, late infantile	Late-infantile variant EPMR (progressive epilepsy with mental retardation)	unknown transmembrane protein, ER, ER-Golgi intermediate complex	transmembrane protein, endoplasmic reticulum , ER-Golgi intermediate complex
CLN10/CTSD	CLN10 disease, congenital CLN10 disease, late infantile CLN10 disease, juvenile CLN10 disease, adult	Congenital classic Late-infantile Adult	Cathepsin D	soluble lysosomal enzyme deficiency
CLN11/GRN	CLN11 disease, adult	Adult (heterozygous mutations cause frontotemporal lobar dementia)	Progranulin	non enzyme; function of protein poorly understood
CLN12/ATP13A2	CLN12 disease, juvenile	CLN12 disease Juvenile (mutations also cause Kufor-Rakeb syndrome)	P-type ATPase	non enzyme; function of protein poorly understood
CLN13	CLN13 disease, adult	Adult Kufs type B	Cathepsin F	soluble lysosomal enzyme deficiency
CLN14/KCTD7	CLN14 disease, infantile	CLN14 disease, infantile	Potassium channel tetramerization domain-containing protein 7	probable transmembrane protein voltage-gated potassium channel complex

Figure 1.12: Classification and nomenclature of NCLs
(© Batten Disease Support and Research Association, 2020)

(H.R.Nelvagala *et al.*, 2020). However, the more research is conducted on each NCL disease, the more we understand how different they are from one another; having diverged causative molecular pathways.

Linkage and biochemical analysis first identified *CLN1*, *CLN2*, and *CLN3* genes causing NCL phenotypes. Improvement in gene identification techniques, with the help of the human genome project, allowed the discovery of *CLN5, CLN6, CLN7*, and *CLN8* genes in affected families. Later, exome sequencing swiftly revealed *CLN4, CLN11, CLN12, CLN13*, and *CLN14* mutations (Mole & Cotman, 2015). While the *CLN4* mutation is autosomal dominantly inherited, the other mutations have autosomal recessive inheritance (Noskova *et al.*, 2011). NCL disease caused by these 13 gene mutations is individually called by the name of the mutated protein of interest.

CLN1

Mutations in the *CLN1* gene, located on chromosome 1, leads to problems in the production of palmitoyl protein thioesterase 1 (PPT1). This protein is a soluble lysosomal enzyme that is trafficked by CI-MPR. It functions as a thioesterase, removing palmitate chains from proteins undergoing lysosomal degradation. Since PPT1 is an important enzyme for lipid digestion (whose actual substrate is still not known), its mutation leads to lipid accumulation in cells (Lu *et al.*, 1996), causing cell death. Symptoms start to show up mostly around the age of 1. Children mostly live up to early-to-mid childhood ages (Mink *et al.*, 2013). The characteristic storage bodies are demonstrated as granular osmiophilic deposits (GRODSs) (Andersona *et al.*, 2013).

CLN2

Mutations in the *CLN2* gene, located on chromosome 11, cause defects in the production of tripeptidyl peptidase1 (TPP1) enzyme. Similar to PPT1, TPP1 is also a soluble lysosomal protein. TPP1 has been shown to degrade fibrillar Aβ (Solé-Domènech *et al.*, 2018).Its mutations cause the accumulation of toxic materials, resulting in cell death. Symptoms usually start with epileptic seizures around the age of 3 and the life span is around 12 years. The characteristic storage bodies are demonstrated as curvilinear bodies (CVB) (Andersona *et al.*, 2013). Coimmunoprecipitation has shown that CLN2 interacts with CLN5 (Vesa *et al.*, 2002) and CLN3 (Persaud-Sawin *et al.*, 2007).

CLN3

Mutations in *CLN3*, located on the short arm of chromosome 16 at position 12.1 (Mirza *et al.*, 2019), cause defects in CLN3 and leads to the most common neurodegenerative disease in children. Symptoms begin with vision loss between age 4-7 and the patient life span is around 30 years. CLN3 disease is more commonly referred to as Batten disease. Clinical features in later stages of CLN3 disease includes parkinsonian features; such as bradykinesia, rigidity, and resting tremor.

CLN3 contains six transmembrane domains with cytosolic N- and C- termini (Ratajczak *et al.*, 2014). It has 438 amino acids, coded by 15 exons. Studies conducted in the 1990s with 200 patients demonstrated that 73% of them have a deletion of exon 7 and 8; causing exon 6 splicing to exon 9 and a newly formed stop codon. This leads to a 1 kb truncated CLN3 protein (CLN3$^{\Delta ex7/8}$, (c.462-

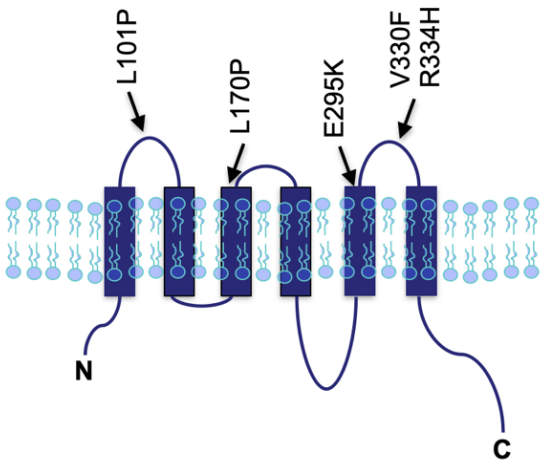

Figure 1.13: Predicted structure of CLN3

CLN3 has six transmembrane domains. Its N and C terminal portions are in the cytosol. Arrows indicate the location of the disease-causing point mutations included in this work.

677del)). The rest of the patients have a variety of different disease-causing missense mutations, including $CLN3^{R334H}$ (22%), $CLN3^{V330F}$, $CLN3^{E295K}$ (9%), and $CLN3^{L101P}$ at exon 13, exon 13, exon 11, and exon 5, respectively (Fig.1.13) (NCL Resource, 2017; Cotman & Staropoli, 2012). Other than the truncated version, none of these CLN3 mutants are associated with its cellular mislocalization (Mirza *et al.*, 2019).

Although the location of CLN3 has been demonstrated on lysosomal membranes (and a small amount in Golgi (Cao *et al.*, 2006)) as a highly glycosylated integral membrane protein (Storch *et al.*, 2004), its function is still poorly understood. Other than glycosylation, CLN3 has been shown to be phosphorylated, myristoylated, and farnesylated. All of which contribute to its stability, membrane targeting, and anchoring. Although it is ubiquitously expressed in human tissues, its level is highest in astrocytes, microglia, and neurons. Interestingly, glioblastomas and neuroblastomas have been shown to have high levels of CLN3 expression (Mirza *et al.*, 2019).

Previously, a role of CLN3 in autophagy and lysosomal trafficking pathways has been proposed (Lojewski *et al.*, 2014; Metcalf *et al.*, 2008). CD8-CIMPR transfection followed by anti-CIMPR feeding protocol demonstrated the deficient cellular trafficking of sorting receptors and a decreased lysosomal enzyme activity in $CLN3^{KD}$ cells (Metcalf *et al.*, 2008). Moreover, multiple enzyme deficiencies were observed in cells having mutated CLN3 protein (Schmidtke *et al.*, 2019). Also, its interaction with Rab7, RILP, and the motor proteins (tubulin, dynactin, dynein, kinesin-2) has been shown (Luiro *et al.*, 2004; Uusi-Rauva *et al.*, 2012) to regulate the mobility of late endocytic

compartments. However, neither the function of these interactions nor the disease-causing mutations on downstream functions of CLN3 and the cause of enzyme deficiency have been determined.

CLN4

DNAJC5 gene, located on chromosome 20, codes for CLN4 protein. Its gene mutations cause defects in cysteine string protein (CSP; a co-chaperon) and leads to NCL disease with an unknown mechanism. CLN4, also called Kufs or Parry disease, is the only NCL having autosomal dominant inheritance. Symptoms start after the age of 30. CLN4 symptoms do not include vision loss that makes it different form other CLN disorders. It has parkinsonian features including the degeneration of the substantia nigra.

CLN5

Mutations in *CLN5*, located on chromosome 13 at position q22.3 (Schmiedt *et al.*, 2009),cause defects in the CLN5 protein. Like CLN1 and CLN2, CLN5 is also a soluble lysosomal protein, although it doesn't appear to have enzymatic activity. Its mutations cause the accumulation of materials with GRODs, CVBs, rectilinear profiles (RLP), and/or fingerprint profiles (FPP) as characteristic storage bodies (Andersona *et al.*, 2013). Symptoms start between age 3 - 7 and patients can live up to their teenage years. CLN5 does not have any homology to any known protein. It is translated as a 407 aa integral membrane protein. It is subsequently cleaved at its N-terminal into a mature soluble protein from 93-407 aa for its endolysosomal transportation (Jules *et al.*, 2017). The most common disease-causing mutation on CLN5 is $CLN5^{Y392X}$ at exon 4. It creates a premature stop codon, leading to a 2bp deletion. Truncated CLN5 protein has been demonstrated to be retained in the ER (although some papers argue) caused by an N-glycosylation loss, preventing its proper folding (Moharir *et al.*, 2013). Other germline mutations causing damaging missense mutations include $CLN5^{D279N}$, $CLN5^{N192S}$, and $CLN5^{R112P}$ at exon 4, exon 3, and exon 2, respectively. $CLN5^{D279N}$ has been shown to add additional glycosylation on CLN5 protein, preventing its processing, thus promoting its ER retention (Lee *et al.*, 2015). $CLN5^{N192S}$, on the other hand, is shown to localize lysosomes normally, indicating its main effect on the protein function other than its localization (Moharir *et al.*, 2013). While $CLN5^{R112P}$ was clearly shown to be an ER-localized protein (Moharir *et al.*, 2013).

Recently, the function of CLN5 as a potential glycoside hydrolase in *Dictyostelium discoideum* has been proposed (Huber & Mathavarajah, 2018). However, no target has been identified and this function has not been shown in mammals. Other studies have shown a role for CLN5 in the regulation of lysosomal pH (Best *et al.*, 2016) and mitophagy (Doccini *et al.*, 2020). Our group has shown a decrease in Rab7 and retromer membrane recruitment in CLN5 knockdown ($CLN5^{KD}$) HeLa cells (Mamo *et al.*, 2012). Using co-immunoprecipitation, CLN5 was shown to interact with CLN1, CLN2, CLN3, CLN6, and CLN8 (Schmiedt *et al.*, 2009)) (Vesa *et al.*, 2002). However, the function of CLN5-CLN3 interaction, the CLN5 disease-causing mutations on the downstream functions of Rab7, and the role of CLN5 to regulate lysosomal acidity has not been determined.

CLN6

CLN6 is an ER-localized integral membrane protein containing seven transmembrane domains. Its mutations cause abnormal protein accumulation with a mixed appearance of GRODS, CVBs, RLPs, and/or FPPs (Andersona *et al.*, 2013). Disease age of onset varies from 18 months to 8 years of age. Since it has a fast progression, patients die around late childhood or early teenage years (Mink *et al.*, 2013). A subset of CLN6 mutations causing Kufs disease has an adult onset. A role for CLN6 in lysosomal acidification has been proposed; through the selective transport of molecules important for lysosomal function (Storch *et al.*, 2004). Recently, it was demonstrated that CLN6 forms complex with CLN8 to regulate lysosomal enzyme transportation from ER to Golgi (Bajaj *et al.*, 2020).

CLN7

Mutations in the *CLN7* gene, located on chromosome 4 at positions q28.1-q28.2, cause defects in the production of the MFSD8 (major facilitator superfamily) protein. Being a lysosomal transmembrane protein, this protein is predicted to function as a membrane transporter. Its mutations cause abnormal storage material accumulation of GRODs, CVBs, RLPs, and/or FPPs (Andersona *et al.*, 2013). Age of disease onset is between 3-7 years of age with a lifespan up to their late childhood or teenage years (Mink *et al.*, 2013). *CLN7* is translated as 518 aa resulting in a 58 kDa protein with 12 transmembrane domains. N- and C- terminals are both cytosolic, as is the case for CLN3. MFSD8 has dileucine motifs in its N-terminal, which are required for its lysosomal local-

ization (Steenhuis *et al.*, 2010). Recently, Cln7-deficient mouse embryonic fibroblasts demonstrated a significant decrease in their lysosomal content, including the CLN5 protein (Danyukova *et al.*, 2018).

CLN8

Mutations in the *CLN8* gene, located on chromosome 8, cause defects in the production of ER-localized transmembrane protein CLN8. Its mutations cause abnormal storage material accumulation of CVBs and FPPs (Andersona *et al.*, 2013). Disease age of onset is between 5-10 years of age with a lifespan up to their 70s (Mink *et al.*, 2013). Thus, CLN8 disease is also called Epilepsy with Progressive Mental Retardation (EPMR). In 2018, the function of CLN8 as an ER cargo receptor for lysosomal enzyme transportation from ER to Golgi has been shown (Ronza *et al.*, 2018). While CLN8 has been shown to bind the lysosomal enzymes via its second luminal loop, it has been shown to interact with COPI and COPII complexes via the specific signals on its carboxy-terminal for its export and retrieval. So that, ER-to-Golgi transfer of lysosomal enzymes can take place (Ronza *et al.*, 2018).

CLN10

Mutations in the *CLN10* gene, located on chromosome 11 at position p15.5, cause defects in the production of the lysosomal enzyme, cathepsin D (CTSD). Mutations in this protein result in granular deposits and microcephaly in all patients (Andersona *et al.*, 2013) inducing very early symptoms, that may lead to the death of the patient even within the first week of their lives. Previously, the importance of CTSD in synaptic function, trafficking, and recycling has been demonstrated (Koch *et al.*, 2011).

CLN11

Mutations in the *GRN* gene, located on chromosome 17 at position q21.32, cause defects in the production of progranulin (PGRN). Its mutations result in an adult-onset disease and impair cell growth, division, and survival by an unknown mechanism. Previously, PGRN has been suggested to play a role in lysosomes by its interaction with sortilin and effect on mTORC1 activity (Carcel-

Trullolsa *et al.*, 2015). TAR DNA binding protein 43 (TDP-43)- positive inclusions are the characteristic cellular pathology (Cenik *et al.*, 2012). TDP-43 is located in the cell nucleus to regulate transcription by its binding to DNA. It also binds to RNA not only to ensure RNA stability but also to regulate alternative splicing events, thus regulating protein production. Its hyper-phosphorylation and ubiquitination are known to cause TDP-43 deposition in the brain and the spinal cord, as it is in amyotrophic lateral sclerosis (ALS) and frontotemporal lobar degeneration (FTLD) motor neuron diseases (Prasad *et al.*, 2019).

CLN12

Mutations in *CLN12* gene (also known as *ATP13A2*, *KRPPD*, *PARK9*, *HSA9947*, *RP-37C10.4*), located on chromosome 1 at position p36.13, cause defects in the production of polyamine-transporting ATPase 13A2 (ATP13A2), which belongs to the family of P-Type ATPases as a type 5. That family is known to shuttle not only polyamines, but also cations, heavy metals, and lipids across biological membranes (Carcel-Trullolsa *et al.*, 2015) to provide normal functioning of lysosomes. Because of that, CLN12 is predicted to have some of these functions. CLN12 disease, also known as Kufor-Rakeb syndrome (a very rare form of juvenile-onset familial Parkinson's disease), results in NCL disease with characteristic lipofuscin accumulations in the affected cells. Interestingly, in addition to NCL features, ATP13A2-KO mice showed increased α-synuclien depositions as it is in mammalian PD models.

CLN13

Mutations in *CLN13* gene, located on chromosome 11 at position q13, cause defects in the production of a lysosomal enzyme called cathepsin F (CTSF). Its mutations cause excess accumulation of autofluorescent granules with a very slow disease progression with adult-onset. Other than its role as a lysosomal enzyme, the role of CTSF has been shown in proteasome degradation, autophagy, and antigen presentation with unknown mechanisms (Carcel-Trullolsa *et al.*, 2015; Seranova *et al.*, 2017; Shi *et al.*, 2000).

CLN14

Mutations in *CLN14* gene, located on chromosome 7 at position q11.21, cause defects in the production of KCTD7 (potassium channel tetramerization domain-containing protein 7) protein. CLN14 disease is grouped under the infantile-onset of NCL. KCTD7 plays role in cell membrane hyperpolarization by conducting K^+. Also, it is suggested that CLN14 might regulate protein degradation by its interaction with Cullin-3 part of E3 ubiquitin-protein ligase (Carcel-Trullolsa *et al.*, 2015).

Therapies

The CLN genes and most of their disease-causing mutations have been identified by newly developed strategies. These provide accurate genetic diagnosis, aiding competence of the treatment before irreversible damage takes place. Although there are many discoveries about the possible roles of CLN proteins in the cellular machine, their function and mechanism of action are poorly understood. NCLs have complex nature of genotype-phenotype correlations. Each CLN mutation might cause different impacts in different cell types. Yet, all of them are known to affect the central nervous system (CNS), which is protected by the blood-brain barrier (BBB). Together with the many unknowns about their molecular function, it is challenging to generate effective therapies. For the CLN2 lysosomal enzyme, there is a current treatment that we will mention in the next paragraph. Also in recent times, there had been huge progress on the NCL research that some promising drug candidates are under development.

Enzyme replacement therapy (ERT) is the replacement of an enzyme defective in the targeted lysosomal disease. Although the idea has advanced from its discovery, improvements are limited with the quantity, half-life, repeated infusion, and efficient CNS distribution of the needed recombinant protein. In 2017, BioMarin developed the first and only FDA (U.S. Food and Drug Administration) and EMA (European Medicines Agency)-approved CLN treatment called Brineura® (cerliponase alfa) for CLN2 disease. It has been shown to slow the neurological manifestations and the progression of the disorder (Rosenberg *et al.*, 2019). Though, there is still ongoing work on CLN2 for better treatment opportunities.

Therapies for the transmembrane protein-coding NCLs, on the other hand, need more sophisticated technologies to program patient cells for the production of the healthy protein. Gene therapy appears to be a promising option. For that purpose, viral vectors are engineered to contain the genetic code for a specific protein. Upon their infection, they will use human cells as a factory

to produce the functional protein. Basically, hematopoietic stem cells (HSC) are isolated from patients for their viral transduction, followed by the infusion of these engineered HSC back into the patient. Adeno-associated virus (AAV) are the most commonly used viral vectors for this purpose against NCL. CLN3 gene encoding scAAV9 vector intravenous administration to diseased mice partially corrected the disease phenotype. Currently, Nationwide Children's Hospital is recruiting patients for AAV9 clinical trials (Bosch *et al.*, 2016). Gene therapy is also performed against CLN5 disease. The sheep disease model is used for that purpose. AAV9-CLN5 or lentivirus-CLN5 are both successfully delivered by intraparenchymal and intracerebroventricular injections. Although the therapy decreased the storage accumulation and extended the lifespan, had no impact on vision loss (Mitchell *et al.*, 2018). However, there is also a great concern over gene therapy efficacy, mostly because of its inability to reverse the existing disease features. Since NCL is a rapidly progressing disorder with increased cell death, its early diagnosis holds the key to the treatment. Another difficulty is to find an HLA-matched donor to prevent graft rejection, which brings the life-long usage of immunosuppressive drugs. Even isolated patient stem cells has drawbacks; they need careful handling and time to proliferate to reach sufficient amount of number for infusion. Although the systemic delivery of gene therapy is favourable for its safety, BBB in humans poses a risk factor for its efficacy.

Also, there are pharmacological treatment options with easy production, characterization features together with their immediate usability for the existing patients. Yet, there are undesired aspects of these small molecules, such as their unpredictable side- or off-target effects. CLN3$^{\Delta ex7/8}$ mice are known to have reduced brain cAMP levels. cAMP degradation is regulated by PDE4 phosphodiesterase. Rolipram, roflumilast, and PF-06266047 are PDE4 inhibitors. Testing these drugs in diseased mice resulted in decreased neuroinflammation, glial activation, and lysosomal pathology. Being the only FDA-approved drug among three of them, roflumilast has a high potential to treat CLN3 disease (Rosenberg *et al.*, 2019). Elevated autoantibodies in CLN3 patients make immunosuppressive drugs a good target for CLN3 treatment. FDA-approved mycophenolate mofetil (CellCept®) has already been tested in CLN3 patients and showed good drug toleration in the short-term interval. Its long-term effects need to be tested. Anti-inflammatory prednisolone eye drops were tested in CLN3 disease patients against vision loss. Promising results support the role of retinal inflammation in blindness (Drack *et al.*, 2015). More interestingly, MK2206 can be a good option by its action on TFEB (transcription factor EB) through inhibiting protein ki-

nase B (AKT serine/threonine kinase). Because MK2206 treated CLN3$^{\Delta ex7/8}$ mice showed TFEB nuclear localization followed by increased autophagic activity and the lysosomal storage clearance (Palmieri *et al.*, 2017). Another AKT inhibitor, trehalose disaccharide, is also shown to be effective against lipofuscin buildup by activating TFEB in preclinical studies. A recent study showed that a combination of AKT inhibition and miglustat (glucosylceramide synthase inhibitor) can enhance its pharmacological action. Theranexus is the company having the license to develop this drug so-called BBDF-101. Orphan drug designation has been granted for BBDF-101 to start its clinical trials in CLN3 patients (Masten *et al.*, 2020).

Another interesting approach is the use of antisense oligonucleotides (ASO). They are small molecules used to treat the gene itself. They induce exon skipping to the mutated part of the gene so that, the functional part of the gene can be produced. This technology has been used for a CLN7 patient bearing an intronic mutation. The ASO created for that patient (called milasen) significantly decreased the course of seizures. With time, we will see the efficacy of milasen. Likewise, the frameshift caused by CLN3$^{\Delta ex7/8}$ mutation is treated with exon 5-targeted ASO. Its effect lasted more than a year in CLN3$^{\Delta ex7/8}$ mice; improved symptoms, disease pathology, and the lifespan (Centa *et al.*, 2020). Thus, reading-frame correction by ASO seems to be a promising approach for CLN3 treatment.

Lysosomal problems are also associated with common neurodegenerative disorders (NDs) (Follett *et al.*, 2014; Reitz, 2018; Aoki *et al.*, 2017; Mohassel *et al.*, 2021; Small & Petsko, 2015). A recent review has highlighted the early endosomal trafficking and endolysosomal degradation defects in Alzheimer's disease (AD), Parkinson's disease (PD), Amyotrophic Lateral Sclerosis (ALS), and Frontotemporal dementia (FTD) (Kiral *et al.*, 2018). Excitingly, there are small molecule trials targeted to either stimulate or block cellular trafficking pathways implicated in various pathologies of AD and PD (Mecozzi *et al.*, 2014; Breijyeh & Karaman, 2020). These therapies are expected to ameliorate other lysosomal-related disorders. Similarly, the knowledge gained from the molecular function of CLN proteins can hopefully reveal better therapeutic targets for AD, PD, ALS, and FTD.

1.6.2 Alzheimer's Disease

AD is the most common form of adult dementia and neurodegeneration with slow disease progression. Symptoms include impairment in learning and memory, which worsens by time through problems in decision making, reasoning, language, attention, orientation, and visuospatial functions. Accumulation of neurofibrillary tangles (NFTs), amyloid plaques, dystrophic neurites, neuropil threads, and brain lesions are the AD pathologies. Abnormal processing of integral plasma membrane amyloid precursor protein (APP) by β- and γ-secretases result in the formation of amyloid-beta (Aβ40 and Aβ42) plaques (DeTure & Dickson, 2019). NFTs, on the other hand, are formed because of the hyperphosphorylation of tau proteins inside the cytoplasm. Together with mitochondrial damage and oxidative stress, neurodegenerative events take over. The main mechanism leading to AD phenotypes is not known. Since both genetic and epigenetic factors are the risk factors, AD is considered a complex multifactorial disorder. Mutation in APP, Presenilin-1 (PSEN-1), Presenilin-2 (PSEN-2), and apolipoprotein E (ApoE) is the cause of 70% of familial AD cases around the world. Besides, sporadic AD is related to age, gender, head injuries, infectious diseases, cardiovascular disorders, environmental factors, diet, and so on. Cholinergic neuronal loss is observed in AD diseases. These cells are synthesizing acetylcholine (ACh), which is essential for cognitive functions. ACh synthesis follows the secretory trafficking pathway inside synaptic vesicles. Aβ accumulation is the hypothetical cause of AD by preventing choline uptake, thus acetylcholine (ACh) release (Breijyeh & Karaman, 2020). Therefore, problems in cellular trafficking seem to be the central mechanism in AD as it is in NCL disorder.

1.6.3 Parkinson's Disease

PD is the second most common form of adult neurodegeneration, mostly effecting males worldwide. Symptoms include progressive physical limitations caused by rigidity, bradykinesia, tremor, postural instability. Dopaminergic neuronal loss is observed in PD cases, which is thought to be the main reason of motor dysfunctions (Gómez-Benito *et al.*, 2020). Mutation in SNCA (α-synuclein), LRRK2, PINK1, PARK7 (DJ-1), ATPase type 13A2 (ATP13A2), and PARK2 (Parkin) is the cause of 10-15% of familial PD cases worldwide. The rest is caused by the environmental factors. Intraneuronal Lewy body formations composed of α-synuclein protein inclusions are the hallmarks of PD. Although the main mechanism leading to PD phenotype is not known, α-synuclein accu-

mulation is thought to be the main reason for neurodegeneration. The toxic effect of α-synuclein on neurons has been demonstrated. Thus, its adverse effect on neuronal integrity, mitochondrial function, endoplasmic reticulum and synaptic transmission seem to be the main mechanism in PD. Moreover, endocytic trafficking defects are observed in PD patient cells (Small & Petsko, 2015).

1.6.4 Amyotrophic Lateral Sclerosis

ALS is the most frequent motor neuron disease with a late age of onset. Symptoms include weakness in the hand and feet, which worsens by time through problems in speech, swallowing, and cognitive functions. Mutation in Fused in Sarcoma (FUS), Superoxide dismutase (SOD1), TAR DNA-binding protein 43 (TDP-43), and Chromosome 9 open reading frame 72 (C9orf72) are some of the causative genes of ALS. 20% of ALS cases are familial. The rest depends on the epigenetic factors. Most of the cases show TDP-43 positive neuronal inclusions as pathological hallmark of the disease. Mitochondrial dysfunction, oxidative stress, axonal transport dysregulation, glutamate excitotoxicity, endosomal and vesicular transport impairment, impaired protein homeostasis, and aberrant RNA metabolism are the observed phenotypes in ALS patients (Gall *et al.*, 2020).

1.7 Bioluminescence Resonance Energy Transfer (BRET)

One good way to understand the function of a protein is to look at its interacting partners. In this work, we first performed interaction studies to understand the CLN3 and CLN5- related pathways. Then, we conducted functional assays to figure out their potential role within the cell. We have mentioned the dynamic nature of GTPases and their impact on the association/dissociation of effector proteins to accomplish diverse cellular functions. Considering the CLN3 as a transmembrane protein, it is important to test the protein interactions in their correct membrane environment and cellular localization. The BRET technique provides interaction information from live cells, making it a perfect technology for our research. As the name indicates, BRET uses the "resonance energy transfer" phenomenon. Fusion protein constructs are used to produce the protein of interest with a chromophore tag. In our work, we have used the bioluminescent enzyme Renilla luciferase (Rluc) as the donor chromophore and the yellow (eYFP)/ green (GFP10) fluorescent proteins as an acceptor fluorophore. In the presence of its substrate (Benzyl-coelenterazine or

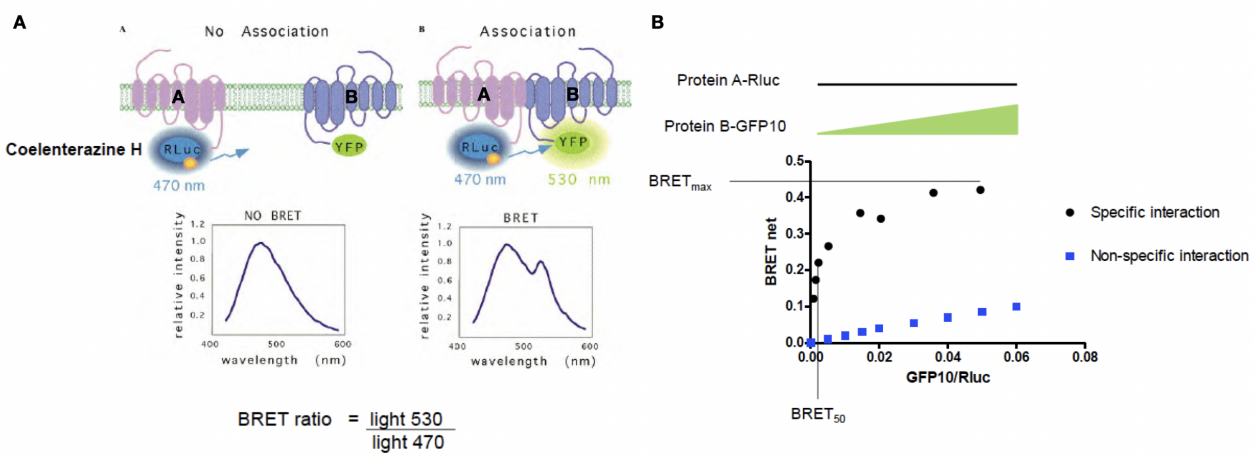

Figure 1.14: Schematic of a BRET interaction and titration curve. (Mercier *et al.*, 2002; Sauvageau & Lefrancois, 2019)

A) In case of an interaction, donor transmits its energy to the acceptor giving a light emission. B) From the emission signal, BRET titration curve can be plotted.

DeepBlueC (didehydro-coelenterazine or coelenterazine-400a)), Rluc oxidizes it into coelenteramide that produces a concomitant light emission (at 395nm). The produced light engrid then excites the fluorophore, which emits a green light (at 510nm) (Fig. 1.14A). That will only happen if these two proteins are in close proximity to interact, which is less than ∼10 nm. While the donor protein loses its energy because of the energy transfer, the fluorescence of the acceptor protein will increase and give a light emission. From the emission signals, we can plot the BRET titration curves giving the specificity of the interaction. To do so, up to 12 points are generated, all of which are transfected with a constant amount of donor and an increasing amount of acceptor (Fig. 1.14B). The light coming from the acceptor (fluorescence) / the light coming from the Rluc (luminescence) will give the BRET_{net}. If the interaction is specific, a hyperbolic increase in the curve should reach saturation (Fig. 1.14B), because a certain amount of donors can specifically interact with a limited number of acceptor proteins. The propensity of the interaction can be interpreted from the BRET_{50} values, which is the 50% of the maximum BRET signal at saturation. The smaller the BRET_{50}, the stronger the interaction. To conclude, BRET is a highly fast, reproducible, and sensitive technique to test interaction partners, membrane association/dissociation, and conformational changes of a protein in its native environment. Taken together, the function of a protein can be scientifically interpreted.

In this work, we used HeLa cells in our BRET transfections to test the biophysical interactions of CLN3 and CLN5 proteins. Since we are interested in the cell biology of these proteins, that is

convenient to use HeLa cells in our research study. It is the first immortal human cell line isolated from the cervical cancer of Henrietta Lacks in 1951. While cancer cells die at some point, Henrietta's cells kept on dividing under certain conditions. That has made HeLa a perfect cell line for research that can be shared with different labs worldwide to study different cellular pathways for a long time. In this way, the comparison, validation, and completion of the unknown pathways can be achieved to build scientific knowledge. Although HeLa cells are not a perfect model to study a neurodegenerative disorder, their easy handling and transfection make them a perfect candidate for our BRET studies. Moreover, it was straightforward to generate CLN3-KO and CLN5-KO HeLa cells using CRISPR/Cas9. These knock-out lines remarkably advanced our understanding of the role of CLN3 and CLN5 at endosomes. At this moment, the indicated functional roles of these proteins can be confirmed and further studied in a more disease-relevant model like patient-derived induced pluripotent stem cells (also known as iPS cells or iPSCs).

1.8 Thesis structure

This thesis is organized into three parts; "General Introduction", "Articles", and "General Discussion & Conclusion". The research focus of this work is on two different Batten-associated proteins; CLN3 and CLN5. My contributions to the discovery of CLN3 and CLN5 protein functions are presented here in the form of two separate scientific papers.

Following the introduction (Part I) in Chapter-1, Article-I in Chapter-2 presents the first study describing "CLN3 regulates endosomal function by modulating Rab7A–effector interactions" published in the Journal of Cell Science in January 2020. In this work, we demonstrate that the endolysosomal integral membrane protein CLN3 is required for retromer function at endosomal membranes for normal lysosomal function. This study is driven by understanding the role of CLN3 in lysosomal homeostasis, whose protein dysfunction leads to an incurable form of the lysosomal disorder, so that the pathogenic mechanism behind CLN3 disease can be targeted for therapies. CLN3 is an integral membrane protein that localizes to endosomes and lysosomes. Although it has been implicated in autophagy, the function of the protein remains unknown. Mutations in the protein result in a childhood dementia known as juvenile neuronal ceroid lipofuscinosis (NCL). Children with this disease suffer from visual failure, cognitive regression, and seizures with premature death usually occurring in the second decade of life. Recent work has also linked CLN3 expression to

various forms of cancer, highlighting the importance of this protein and its deregulation in human disease.

In this work, we demonstrate that CLN3 interacts with the small GTPase Rab7 using bioluminescence resonance energy transfer (BRET). Compared to co-immunoprecipitation, BRET enables the study of protein-protein interaction in live cells with proteins in their native environments. Furthermore, by extrapolating the $BRET_{50}$ from BRET titration curves, the propensity to interact can be determined, therefore the method is well suited to determine how mutations in a protein can affect an interaction or how a protein can affect the interaction of two other proteins. Using BRET, we also found that disease-causing mutations in CLN3 affect its interaction with Rab7. Rab7 is a key regulator of endosomal function which modulates the endosome-to-TGN trafficking, endocytic cargo degradation, and autophagy. We demonstrate that CLN3 is required for retromer and PLEKHM1 interactions of Rab7. Lack of retromer function in CLN3 knockout (CLN3-KO) HeLa cells results in the degradation of the lysosomal sorting receptors, sortilin, and CI-MPR. The deficient function of PLEKHM1 results in a significant delay in EGFR degradation and could also explain deficiencies in autophagy in CLN3-KO cells as PLEKHM1 is required for fusion to lysosomes.

Article-II in Chapter-3 presents the second project "CLN5 and CLN3 function as a complex to regulate endolysosome function", which was published in Biochemical Journal in May 2021. In this work, we demonstrate an upstream modulatory role of CLN5 for retromer function by modulating both Rab7 palmitoylation status and CLN3 interactions. Also, extended the study to explain the autophagy defects observed in CLN5 patient cells. Our observations of decreased retromer membrane recruitment in CLN5-KO HeLa cells drives us to understand the role of CLN5, which is known to interact with CLN3 with unknown function, so that we could answer how a soluble lysosomal protein (CLN5) can modulate the recruitment of a protein in the cytosol.

Retromer is a protein complex that mediates the endosome-to-trans Golgi Network (TGN) trafficking of the lysosomal sorting receptor sortilin, under the regulation of the small GTPase Rab7A. Only GTP-bound active Rab7 can localize to late endosomal membranes, so that, retromer can be recruited to membrane-anchored Rab7A for its effector function. In this work, we showed that CLN5 is required for the palmitoylation of Rab7A, which is required for retromer membrane recruitment. We found that sortilin is degraded in CLN5 knockout HeLa cells. CLN3 is also required for the endosome-to-TGN sorting of sortilin by interacting with sortilin and regulating its retromer

interaction. The CLN3/sortilin interaction was disrupted in CLN5 knockout HeLa cells. Other than that, another Rab7 effector, RILP, is known to regulate the movement of lysosomes allowing them to fuse with autophagosomes. In our CLN5-KO cells, we found a decreased Rab7A/RILP interaction, along with the inefficient movement of lysosomes, resulting in decreased fusion with autophagosomes, and decreased autophagic flux. Together, we demonstrate a role for CLN5/CLN3 as a complex on the sorting of sortilin and extend the role of CLN5 to other Rab7A effectors.

In Part-III, we discuss the results and give the concluding remarks under Chapter-4. In short, upon completion of these two projects, we were able to identify a novel role of CLN3 and the upstream modulatory role of CLN5 to regulate the retromer function of Rab7. Briefly, this thesis demonstrates the cooperation of CLN3 and CLN5, whose mutations cause NCL disorder, in the regulation of endolysosome function.

Part II

Articles

Summary of contributions

I, Seda Yasa, have generated the following data as the first author of my first article, titled "CLN3 regulates endosomal function by modulating Rab7-effector interactions".

- RlucII-CLN3 plasmid cloning and GFP10-CLN3^{R334H}, GFP10-CLN3^{V330F}, GFP10-CLN3^{E295K}, GFP10-CLN3^{L101P}, and FLAG-CLN3^{R334H}, FLAG-CLN3^{V330F}, FLAG-CLN3^{E295K} and FLAG-CLN3^{L101P} vector constructs by site-directed mutagenesis

- Fig. 2.1

- Fig.2.2

- Fig.2.3 A,B

- Fig.2.4 A,B,C,D

- Fig.2.5

- Fig.2.6

- Fig.2.7

- Fig.2.8

- Fig.2.9 B,C,D

- Fig.2.10 B

- Fig.2.11

While CLN3^{KO} HeLa cells are generated by Abuzar Kaleem, Rab7^{KO} HeLa cells are generated by Graziana Modica using CRISPR/Cas9.

Graziana also generated RlucII-Rab7A, RlucII-Rab7^{C205,207S}, RlucII-Rab1a, GFP10-FYCO1, PLEKHM1-GFP10 and performed Fig.2.3 C,D.

And Etienne Sauvageau generated GFP10-CLN3, FLAG-CLN3, Vps26-nLuc, Vps26A-GFP10, RlucII-Arf6, S1R-YFP and performed Fig.2.3 E, Fig.2.4 E,F, and Fig.2.10 A.

Chapter 2

Article I: CLN3 regulates endosomal function by modulating Rab7-effector interactions

CLN3 régule la fonction endosomale en modulant les interactions Rab7-effecteur

Authors

Seda Yasa[1], Graziana Modica[1], Etienne Sauvageau[1], Abuzar Kaleem[2], Guido Hermey[2], Stephane Lefrancois[1,3,4]

[1] Centre Armand-Frappier Santé Biotechnologie, Institut National de la Recherche Scientifique, Laval, Canada H7V 1B7.

[2] Institute for Molecular and Cellular Cognition, Center for Molecular Neurobiology Hamburg, University Medical Center Hamburg-Eppendorf, 20251 Hamburg, Germany.

[3] Department of Anatomy and Cell Biology, McGill University, Montreal, Canada H3A 0C7.

[4] Centre d'Excellence en Recherche sur les Maladies Orphelines - Fondation Courtois (CERMO-FC), Université du Québec a Montréal (UQAM), Montréal, Canada H2X 3Y7.

Contributions

Conceptualization: S.Y., G.M., E.S., G.H., S.L.; Methodology: S.Y., G.M., E.S., A.K., G.H., S.L.; Validation: G.H., S.L.; Formal analysis: S.Y., G.M., E.S., A.K., S.L.; Investigation: S.Y., G.M.,

E.S., A.K.; Resources: A.K.; Writing - original draft: S.Y., S.L.; Writing - review & editing: S.Y., G.M., E.S., G.H., S.L.; Supervision: G.H., S.L.; Project administration: S.L.; Funding acquisition: G.H., S.L.

Journal of Cell Science

doi:10.1242/jcs.234047

Received 10 May 2019; Accepted 22 January 2020

Abstract

Mutations in CLN3 are a cause of juvenile neuronal ceroid lipofuscinosis (JNCL), also known as Batten disease. Clinical manifestations include cognitive regression, progressive loss of vision and motor function, epileptic seizures and a significantly reduced lifespan. CLN3 localizes to endosomes and lysosomes, and has been implicated in intracellular trafficking and autophagy. However, the precise molecular function of CLN3 remains to be elucidated. Previous studies showed an interaction between CLN3 and Rab7A, a small GTPase that regulates several functions at late endosomes. We confirmed this interaction in live cells and found that CLN3 is required for the efficient endosome-to-TGN trafficking of the lysosomal sorting receptors because it regulates the Rab7A interaction with retromer. In cells lacking CLN3 or expressing CLN3 harbouring a disease-causing mutation, the lysosomal sorting receptors were degraded. We also demonstrated that CLN3 is required for the Rab7A–PLEKHM1 interaction, which is required for fusion of autophagosomes to lysosomes. Overall, our data provide a molecular explanation behind phenotypes observed in JNCL and give an indication of the pathogenic mechanism behind Batten disease.

This article has an associated (First-Person, 2020) interview with the first author of the paper.

2.1 Introduction

The neuronal ceroid lipofuscinoses (NCLs) are a group of rare neurodegenerative diseases linked to over 430 mutations in 13 genetically distinct genes (*CLN1–CLN8* and *CLN10–CLN14*)(Mole & Cotman, 2015). Clinical manifestations of NCLs include intellectual impairment, progressive loss of vision and motor function, epileptic seizures and a significantly reduced lifespan (Andersona *et al.*, 2013). At the cellular level, NCLs display aberrant lysosomal function and an excessive

accumulation of ceroid lipofuscin in neurons as well as other cell types outside of the central nervous system (Andersona *et al.*, 2013).

Juvenile neuronal ceroid lipofuscinosis (JNCL) is caused by germline mutations in ceroid lipofuscinosis neuronal-3 (*CLN3*). More often referred to as Batten disease, it is the most common paediatric neurodegenerative disease (Andersona *et al.*, 2013; Mole & Cotman, 2015). CLN3 is a protein of 438 amino acids with six transmembrane domains whose N- and C-terminal ends are located in the cytosol (Ratajczak *et al.*, 2014). The most common mutation results in the deletion of exon 7 and 8 ($CLN3^{\Delta ex7/8}$), but several other mutations have been identified (Cotman & Staropoli, 2012). CLN3 is a highly glycosylated integral membrane protein (Storch *et al.*, 2004) that localizes to the endosomal/lysosomal membrane (Oetjen *et al.*, 2016) among other intracellular locations and has proposed roles in lysosomal trafficking and autophagy (Lojewski *et al.*, 2014; Metcalf *et al.*, 2008). CLN3 interacts with and has been implicated in Rab7A recruitment to endosomal membranes (Luiro *et al.*, 2004; Uusi-Rauva *et al.*, 2012); however, the function of this interaction is unknown. Furthermore, how disease-causing mutations in CLN3 affect this interaction or the downstream functions of Rab7A has not been elucidated.

The Ras-like proteins in brain (Rabs) are key regulators of the formation, trafficking, and fusion of transport vesicles at the endoplasmic reticulum (ER), Golgi apparatus and early and late endosomes (Hutagalung & Novick, 2011). Rabs function by interacting with downstream effectors (Grosshans *et al.*, 2006) and a key process regulating these interactions is the GTP loading or 'activation' of Rab GTPases at specific membrane sites (Pfeffer & Aivazian, 2004). This GDP to GTP switch is regulated by guanine exchange factors (GEFs) that load Rab GTPases with GTP, while GTPase activating proteins (GAPs) terminate their activity by hydrolysing the GTP to GDP (Barr & Lambright, 2010).

Active GTP-loaded Rab7A localizes to endosomal membranes and recruits numerous effectors to perform a variety of functions such as endosome-to-trans Golgi network (TGN) trafficking (Rojas *et al.*, 2008; Seaman, 2009), autophagosome–lysosome fusion (McEwan *et al.*, 2014), lysosomal positioning (Wijdeven *et al.*, 2016) and degradation of endocytic cargo, such as epidermal growth factor (EGF) receptor (EGFR) (Vanlandingham & Ceresa, 2009).

In this study, we systematically analysed several of these Rab7A mediated pathways to determine which was under the control of CLN3. We identified defects in endosome-to-TGN sorting and EGFR

degradation. Overall, our data suggest a role for CLN3 as a regulator of Rab7A function. Our data provide insight into the possible pathogenic mechanism in Batten disease.

2.2 Results

2.2.1 A subset of disease-causing mutations in CLN3 alters its interactions

It has been reported that CLN3 interacts with the small GTPase (Uusi-Rauva *et al.*, 2012), but the functional role of this interaction is not understood and it is not clear how disease-causing mutations in CLN3 affect this interaction.We used bioluminescence resonance energy transfer (BRET) to confirm the CLN3–Rab7A interaction in live cells and to determine how disease-causing mutations affect this interaction. Compared with coimmunoprecipitation, BRET is performed in live cells, with proteins localized to their native environment. From BRET titration curves, the $BRET_{50}$ can be calculated which is the value at which the concentration of the acceptor is required to obtain 50% of the maximal BRET signal ($BRET_{MAX}$) and is indicative of the propensity of the protein pair to interact (Kobayashi *et al.*, 2009; Mercier *et al.*, 2002). The smaller the $BRET_{50}$, the stronger the interaction. Renilla luciferase II (RlucII) was fused at the N-terminus to wild-type Rab7A (RlucII-Rab7A). As previously shown, this tag had little effect on the distribution or function of Rab7A, as expressing RlucII-Rab7A in Rab7A-knockout cells (Rab7A-KO) rescued retromer recruitment (Modica *et al.*, 2017). The energy acceptor green fluorescent protein 10 (GFP10) was fused to the N-terminus of wild-type and various CLN3 mutants (GFP10-CLN3, GFP10-$CLN3^{R334H}$, GFP10-GFP10-$CLN3^{V330F}$, GFP10- GFP10-$CLN3^{E295K}$, GFP10-GFP10-$CLN3^{L101P}$). These mutations have been previously studied and were shown to localize to late endosomes/ lysosomes similarly to wild-type CLN3 (Haskell *et al.*, 2000). We engineered a CLN3 mutant harbouring the common exon 7 and 8 deletion ($CLN3^{\Delta ex7/8}$), but we could not efficiently express this protein in our lab. HeLa cells were co-transfected with a constant amount of RlucII-Rab7A and increasing amounts of GFP10-CLN3 to generate BRET titration curves. The BRET signal between RlucII-Rab7A and GFP10-CLN3 rapidly increased with increasing amounts of expressed GFP10-CLN3 until it reached saturation, suggesting a specific interaction (Fig. 2.1A, blue curve). We also tested another Rab GTPase, Rab1a, which is localized to the Golgi (Dumaresq-Doiron *et al.*, 2010), to confirm the specificity of the CLN3–Rab7A interaction. We generated BRET titration curves with

RlucII-Rab1a (Fig. 2.1A, red curve) in HeLa cells. We extrapolated the $BRET_{50}$ for the interaction between CLN3 and the two Rab GTPases and found that the Rab7A–CLN3 interaction had a much smaller $BRET_{50}$ (0.004) compared with the value (0.020) for the Rab1a–CLN3 interaction, indicating that Rab7A has a higher propensity to interact with CLN3 compared with Rab1a (Fig. 2.1B). A small fraction of CLN3 localizes to the Golgi (Cao *et al.*, 2006), hence we were not surprised to detect an interaction between CLN3 and Rab1a. Next, we tested the interaction between CLN3 and $Rab7A^{C205,207S}$ which is a mutant form of Rab7A that cannot be recruited to membranes owing to its lack of prenylation (Modica *et al.*, 2017). We found no interaction between $Rab7A^{C205,207S}$ and CLN3 (Fig. 2.1A, green line). Finally, we tested if the small GTPase Arf6 can interact with CLN3 (Fig. 2.1A, orange line) and found no interaction, indicating that the signal we observed between Rab7a and CLN3 is due to a specific interaction between the two proteins.We next performed a BRET experiment to determine the impact of CLN3 disease-causing mutations on the CLN3–Rab7A interaction (Fig. 2.1C). Compared with wild-type CLN3, we found a significantly stronger (smaller $BRET_{50}$) interaction between Rab7A and $CLN3^{R334H}$ or $CLN3^{V330F}$ (Fig. 2.1D), whereas the $CLN3^{E295K}$ and $CLN3^{L101P}$ mutations had negligible effects on the CLN3–Rab7A interaction (Fig. 2.1D). To confirm our BRET data, we tested these interactions via co-immunoprecipitation (co-IP). We expressed FLAG-tagged wild-type CLN3 and the various CLN3 mutants in HeLa cells, immunoprecipitated the various forms of CLN3 with anti-FLAG antibody and blotted for endogenous Rab7A. By co-IP, we confirmed the CLN3–Rab7A interaction and found that only $CLN3^{L101P}$ did not interact with Rab7A (Fig. 2.8A).

Mutations in CLN5, which interacts with CLN3, cause a form of NCL with overlapping symptoms to CLN3 disease (Vesa *et al.*, 2002). In our previous work, we showed that CLN5 interacts with sortilin (also known as SORT1) (Mamo *et al.*, 2012). Therefore, we rationalized that CLN3 could also interact with this lysosomal sorting receptor. To test this hypothesis, we performed a BRET experiment by expressing a constant amount of RlucII-tagged wildtype CLN3 (RlucII-CLN3) and increasing amounts of yellow fluorescence protein (YFP) tagged sortilin.We found an interaction between CLN3 and sortilin, as the curve reached saturation (Fig. 2.1E, blue curve). We next determined the impact CLN3 disease-causing mutations could have on this interaction. We generated BRET titration curves between sortilin-YFP and RlucII-$CLN3^{R334H}$ (Fig. 2.1E, red curve), RlucII-$CLN3^{V330F}$ (Fig. 2.1E, green curve), RlucII-$CLN3^{E295K}$ (Fig. 2.1E, black curve) and RlucII-$CLN3^{L101P}$ (Fig. 2.1E, purple curve). As a control, we used Sigma-1 receptor (S1R-YFP),

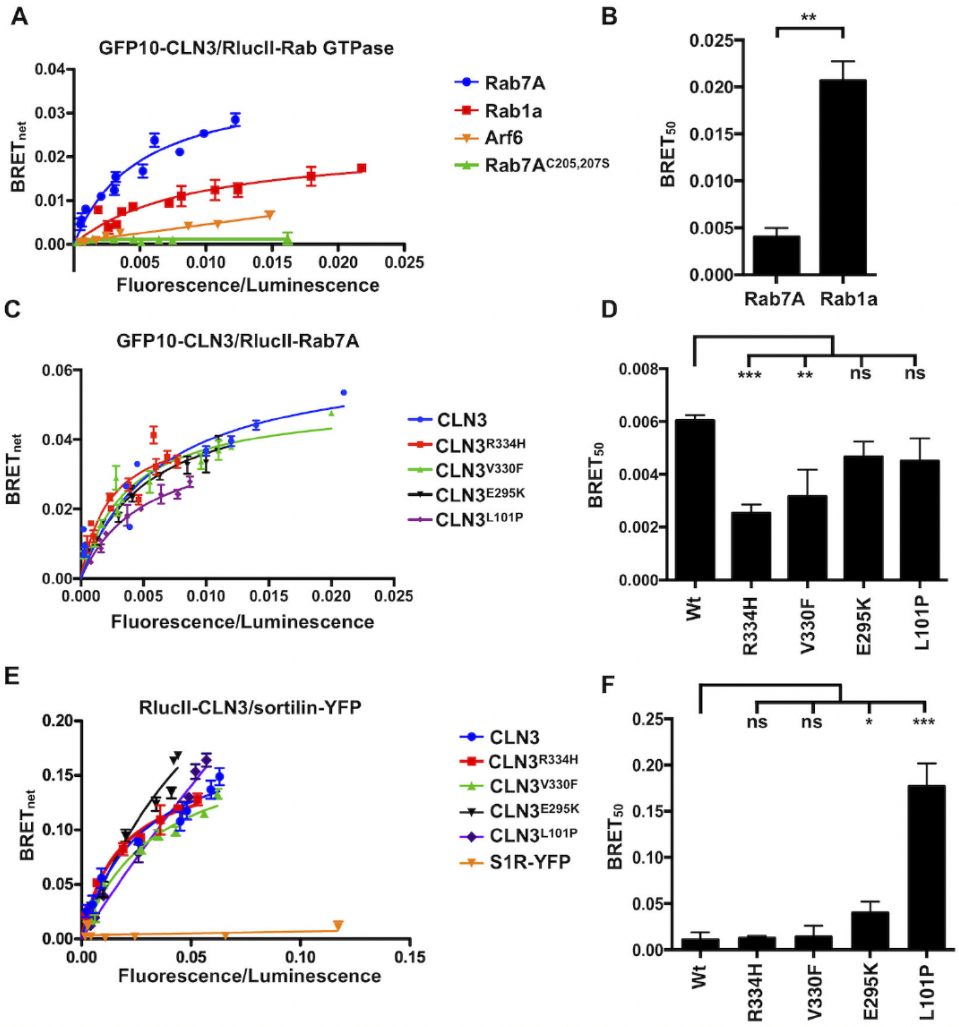

Figure 2.1: CLN3 interacts with Rab7A and sortilin.

(A) HeLa cells were transfected with a constant amount of RlucII-Rab7A (blue curve), RlucII-Rab1a (red curve), Arf6-RlucII (orange line) or RlucII-Rab7A^{C205,207S} (green line) and increasing amounts of GFP10-CLN3 to generate BRET titration curves. 48 h post-transfection, BRET analysis was performed. BRET signals are plotted as a function of the ratio between the GFP10 fluorescence over RlucII luminescence. (B) BRET$_{50}$ was extrapolated from three independent experiments. (C) HeLa cells were transfected with a constant amount of RlucII-Rab7A and increasing amounts of GFP10-CLN3, GFP10-CLN3^{R334H}, GFP10-CLN3^{V330F}, GFP10-CLN3^{E295K} or GFP10-CLN3^{L101P} to generate BRET titration curves. BRET$_{MAX}$, maximal BRET signal. (D) BRET$_{50}$ was extrapolated from three independent experiments. (E) HeLa cells were transfected with a constant amount of RlucII CLN3 or RlucII-CLN3 harbouring a disease-causing mutation and increasing amounts of sortilin-YFP or Sigma-1 receptor-YFP (S1R-YFP) to generate BRET titration curves. 48 h post-transfection, BRET analysis was performed. BRET signals are plotted as a function of the ratio between the YFP fluorescence over RlucII luminescence. (F) BRET$_{50}$ was extrapolated from three independent experiments. Data are mean±s.d.; ns, not significant; $^{*}P \leq 0.05$; $^{**}P \leq 0.01$; $^{***}P \leq 0.001$; two-way ANOVA followed by Tukey's *post hoc* test in D and F; Student's t-test in B.

a type I integral membrane protein also known as SIGMAR1 (Fig. 2.1E, orange line) (Prause *et al.*, 2013). We found no interaction between CLN3 and Sigma-1 receptor. Compared with wild-type CLN3, we found a significant increase in the BRET$_{50}$ values for the sortilin–CLN3^{E295K} and sortilin–CLN3^{L101P} interactions, suggesting weaker interactions (Fig. 2.1F). Interestingly,we found no change in the sortilin–CLN3^{R334H} and sortilin–CLN3^{V330F} interactions compared with

the sortilin– CLN3 interaction (Fig. 2.1F). To confirm these BRET results by co-IP, we expressed FLAG-tagged wild-type CLN3 and the various CLN3 mutants in HeLa cells, immunoprecipitated the various forms of CLN3 with anti-FLAG antibody, and blotted for endogenous sortilin. We found that $CLN3^{L101P}$ had a significant negative impact on the CLN3– sortilin, which is consistent with our BRET data (Fig. 2.8A).

2.2.2 CLN3 is not required for the steady-state membrane distribution of Rab7A

A previous study had found that Rab7A immunofluorescence staining was decreased in cells harbouring the homozygous mutation ($CLN3^{\Delta ex7/8}$/$CLN3^{\Delta ex7/8}$) compared with wild-type cells (Fossale *et al.*, 2004). Based on this, we investigated whether CLN3 is required for the membrane recruitment of Rab7A by generating CLN3-KO HeLa cells using CRISPR/Cas9 (Fig. 2.9A). We also generated Rab7A-KO cells using the same parental HeLa strain to serve as a control in our experiments (Fig. 2.9B). Previous work has demonstrated that cells harbouring CLN3 mutations accumulate LC3II-positive autophagosomes (Fossale *et al.*, 2004; FVidal-Donet *et al.*, 2013). Soluble microtubule-associated protein 1A/1B-light chain 3 (LC3; also known as MAP1LC3B) forms LC3-II through lipidation upon activation of autophagy. LC3-II then localizes to autophagosomal membranes and remains there until autophagosomes fuse with lysosomes, resulting in its degradation (Ganley *et al.*, 2011). If autophagosome–lysosome fusion is inhibited, or if lysosomal function is blocked, either by a compound such as bafilomycin A1 (BafA1) or a defective protein, degradation of LC3-II cannot occur. Therefore, comparing the turnover of LC3-II levels is a good measure of autophagic activity and competence. To test if our CLN3-KO cells behaved as expected with respect to autophagy, we initiated autophagy through nutrient starvation by incubating wild-type, CLN3-KO and Rab7A-KO cells in the presence or absence of BafA1. We found an increase in the LC3-II/total LC3 ratio in wildtype cells upon starvation compared with fed conditions, which was further increased in BafA1-treated cells (Fig. 2.9C,D) suggesting that wild-type HeLa cells could initiate LC3 recruitment and degrade it, unless lysosomal function was inhibited pharmacologically. Next, we used Rab7A-KO HeLa cells as a control group, since without Rab7A, we would expect defects in LC3 degradation and therefore a higher ratio of LC3-II/total LC3 (Fig. 2.9C,D). As expected, we found a higher basal level of LC3-II/total LC3 levels, which increased upon the induction of autophagy. The addition of BafA1 did not increase this ratio (Fig. 2.9C,D), suggesting a defect in late stages of autophagy in Rab7A-KO cells as expected. In CLN3-KO HeLa cells, we

observed a higher LC3-II/total LC3 ratio compared with wild-type cells. Much like Rab7A-KO cells, the LC3-II/Total LC3 ratio increased in starvation conditions, and was not increased further by BafA1 treatment (Fig. 2.9C,D). Overall, our data from the CLN3-KO HeLa cells support previously published results suggesting that cells lacking CLN3 are defective in late stages of autophagy. Combined with our sequencing data, this confirms ablation of CLN3 in this cell line.

To determine if CLN3 is required for the membrane recruitment of Rab7A, we performed a membrane isolation technique that we have used previously (Mamo *et al.*, 2012; Modica *et al.*, 2017), in wild-type, CLN3-KO and CLN3-KO HeLa cells expressing FLAG-CLN3 (Fig. 2.2A). Our membrane separation was successful, as the integral membrane protein Lamp2 was found in the pellet fraction (P), while the cytosolic protein tubulin was found in the supernatant fraction (S) (Fig. 2.2A). Quantification of 5 independent experiments showed that Rab7A was not significantly displaced from membranes to the cytosolic fraction in CLN3-KO HeLa cells compared with wild-type HeLa cells, while the expression of Flag-CLN3 in CLN3-KO cells did not affect this phenotype (Fig. 2.2B). The small GTPase Rab7A regulates the spatiotemporal recruitment of retromer (Rojas *et al.*, 2008; Seaman, 2009), a protein complex required for efficient endosome-to-TGN traffic of cation-independent mannose 6-phosphate receptor (CI-MPR; also known as IGF2R) and sortilin (Arighi *et al.*, 2004; Canuel *et al.*, 2008; Seaman, 2004). In cells lacking retromer, these receptors do not efficiently recycle to the TGN, accumulate at late endosomes and are subsequently degraded in lysosomes (Seaman, 2004). However, in Rab7A-depleted cells, CI-MPR was not efficiently recycled to the TGN, but was not degraded either (Rojas *et al.*, 2008). We repeated the membrane assay as above, but we included Rab7A-KO HeLa cells as a control, as we previously demonstrated a reduction of retromer recruitment in Rab7A-KO HEK293 cells (Modica *et al.*, 2017). Lamp2 and tubulin were used as markers of membrane (P) and cytosolic fractions (S), respectively (Fig. 2.2C). Compared with wild-type HeLa cells, we observed a significant decrease in retromer recruitment (as detected by staining with the retromer subunit Vps26A) in Rab7A-KO HeLa cells, but we did not observe any significant changes in CLN3-KO cells (Fig. 2.2C). Quantification from 3 independent experiments found no changes in the membrane distribution of retromer in CLN3-KO and CLN3-KO cells expressing FLAG-CLN3 compared with wild-type cells (Fig. 2.2D). However, we found a 26% increase of retromer in the supernatant (cytosolic fraction) of Rab7A-KO cells compared with wild-type cells (Fig. 2.2D), which is comparable to other previously published studies (Mamo *et al.*, 2012; Seaman, 2009).

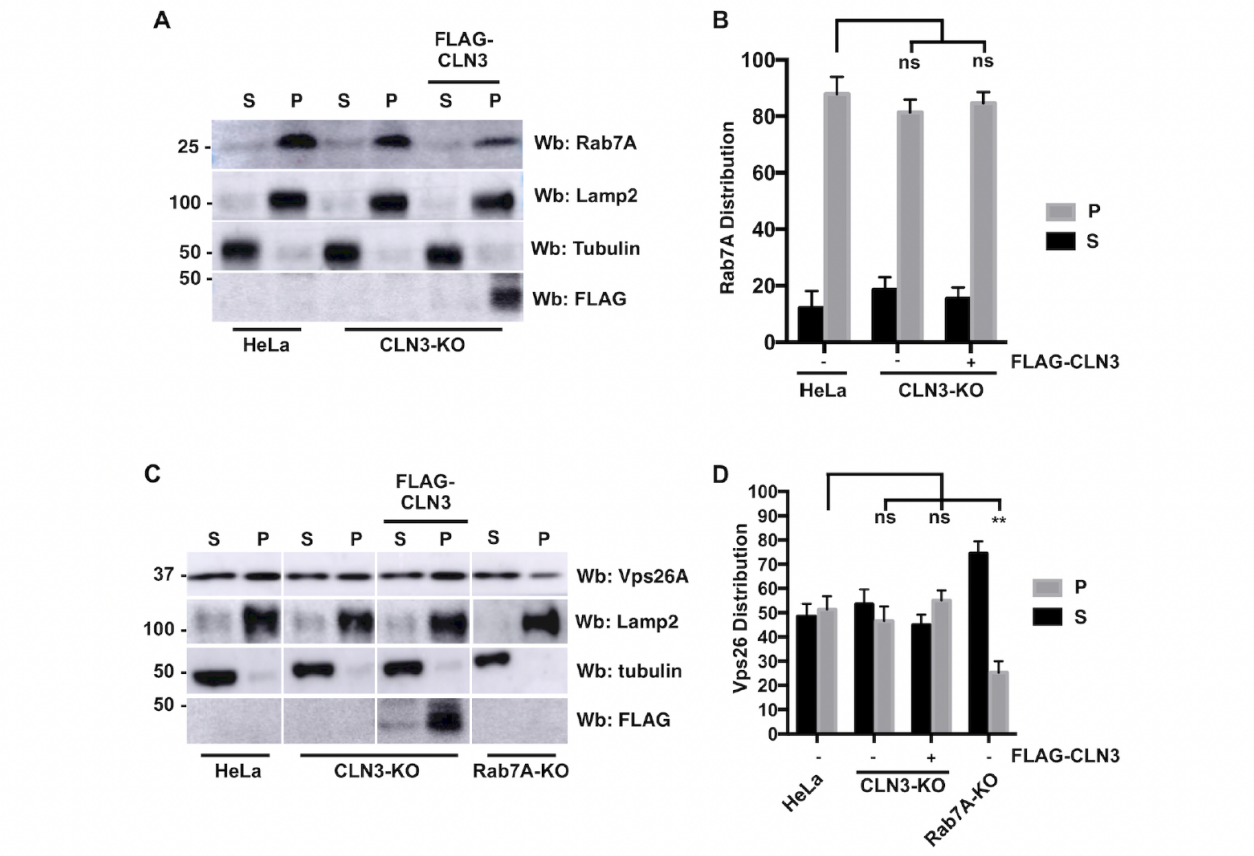

Figure 2.2: CLN3 is not required for the recruitment of Rab7A to membrane.

(A) Wild-type, CLN3-KO and FLAG-CLN3 expressing CLN3-KO HeLa cells were collected for membrane isolation assay. Samples were subjected to western blotting with anti-Rab7A antibody, anti-Lamp2 antibody (a marker for the membrane fraction) and anti-tubulin antibody (a marker for the cytosolic fraction). Anti FLAG staining shows the expression of wild-type CLN3 rescue. S, supernatant, P, pellet. (B) Quantification of 5 separate membrane isolation assay experiments. (C) Wild-type, CLN3-KO, FLAG-CLN3 expressing CLN3-KO and Rab7A-KO HeLa cells were collected for a membrane isolation assay. After the isolation, samples were subjected to western blotting with anti-Vps26A antibody (a retromer subunit), anti-Lamp2 antibody and anti-tubulin antibody. Anti-FLAG staining shows expression of wild-type CLN3. S, supernatant, P, pellet. (D) Quantification of 5 separate membrane isolation assay experiments. Data in B and D are mean±s.d. ns, not significant; $^{**}P \leq 0.01$; two-way ANOVA followed by Tukey's *post hoc* test.

2.2.3 CLN3 is required for efficient retromer interactions

Although we found no defects in the membrane distribution of retromer in CLN3-KO cells, we wondered if we could observe other changes. Rab7A interacts with retromer, which is required for the spatiotemporal recruitment of the latter. We tested whether or not the interaction between Rab7A and retromer is affected in CLN3- KO cells. We have previously used BRET to study the Rab7A–Vps26A interaction (Modica *et al.*, 2017). This interaction is specific as Rab7A did not interact with AP-1 subunits (a clathrin adaptor that has been localized to both the TGN and endosomes), whereas Vps26A did not interact with Rab1a (Modica *et al.*, 2017). First, we investigated whether Vps26A-GFP10 could be part of the retromer trimer. We found that endogenous Vps35 could

coimmunoprecipitate with both wild-type Vps26A and Vps26A-GFP10, suggesting the GFP10-tagged protein could be included in the retromer trimer (Fig. 2.10A). Next, we generated BRET titration curves between RlucII-Rab7A and Vps26A-GFP10 in wild-type (blue curve) and CLN3-KO (red curve) HeLa cells (Fig. 2.3A). Compared with wild-type HeLa cells, we found a two fold increase in the $BRET_{50}$ values for Rab7A binding to Vps26A in CLN3-KO cells, suggesting a weaker interaction (Fig. 2.3B). As a control, we tested the Rab1a–Vps26A interaction in HeLa cells. We found no interaction between Rab1a and Vps26A in wild-type HeLa cells (Fig. 2.3A, green line). We previously demonstrated that the retromer–Rab7A interaction requires the palmitoylation of Rab7A (Modica *et al.*, 2017). We tested whether the palmitoylation level of Rab7A was lower in CLN3-KO versus wild-type HeLa cells using Acyl-RAC, a technique to determine the palmitoylation status of a protein (Fig. 2.3C). Quantification of three separate Acyl-RAC assays found no significant change in the level of palmitoylation of Rab7A in CLN3-KO cells compared with wild-type HeLa cells (Fig. 2.3D). As we observed no changes in the palmitoylation level of Rab7A in CLN3-KO cells, we next tested if the GTP loading of Rab7A was affected in CLN3-KO, using a well-characterized FRET biosensor (Yasuda *et al.*, 2016). We found no differences in the GTP loading of Rab7A between wild-type and CLN3-KO HeLa cells (Fig. 2.3E), suggesting that CLN3 does not alter the GTP loading of Rab7A.

We next asked if CLN3 can interact with retromer. We generated BRET titration curves using RlucII-CLN3 and Vps26A-GFP10 (Fig. 2.4A, blue curve). As a control, we tested whether or not retromer can interact with ABCD4, a multi-spanning integral membrane protein localized to endolysosomes (Coelho *et al.*, 2012). We identified an interaction between CLN3 and retromer (Fig, 4A, blue curve), but not between ABCD4 and retromer (Fig. 2.4A, orange line). Although the signal increases rapidly, suggesting numerous random collisions, the signal does not saturate, suggesting no interaction. The $CLN3^{R334H}$ (Fig. 2.4A, red curve) and $CLN3^{E295K}$(Fig. 2.4A, black curve) mutations had no impact on this interaction (Fig. 2.4B). Interestingly, the $CLN3^{V330F}$ (Fig. 2.4A, green curve) increased the propensity of CLN3 to interact with retromer, whereas the $CLN3^{L101P}$ mutation (Fig. 2.4A, purple curve), significantly weakened the interaction (Fig. 2.4B). We again used coimmunoprecipitation to confirm these BRET results and found that endogenous Vps26A was able to efficiently interact with all forms of FLAG-tagged CLN3 except $CLN3^{L101P}$, confirming our BRET data (Fig. 2.8A).

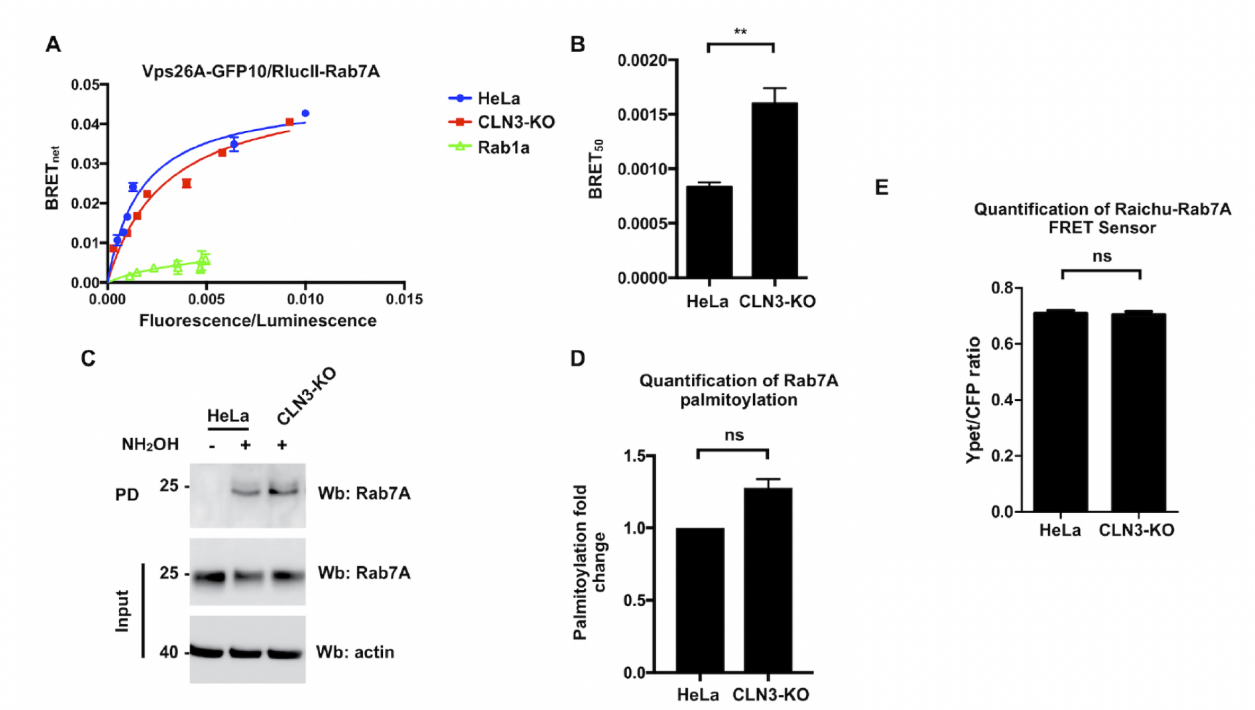

Figure 2.3: CLN3 is required for the efficient interaction of Rab7A with retromer.

(A) Wild-type and CLN3-KO HeLa cells were transfected with a constant amount of RlucII-Rab7A and increasing amounts of Vps26A-GFP10 to generate BRET titration curves. Wild-type HeLa cells were also transfected with RlucII-Rab1a and Vps26A-GFP10 to generate BRET titration curves. BRET analysis was performed 48 h post-transfection. BRET signals are plotted as a function of the ratio between the GFP10 fluorescence over RlucII luminescence. (B) $BRET_{50}$ was extrapolated from 3 independent experiments. (C) Wild-type and CLN3-KO HeLa cell lysates were collected and subjected to Acyl-RAC analysis to determine the palmitoylation status of Rab7A. NH2OH: Hydroxylamine. (D) Quantification of 3 separate Acyl-RAC assay experiments. (E) Wild-type and CLN3-KO HeLa cells were transfected with the FRET sensor, Raichu-Rab7A. Quantification of 4 separate experiments are shown. Data in B, D and E are mean±s.d. ns, not significant; $^{**}P \leq 0.01$; Student's t-test.

We next aimed to determine if the CLN3–retromer interaction was dependent on Rab7A. We generated BRET titration curves between RlucII-CLN3 and Vps26A-GFP10 in wild-type (Fig. 2.4C, black curve) and Rab7A-KO (Fig. 2.4C, blue curve) HeLa cells. We found a significantly weaker CLN3–retromer interaction in Rab7A-KO compared with wild-type HeLa cells. CI-MPR and sortilin are known to interact with retromer, which is necessary for their endosome-to- TGN trafficking (Arighi *et al.*, 2004; Canuel *et al.*, 2008). Using BRET, we confirmed this interaction using Vps26A conjugated to nano-Luciferase (Vps26A-nLuc) and sortilin-YFP (Fig. 2.4E, black curve). As expected, the sortilin–retromer interaction was significantly weaker in Rab7A-KO cells compared with wild-type HeLa cells (Fig. 2.4F, red curve). We next tested the interaction in CLN3-KO HeLa cells to determine if CLN3 played a role in this interaction (Fig. 2.4E, blue curve). We found a significantly weakened interaction between retromer and sortilin in CLN3-KO cells compared with wild-type HeLa cells (Fig. 2.4F). We confirmed these BRET results using co-immunoprecipitation

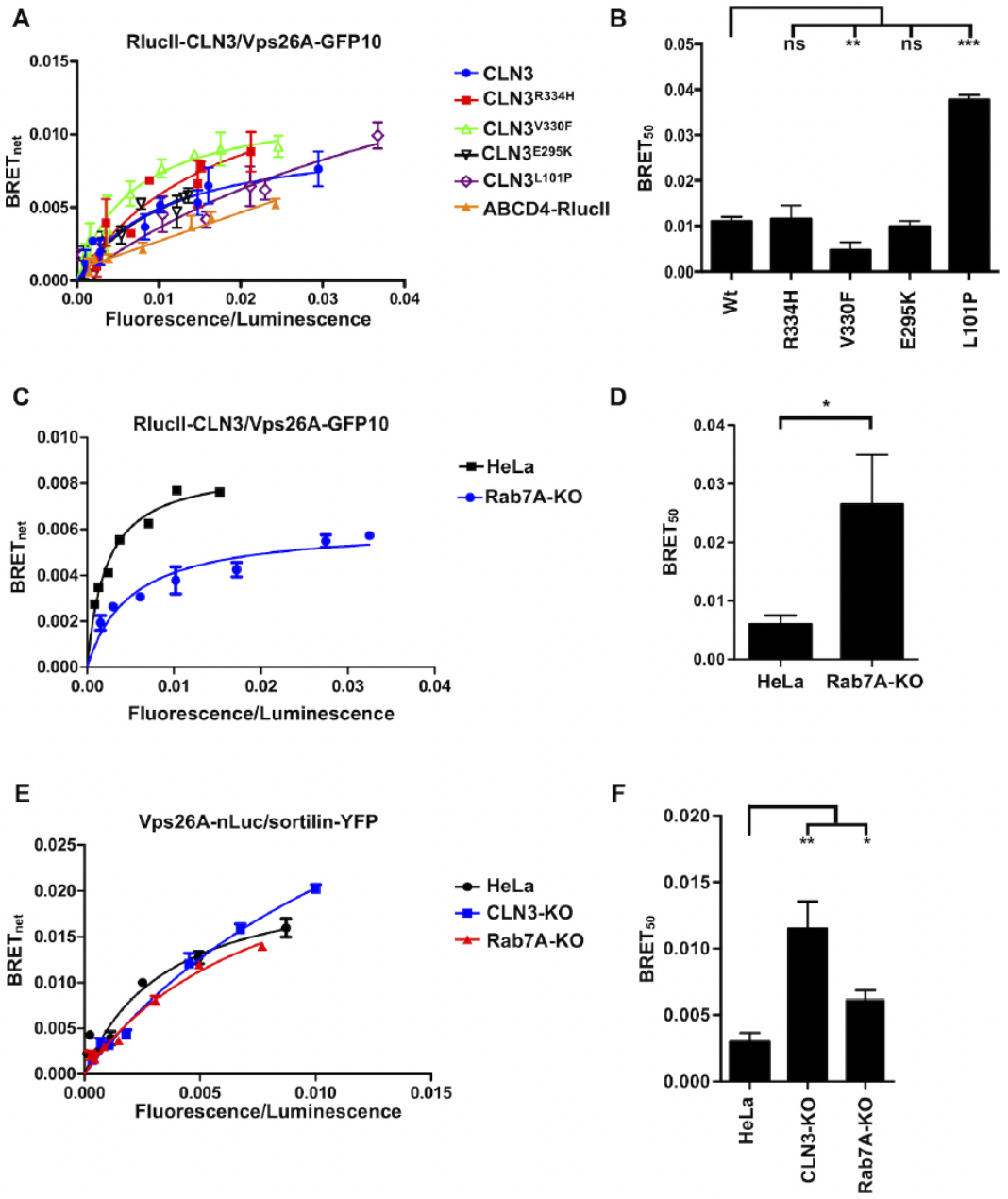

Figure 2.4: CLN3 interacts with retromer and modulates the sortilin–retromer interaction.

(A) HeLa cells were transfected with a constant amount of RlucII-CLN3, RlucII-CLN3 harbouring a disease-causing mutation or ABCD4-RlucII and increasing amounts of Vps26A-GFP10 to generate BRET titration curves. BRET analysis was performed 48 h post-transfection. BRET signals are plotted as a function of the ratio between the GFP10 fluorescence over RlucII luminescence. (B) $BRET_{50}$ was extrapolated from 3 independent experiments. (C)Wild-type and Rab7A-KO HeLa cells were transfected with a constant amount of RlucII-CLN3 and increasing amounts of Vps26A-GFP10 to generate BRET titration curves. 48 h post-transfection BRET analysis was performed. BRET signals are plotted as a function of the ratio between the GFP10 fluorescence over RlucII luminescence. (D) $BRET_{50}$ was extrapolated from 4 independent experiments (E)Wild-type, CLN3-KO and Rab7A-KO HeLa cells were transfected with a constant amount of Vps26A-nLuc and increasing amounts of sortilin-YFP to generate BRET titration curves. BRET analysis was performed 48 h post-transfection. BRET signals are plotted as a function of the ratio between the YFP fluorescence over nLuc luminescence. (F) $BRET_{50}$ was extrapolated from 3 independent experiments. Data are mean±s.d. ns, not significant; $*P \leq 0.05$; $**P \leq 0.01$; two-way ANOVA followed by Tukey's *post hoc* test in B and F; Student's t-test in D.

and found that endogenous Vps26A did not interact as efficiently with endogenous sortilin in CLN3-KO HeLa cells compared with wild-type cells (Fig. 2.10B).

2.2.4 CLN3 regulates the stability of sortilin and CI-MPR

Since we observed a weaker retromer–sortilin interaction in CLN3-KO cells and retromer is required for the efficient endosome-to- TGN trafficking of CI-MPR and sortilin (Arighi *et al.*, 2004; Canuel *et al.*, 2008), we wanted to determine if lysosomal sorting receptor recycling is regulated by CLN3. In cells depleted of retromer, CI-MPR and sortilin are degraded in lysosomes rather than recycled back to the TGN (Arighi *et al.*, 2004). We performed a cycloheximide chase experiment to determine receptor stability as we have previously done (Mamo *et al.*, 2012; McCormick *et al.*, 2008). Wild-type, CLN3-KO and Rab7A-KO HeLa cells were incubated with serum-free medium containing 50 μg/ml cycloheximide and collected after 0, 3, and 6 h of incubation. Western blot analysis shows decreased levels of sortilin and CI-MPR in CLN3-KO HeLa cells compared with Rab7A-KO and wild-type HeLa cells (Fig. 2.11A). Transfecting FLAG-CLN3 in CLN3-KO cells rescued this phenotype (Fig. 2.11A). Actin staining was used as a loading control, while FLAG staining was used to demonstrate the expression level of FLAG-tagged CLN3 constructs.

Compared with wild-type cells, which had 92% and 88% of sortilin remaining (Fig. 2.5A) and 100% and 95% CI-MPR remaining (Fig. 2.5B) at 3 and 6 h, sortilin and CI-MPR were significantly degraded in CLN3-KO cells as they had only 30% and 19% of sortilin (Fig. 2.5A), and 37% and 8% of CI-MPR (Fig. 2.5B) remaining after 3 and 6 h. Expression of FLAG-CLN3 in CLN3-KO cells rescued the stability and hence recycling of sortilin (Fig. 2.5A) and CI-MPR (Fig. 2.5B) as they were no longer degraded and had protein levels remaining that were similar to levels in wild-type HeLa cells with 74% and 85% and 94% and 95% remaining, respectively, at 3 and 6 h. The amount of sortilin and CI-MPR remaining in Rab7A-KO cells (89% and 85%, and 76% and 80% remaining, respectively, after 3 and 6 h) was comparable to wild-type levels (Fig. 2.5A,B), as although endosome-to-TGN trafficking is affected, degradation is also blocked. Next, we sought to determine the effects of CLN3 mutations known to cause human disease on the stability of these two cargo receptors. We expressed FLAG-CLN3^{R334H}, FLAG-CLN3^{V330F}, FLAG-CLN3^{E295K} and FLAG-CLN3^{L101P} in CLN3-KO HeLa cells (Fig. 2.11B). At 48 h post-transfection, a cycloheximide chase was performed as above and total cell lysate was collected. Western blotting with anti-FLAG

antibody was used to indicate the expression level of the various expressed proteins, and anti-actin staining was used as a loading control. Although degradation of sortilin and CI-MPR was not as robust as in CLN3-KO HeLa cells, the receptors were significantly degraded in cells expressing $CLN3^{V330F}$ (74% and 42% of sortilin and 28% and 25% of CI-MPR remaining after 3 and 6 h), $CLN3^{E295K}$ (51% and 51% of sortilin and 57% and 31% of CI-MPR remaining after 3 and 6 h) and $CLN3^{L101P}$ (35% and 44% of sortilin and 53% and 30% of CI-MPR remaining after 3 and 6 h) compared with wild-type cells (Fig. 2.5A,B). Interestingly, $CLN3^{R334H}$ was able to rescue the phenotype (82% remaining at 3 h) for sortilin (Fig. 2.5A), at a level not statistically different from that in wild-type cells, but it only partially rescued sortilin degradation at 6 h (70% remaining). Expression of $CLN3^{R334H}$ was not able to fully rescue CI-MPR (55% and 45% remaining at 3 and 6 h) (Fig. 2.5B). Overall, it appears that CLN3 proteins harbouring disease-causing mutations retain some function as they were able to partially rescue sortilin and CI-MPR degradation. However, they could not rescue as efficiently as wild-type CLN3, and degradation of the two lysosomal sorting receptors was significant in cells expressing CLN3 harbouring disease-causing mutations compared with wildtype cells.

Cathepsin D (also known as CTSD) is a lysosomal hydrolase whose trafficking to lysosomes is mediated by CI-MPR. Disruption of CI-MPR trafficking by depleting cells of retromer subunits or Rab7A using RNAi leads to inefficient processing of cathepsin D, resulting in the accumulation of pro and intermediate forms of the protein, and a reduction of the mature lysosomal form (Rojas *et al.*, 2008; Seaman, 2004). Since we observed the degradation of CI-MPR and sortilin in CLN3-KO HeLa cells, we aimed to determine if this had an impact on the processing of cathepsin D (Fig. 2.5C). Compared with wild-type HeLa cells, which had 7.3% pro and 5.6% intermediate cathepsin D, CLN3-KO and Rab7A-KO HeLa cells had increased levels of pro-cathepsin D (28.3% and 42.3% respectively) and intermediate cathepsin D (11.6% and 26.6% respectively). On the other hand, CLN3-KO and Rab7A-KO HeLa cells had a reduction of mature cathepsin D (60% and 30.6% respectively) compared with wild-type HeLa cells, which had 87% mature form (Fig. 2.5D).

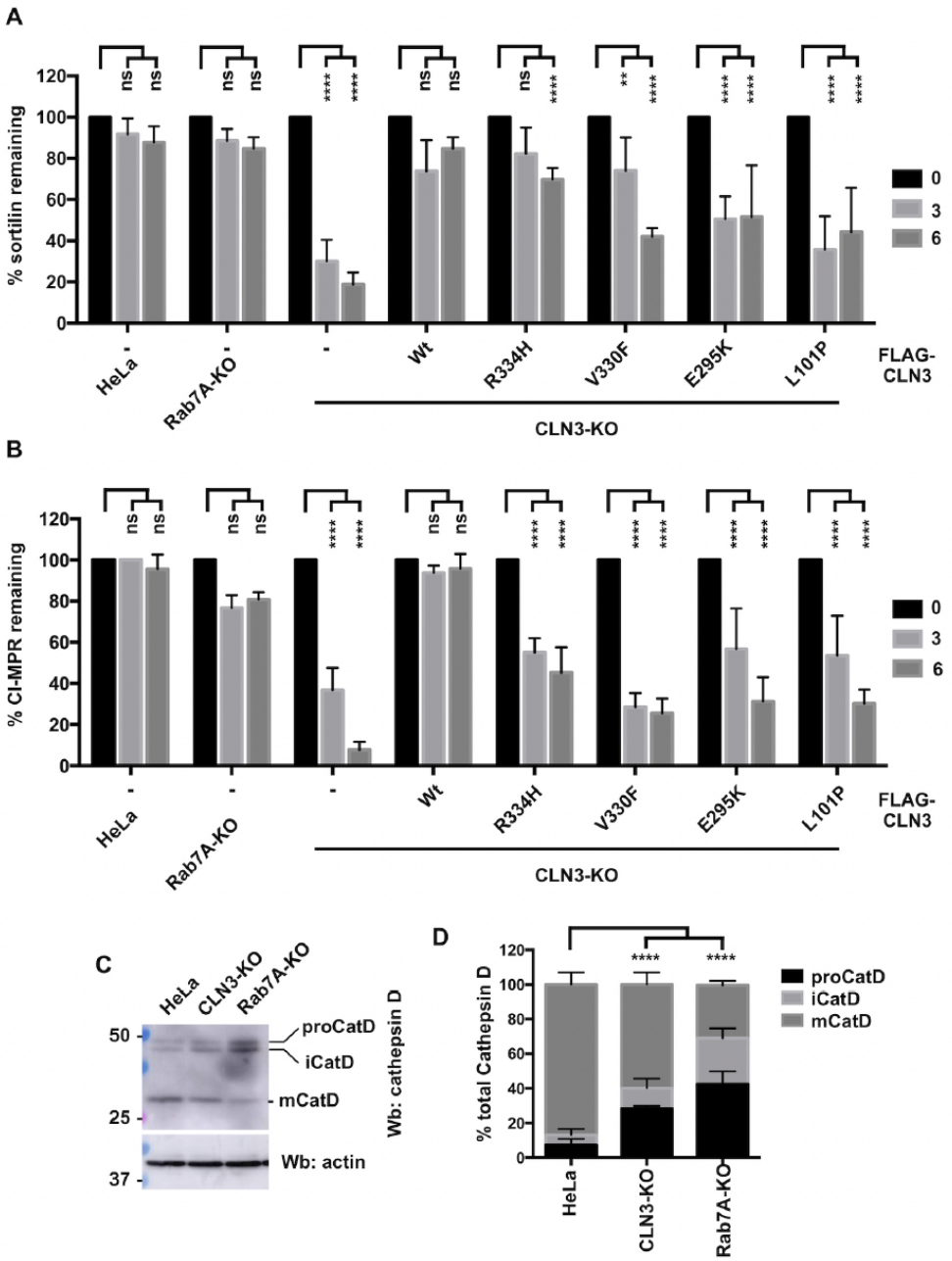

Figure 2.5: CLN3 regulates the stability of sortilin and CI-MPR.

(A) Wild-type, Rab7A-KO, CLN3-KO or CLN3-KO HeLa cells expressing wild-type or mutant FLAG-CLN3 as indicated, were incubated with 50 μg/ml cycloheximide in serum-free medium for 0, 3, or 6 h. Quantification of 5 separate experiments (sample blots are shown in Fig. 2.11) of sortilin remaining is plotted. (B) Wild-type, Rab7A-KO, CLN3-KO or CLN3-KO expressing wild-type or mutant FLAG-CLN3 as indicated were incubated with 50 μg/ml cycloheximide in serum-free media for 0, 3, or 6 h. Quantification of 5 separate experiments (sample blots are shown in Fig. 2.11) of CI-MPR remaining at 6 h in each group. (C) Whole cell lysate from wild-type and CLN3-KO HeLa cells was resolved by 12% SDS-PAGE. Western blotting was performed using anti-cathepsin D and anti-actin antibodies. (D) Quantification of pro-cathepsin D (proCatD, 53 kDa), intermediate cathepsin D (iCatD, 48 kDa) and mature cathepsin D (mCatD, 31 kDa). The amount of each is expressed as a percentage of total cathepsin D. Data in A, B and D are mean±s.d.; ns, not significant; $^{**}P \leq 0.01$,$^{****}P \leq 0.0001$, two-way ANOVA followed by Tukey's *post hoc* test.

2.2.5 CLN3 is required for the efficient degradation of proteins following internalization

Upon EGF stimulation, EGF receptor (EGFR) is internalized and can be either recycled to the cell surface or degraded in lysosomes (Ceresa & Peterson, 2014). Rab7A is a key regulator of the degradative pathway mediating the later steps of this process (Vanlandingham & Ceresa, 2009). At least two Rab7A effectors have been implicated in EGFR degradation, RILP and PLEKHM1. Indeed, depletion of either of these proteins results in significant delays in the degradation kinetics of EGFR (Marwaha *et al.*, 2017; McEwan *et al.*, 2014; Progida *et al.*, 2007). In order to determine whether CLN3 modulates this Rab7A pathway, we investigated the degradation kinetics of EGFR in wild-type, CLN3-KO and Rab7A-KO HeLa cells. Wild-type, CLN3-KO and Rab7A-KO HeLa cells were serum starved for 1 h in the presence of cycloheximide and then stimulated with 100 ng/ml EGF in the presence of cycloheximide for the indicated periods of time. The level of endogenous EGFR was determined by western blotting and anti-actin staining was used as a control (Fig. 2.6A). In wild-type cells, EGFR degradation was observed after 10 min and quantification of 5 independent experiments found substantial degradation at 15 (35% remaining), 30 (21% remaining) and 120 min (6% remaining) (Fig. 2.6B). As expected, Rab7A-KO cells had significantly delayed degradation compared with wild-type cells at most indicated time points with 82% and 76% remaining at 10 and 15 min. However, in the Rab7A-KO HeLa cells, EGFR was degraded at 30 and 120 min (Fig. 2.6B). When we compared the degradation kinetics of EGFR in CLN3-KO cells, we found significant delays at 10 (99% remaining), 15 (97% remaining) and 30 min (77% remaining) compared with wild-type cells, with no significant difference at 120 min (Fig. 2.6B). The delayed degradation kinetics between Rab7A-KO and CLN3-KO was similar at 5, 10, 15 and 120 min, while the CLN3-KO cells contained significantly more EGFR at 30 min than Rab7A-KO HeLa cells.

Next, we tested the degradation kinetics of Alexa Fluor 488- labelled EGF (EGF-488) using the same cell lines to confirm our EGFR degradation result. Following 2 h of serum starvation, cells were incubated with 300 ng/ml EGF-488 for 30 min, washed and then chased for 0 or 30 min (Fig. 2.6C). Images were acquired at random from the 4 different conditions and the number of EGF-488 puncta from 50 cells per condition were counted using ImageJ. At time zero, both wild-type and CLN3-KO HeLa cells had comparable numbers of EGF-488 puncta (an average of 12.57 versus 12.08, respectively). After 30 min of chase, wild-type HeLa cells had an average of 2.6 puncta per cell, whereas CLN3-KO HeLa cells had more than double this, with an average of 8.2 puncta per

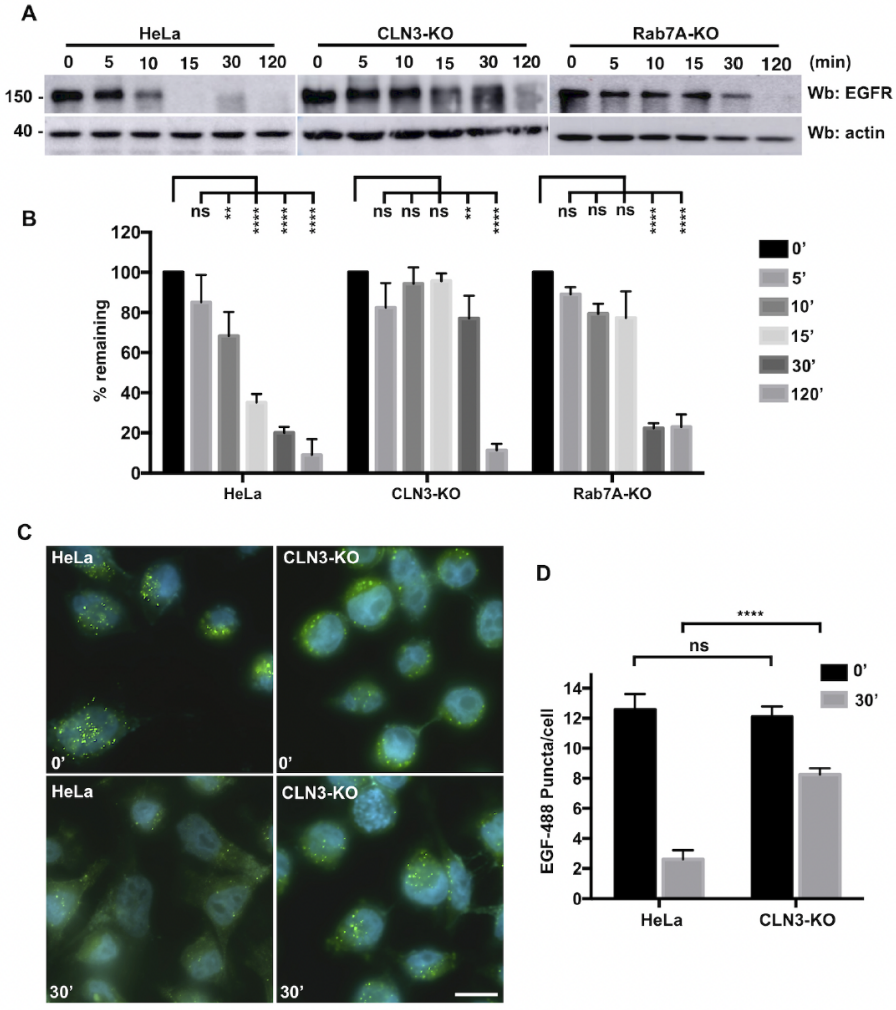

Figure 2.6: CLN3 is required for EGFR degradation.

(A) Wild-type, CLN3-KO and Rab7A-KO HeLa cells were incubated with 50 μg/ml cycloheximide for 1 h and subsequently treated with 100 ng/ml EGF in Opti-MEM for 0, 5, 10, 15, 30 and 120 min. Whole cell lysatewas then resolved by SDS-PAGE and awestern blot was performed using anti-EGFR antibody. Anti-actin staining was used as a loading control. (B) Quantification of the remaining EGFR as detected in A was performed in 5 independent experiments. (C) Wild-type and CLN3-KO HeLa cells were grown on coverslips and incubated with 300 ng/ml EGF-488 for 0 or 30 min. The cells were fixed with 4% PFA for 12 min, followed by staining with DAPI to visualize the nucleus. Images were taken on a Zeiss Fluorescence microscope using a 63× objective. (D) EGF-488 (green puncta) were counted using ImageJ in 50 cells per condition. The results shown are the average number of puncta per cell per condition. Data in B and D are mean±s.d. ns, not significant; $^{**}P \leq 0.01$, $^{****}P \leq 0.0001$; two-way ANOVA followed by Tukey's *post hoc* test. Scale bar: 10 μm.

cell (Fig. 2.6D). The delayed degradation kinetics observed in the CLN3-KO cells can be explained by decreased lysosomal function as a result of defective endosome-to-TGN trafficking, or it could be that EGF and EGFR do not reach the lysosomes efficiently owing to a lack of fusion.

In order to understand the mechanism behind the delayed EGFR degradation, we used BRET to determine if the Rab7A–RILP, Rab7A–PLEKHM1 and/or Rab7A–FYCO1 interactions were affected (Fig. 2.7A–F). FYCO1 is a Rab7A effector required for anterograde traffic of vesicles (Pankiv

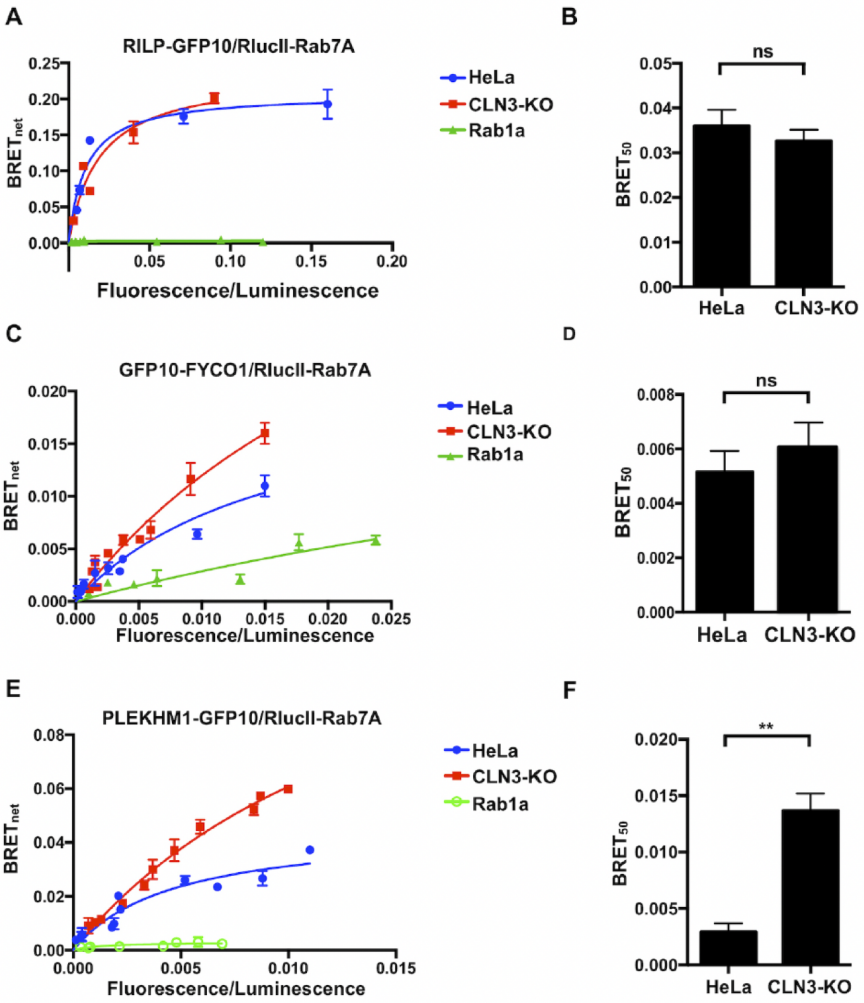

Figure 2.7: CLN3 regulates endocytic degradation by modulating the Rab7A– PLEKHM1 interaction.

(A) Wild-type and CLN3-KO HeLa cells were transfected with a constant amount of RlucII-Rab7A and increasing amounts of RILP-GFP10 to generate BRET titration curves. RlucII-Rab1a was also used in wild-type cells as a control. BRET signals are plotted as a function of the ratio between the GFP10 fluorescence over RlucII luminescence. (B) $BRET_{50}$ was extrapolated from 3 independent experiments. (C) Wild-type and CLN3-KO HeLa cells were transfected with a constant amount of RlucII-Rab7A and increasing amounts of GFP10-FYCO1 to generate BRET titration curves. RlucII-Rab1a was also used in wild-type cells as a control. BRET signals are plotted as a function of the ratio between the GFP10 fluorescence over RlucII luminescence. (D) $BRET_{50}$ was extrapolated from 3 independent experiments. (E) Wildtype and CLN3-KO HeLa cells were transfected with a constant amount of RlucII-Rab7A and increasing amounts of PLEKHM1-GFP10 to generate BRET titration curves. RlucII-Rab1a was also used in wildtype cells as a control. BRET signals are plotted as a function of the ratio between the GFP10 fluorescence over RlucII luminescence. (F) $BRET_{50}$ was extrapolated from 3 independent experiments. Data in B, D and F are mean±s.d.; ns, not significant; $^{**}P \leq 0.01$; Student's t-test.

et al., 2010), while RILP and PLEKHM1 are implicated in membrane fusion and degradation (Marwaha *et al.*, 2017; McEwan *et al.*, 2014; Progida *et al.*, 2007). We found no significant change in the interaction between RILP and Rab7A (Fig. 2.7A,B) or FYCO1 and Rab7A (Fig. 2.7C,D) in either wild-type or CLN3-KO HeLa cells as shown by the $BRET_{50}$ values.We did find a change in the interaction between PLEKHM1 and Rab7A, as the $BRET_{50}$ value was 3.5-fold higher for

the Rab7A–PLEKHM1 interaction in CLN3-KO cells compared with wild-type cells, suggesting a weaker interaction (Fig. 2.7E,F). As a control, we tested if Rab1a could interact with the Rab7A effectors above. Rab1a did not interact with any of the Rab7A effectors (Fig. 2.7A,C,E, green line).

2.3 Discussion

CLN3 is an integral membrane protein localized to endosomes and lysosomes whose function has been implicated in intracellular trafficking and autophagy (Metcalf *et al.*, 2008; Chandrachud *et al.*, 2015; Oetjen *et al.*, 2016). Previous work using in vitro techniques had demonstrated an interaction between CLN3 and the small GTPase Rab7A (Uusi-Rauva *et al.*, 2012). We confirmed this interaction using BRET in live cells. Furthermore, we showed that two CLN3 mutations, $CLN3^{R334H}$ and $CLN3^{V330F}$, increased this interaction. This suggests that these two mutations could retain Rab7A on membranes longer or prevent its efficient cycling, a process required for optimal function. Interestingly, two other point mutations, $CLN3^{E295K}$ and $CLN3^{L101P}$, had no effect on this interaction. However, these two mutations weakened the CLN3– sortilin interaction. Combined with CLN3 being required for both the Rab7A–retromer and retromer–sortilin interactions, our data reveal a role for CLN3 in modulating retromer function. It is well established that defects in retromer function or sortilin affect cathepsin D sorting and processing (Arighi *et al.*, 2004; Canuel *et al.*, 2008). A previous publication demonstrated defects in the trafficking and processing of the lysosomal enzyme cathepsin D in $CLN3^{\Delta ex7/8}$/$CLN3^{\Delta ex7/8}$ cells (Fossale *et al.*, 2004). Ablation of CLN3 results in the lysosomal degradation of sortilin and CI-MPR, which is most likely due to deficient endosome-to-TGN trafficking of sortilin and CI-MPR. Furthermore, a recently published study using proteomics to determine the impact of CLN3 mutations on lysosomal content found a decrease in 28 lysosomal proteins, including cathepsin D and prosaposin (Mirza *et al.*, 2019). While the trafficking of cathepsin D to lysosomes is mediated by CI-MPR, prosaposin requires sortilin (Lefrancois *et al.*, 2003). Combined, CLN3 appears to play a crucial role in regulating lysosomal sorting and trafficking. As such, our results provide a molecular explanation to those previous observations.

Rab7A also plays a crucial role in the degradation of endocytic cargo such as EGFR (Vanlandingham & Ceresa, 2009).We found significant delays in the degradation of both EGFR and EGF in CLN3-KO cells. This could be explained in two ways. First, CLN3 is involved in the trafficking of

the lysosomal sorting receptor sortilin. Defects in trafficking of this protein, or defects in retromer function have been shown to have a significant impact on lysosome function (Arighi *et al.*, 2004; Lefrancois *et al.*, 2003; Seaman, 2004). Second, Rab7A is required for the fusion of endosomes and lysosomes, a process requiring RILP and PLEKHM1 (Marwaha *et al.*, 2017; McEwan *et al.*, 2014; Progida *et al.*, 2007). Although we found no change in the Rab7A–RILP interaction in CLN3-KO cells, we found a significant decrease in the Rab7A–PLEKHM1 interaction. This suggests defective fusion events. Combined with decreased lysosomal function, this could explain the significant delay in EGF and EGFR degradation. The Akt–mTOR pathway is upregulated in JNCL patient fibroblasts (FVidal-Donet *et al.*, 2013). EGFR is known to activate several signalling pathways, including Akt (Mattoon *et al.*, 2004). Dysregulated trafficking and degradation of EGFR can lead to increased signalling (Sorkin & von Zastrow, 2009). Our results could at least partially explain the upregulation of the Akt–mTOR pathway found in JNCL patient fibroblasts.

Autophagy is affected in CLN3-deficient cells (Chandrachud *et al.*, 2015; Chang *et al.*, 2011; FVidal-Donet *et al.*, 2013). Our CLN3-KO HeLa cells also show defective autophagy, similar to the defects observed in the Rab7A-KO. This suggests defects late in the autophagy pathway, possibly at the fusion step with lysosomes. PLEKHM1, among other factors, plays a critical role in modulating autophagosome fusion with lysosomes (McEwan *et al.*, 2014). Defects in this fusion machinery lead-to defective autophagy, but also delayed EGFR degradation kinetics. We propose that defects in autophagy observed in patients with JNCL could be due to defects in PLEKHM1 function, along with defects in lysosome function due to decreased sorting of sortilin and CI-MPR.

In conclusion, our results point to a role of CLN3 in the regulation of a subset of Rab7A functions. We have previously shown a similar role for CLN5, a soluble protein found within the lumen of endosomes and lysosomes (Mamo *et al.*, 2012). As CLN3 and CLN5 are known to interact, we speculate that the two proteins could function as a complex to regulate Rab7A and retromer function, demonstrating, at least partially, the molecular mechanisms deficient in JNCL.

2.4 Materials and Methods

2.4.1 Plasmids and mutagenesis

RlucII-CLN3 and GFP10-CLN3 were generated by amplifying CLN3 cDNA from FLAG-CLN3 (EX-Q0362-M12, Genecopoeia, Rockville, MD) and cloned into the EcoRV-XhoI and EcoRV-XbaI sites of pcDNA3.1Hygro(+)RlucII-GFP10-st2 and pcDNA3.1Hygro(+)GFP10-RlucII-st2 plasmids, respectively (a gift from Michel Bouvier, University de Montreal). To generate Vps26A-nLuc, Vps26A cDNA was obtained by PCR from Vps26A-YFP plasmid. pnLuc-N1 was generated by replacing the eYFP of pEYFP-N1 with nano-Luc (a gift from Regis Grailhe, Pasteur Institute Korea). Cloning was done after digestion of pnLuc-N1 plasmid with XhoI-HindIII restriction enzymes. PLEKHM1-GFP10 was engineered by inserting PLEKHM1 (Addgene plasmid #73592, deposited by Paul Odgren) into the NheI-EcoRV sites of pcDNA3.1 Hygro (+) GFP10-RLucII-st2. To generate GFP10-FYCOI, cDNA of FYCOI was obtained by PCR from mCherry-FYCOI (a gift from John H. Brumell, Sickkids Hospital) and cloned into the KpnI-XbaI sites of pcDNA3.1 Hygro (+) GFP10-RLucII. The various mutants were engineered using site-directed mutagenesis from the previously described FLAG-CLN3, GFP10 CLN3, RlucII-CLN3 constructs. Sortilin-YFP was a gift from Makoto Kanzaki, Tohoku University. Raichu-Rab7A was a gift from Takeshi Nakamura, Tokyo University of Science. RlucII-Rab7A, RlucII-Rab1a, Vps26AGFP10 and RILP-GFP10 were previously described (Modica et al., 2017).

2.4.2 Antibodies

The following mouse monoclonal antibodies were used: anti-actin (WB: 1:3000, BD Biosciences, 612657); anti-α-tubulin (WB: 1:1000, Sigma- Aldrich, T9026); anti-Lamp1 (WB: 1:500, Abcam ab25631); anti-CI-MPR (WB: 1 μg/ml, Serotec, MCA2048); anti-Cathepsin D (WB: 1:100, Sigma-Aldrich, IM03). The following rabbit monoclonal antibodies were used: anti-Rab7A (WB: 1:1000, Cell Signaling Technology D95F2); anti-EGFR (WB: 1:1000, Abcam ab52894); anti-LC3 (WB: 1:2000, Abcam ab192890). The following rabbit polyclonal antibodies were used: anti- Vps26A (WB: 1:2000, Abcam ab23892); anti-RILP (WB: 1:1000, Abcam ab128616); anti-FLAG (WB: 1:1000, Sigma-Aldrich F7425); anti-sortilin (WB: 1 μg/ml, Abcam ab16640). The following goat polyclonal antibody was used: anti-Vps35 (WB: 1:000, Novus Biologicals NB1001397).

2.4.3 Cell culture and transient transfections

HeLa cells were cultured in Dulbecco's modified Eagle's medium (DMEM) supplemented with 2 mM L-glutamine, 100 U/ml penicillin, 100 g/ml streptomycin and 10% FBS (Thermo Fisher Scientific, Burlington, ON) at 37°C in a humidified chamber at 95% air and 5% CO2. Cells were seeded at a density of 2×10^5/well for 12-well plates and 5×10^5/well for 6-well plates 24 h prior to transfection. Transfections were performed with polyethylenimine (PEI) (Thermo Fisher Scientific). Briefly, solution 1 was prepared by diluting plasmid into Opti-MEM (Thermo Fisher Scientific). Solution 2 was prepared by diluting PEI (1 μg/μl) in Opti- MEM in a 1:3 ratio with the DNA to be transfected. After a 5 min incubation, the two solutions were mixed, vortexed for 3 s, incubated at room temperature (RT) for 15 min and added to the cells.

2.4.4 CRISPR/Cas9 editing

In order to generate CLN3-knockout cells, a guide RNA (gRNA) corresponding to the first exon of CLN3 was designed (CACCGCGGCGCTTTTCGGATTCCGA) and cloned into pX330-U6 expressing a humanized Cas9 (Cong et al., 2013). HeLa cells were co-transfected with pX330-U6-gRNA-CLN3 and pcDNA3.1-zeocin (Thermo Fisher Scientific). 24 h after transfection, cells were selected with zeocin (250 μg/ml) for 5 days. Cells were cultured for 2 weeks, single clones were isolated and genomic DNA extracted. DNA sequencing was performed to identify CLN3-knockout cells carrying a specific indel mutation. HeLa cells were transfected with an all-in-one CRISPR/Cas9 plasmid for Rab7A (plasmid number HTN218819, Genecopoeia, Rockville, MD). 72 h posttransfection, the cells were treated with 1 mg/ml geneticin (Thermo Fisher Scientific) for 1 week. Limited dilution was performed to isolate single cells which were allowed to grow for 2 weeks. Western blotting was used to identify Rab7A-KO cells.

2.4.5 BRET titration experiments

HeLa cells were seeded in 12-well plates and transfected with the indicated plasmids. 48 h post-transfection, cells were washed in PBS, detached with 5 mM EDTA in PBS and collected in 500 μl PBS. Cells were transferred to opaque 96-well plates (VWR Canada, Mississauga, ON) in triplicate. Total fluorescence was first measured with the Tecan Infinite M1000 Pro plate reader (Tecan Group

Ltd., Mannedorf, Switzerland) with the excitation and emission set at 400 nm and 510 nm, respectively, for $BRET^2$ and 500 nm and 530 nm for $BRET^1$. The $BRET^2$ substrate coelenterazine 400a and $BRET^1$ substrate h-coelenterazine were then added to all wells (5 μM final concentration) and the $BRET^2$ and $BRET^1$ signals were measured 2 min later. The BRET signals were calculated as a ratio of the light emitted at 525±15 nm over the light emitted at 410±40 nm. The $BRET_{net}$ signals were calculated as the difference between the BRET signal in cells expressing both fluorescence and luminescence constructs and the BRET signal from cells where only the luminescence fused construct was expressed.

2.4.6 Western blotting

Cells were detached using 5 mM EDTA in PBS, washed in 1× PBS and collected by centrifugation. TNE buffer (150 mMNaCl, 50 mM Tris-HCl, pH 7.5, 2 mM EDTA, 0.5% Triton X-100 and protease inhibitor cocktail) was used to lyse cells by incubating them for 30 min on ice. Lysates were centrifuged at high speed for 10 min and the supernatants (cell lysate) were collected to be analyzed by western blotting. Samples were mixed with sample buffer 3× to obtain a final concentration of 1× (62.5 mM Tris- HCl, pH 6.5, 2.5% SDS, 10% glycerol, 0.01% Bromophenol Blue). Prior to electrophoresis, samples were incubated at 95°C for 5 min and resolved on SDS-PAGE followed by wet-transfer to nitrocellulose membranes. Detection was done by immunoblotting using the indicated antibodies.

2.4.7 Membrane separation assay

24 h post-transfection, cells were collected in 5 mM EDTA in PBS. The cells were subsequently snap frozen in liquid nitrogen and allowed to thaw at room temperature for 5 min. The cells were resuspended in Buffer 1 (0.1 M Mes- NaOH, pH 6.5, 1 mM magnesium acetate, 0.5 mM EGTA, 200 M sodium orthovanadate, 0.2 M sucrose) and centrifuged at 10,000 g for 5 min at 4°C. The supernatant containing the cytosolic proteins (S, soluble fraction) was collected. The remaining pellet was resuspended in Buffer 2 (50 mM Tris- HCl, 150 mM NaCl, 1 mM EDTA, 0.1% SDS, 1% Triton X-100) and centrifuged at 10,000 g for 5 min at 4°C. Samples were loaded into SDS-PAGE gels in equal volumes. Fiji was used to quantify the intensity of the bands (Schindelin et al., 2012).

The intensity of each fraction was calculated and divided by the total intensity to determine the distribution of proteins.

2.4.8 Cycloheximide chase

Wild-type, CLN3-KO, Rab7A-KO HeLa cells were seeded in 6-well plates the day prior to transfection. 500 ng of FLAG fused wild-type and mutation harbouring CLN3 was transfected into CLN3-KO HeLa cells. 48 h after transfection, cells were treated with 50 μg/ml of cycloheximide in Opti-MEM. Lysates were collected at 0, 3 or 6 h time points and run on 10% SDS-PAGE gels. Fiji was used to quantify the intensity of the bands (Schindelin et al., 2012). All protein levels were standardized to the actin loading control. Amount of remaining protein is expressed as a percentage of the 0 time point in each group.

2.4.9 EGFR degradation assay

Wild-type, CLN3-KO and Rab7A-KO cells were seeded in 6-well plates the day before the assay. In order to prevent *de novo* synthesis EGFR during EGF stimulation, cells were treated with 50 μg/ml cycloheximide in Opti- MEM for 1 h. EGF stimulation was performed with 100 ng/ml EGF in Opti-MEM containing 50 μg/ml of cycloheximide. Cell lysates were collected as indicated above and western blotting was performed. Fiji was used to quantify the intensity of the bands (Schindelin et al., 2012). All protein levels were standardized to the actin loading control. Amount of remaining protein is expressed as a percentage of the 0 time point in each group.

2.4.10 EGF-488 pulse-chase

Wild-type and CLN3-KO HeLa cells were seeded on coverslips the day before the experiment. Cells were serum starved in Opti-MEM for 1 h followed by a 30-min pulse of 300 ng/ml of EGF-488. Cells were then washed with PBS, fixed in 4% paraformaldehyde at 0 and 30 min and mounted onto slide using Fluoromount-G (Thermo Fisher). The coverslips were sealed using nail polish. Cells were imaged using fluorescence microscope. The number of puncta per cell was counted using Fiji. Briefly, the images were split into their individual channels. Using the green channel, the threshold was adjusted to 0.93% in order to get signal only from the puncta. The number of puncta counted

from an image was divided by the number of nuclei within that image, which gave us the number of puncta per cell. 50 cells per condition for each time point were analyzed.

2.4.11 Autophagic flux

Wild-type, CLN3-KO, Rab7A-KO HeLa cells were seeded in 6-well plates the day before autophagy induction. Cells were starved with Earle's balanced salt solution (EBSS) for 4 h to induce autophagy. 100 nM Bafilomycin A1 (BafA1) was used to inhibit lysosomal function and therefore inhibit autophagy. Lysates were resolved by SDS-PAGE and blotted with anti-LC3 and anti-actin antibodies. Band intensity was determined using Fiji, and quantification was performed as LC3-II over LC3-I+LC3-II.

2.4.12 Acyl-RAC to isolate palmitoylated proteins

The protocol to detect palmitoylated protein was adapted from a published protocol (Ren et al., 2013). Briefly, protein lysates were incubated overnight at room temperature with 0.5% methyl methanethiosulfonate (MMTS) (Sigma-Aldrich) to block free cysteine residues. Proteins were then precipitated by adding two volumes of cold acetone and incubated at $-20°$C. for 2 h. After washing with cold acetone, the pellet was resuspended in binding buffer (100 mM HEPES, 1 mM EDTA, 1% SDS).Water-swollen thiopropyl Sepharose 6B (GE Healthcare Life Sciences) was added and samples were divided into two equal parts. One part was treated with hydroxylamine (Sigma-Aldrich), pH 7.5, to a final concentration of 0.2 M to cleave palmitate residues from proteins; the other part was treated with an equal amount of NaCl as a control. After 3 h incubation at room temperature, beads were washed five times with binding buffer and captured proteins were eluted with 75 mM dithiothreitol.

2.4.13 Raichu-Rab7A FRET sensor

Wild-type or CLN3-KO HeLa cells were seeded in 12-well plates and transfected with the Raichu-Rab7A sensor. 36 h post-transfection, cells were washed in PBS, detached with 5 mM EDTA in PBS and collected in 500 μl PBS. Cells were transferred to white opaque 96-well plates (VWR Canada, Mississauga, ON) in triplicate. After excitation at 433 nm, the light emitted at the maximal emission

of CFP (475 nm) and Ypet (525 nm) was measured on a Tecan Infinite M1000 Pro plate reader (Tecan Group Ltd., Mannedorf, Switzerland). Data are presented as a ratio of the light emitted at 525 nm (Ypet) divided by the light emitted at 475 nm (CFP).

2.4.14 Statistics

Statistical analysis was performed using GraphPad Prism v.7. The statistical tests used are described in the respective figure legends.

Acknowledgements

We would like to thank Michel Bouvier (IRIC and University de Montreal), Regis Grailhe (Pasteur Institute Korea), Paul Odgren (University of Massachusetts Medical School), Makoto Kanzaki (Tohoku University) and Takeshi Nakamura (Tokyo University of Science) for providing plasmids.

Competing interests

The authors declare no competing or financial interests.

Funding

This work was supported by an EU Joint Programme in Neurodegenerative Diseases Grant (Neuronode to S.L.), the Canadian Institutes for Health Research (ENG-387575 to S.L.), the Canadian Foundation for Innovation (35258 to S.L.), the National Contest for Life Foundation Germany (NCL) (to G.H.) and by the Deutsche Forschungsgemeinschaft (DFG; 425373668, HE 3220/4-1 to G.H.). S.Y. is supported by a Fondation Universitaire Armand-Frappier scholarship. G.M. is supported by a scholarship from Fond de Recherche du Quebec - Santé.

Supplementary information

Supplementary information available online at (Supplementary-figures, 2020).

2.5 Supplementary figures

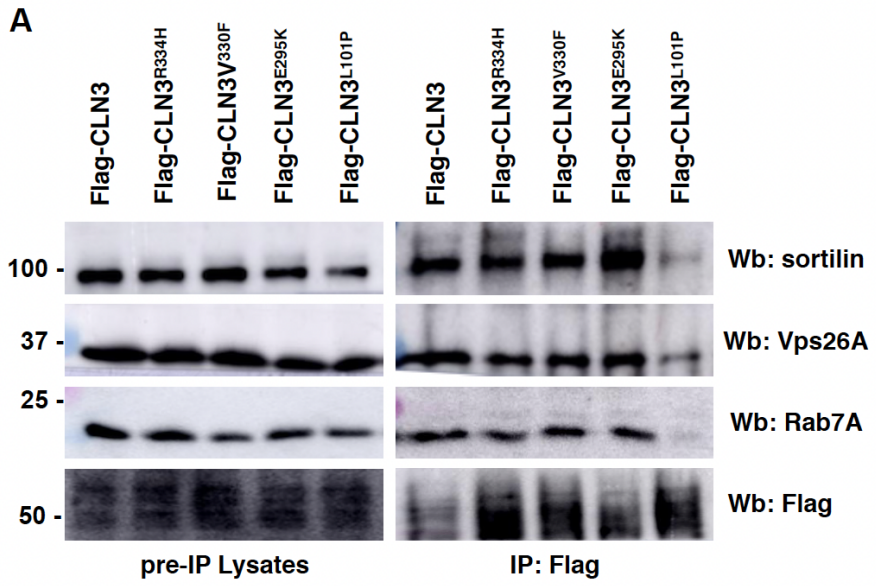

Figure 2.8: Co-immunoprecipitation confirming our BRET data.

(A) HeLa cells were transfected with Flag-CLN3 or Flag-CLN3 harbouring diseasecausing mutations. 24 hours post-transfection, cells were lysed and immunoprecipitation was performed using an anti-Flag antibody. Pre and Post IP samples were run on a 12% SDS-PAGE gel and Western blotting (Wb) was done with anti-sortilin, anti-Vps26, anti-Rab7A and anti-Flag antibodies

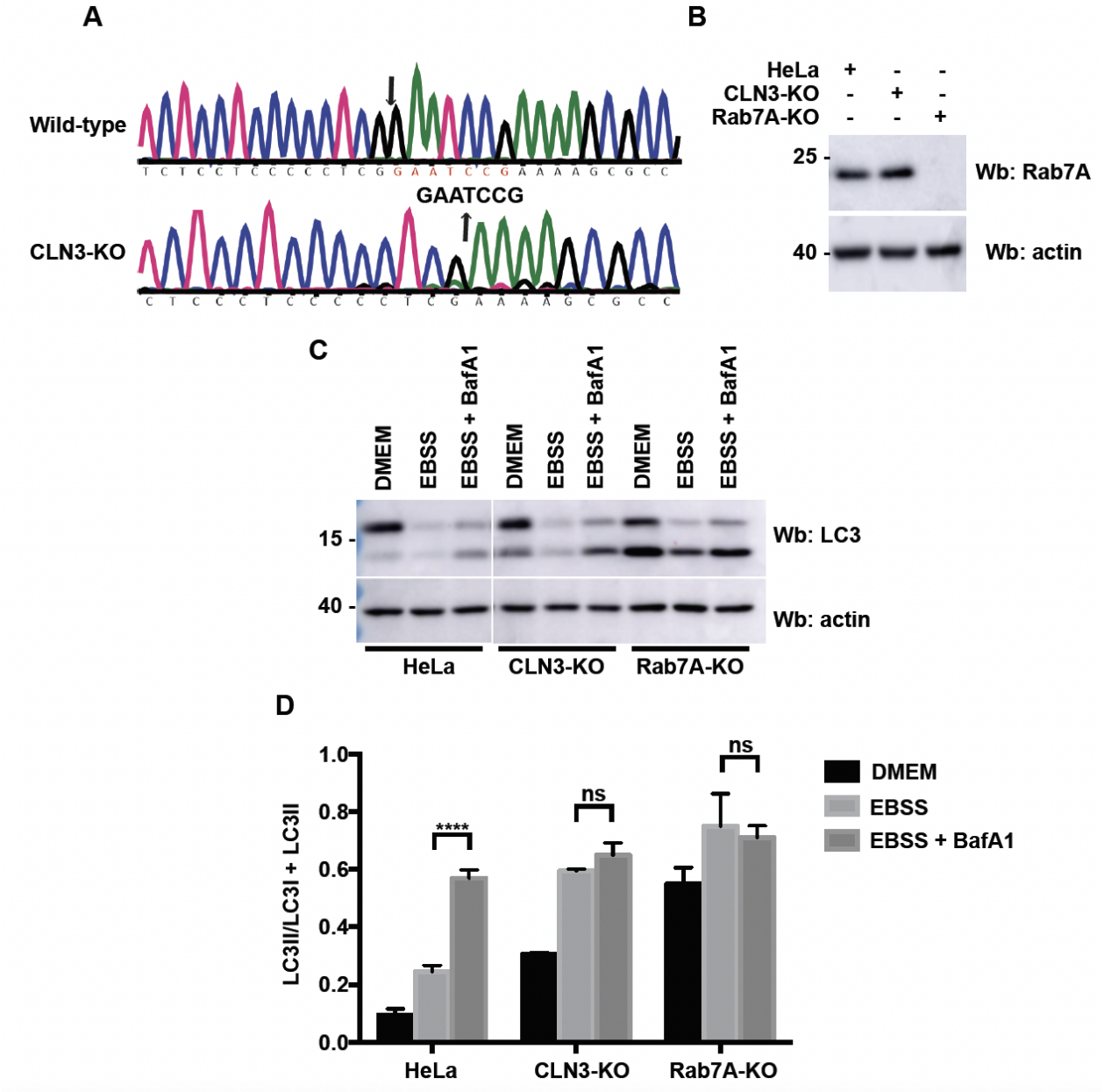

Figure 2.9: Engineering of CLN3 and Rab7A knockout HeLa cells

(A) DNA sequencing of genomic DNA of wild type (upper panel) and CLN3 knockout HeLa cells demonstrates the deletion of 7 base pairs in the CLN3 gene from position 35 to 41 after the start codon. Note that the reverse complementary sequence is shown. The deletion causes a frameshift, changes the encoded amino acid sequence starting at position 13 (D^{13} to R) and leads to a premature stop codon after amino acid 52. Arrow indicates the position of the Indel mutation. (B) Total cell lysate from wild-type, CLN3-KO and Rab7A-KO cells was run on an SDS-PAGE and Western blotting (Wb) was performed using anti-Rab7A and anti-actin antibodies. (C) Wild-type, CLN3-KO and Rab7A KO HeLa cells were cultured in DMEM, EBSS, EBSS + Bafilomycin A1 (BafA1) for 4 hours. Total cells lysates were run on a SDS-PAGE and Western blotting (Wb) was performed with anti-LC3 and anti actin antibodies. The amount of LC3-II was calculated as a ratio between the amount of LC3-II over total LC3 (LC3-I +LC3-II). (D) The results shown are representative of 5 independent experiments. Data is represented as mean ± SD. ns, not significant; ****, $P \leq 0.0001$; two-way ANOVA followed by Tukey's *post hoc* test.

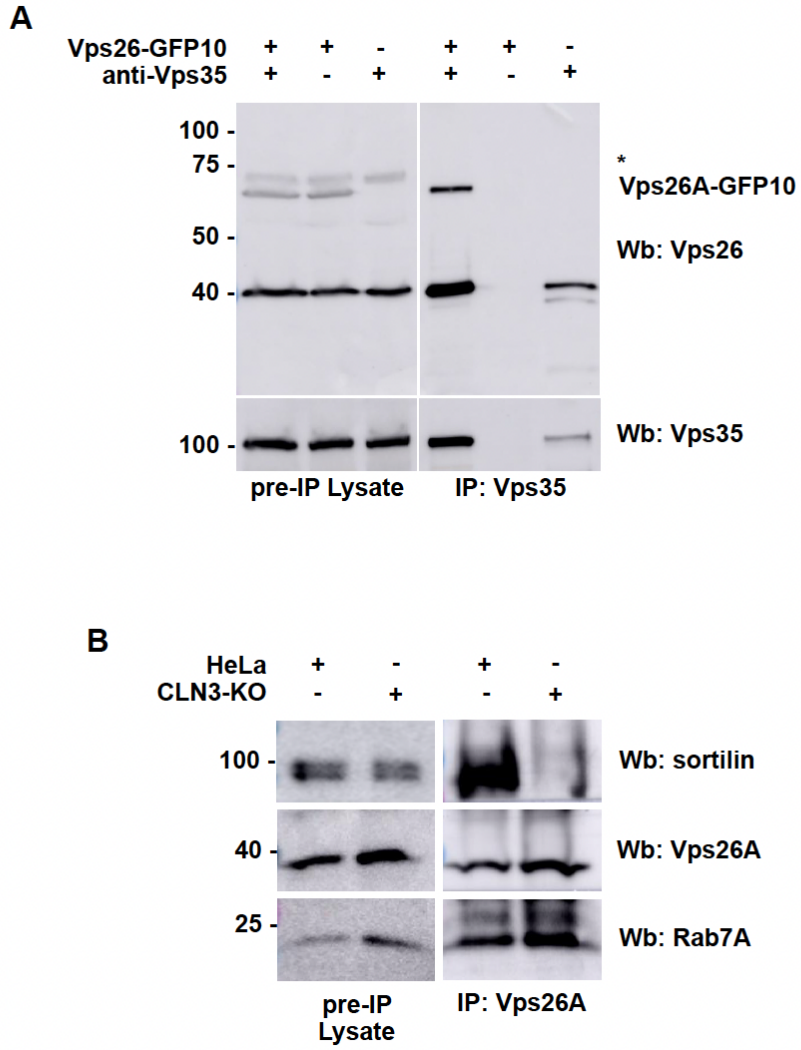

Figure 2.10: Co-immunoprecipitation confirming our BRET data

(A) Wild-type HeLa cells were transfected with Vps26A-GFP10. 24 hours post-transfection, the cells were lysed and Vps35 was immunoprecipitated with anti-Vps35 antibodies. Eluted samples were run on a 12% SDS gel and Western blotting was performed with anti-Vps26 and anti-Vps35 antibodies. Star indicates non-specific bands in the pre-IP lysate. (B) Wildtype and CLN3-KO HeLa cells were lysed and immunoprecipitation was performed an anti-Vps26A antibody. Pre and Post-IP samples were run on a 12% SDS-PAGE gel and Western blotting (Wb) was done with anti-sortilin, anti-Vps26A and anti-Rab7A antibodies.

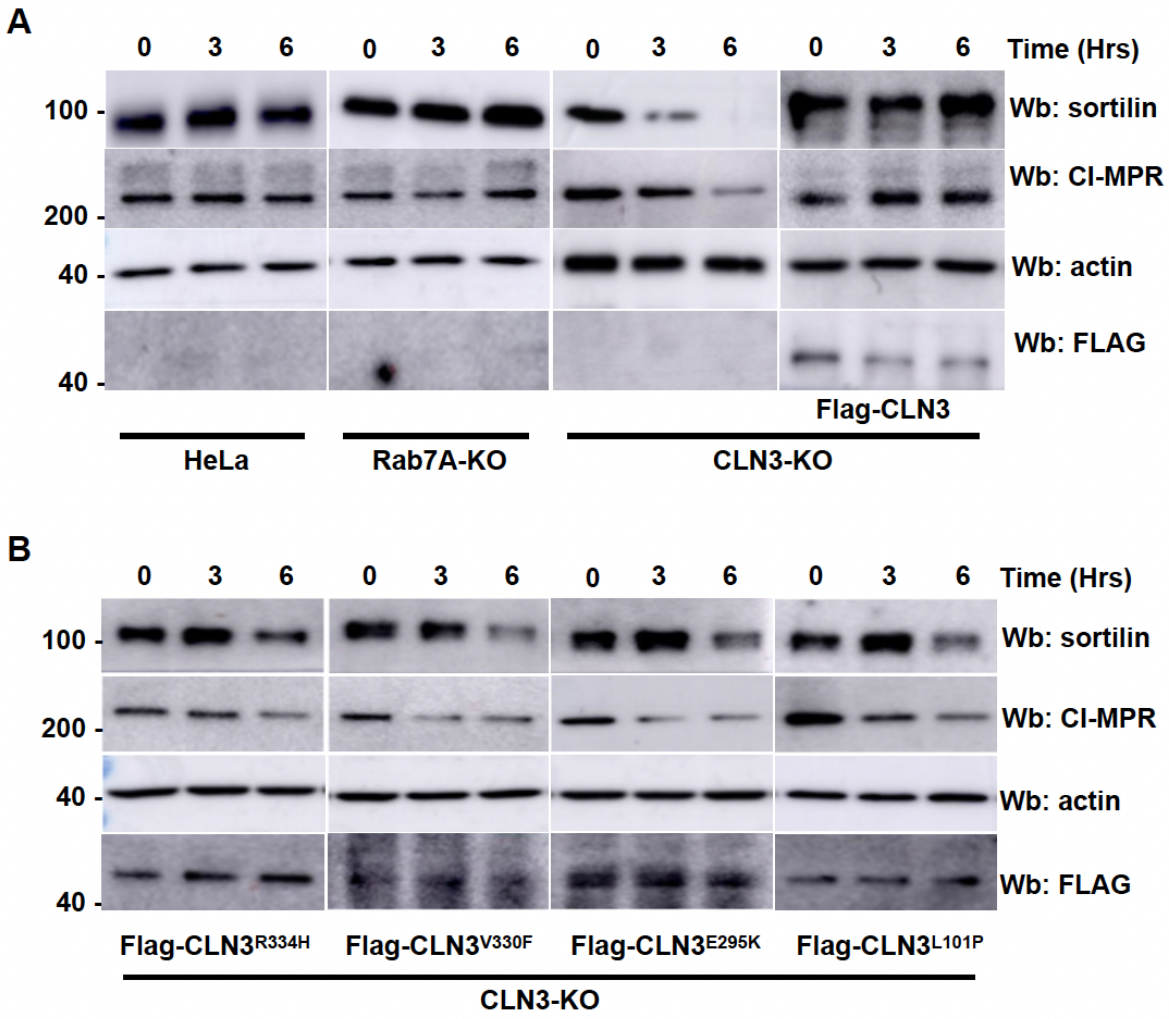

Figure 2.11: Stability of sortilin and CI-MPR

(A) Wild-type, Rab7A-KO, CLN3-KO and CLN3-KO expressing FLAG-CLN3 HeLa cells were incubated with 50 μg/ml of cycloheximide for the indicated times. Total cell lysate was run on SDS-PAGE and Western blotting was performed using anti-sortilin, anti-CI-MPR, anti-actin and anti-FLAG antibodies. Blots are representative from 5 independent experiments. (B) CLN3-KO HeLa cells expressing wild-type and mutant FLAG-CLN3 as indicated were incubated with 50 μg/ml of cycloheximide for the indicated times. Total cell lysate was run on SDS-PAGE and Western blotting was performed using anti-sortilin, anti-CI-MPR, anti-actin and anti-FLAG antibodies. Blots are representative from 5 independent experiments

Summary of contributions

I, Seda Yasa, have generated the following data as the first author of my second article, titled "CLN5 and CLN3 function as a complex to regulate endolysosome function".

- $CLN5^{KO}$ HeLa cells by CRISPR/Cas9

- $CLN5^{Y392X}$-HA by site-directed mutagenesis and RlucII-CLN3 vector constructs

- Fig. 3.1

- Fig.3.2

- Fig.3.3

- Fig.3.4

- Fig.3.5

- Fig.3.6

- Fig.3.7

- Fig.3.9

- Fig.3.10

Etienne Sauvageau generated CLN5-HA, HA-$CLN5^{Y392X}$, GFP10-CLN3, Vps26-nLuc, Vps26A-GFP10 plasmids.

And $Rab7^{KO}$ HeLa cells, and RlucII-Rab7A, PLEKHM1-GFP10 constructs are generated by Graziana Modica.

Chapter 3

Article II: CLN5 and CLN3 function as a complex to regulate endolysosome function

CLN5 et CLN3 fonctionnent comme un complexe pour réguler la fonction de l'endolysosome

Running title: Endolysosome function of CLN3 and CLN5

Authors

Seda Yasa[1], Etienne Sauvageau[1], Graziana Modica[1], Stephane Lefrancois[1,2]

[1] Centre Armand-Frappier Santé Biotechnologie, Institut National de la Recherche Scientifique, Laval, Canada H7V 1B7.

[2] Department of Anatomy and Cell Biology, McGill University, Montreal, Canada H3A 0C7 and Centre d'Excellence en Recherche sur les Maladies Orphelines - Fondation Courtois (CERMOFC), Université du Québec à Montréal (UQAM), Montréal, Canada H2X 3Y7

Contribution

Stephane Lefrancois: Conceptualization, Supervision, Funding acquisition, Formal Analysis, Writing — original draft, Project administration, Writing - review and editing.

Seda Yasa: Conceptualization, Investigation, Methodology, Formal Analysis, Writing — original

draft, Writing — review and editing.

Graziana Modica: Conceptualization, Investigation, Formal Analysis, Writing — review and editing.

Etienne Sauvageau: Investigation, Methodology, Formal Analysis, Writing — review and editing.

Biochemical Journal

Accepted 28 May 2021

Abstract

CLN5 is a soluble endolysosomal protein whose function is poorly understood. Mutations in this protein cause a rare neurodegenerative disease, neuronal ceroid lipofuscinosis (NCL). We previously found that depletion of CLN5 leads to dysfunctional retromer, resulting in the degradation of the lysosomal sorting receptor, sortilin. However, how a soluble lysosomal protein can modulate the function of a cytosolic protein, retromer, is not known. In this work, we show that deletion of CLN5 not only results in retromer dysfunction, but also in impaired endolysosome fusion events. This results in delayed degradation of endocytic proteins and in defective autophagy. CLN5 modulates these various pathways by regulating downstream interactions between CLN3, an endolysosomal integral membrane protein whose mutations also result in NCL, RAB7A, and a subset of RAB7A effectors. Our data support a model where CLN3 and CLN5 function as an endolysosomal complex regulating various functions.

Summary Statement

We have previously demonstrated that CLN3 is required for efficient endosome-to-trans Golgi Network (TGN) trafficking of sortilin by regulating retromer function. In this work, we show that CLN5, which interacts with CLN3, regulates retromer function by modulating key interactions between CLN3, Rab7A, retromer, and sortilin. Therefore, CLN3 and CLN5 serve as endosomal switch regulating the itinerary of the lysosomal sorting receptors.

3.1 Introduction

The Neuronal Ceroid Lipofuscinoses (NCLs) are a group of inherited lysosomal diseases with over 430 mutations in 13 genetically distinct genes (*CLN1-8* and *CLN10-14*) (Mole & Cotman, 2015). Germline mutations in CLN5, resulting in either amino acid conversion (R112H, N192S, D279N)

or truncations due to premature stop codons (W75X and Y392X), are causes of CLN5 disease. The truncation mutation, $CLN5^{Y392X}$, is the most common mutation in patients. This form of NCL has an early onset between the ages of 3 - 7, with a lifespan into the teenage years. Patients exhibit symptoms including retinopathy, motor disorders, epilepsy, and cognitive regression. The principal characteristics leading to the identification of NCL disorder is aberrant lysosomal function and excess accumulation of auto fluorescent ceroid lipopigments in neurons and peripheral tissues (Andersona *et al.*, 2013).

CLN5 is a glycosylated endolysosomal protein that is translated as a type II integral membrane protein (residues 1 - 407), prior to being cleaved into a mature soluble form (93 - 407), which is then transported to endolysosomes (Jules *et al.*, 2017). Recent work has suggested that CLN5 could function as a glycoside hydrolase, but endogenous targets have not been identified (Huber & Mathavarajah, 2018). Furthermore, CLN5 has been linked to the regulation of lysosomal pH (Best *et al.*, 2016) and mitophagy (Doccini *et al.*, 2020). To further our understanding of this protein, using small interfering RNA (siRNA), we generated CLN5 knockdown ($CLN5^{KD}$) HeLa cells. In these cells, we found less membrane bound Rab7A (Mamo *et al.*, 2012). Rab7A is a small GTPases that can bind to and recruit retromer, a protein complex that mediates endosome-to-trans Golgi Network (TGN) trafficking. Once recruited, retromer interacts with the cytosolic tails of the lysosomal sorting receptors cationic independent mannose 6- phosphate receptor (CI-MPR) and sortilin to drive their endosome-to-TGN retrieval (Canuel *et al.*, 2008; Rojas *et al.*, 2008; Seaman, 2009). In CLN5-KD HeLa cells, the lack of Rab7A recruitment resulted in the lysosomal degradation of CI-MPR and sortilin, and misrouting of the lysosomal enzyme cathepsin D, due to lack of retromer recruitment (Mamo *et al.*, 2012). Beyond retromer recruitment, Rab7A also regulates the degradation of endocytic cargo such as the epidermal growth factor (EGF) receptor (EGFR) (Vanlandingham & Ceresa, 2009) by interacting with PLEKHM1 (McEwan *et al.*, 2014), regulates organelle movement by interacting with RILP (Pankiv *et al.*, 2010; van der Kant *et al.*, 2013), and regulates the late stages of autophagy by mediating autophagosome/lysosome fusion through HOPS and other tethering factors (Ao *et al.*, 2014).

Recently, we have shown that CLN3 is also required in the endosome-to-TGN retrieval of the lysosomal sorting receptors (Yasa *et al.*, 2020). Mutations in the gene encoding for CLN3 results in the juvenile variant of NCL (JNCL), commonly known as Batten disease. JNCL is the most common cause of childhood dementia, with an age of onset between 5 to 10 years (Butz *et al.*, 2019). CLN3

is a protein of 438 amino acids with six transmembrane domains, whose N- and C- terminal ends are located in the cytosol. This glycosylated protein localizes to endolysosomal membranes among other intracellular locations (Storch *et al.*, 2004; Oetjen *et al.*, 2016), and can interact with other CLN proteins including CLN5. However, the molecular function of these interactions are not known (Vesa *et al.*, 2002). Unlike depletion of CLN5, deletion of CLN3 did not affect the localization or activation of Rab7A or its effector retromer. Rather, CLN3 is required for the efficient Rab7A interaction with retromer, and for the retromer/sortilin interaction, most likely acting as a scaffold protein (Yasa *et al.*, 2020).

In this study, we generated CLN5 knockout ($CLN5^{KO}$) HeLa cells on the same parental cell line used to generate CLN3 knockout ($CLN3^{KO}$) and Rab7A knockout ($Rab7A^{KO}$) cells (Yasa *et al.*, 2020). This knockout system has enabled us to study the effects of a CLN5 disease-causing mutation. We extended our studies to identify defects in endocytic degradation and autophagy. Importantly, we identified significant decreases in previously known interactions between CLN3 and sortilin, retromer and Rab7A in $CLN5^{KO}$ cells compared to wild-type cells. This leads to decreases in the Rab7A/retromer and retromer/sortilin interactions. Overall, our data suggest that CLN3 and CLN5 form a late endolysosome complex that modulates a subset of Rab7A functions. These finding provides insights into the pathogenic mechanisms observed in CLN3 and CLN5 disease.

3.2 Results

3.2.1 Retromer is not efficiently recruited to endosomal membranes in $CLN5^{KO}$ HeLa cells

In our previous work conducted in $CLN5^{KD}$ HeLa cells, we showed decreased membrane recruitment of Rab7A leading to a significant decrease in the membrane recruitment of its effector, retromer (Mamo *et al.*, 2012). In order to study the role of CLN5 disease-causing mutations, we generated $CLN5^{KO}$ HeLa cells using CRISPR/Cas9. Our sequencing data and Western blot analysis confirm the deletion of CLN5 in this cell line (Fig. S1A and B). To confirm our previous results obtained in $CLN5^{KD}$ cells, we performed a membrane isolation experiment in our $CLN5^{KO}$ HeLa cells as we have previously done (Mamo *et al.*, 2012; Yasa *et al.*, 2020; Modica *et al.*, 2017), and compared the membrane distribution of Rab7A in wild-type and $CLN5^{KO}$ HeLa cells (Fig. 3.1A). Our membrane

separation was successful, as the integral membrane protein Lamp2 was found in the pellet fraction (P) containing membranes, and not in the supernatant fraction (S) contains the cytosol (Fig. 3.1A). Quantification of 3 independent experiments showed that CLN5 deletion had no significant effect on Rab7A membrane distribution (Fig. 3.1B). We sought to determine the effect of a CLN5 mutation known to cause human disease on Rab7A membrane recruitment. Thus, we engineered a CLN5 disease-causing mutation expression plasmid using site directed mutagenesis to generate CLN5^{Y392X}-HA, and expressed it in CLN5^{KO} HeLa cells (Fig. 3.1A). Rab7A distribution was not affected in CLN5^{KO} HeLa cells expressing CLN5-HA or expressing the disease causing mutation, CLN5^{Y392X}-HA (Fig. 3.1B). The small GTPase Rab7A regulates the spatiotemporal recruitment of retromer (Rojas *et al.*, 2008; Seaman, 2009). Therefore, we repeated the membrane assay as above to test if CLN5 is required for membrane recruitment of retromer. This time we included Rab7A^{KO} HeLa cells as a control, as we previously demonstrated a reduction of retromer recruitment in these cells (Yasa *et al.*, 2020). Compared to wild-type HeLa cells, we observed a significant decrease in retromer recruitment (as detected by the retromer subunit Vps26A) in CLN5^{KO} and Rab7A^{KO} HeLa cells (Fig. 3.1A). Quantification of 6 independent experiments found a reduction of 21.4% in the membrane recruitment of retromer in CLN5^{KO}, compared to a 31.4% decrease in recruitment in Rab7A^{KO} HeLa cells (Fig. 3.1C). These values are comparable to previous studies (Rojas *et al.*, 2008; Seaman, 2009). This decrease in retromer membrane recruitment was rescued by expressing CLN5-HA in CLN5^{KO} cells, indicating the effect seen on Vps26A recruitment is specific to CLN5 deletion, and likely not an off-target effect (Fig. 3.1A and C). The expression of CLN5^{Y392X}-HA in CLN5^{KO} cells partially rescued retromer recruitment, but not to levels comparable as that of wild-type CLN5 (Fig. 3.1C).

The question remained as to how Rab7A was membrane bound, but not able to recruit retromer. In recent years, Rab7A has been shown to be phosphorylated (Francavilla *et al.*, 2016; Lin *et al.*, 2017a; Heo *et al.*, 2018), ubiquitinated (Song *et al.*, 2016) and palmitoylated (Modica *et al.*, 2017). These post-translational modifications have been demonstrated to regulate various functions of this small GTPase, often by modulating the interaction with its effectors. In particular, we have previously shown that Rab7A palmitoylation is required for the recruitment of retromer to endosomal membranes. While non-palmitoylatable Rab7A is still membrane bound, it does not efficiently interact with retromer, and is not capable of rescuing retromer membrane recruitment in Rab7A^{KO} HEK293 cells (Modica *et al.*, 2017). Since RAB7A was still membrane bound in CLN5KO HeLa

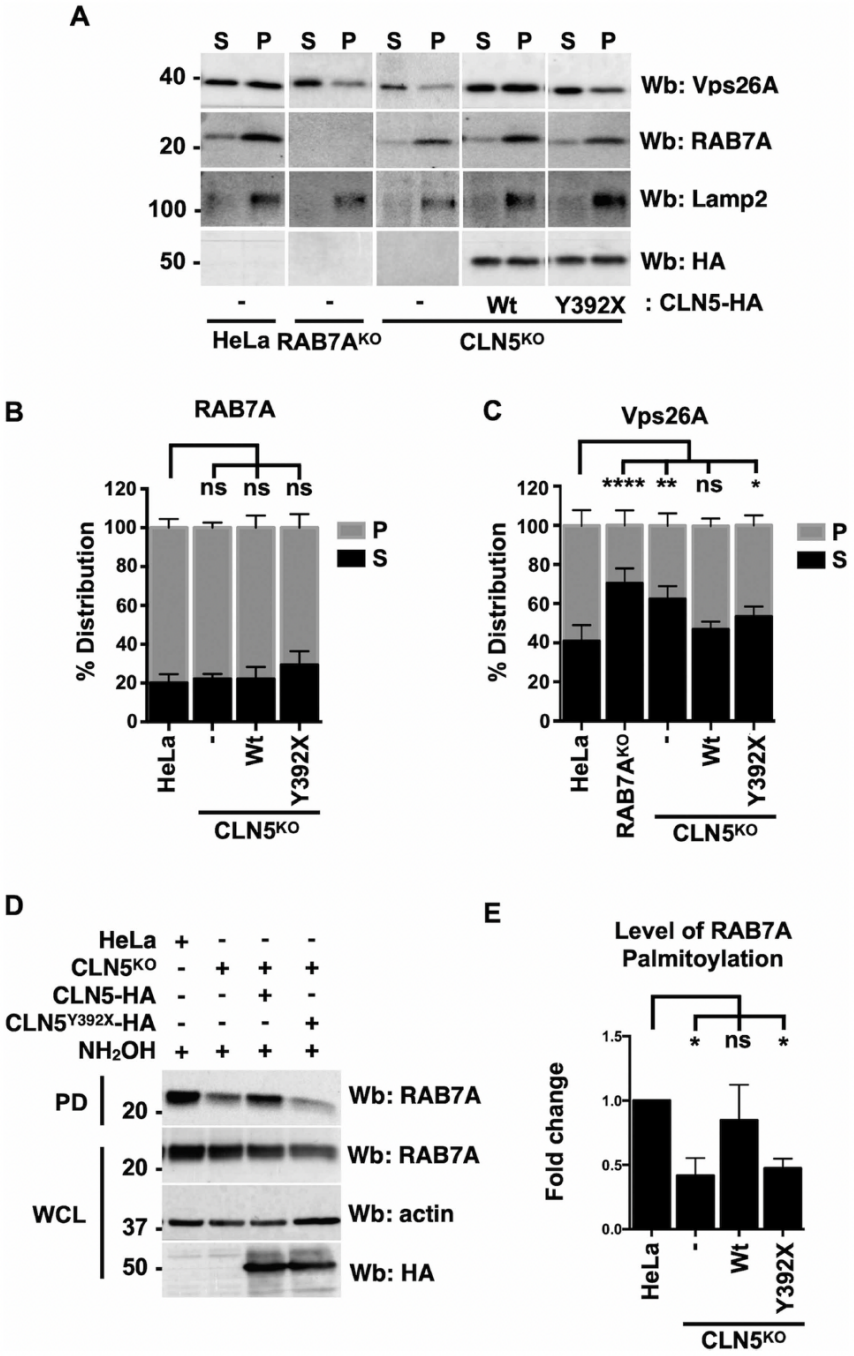

Figure 3.1: Rab7A palmitoylation is reduced in CLN5^{KO} HeLa cells affecting retromer recruitment.

(A) A membrane separation assay was performed on wild-type, Rab7A^{KO}, CLN5^{KO}, and CLN5^{KO} HeLa cells expressing CLN5-HA or CLN5^{Y392X}-HA. Western blotting (Wb) was performed with anti-Rab7A, anti-Vps26A, anti-Lamp2 (as a marker of the membrane fraction) and anti-HA (to identify cells expressing CLN5-HA) antibodies. S; supernatant fraction, P; pellet fraction. (B) Quantification of 3 separate membrane isolation assay experiments for Rab7A distribution. Data is shown as mean±s.d.; ns, not significant; two-way ANOVA followed by Tukey's *post hoc* test. (C) Quantification of 3 separate membrane isolation assay experiments for Vps26A distribution. Data is shown as mean±s.d.; ns, not significant; $^{*}P \leq 0.05$, $^{**}P \leq 0.01$,$^{****}P \leq 0.0001$, two-way ANOVA followed by Tukey's *post hoc* test (D) Whole cell lysate (WCL) from wild-type and CLN5^{KO} HeLa cells were subjected to Acyl-RAC analysis to determine the palmitoylation status of Rab7A. NH2OH: hydroxylamine, PD: pull-down (E) Quantification of 3 separate Acyl-RAC assay experiments. Data is shown as mean±s.d.; $^{**}P \leq 0.01$, Student's t-test.

cells, but retromer was not, we used Acyl-RAC to test if RAB7A palmitoylation is affected in these cells and to test the effects of the CLN5 disease causing mutation, CLN5Y392X, on RAB7A palmitoylation (Fig. 3.1D). We found that RAB7A palmitoylation is significantly decreased by more that 50% in CLN5KO HeLa cells compared with wild-type cells (Fig. 3.1E). RAB7A palmitoylation was rescued by expressing CLN5-HA in CLN5KO HeLa cells, while expressing CLN5Y392X-HA did not (Fig. 3.1E).

3.2.2 CLN5 is required for efficient retromer interactions

Rab7A coordinates the spatiotemporal recruitment of retromer to endosomal membranes (Rojas *et al.*, 2008; Seaman, 2009). Since we observed decreased retromer membrane recruitment along with decreased Rab7A palmitoylation, we expected to observe a weaker interaction between Rab7A and retromer in $CLN5^{KO}$ HeLa cells. To test our hypothesis, we used bioluminescence resonance energy transfer (BRET), as we have previously done (Yasa *et al.*, 2020; Modica *et al.*, 2017). Compared to coimmunoprecipitation, BRET is performed in live cells, with proteins localized to their native environment. From BRET titration curves, the $BRET_{50}$ can be calculated, which is the value at which the concentration of the acceptor is required to obtain 50% of the maximal BRET signal ($BRET_{max}$). The $BRET_{50}$ is indicative of the propensity of a pair of protein to interact, as the smaller the $BRET_{50}$, the stronger the interaction (Mercier *et al.*, 2002; Kobayashi *et al.*, 2009). The energy donor Renilla Luciferase II (RlucII) was fused at the N-terminus to wild-type Rab7A (RlucII-Rab7A), while the energy acceptor GFP10 was fused at the C-terminus of the retromer subunit Vps26A. Neither of these tags appear to interfere with the function of the proteins, as we have previously shown that RlucII had little effect on the distribution or function of Rab7A (Modica *et al.*, 2017), while we confirmed that Vps26A-GFP10 is efficiently integrated into the retromer trimer (Yasa *et al.*, 2020). We have previously used BRET to study the Rab7A/Vps26A interaction (Modica *et al.*, 2017). This interaction is specific as Rab7A did not interact with AP-1 subunits (a clathrin adaptor that has been localized to both the TGN and endosomes), while Vps26A did not interact with RlucII-Rab1a, which is localized to the Golgi apparatus (Modica *et al.*, 2017). Wild-type and $CLN5^{KO}$ HeLa cells were co-transfected with a constant amount of RlucII-Rab7A, and increasing amounts of Vps26A-GFP10 to generate BRET titration curves (Fig. 3.2A, blue and red curves). The BRET signal between RlucII-Rab7A and Vps26A-GFP10 rapidly increased with increasing amounts of expressed Vps26A-GFP10 until it reached saturation,

suggesting a specific interaction. Compared to wild-type HeLa cells, we found a 5- fold increase in the $BRET_{50}$ value for Rab7A binding to Vps26A in $CLN5^{KO}$ cells, suggesting a weaker interaction (Fig. 3.2B). To test if the disease-causing mutation in CLN5 affected the Rab7A/retromer interaction, we expressed wild-type HA-CLN5 (Figure 2A, green curve) or HA-$CLN5^{Y392X}$ (Figure 2A, purple curve) in $CLN5^{KO}$ cells and generated BRET titration curves as above. While expressing HA-CLN5 rescued the Rab7/retromer interaction as the $BRET_{50}$ was similar to the $BRET_{50}$ in wild-type HeLa cells (Fig. 3.2B), expression of HA-$CLN5^{Y392X}$ did not, as the $BRET_{50}$ value was 4 fold larger (Fig. 3.2B). Our previous work suggests that palmitoylation favours the association of Rab7A to a specific endosomal domain to optimize its interaction with retromer (Modica *et al.*, 2017), without affecting the overall ability of the small GTPase to interact with this effector. As such, when the Rab7A/retromer interaction was analyzed with BRET, hence preserving cellular membranes, we observed a decreased interaction, while no change in the interaction was observed in co-immunoprecipitation where cellular compartments are lost. To confirm if this was the case in $CLN5^{KO}$ HeLa cells, we performed co-immunoprecipitation between Rab7A and retromer in wild-type and $CLN5^{KO}$ HeLa cells (Fig. S1C). We found no change in the Rab7A/retromer interaction using this method.

CI-MPR and sortilin are known to interact with retromer, which is necessary for their endosome-to-TGN trafficking (Canuel *et al.*, 2008; Arighi *et al.*, 2004; Seaman, 2004). Using BRET, we have previously shown that nanoLuciferase-tagged Vps26A (Vps26A-nLuc) and YFP-tagged sortilin (sortilin-YFP) interact, and that this interaction is significantly weaker in $CLN3^{KO}$ cells compared to wild-type HeLa cells (Yasa *et al.*, 2020). We tested the sortilin/retromer interaction in $CLN5^{KO}$ HeLa cells to determine if this protein plays a role in this interaction. Wild-type and $CLN5^{KO}$ HeLa cells were co-transfected with a constant amount of Vps26A-nLuc and increasing amounts of sortilin-YFP to generate BRET titration curves (Fig. 3.2C, blue and red curves). We found a significantly weakened interaction between retromer and sortilin in $CLN5^{KO}$ cells compared to wild-type HeLa cells, as we observed a 4 fold increase in the $BRET_{50}$ value (Fig. 3.2D). The retromer sortilin interaction in $CLN5^{KO}$ HeLa cells could be rescued by expressing HA-CLN5 (Fig. 3.2C, green curve), as the $BRET_{50}$ value was similar to the one we calculated in wild-type HeLa cells. We next performed BRET experiments to determine the impact of the $CLN5^{Y392X}$ disease-causing mutation on the Vps26A/sortilin interaction. Expression of HA-$CLN5^{Y392X}$ in $CLN5^{KO}$ HeLa cells (Fig. 3.2C, purple curve) did not rescue the interaction as shown by the $BRET_{50}$ value (Fig.

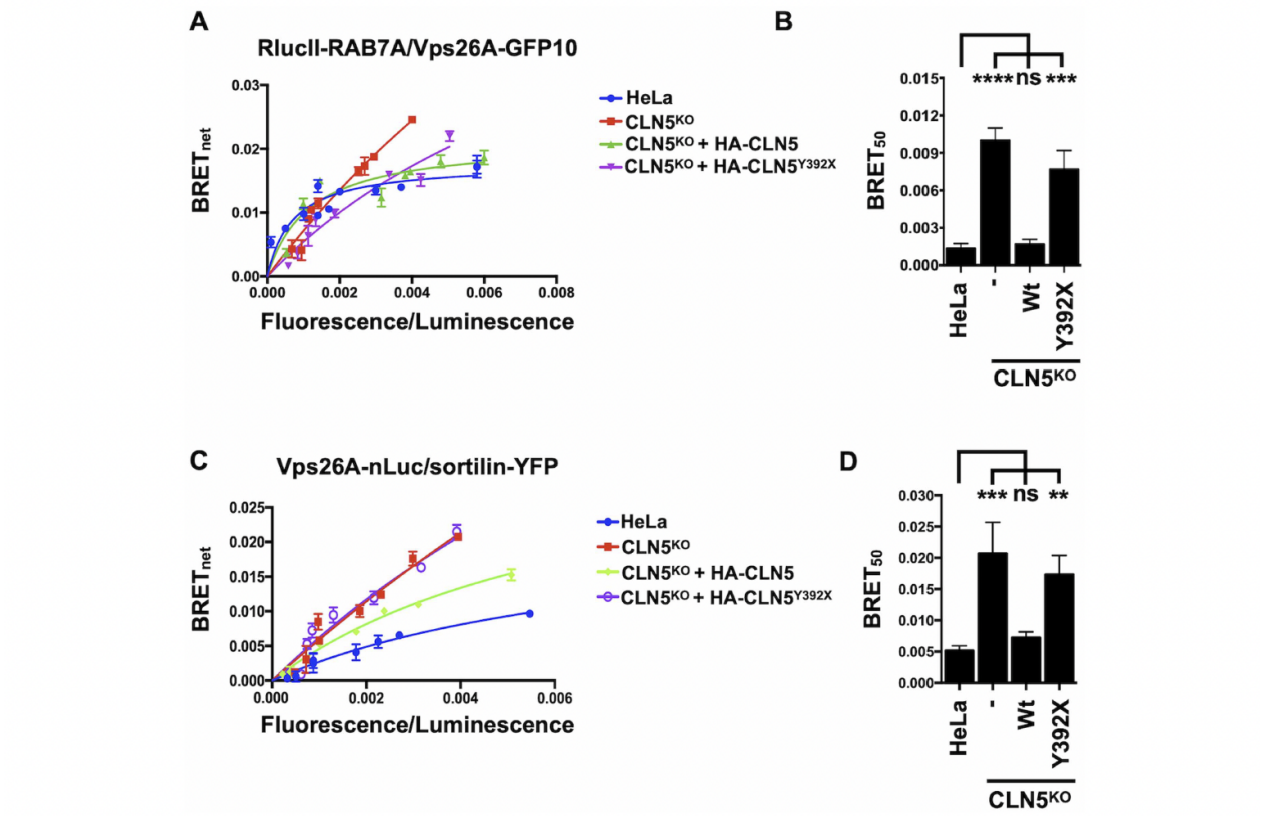

Figure 3.2: Weaker Rab7A/retromer and retromer/sortilin interactions in CLN5^{KO} HeLa cells.

(A) Wild-type, CLN5^{KO} and CLN5^{KO} HeLa rescued with wild-type HA-CLN5 or HA-CLN5^{Y392X} were transfected with a constant amount of RlucII-Rab7A and increasing amounts of Vps26A-GFP10 to generate BRET titration curves. BRET signals are plotted as a function of the ratio between the GFP10 fluorescence over RlucII luminescence. (B) BRET$_{50}$ was extrapolated from 3 independent experiments. Data is shown as mean±s.d.; ns, not significant, $^{***}P \leq 0.001$, $^{****}P \leq 0.0001$, one-way ANOVA followed by Tukey's *post hoc* test (C) Wild-type, CLN5^{KO} and CLN5^{KO} HeLa rescued with wild-type HA-CLN5 or HA-CLN5^{Y392X} were transfected with a constant amount of Vps26A-nLuc and increasing amounts of sortilin-YFP to generate BRET titration curves. BRET signals are plotted as a function of the ratio between the YFP fluorescence over nLuc luminescence. (D) Quantification of 3 independent experiments. Data is shown as mean±s.d.; ns, not significant; $^{**}P \leq 0.01$, $^{***}P \leq 0.001$, one-way ANOVA followed by Tukey's post hoc test.

3.2D). To confirm our BRET data, we immunoprecipitated endogenous Vps26A with anti-Vps26A antibody, and blotted for endogenous sortilin (Fig. S1C). By co-immunoprecipitation, we observed no change in the Vps26A/sortilin interaction in CLN5^{KO} cells, suggesting that the proteins can interact when the contribution of membrane distribution is not considered.

3.2.3 Sortilin is degraded in CLN5^{KO} HeLa cells

In cells lacking functional retromer, sortilin does not efficiently recycle to the TGN, accumulates in late endosomes, and is subsequently degraded in lysosomes (Yasa *et al.*, 2020). We have previously demonstrated the same phenotype in cells depleted of CLN5 (Mamo *et al.*, 2012). Using our CLN5^{KO}

HeLa cells, we performed a cycloheximide chase experiment to determine receptor stability as we have previously done (Mamo *et al.*, 2012; Yasa *et al.*, 2020; McCormick *et al.*, 2008). Wild-type, Rab7A^{KO} and CLN5^{KO} HeLa cells were incubated with serum free medium containing 50 μg/ml cycloheximide and collected after 0, 3, and 6 hours of incubation. Western blotting was performed using anti-sortilin antibody, anti-actin antibody (as a loading control), while HA staining was used to demonstrate the expression level of HA tagged CLN5 constructs. Western blot (Wb) analysis shows decreased levels of sortilin in CLN5^{KO} HeLa cells at 3 and 6 hours compared to Rab7A^{KO} and wild-type HeLa cells (Fig. 3.3A). Transfecting CLN5-HA in CLN5^{KO} cells rescued this phenotype (Fig. 3.3A). We next aimed to determine the impact of CLN5^{Y392X} on the stability of sortilin. Expression of CLN5^{Y392X}-HA in CLN5^{KO} cells did not rescue the degradation of sortilin (Fig. 3.3A). Quantitative analysis of 3 independent cycloheximide chase experiments showed that compared to wild-type cells which had 76.6% and 74.75% of sortilin remaining at 3 and 6 hours respectively (Fig. 3.3B), sortilin was significantly degraded in CLN5^{KO} cells, as only 23.8% and 22.8% of sortilin remained after 3 and 6 hours (Fig. 3.3B). As expected, we observed no significant degradation in Rab7A^{KO} cells, which had 75.7% and 84.3% sortilin remaining at 3 and 6 hours respectively (Fig. 3.3B). Expressing CLN5-HA in CLN5^{KO} cells rescued the stability and hence recycling of sortilin, as it was no longer degraded and had protein levels remaining of 79.6% and 77% respectively at 3 and 6 hours, which is similar to wild-type HeLa cells (Fig. 3.3B). We observed a partial rescue of sortilin degradation in CLN5^{KO} cells expressing CLN5^{Y392X}-HA at the 3 hours time point, as 38.4% was remaining. However, after 6 hours, only 17.7% was remaining, suggesting that this disease-causing mutation did not rescue the knockout phenotype.

3.2.4 Lysosomal dysfunction in CLN5^{KO} cells

Since we observed the degradation of sortilin in CLN5^{KO} HeLa cells, we aimed to determine if this had an impact on lysosomal function. Cathepsin D is generated as a 53 kDa pro-cathepsin D (proCatD), which is processed to a 47 kDa intermediate form (iCatD), before being fully processed to a 31 kDa mature cathepsin D (mCatD) once it reaches the lysosome (Laurent-Matha *et al.*, 2006). Depletion of Rab7A by siRNA affects this processing, resulting in increased amounts of the pro and intermediate forms (Rojas *et al.*, 2008). Total cell lysate from wild-type, CLN5^{KO}, and Rab7A^{KO} HeLa cells was run on a SDS-PAGE and Western blotting was performed using anti-cathepsin D antibody (Fig. 3.4A). Compared to wild-type HeLa cells which had 24.6% pro-cathepsin

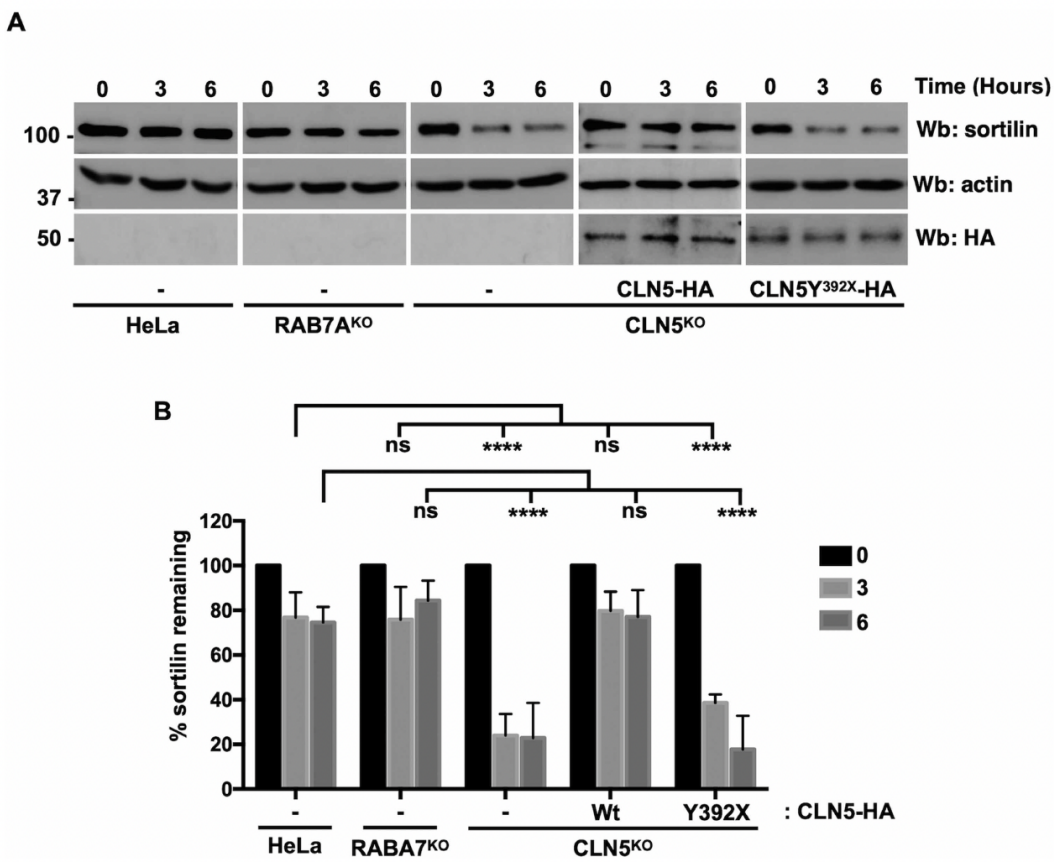

Figure 3.3: The lysosomal sorting receptor sortilin is degraded in CLN5^{KO} HeLa cells.

(A) Wild-type, Rab7A^{KO}, CLN5^{KO}, and CLN5^{KO} HeLa cells expressing CLN5-HA or CLN5^{Y392X}-HA were treated with 50 μg/ml of cycloheximide in serum free media for the indicated times. Whole cell lysate was run on a SDS-PAGE and Western blotting (Wb) was performed with anti-sortilin, anti-actin and anti-HA antibodies. (B) Quantification of 3 independent experiments. Data is shown as mean±s.d.; ns, not significant; $^{****}P \leq 0.0001$, two-way ANOVA followed by Tukey's post hoc test.

(proCatD), 9.8% intermediate (iCatD) and 65.6% mature cathepsin D (mCatD), CLN5^{KO} HeLa had significantly increased iCatD (24.6% and significantly reduced mCatD (48%with similar levels of proCatD (27.4%). On the other hand, Rab7A^{KO} HeLa cells had increased levels of proCatD (37.6%) and iCatD (30.3%), and had decreased amounts of mCatD (32.1%) (Fig. 3.4B). As the processing of cathepsin D was affected in CLN5^{KO} HeLa cells, we aimed to determine if lysosomal enzyme function was decreased by assessing the function of cathepsin B using a fluorescent substrate assay, MagicRed. The substrate is cleaved by active cathepsin B, which results in an increase in fluorescence emission. Therefore, lack or decreased fluorescence can be interpreted as a lack of active enzyme. The fluorescence emission was decreased by 35.6% and 25.7% in CLN5^{KO} and RAB7A^{KO} HeLa cells, respectively, compared with wild-type HeLa cells (Fig. 3.4C). This suggests decreased activity of cathepsin B in the KO cells compared with wild-type cells. β-glucuronidase is a soluble

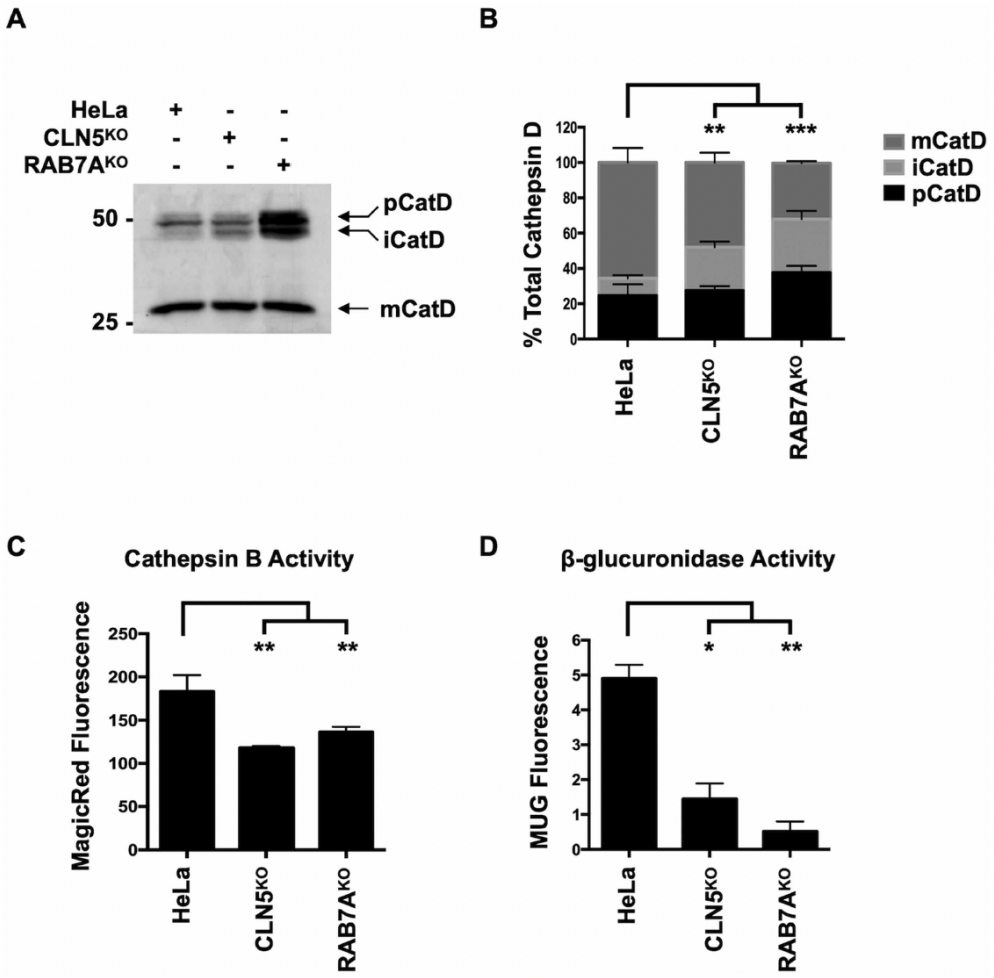

Figure 3.4: Lysosomal function is deficient in CLN5^{KO} cells.

(A) Whole cell lysate from wild-type, CLN5^{KO} and RAB7A^{KO} HeLa cells was resolved by SDS–PAGE and Western blotting (Wb) was performed using anti-cathepsin D antibody. (B) Quantification of pro-cathepsin D (proCatD, 53 kDa), intermediate cathepsin D (iCatD, 48 kDa) and mature cathepsin D (mCatD, 31 kDa). The amount of each is expressed as a percentage of total cathepsin D. Statistical significance refers to mature Cathepsin D (mCatD). Data are mean ± s.d.; ns, not significant; **P $\leq$ 0.01,***P $\leq$ 0.001, two-way ANOVA followed by Tukey's *post hoc* test. (C) Wild-type, CLN5^{KO} and RAB7A^{KO} HeLa cells were incubated in Magic Red substrate to measure the activity of cathepsin B. The fluorescence emission at 628 nm was measured in each sample. Data are mean ± s.d.; **P $\leq$ 0.01, one-way ANOVA followed by Tukey's *post hoc* test. (D) Whole cell lysate from wild-type, CLN5^{KO} and RAB7A^{KO} HeLa cells was incubated with methylumbelliferyl-β-D-glucuronide (MUG) to test the activity of β-glucuronidase. The fluorescence emission at 445 nm was measured in each sample. Data are mean ± s.d.; *P $\leq$ 0.005, **P $\leq$ 0.01, one-way ANOVA followed by Tukey's post hoc test.

lysosomal enzyme whose activity is affected in retromer-depleted cells (Arighi *et al.*, 2004). Activity of this enzyme can be evaluated using the substrate MUG, which emits a fluorescent signal when cleaved (Tropak *et al.*, 2004). Fluorescence emission was 3.4 and 9.60 fold decreased in CLN5^{KO} and RAB7A^{KO} HeLa cells, respectively, compared with wild-type HeLa cells, suggesting reduced β-glucuronidase activity (Fig. 3.4D).

3.2.5 CLN5 is required for efficient CLN3 interactions

Recently, we showed that CLN3 functions as a scaffold protein to ensure the Rab7A/retromer and retromer/sortilin interactions, which are sequentially required to regulate the endosome-to-TGN retrieval of sortilin (Yasa *et al.*, 2020). In this current study, we demonstrated a role for CLN5 in regulating the stability of sortilin. However, the question remains how a soluble lysosomal protein, CLN5, can regulate the Rab7A/retromer and retromer/sortilin interactions, which occur in the cytosol. In order to better understand the relationship of CLN5 and CLN3 in this trafficking pathway, we wanted to determine the role of CLN5 in modulating CLN3 interactions. Previous studies have shown that CLN3 and CLN5 interact (Vesa *et al.*, 2002; Schmiedt *et al.*, 2009). We confirmed the CLN3/CLN5 interaction using co-immunoprecipitation, and tested the impact of a disease-causing mutation in CLN5 on this interaction (Fig. S2A). The disease-causing mutation we tested, CLN5^{Y392X}, had no impact on the CLN3/CLN5 interaction (Fig. S2A). The CLN3/Rab7A interaction has been previously shown using co-immunoprecipitation and BRET experiments (Yasa *et al.*, 2020; Uusi-Rauva *et al.*, 2012). To determine if CLN5 plays a role in this interaction, wild-type (Fig. 3.5A, blue curve) and CLN5^{KO} HeLa cells (Fig. 3.5A, red curve) were co-transfected with a constant amount of RlucII-Rab7A and increasing amounts of GFP10-CLN3 to generate BRET titration curves. We extrapolated the BRET$_{50}$ for the interaction between CLN3 and Rab7A and found that the BRET$_{50}$ was 2.85 fold larger in CLN5^{KO} HeLa cells compared to wild-type cells, indicating a weaker CLN3/Rab7A interaction in cells lacking CLN5 (Fig. 3.5B). Expressing HA-CLN5 in CLN5^{KO} cells rescued the CLN3/Rab7A interaction (Fig. 3.5A, green curve) as the BRET$_{50}$ was similar to wild-type HeLa cells (Fig. 3.5B). Expressing HA-CLN5^{Y392X} in CLN5^{KO} cells had a partial rescue effect on the CLN3/Rab7A interaction (Fig. 3.5A, purple curve), but the BRET$_{50}$ was still more than 2 fold larger (Fig. 3.5B).

We previously demonstrated an interaction between CLN3 and retromer (Yasa *et al.*, 2020). To test if CLN5 plays a role in modulating this interaction, we generated BRET titration curves using RlucII-CLN3 and Vps26A-GFP10 in wild-type (Fig. 3.5C, blue curve) and CLN5^{KO} HeLa cells (Fig. 3.5C, red curve). We found a significantly weaker CLN3/retromer interaction in CLN5^{KO} cells compared to wild-type HeLa cells as shown by the 4 fold increase of the BRET$_{50}$ in CLN5^{KO} HeLa cells compared to wild-type cells (Fig. 3.5D). As expected, expressing HA-CLN5 in CLN5^{KO} cells rescued the CLN3/retromer interaction (Fig. 3.5B, green curve) as the BRET$_{50}$ was similar to wild-type HeLA cells (Fig. 3.5C). Expressing HA-CLN5^{Y392X} in CLN5^{KO} HeLa cells had a partial

rescue effect on the CLN3/retromer interaction (Fig. 3.5C, purple curve), but the $BRET_{50}$ was still more than 3 fold larger (Fig. 3.5D).

We have also shown an interaction between CLN3 and sortilin (Yasa *et al.*, 2020) and between CLN5 and sortilin (Mamo *et al.*, 2012). To test if a disease-causing mutation in CLN5 affected its ability to interact with sortilin, we performed a co-immunoprecipitation assay (Fig. S2C). Wild-type CLN5, as well as the disease-causing mutant tested, $CLN5^{Y392X}$, were able to interact with sortilin. We next generated BRET titration curves using RlucII-CLN3 and sortilin-YFP in wild-type (Fig. 3.5E, blue curve) and $CLN5^{KO}$ HeLa cells (Fig. 3.5E, red curve). We extrapolated the $BRET_{50}$ for the interaction between CLN3 and sortilin and found that the $BRET_{50}$ in $CLN5^{KO}$ HeLa cells was 6 fold larger than in wild-type cells, indicating a decreased interaction in $CLN5^{KO}$ cells (Fig. 3.5F). Expressing HA-CLN5 in $CLN5^{KO}$ HeLa cells rescued the phenotype as the $BRET_{50}$ value was similar to wild-type cells (Fig. 3.5F, green curve), while expressing HA-$CLN5^{Y392X}$ (Fig. 3.5F, purple curve) did not. Although expression of $CLN5^{Y392X}$ had a partial rescue of the CLN3/sortilin interaction, the $BRET_{50}$ values were not restored to levels comparable to rescuing with wild-type CLN5 (Fig. 3.5F). To confirm our BRET results, we performed a co-immunoprecipitation experiment to determine the role of CLN5 in the modulating the CLN3/Rab7A, CLN3/retromer and sortilin/CLN3 interactions (Fig. S2B). We found that retromer (Vps26A), Rab7A and sortilin could co-immunoprecipitate with Flag-CLN3 in wild-type HeLa cells, but not in $CLN5^{KO}$ HeLa cells. The interaction was specific as expressing empty Flag vector did not coimmunoprecipitate retromer or Rab7A (Fig. S2B).

3.2.6 CLN5 is required for the efficient degradation of proteins following internalization

Another function of Rab7A is mediating key steps in the degradation of endocytic cargo (Vanlandingham & Ceresa, 2009; Ceresa & Bahr, 2006). Upon Epidermal Growth Factor (EGF) stimulation, EGF receptor (EGFR) is internalized and can be either recycled to the cell surface, or degraded in lysosomes (Ceresa & Peterson, 2014). At least two Rab7A effectors have been implicated in EGFR degradation, RILP and PLEKHM1. Depletion of either of these proteins results in significant delays in the degradation kinetics of EGFR (McEwan *et al.*, 2014; Progida *et al.*, 2007; Marwaha *et al.*, 2017). To determine whether CLN5 is implicated in this pathway, we investigated the degradation

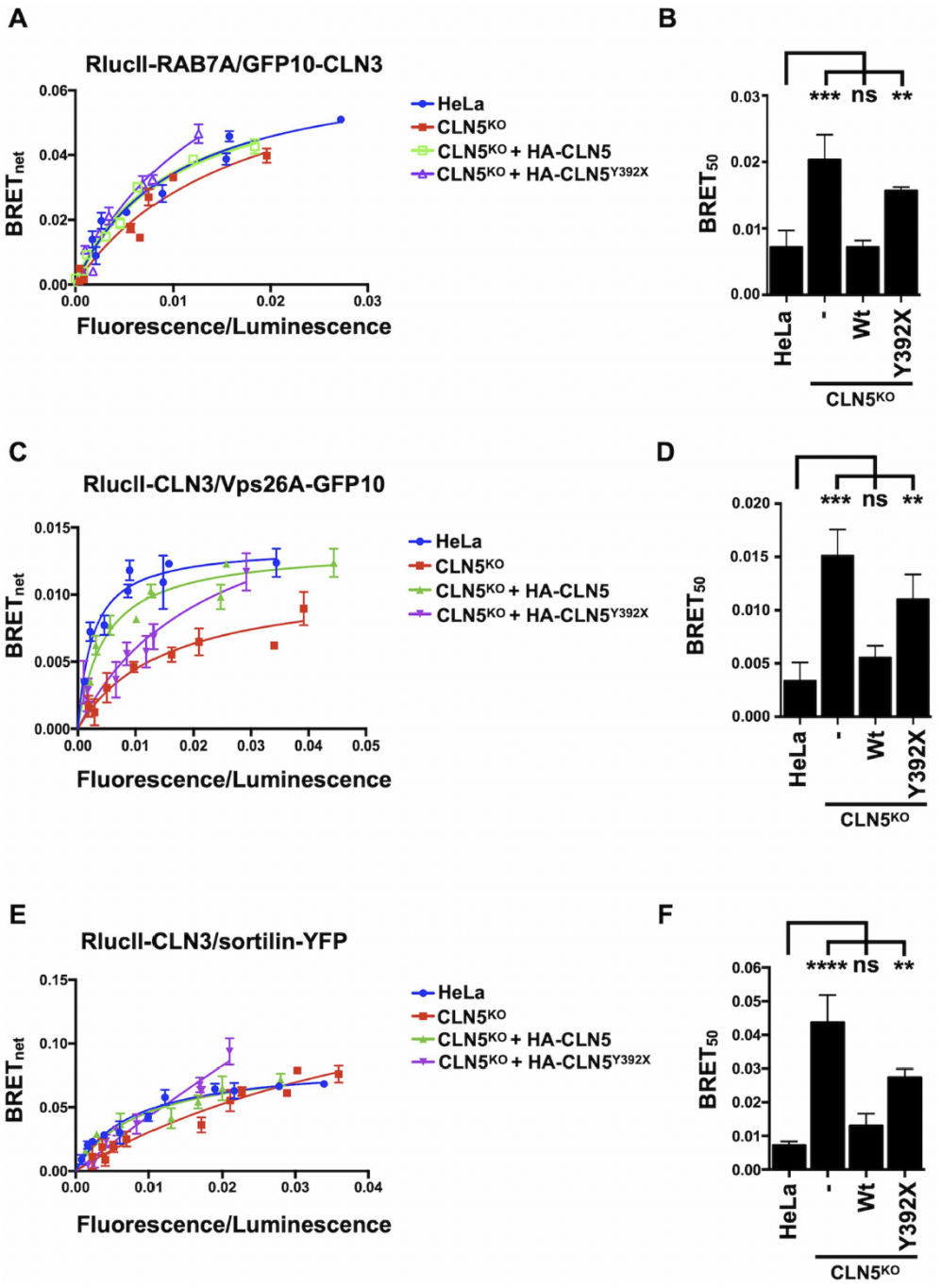

Figure 3.5: CLN5 modulates CLN3 interactions.

(A) Wild-type, $CLN5^{KO}$ and $CLN5^{KO}$ HeLa rescued with wild-type HA-CLN5 or HA-$CLN5^{Y392X}$ were transfected with a constant amount of RlucII-Rab7A and increasing amounts of GFP10- CLN3 to generate BRET titration curves. BRET signals are plotted as a function of the ratio between the GFP10 fluorescence over RlucII luminescence. (B) $BRET_{50}$ was extrapolated from 3 independent experiments. Data is shown as mean±s.d.; ns, not significant, $^{**}P \leq 0.01$, $^{****}P \leq 0.0001$, one-way ANOVA followed by Tukey's *post hoc* test. (C) Wild-type, $CLN5^{KO}$ and $CLN5^{KO}$ HeLa rescued with wild-type HA-CLN5 or HA-$CLN5^{Y392X}$ were transfected with a constant amount of RlucII-CLN3 and increasing amounts of Vps26A-GFP10 to generate BRET titration curves. BRET signals are plotted as a function of the ratio between the GFP10 fluorescence over RlucII luminescence. (D) $BRET_{50}$ was extrapolated from 3 independent experiments. Data is shown as mean±s.d.; ns, not significant, $^{**}P \leq 0.01$, $^{***}P \leq 0.0001$, one-way ANOVA followed by Tukey's *post hoc* test. (E) Wild-type, $CLN5^{KO}$ and $CLN5^{KO}$ HeLa rescued with wild-type HA-CLN5 or HA-$CLN5^{392X}$ were transfected with a constant amount of RlucII-CLN3 and increasing amounts of sortilin-YFP to generate BRET titration curves. BRET signals are plotted as a function of the ratio between the YFP fluorescence over RlucII luminescence.

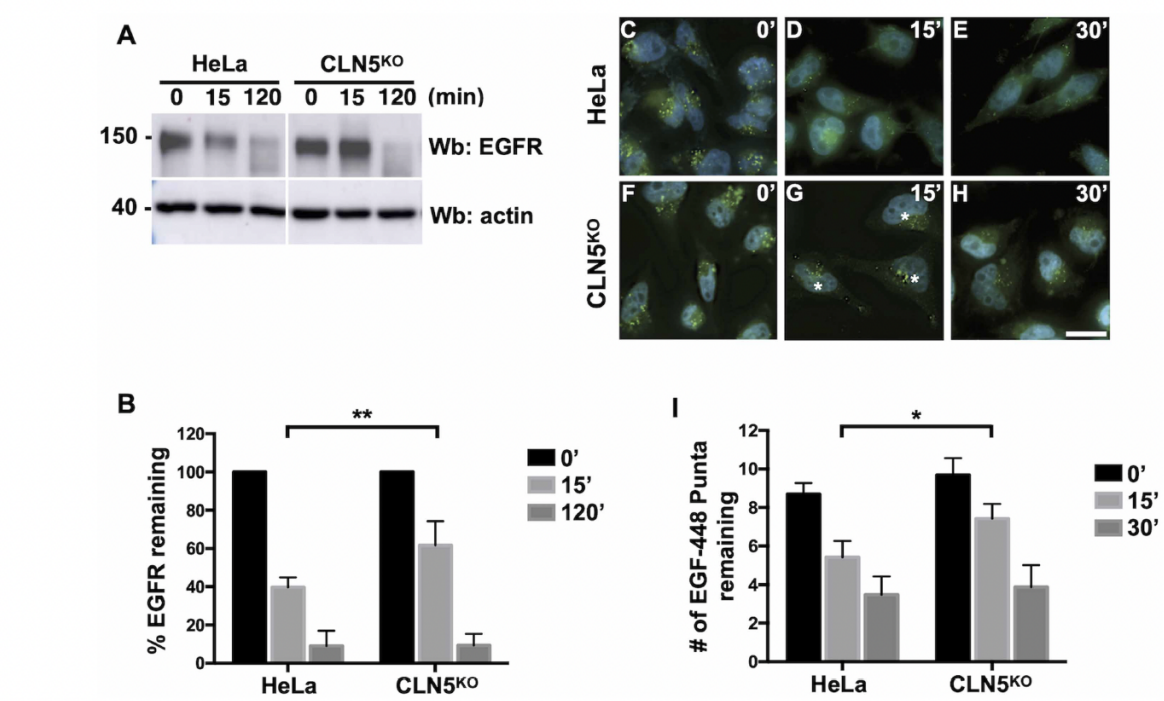

Figure 3.6: EGF and EGFR degradation is delayed in CLN5^{KO} cells.

(A) Wild-type and CLN5^{KO} HeLa cells were incubated with 50 μg/ml cycloheximide for 1 h and subsequently treated with 100 ng/ml EGF in Opti-MEM for 0, 15 and 120 min. Whole cell lysate was then resolved by SDS-PAGE and a Western blot (Wb) was performed using anti-EGFR antibody. Anti-actin staining was used as a loading control. (B) Quantification of the remaining EGFR as detected in A was performed in 3 independent experiments. Data are mean±s.d. ns, not significant; $^{**}P \leq 0.01$; one-way ANOVA followed by Tukey's *post hoc* test. Scale bar: 10 μm. (C - H) Wild-type (C - E) and CLN5^{KO} (F - H) HeLa cells were grown on coverslips and incubated with 300 ng/ml EGF-488 for 0, 15 or 30 min. The cells were fixed with 4% PFA for 12 min, followed by staining with DAPI to visualize the nucleus. Images were taken on a Zeiss Fluorescence microscope using a 63× objective. Stars indicate remaining EGF-488. (I) EGF-488 (green puncta) were counted using ImageJ in 50 cells per condition. The results shown are the average number of puncta per cell per condition. Data are mean±s.d. ns, not significant; $^{*}P \leq 0.05$; one-way ANOVA followed by Tukey's *post hoc* test. Scale bar: 10 μm.

kinetics of EGFR in wild-type and CLN5^{KO} HeLa cells. The cells were serum starved for 1 hour in the presence of cycloheximide and then stimulated with 100 ng/ml of EGF in the presence of cycloheximide for the indicated periods of time. The level of endogenous EGFR was determined by Western blot using anti-EGFR antibody. Anti-actin staining was used as a loading control (Fig. 3.6A). In wild-type cells, EGFR degradation was observed after 15 minutes and quantification of 3 independent experiments found substantial degradation at 15 (34.3% remaining) and 120 minutes (9% remaining) (Fig. 3.6B). When we compared the degradation kinetics of EGFR in CLN5^{KO} cells, we found significant delay at 15 (75.6% remaining) compared to wild-type cells, with no significant difference at 120 minutes (10.3% remaining) (Fig. 3.6B).

Next, we tested the degradation kinetics of Alexa-488 labeled EGF (EGF-488) using the same cell lines to confirm our EGFR degradation results. Following 2 hours of serum starvation, wild type

(Fig. 3.6C - E) and CLN5^{KO} (Fig. 3.6F - H) HeLa cells were incubated with 300 ng/ml EGF-488 for 30 minutes, washed and then chased for 0 (Fig. 3.6C and F), 15 (Fig. 3.6D and G) or 30 minutes (Fig. 3.6E and H). Images were acquired at random from the different conditions and the number of EGF-488 puncta from 35 cells per condition were counted using Image J as we have previously done (Yasa *et al.*, 2020). At time 0 min, both wild-type and CLN5^{KO} HeLa cells had comparable number of EGF-488 puncta (an average of 8.7 versus 9.7 respectively). After 15 minutes of chase, wild-type HeLa cells had an average of 5.4 puncta per cell, while CLN5^{KO} HeLa had on average 7.4 puncta per cell, an increase of 37% (Fig. 3.6I). After 30 minutes of chase, wild-type HeLa cells had an average of 3.4 puncta per cell, while CLN5^{KO} HeLa had on average 3.8 puncta per cell (Fig. 3.6I).

3.2.7 CLN5 is required for the RAB7A–RILP interaction

To understand the mechanism behind the delayed EGF and EGFR degradation, we used BRET to determine if the Rab7A/PLEKHM1 or Rab7A/RILP interactions were affected (Fig. 3.7A - D). RILP and PLEKHM1 are implicated in the degradation of internalized cargo such as EGFR by either participating in the tethering of vesicles, as is the case for PLEKHM1 (McEwan *et al.*, 2014), or by mediating the movement of vesicles, as is the case for RILP (Wijdeven *et al.*, 2016). We generated BRET titration curves by transfecting a constant amount of RlucII-Rab7A and increasing amounts of PLEKHM1-GFP10 (Fig. 3.7A) or increasing amounts of RILP-GFP10 (Fig. 3.7C). We found no significant change in the interaction between PLEKHM1 and Rab7A in CLN5^{KO} HeLa cells compared to wild-type HeLa cells as shown by the similar BRET$_{50}$ values (Fig. 3.7B). On the other hand, the interaction between RILP and Rab7A was significantly disrupted in CLN5^{KO} cells, as the BRET50 value was 3 fold higher for the Rab7A/RILP interaction in CLN5^{KO} cells compared to wild-type cells, suggesting a weaker interaction (Fig. 3.7D). Rab7A can interact with RILP to subsequently engage dynein motors for minus-end transport of lysosomes (van der Kant *et al.*, 2013; Johansson *et al.*, 2007). If this transport system is affected due to the decreased Rab7A/RILP interaction, we would expect dysfunctional minus-end movement of lysosomes following starvation and the induction of autophagy. We compared the positioning of lysosomes, by staining with the lysosomal membrane protein CD63, in wild-type and CLN5^{KO} cells that were starved in EBSS for 3 hours or maintained in DMEM (Fig. 3.7E - H). In both wild-type (Fig. 3.7E and E') and CLN5^{KO} (Fig. 3.7F and F') HeLa cells cultured in DMEM, CD63 positive lysosomes were

distributed throughout the cells. In nutrient starved wild-type cells, lysosomes efficiently moved in a retrograde manner towards the perinuclear region of the cell (Fig. 3.7G and G', white arrows). However, while CLN5^{KO} HeLa cells were able to move some lysosomes, they were not as efficient as wild-type HeLa cells (Fig. 3.7H and H'). Quantification of 30 cells per condition showed that as a percentage of total CD63 fluorescence, CLN5^{KO} cells had significantly less perinuclear lysosomes compared to wild-type HeLa cells (Fig. 3.7I).

3.2.8 CLN5 is required for autophagosome/lysosome fusion

A role for minus-end movement of lysosomes is to enable efficient fusion with autophagosomes, a step required for efficient autophagic degradation (Cabukusta & Neefjes, 2018). Previous studies have reported autophagic defects in cells depleted of CLN5 by RNAi (Adams *et al.*, 2019), or CLN5 deficient cells (Doccini *et al.*, 2020; Leinonen *et al.*, 2017). Therefore, in CLN5^{KO} HeLa cells, we would expect less autophagosome/lysosome fusions and defective autophagic flux. To test fusion ability, we expressed mCherry-LC3 and Lamp1-GFP in wild-type (Fig. 3.9A - C), CLN5^{KO} (Fig. 3.9D - F) and Rab7A^{KO} HeLa cells (Fig. 3.9G - I). LC3 is a marker of autophagosomes, while Lamp1 is a marker of lysosomes. Upon the initiation of autophagy by starvation, LC3-positive autophagosomes fuse with Lamp1-positive lysosomes, forming autolysosomes in order to degrade material (Nakamura & Yoshimori, 2017). Cells were nutrient starved for 3 hours in EBSS and the co-localization of mCherry-LC3 and Lamp1-GFP was determined. Quantification of the co-localization using Pearson's coefficient in 30 cells per condition showed a high level of co-localization of mCherry-LC3 and Lamp1-GFP in wild-type HeLa cells, suggesting that autophagosomes were fusing with lysosomes (Fig. 3.9J). Rab7A participates not only in the movement of lysosomes, but also in the fusion process (Birgisdottir & Johansen, 2020). As such, we would expect significantly less co-localization in Rab7A^{KO} HeLa cells. Compared to wild-type cells, the co-localization between LC3 and Lamp1 was significantly reduced in Rab7A^{KO} HeLa cells (Fig. 3.9J). We also found significantly less co-localization between LC3 and Lamp1 in CLN5^{KO} HeLa cells (Fig. 3.9J), suggesting that the deficient retrograde movement of lysosomes was preventing fusion between autophagosomes and lysosomes.

Next, we used a tandem LC3 probe (mTagRFP-mWasabi-LC3) to determine autophagic flux (Zhou *et al.*, 2012). mWasabi is pH sensitive (more sensitive compared to EGFP), while mTagRFP

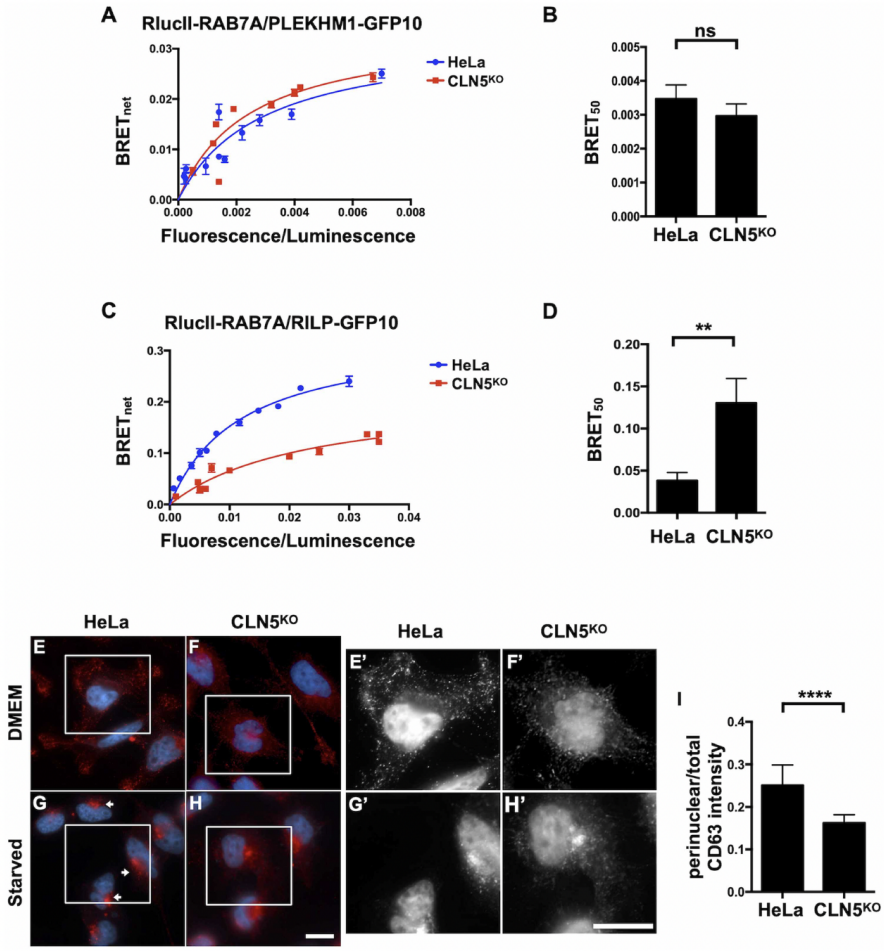

Figure 3.7: Retrograde transport of lysosomes is deficient in CLN5^{KO} HeLa cells.

(A) Wild-type and CLN5^{KO} HeLa cells were transfected with a constant amount of RlucII-Rab7A and increasing amounts of PLEKHM1-GFP10 to generate BRET titration curves. BRET signals are plotted as a function of the ratio between the GFP10 fluorescence over RlucII luminescence. (B) BRET$_{50}$ was extrapolated from 3 independent experiments. Data is shown as mean±s.d.; ns, not significant. (C) Wild-type and CLN5^{KO} HeLa cells were transfected with a constant amount of RlucII-Rab7A and increasing amounts of RILP-GFP10 to generate BRET titration curves. BRET signals are plotted as a function of the ratio between the GFP10 fluorescence over RlucII luminescence. (D) BRET$_{50}$ was extrapolated from 3 independent experiments. Data is shown as mean±s.d.; $^{**}P \leq 0.01$, Student's t-test. (E–H) Wild-type (E,G) and CLN5^{KO} (F,H) HeLa cells were cultured in standard DMEM (E,F) or starved (G,H) for 3 h in EBSS. The cells were subsequently immunostained with anti-CD63 antibody. The cells were then fixed with 4% PFA for 12 min, followed by staining with DAPI to visualize the nucleus. Images were taken on a Zeiss Fluorescence microscope using a 63× objective. Representative images are shown. Scale bar: 10 μm. (E0 –H0) Magnified view of white square area shown in (E–H). Scale bar 10 μm. (I) Fluorescence intensity of CD63 in the perinuclear region and total cellular CD63 fluorescence was determined using ImageJ. Results shown are the ratio of perinuclear intensity divided by total CD63 fluorescence intensity from 30 cells. Data are shown as mean ± s.d.; ****P $\leq$ 0.0001, Student's t-test. Scale bar: 10 μm.

is not. If cells can proceed with autophagy, the fusion of autophagosomes with lysosomes quenches the mWasabi so red is observed, while late blocks in autophagy (no autophagosome fusion with lysosomes) results in an increase in yellow puncta, with a corresponding decrease in red signal, since mWasabi is not quenched. We expressed mTagRFP-mWasabi-LC3 in wild-type (Fig. 3.9K), CLN5^{KO} (Fig. 3.9L) and Rab7A^{KO} HeLa cells (Fig. 3.9M), and the cells were starved in EBSS

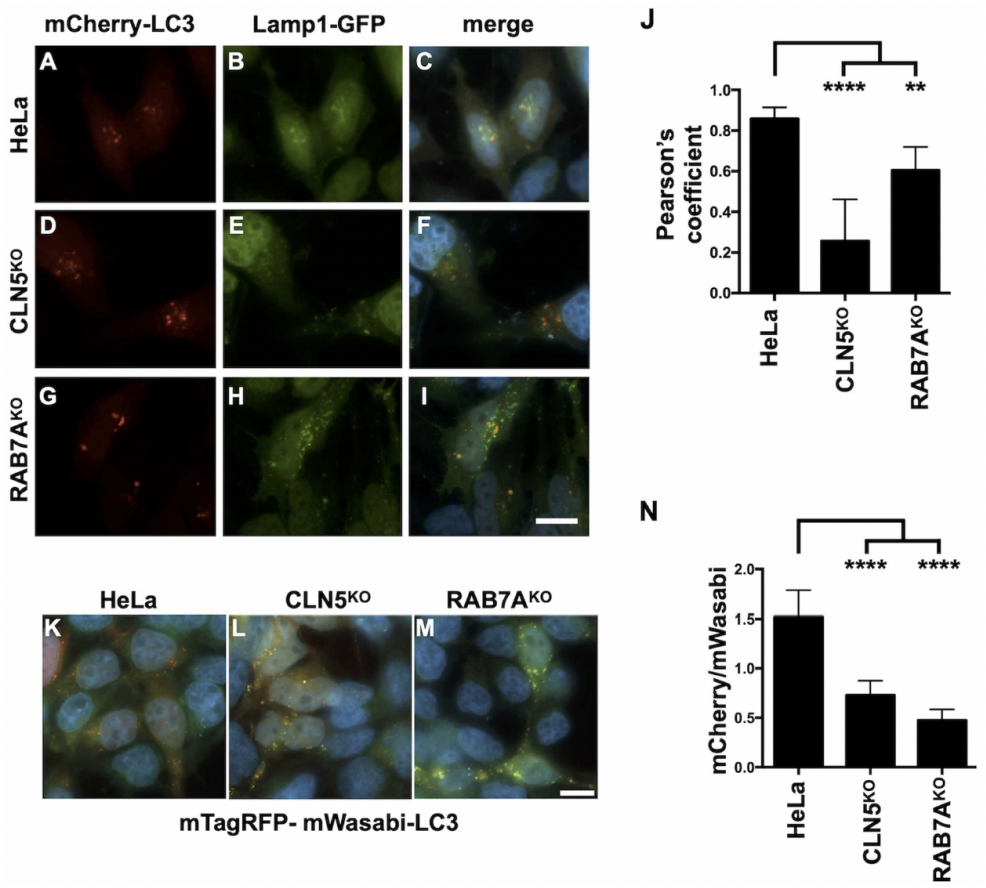

Figure 3.8: Lack of fusion of autophagosomes to lysosomes in CLN5^{KO} HeLa cells.

(A - I) mCherry-LC3 and Lamp1-GFP were co-transfected into wild-type (A - C), CLN5^{KO} (D - F) and Rab7A^{KO} (G - I) HeLa cells and imaged on a Zeiss Fluorescence microscope using a 63× objective. Representative images are shown. Scale bar = 10 μm. (J) Quantification of the fluorescence from 35 cells to determine the Pearson's coefficient of mCherry-LC3 and Lamp1-GFP in wild-type, CLN5^{KO} and Rab7A^{KO} HeLa cells. $^{**}P \leq 0.01$; $^{****}P \leq 0.0001$; one-way ANOVA followed by Tukey's *post hoc* test. (K - N) mTagRFP-mWasabi-LC3 was transfected into wildtype (K), CLN5^{KO} (L) and Rab7A^{KO} (M) HeLa cells. Representative images are shown. Scale bar: 10 μm (N) Quantification of mCherry divided by mWasabi was calculated for 30 cells. $^{****}P \leq 0.0001$; one-way ANOVA followed by Tukey's *post hoc* test.

for 3 hours. In wild-type cells, autophagosome/lysosome fusion occurs, resulting in a red signal as the mWasabi is quenched (Fig. 3.9K and N). In CLN5^{KO} HeLa cells, fusion is deficient, and therefore mWasabi is not exposed to the acidic pH of the lysosomal lumen and no quenching occurs. Therefore, the red signal is significantly decreased (Fig. 3.9L and N). Since Rab7A^{KO} is required for efficient fusion, a similar observation was made in Rab7A^{KO} HeLa cells as expected (Fig. 3.9M and N).

3.3 Discussion

CLN5 is a soluble endolysosomal protein whose function remains poorly understood. Mutations in this protein cause a rare neurodegenerative disease that affects children, so understanding the function of CLN5 could lead to new therapeutic targets. Work using the model organism Dictyostelium discoideum showed that CLN5 has glycoside hydrolase activity (Huber & Mathavarajah, 2018), and previous reports found that CLN5 regulates lysosomal pH (Best *et al.*, 2016) and autophagy (Adams *et al.*, 2019; Leinonen *et al.*, 2017). More recent work has implicated CLN5 in mitochondrial function (Doccini *et al.*, 2020). Using siRNA ($CLN5^{KD}$), we previously demonstrated that CLN5 regulates the stability of the lysosomal sorting receptor sortilin by enabling its endosome-to-TGN trafficking (Mamo *et al.*, 2012). However, using this KD system, we never tested the effects of disease-causing mutations on this trafficking pathway, or whether CLN5 modulated other Rab7A functions. Furthermore, it is not known how a soluble endolysosomal protein can regulate protein-protein interactions in the cytosol. In this current work, we generated a CLN5 knockout ($CLN5^{KO}$) HeLa cell line that can be rescued with wildtype or mutant CLN5. Using this tool, we have confirmed our previous work and expanded our understanding of the function of this protein.

In our $CLN5^{KD}$ HeLa cells, we observed less membrane bound Rab7A and retromer (Mamo *et al.*, 2012). We found less membrane bound retromer in our $CLN5^{KO}$ HeLa cells, which was rescued by expressing wild-type CLN5, but not the disease-causing mutant ($CLN5^{Y392X}$). Although retromer recruitment was deficient in $CLN5^{KO}$ HeLa cells, Rab7A was still membrane bound. This raised two points. Why the discrepancy between the KD and KO models, and how could Rab7A be membrane bound but not recruit retromer? We hypothesize that chronic loss of CLN5 in the KO model results in the cell overcoming the effect, while acute depletion of CLN5 by siRNA does not allow time for the cell to compensate. We have previously shown that Rab7A palmitoylation is required for the efficient recruitment of retromer to endosomal membranes, but is not required for Rab7A membrane localization (Modica *et al.*, 2017). We found that Rab7A palmitoylation is significantly decreased in $CLN5^{KO}$ HeLa cells, providing an explanation for the decrease in the Rab7A/ retromer interaction as measured in live cells by BRET, and the subsequent lack of retromer recruitment. Palmitoylation of Rab7A is not required to modulate the Rab7A/retromer interaction *per se*, but serves to localize Rab7A to specific endosomal membrane domains to favour the interaction (Modica *et al.*, 2017). When membranes are disrupted such as in co-immunoprecipitation, non-palmitoylatable Rab7A can

interact with retromer (Modica *et al.*, 2017). As such, it is not surprising that Rab7A and retromer interacted by co-immunoprecipitation in CLN5^{KO} HeLa cells.

The recruitment of retromer to endosomal membranes enables the endosome-to-TGN retrieval of the lysosomal sorting receptor sortilin (Canuel *et al.*, 2008). The sortilin/retromer interaction was perturbed in CLN5^{KO} HeLa cells compared to wild-type HeLa cells. While the expression of wildtype CLN5 in CLN5^{KO} HeLa cells rescued the sortilin/retromer interaction, the expression CLN5^{Y392X} did not. This would suggest that the residues at the C-terminal end of CLN5 are required for the sortilin/retromer interaction, however how those residues modulate this interaction is yet to be determined. The decrease in the sortilin/retromer interaction observed in the CLN5^{KO} HeLa cells should result in the lysosomal degradation of the lysosomal sorting receptor. As in the CLN5^{KD} HeLa cells (Mamo *et al.*, 2012), sortilin is degraded in CLN5^{KO} HeLa cells. Expression of wild-type CLN5 rescued this degradation, while expressing the disease-causing mutant CLN5^{Y392X} did not rescue. Taken together, these observations point to a crucial role of CLN5 in modulating Rab7A-dependent retromer recruitment and function. Indeed by modulating the palmitoylation level of the small GTPase, CLN5 establishes the conditions for an optimal Rab7/ retromer interaction, hence efficient retromer/sortilin binding and recycling to the TGN, which in turns translates in proper lysosomal function.

In our recently published paper, we demonstrated that CLN3 functions as a scaffold to ensure efficient protein-protein interactions. In that study, we demonstrated decreased Rab7A/ retromer and retromer/sortilin interactions in CLN3^{KO} HeLa cells, which consequently lead to the degradation of sortilin (Yasa *et al.*, 2020). We found similar results in our CLN5^{KO} HeLa cells. Furthermore, we found that CLN5 is required for the CLN3/retromer and CLN3/sortilin interactions. Although wild-type CLN5 rescued the CLN3/sortilin interaction in CLN5^{KO} HeLa cells, the expression of the disease-causing mutant did not. Based on this data, we propose a model where CLN3 and CLN5 function as an endosomal complex required for the efficient endosome-to-TGN trafficking of sortilin. This inefficient recycling results in defective lysosomal function, which is a hallmark of CLN5 disease. Our results suggest a potential pathogenic mechanism for CLN5 disease.

We next asked if other Rab7A mediated pathways are affected in CLN5^{KO} HeLa cells. We found significant delays in the degradation of both EGFR and EGF. This delayed degradation could be due to less efficient lysosomal function, or due to decreased fusion of endocytic cargo

with lysosomes, a mechanism also modulated by Rab7A. The Rab7A effector RILP is implicated in the degradation of internalized cargo such as EGFR by mediating the movement of vesicles (Wijdeven *et al.*, 2016), while the Rab7A effector PLEKHM1 is a tether required for fusion in both endocytic degradation and autophagy (McEwan *et al.*, 2014). In CLN5^{KO} HeLa cells, we found no changes to the Rab7A/PLEKMH1 interaction, but we found a decreased Rab7A/RILP interaction. This resulted in deficient movement of CD63 positive lysosomes toward the perinuclear region, an important step in the autophagic process. Indeed, we observed less colocalization of LC3II containing autophagosomes with Lamp1 positive lysosomes upon starvation in CLN5^{KO} HeLa cells, and less autophagic flux as demonstrated using a tandem LC3 probe (mTagRFP mWasabi-LC3). While decreased lysosomal function plays a role in the pathogenic mechanism of CLN5 disease, defective endocytic degradation and autophagy are most likely due to defective lysosomal movement and thus decreased fusion events.

In conclusion, in this study we demonstrate a role for CLN5, together with CLN3, acting as a complex to regulate endosome-to-TGN trafficking. While CLN3 behaves like an interaction platform, CLN5 ensures those CLN3 interactions, which are vital for lysosomal functioning are maintained and regulated. These findings enlighten the molecular mechanisms behind NCL pathogenesis caused by defected CLN5 and CLN3 proteins.

Data Availability

All of the primary data that is presented in this study can be requested in electronic form by contacting Stephane Lefrancois (stephane.lefrancois@inrs.ca). All reagents generated by our group are available upon request to Stephane Lefrancois (stephane.lefrancois@inrs.ca).

Competing Interests

The authors declare that there are no competing interests associated with the manuscript.

Funding

This work was supported by the Joint Programme in Neurodegenerative Diseases (Neuronode), the Canadian Institutes for Health Research (ENG-155186), the Canadian Foundation for Innovation (35258), and ForeBatten Foundation grants to SL. SY and GM are supported by a scholarship from Fond de recherche du Quebec - Santé.

Acknowledgements

We would like to thank Michel Bouvier (IRIC and University de Montreal), Regis Grailhe, (Pasteur Institute Korea), Paul Odgren (University of Massachusetts Medical School, Addgene #73592), Makoto Kanzaki (Tohoku University), Takeshi Nakamura (Tokyo University of Science) , Peter J. McCormick (Queen Mary University), Juan S. Bonifacino (NICHD, NIH), Jian Lin (Peking University) for providing plasmids. We would like to thank Guido Hermey (Institute for Molecular and Cellular Cognition, Center for Molecular Neurobiology Hamburg, University Medical Center Hamburg-Eppendorf) for providing the parental HeLa cells.

3.4 Materials and methods

3.4.1 Plasmids and mutagenesis

RlucII-CLN3, GFP10-CLN3, Vps26A-nLuc, PLEKHM1-GFP10, RlucII-Rab7A, Vps26A-GFP10, RILP-GFP10 and sortilin-myc were previously described [16, 21, 22]. The various CLN5 mutants were engineered using site-directed mutagenesis from the previously described HA-CLN5 and CLN5-HA constructs [3]. Sortilin-YFP was a generous gift from Dr. Makoto Kanzaki, Tohoku University. mCherry-LC3 was a generous gift from Dr. Peter K. Kim, Sickkids Hospital. Lamp1-GFP was a generous gift from Dr. Juan Bonifacino, NICHD, NIH. mTagRFP-mWasabi- LC3 was a generous gift from Jian Lin, Peking University.

3.4.2 Antibodies

The following mouse monoclonal antibodies were used: anti-actin (Wb: 1 : 3000, BD Biosciences 612657); anti-Lamp2 (Wb: 1 : 500, Abcam ab25631); anti-HA (Wb: 1 : 1000, Cedarlane Labs 901503); anti-myc (Wb: 1 : 1000, ThermoFisher Scientific LS132500), anti-Cathepsin D (Wb: 1 : 100, Sigma–Aldrich, IM03); anti-Flag (Wb: 1 : 1000, Sigma–Aldrich F1804); anti-CD63 (IF: 1 : 500, BD Bioscience 556019). The following rabbit monoclonal antibodies were used: anti-RAB7A (Wb: 1 : 1000, Cell Signalling Technology D95F2); anti-EGFR (Wb: 1 : 1000, Abcam ab52894); anti-CLN5 (Wb: 1 : 1000 Abcam ab1700899). The following rabbit polyclonal antibodies were used: anti-Vps26A (Wb: 1 : 2000, Abcam ab23892); anti-FLAG (Wb: 1 : 1000, BioLegend, 902401); anti-sortilin (Wb: 1 μg/ml, Abcam ab16640).

3.4.3 Cell culture and transient transfections

HeLa cells were cultured in Dulbecco's modified Eagle's medium (DMEM) supplemented with 2mM L-Glutamine, 100 U/ml penicillin, 100g/ml streptomycin and 10% FBS (Wisent Bioproducts, St-Bruno, QC) at 37°C. in a humidified chamber at 95% air and 5% CO2. Cells were seeded at a density of 2 X 10^5/well for 12 well plates and 5 X 10^5/well for 6 well plates 24 hours prior to transfection. Transfections were performed with polyethylenimine (PEI) (ThermoFisher Scientific, Ottawa, ON). Briefly, solution 1 was prepared by diluting plasmid into Opti-MEM (ThermoFisher Scientific). Solution 2 was prepared by diluting PEI (1 μg/μl) into Opti-MEM in a ration of 1:3 with the DNA to be transfected. After a 5 min incubation, the two solutions were mixed, vortexed for 3 s, incubated at room temperature (RT) for 15 min and subsequently added to the cells.

3.4.4 CRISPR/Cas9 Editing

HeLa cells were transfected with an all-in-one CRISPR/Cas9 plasmid for CLN5 (plasmid number HCP202087-CG01-1-B, Genecopoeia, Rockville, MD). 72 hours post-transfection, cells were treated with 1mg/ml Geneticin (ThermoFisher Scientific) for 1 week. Limited dilution was performed to isolate single cells, which were allowed to grow for 2 weeks. Western blotting was used to identify $CLN5^{KO}$ cells. Genomic DNA extracted form $CLN5^{KO}$ HeLa cells was sequenced to confirm $CLN5^{KO}$ cells. $Rab7A^{KO}$ HeLa cells were previously described [16].

3.4.5 BRET titration experiments

HeLa cells were seeded in 12-well plates and transfected with the indicated plasmids. 48 hours post transfection, cells were washed in PBS, detached with 5mM EDTA in PBS and collected in 500 μl of PBS. Cells were transferred to opaque 96-well plates (VWR Canada, Mississauga, ON) in triplicates. Total fluorescence was first measured with the Tecan Infinite M1000 Pro plate reader (Tecan Group Ltd., Mannedorf, Switzerland) with the excitation and emission set at 400 nm and 510 nm respectively for BRET^2 and 500 nm and 530 nm for BRET^1. The BRET^2 substrate coelenterazine 400a and BRET^1 substrate h-coelenterazine were then added to all wells (5 μM final concentration) and the BRET^2 or BRET^1 signals measured 2 min later. The BRET signals were calculated as a ratio of the light emitted at 525 $\pm$ 15 nm over the light emitted at 410 $\pm$ 40 nm. The BRET$_{net}$ signals were calculated as the difference between the BRET signal in cells expressing both fluorescence and luminescence constructs and the BRET signal from cells where only the luminescence fused construct was expressed.

3.4.6 Western blotting

Cell were detached using 5mM EDTA in PBS, washed in 1X PBS and collected by centrifugation. TNE buffer (150 mM NaCl, 50 mM Tris, pH 7.5, 2 mM EDTA, 0.5% Triton X-100 and protease inhibitor cocktail) was used to lyse cells by incubating them for 30 minutes on ice. Lysates were centrifuged at high speed for 10 minutes and the supernatants (whole cell lysate) were collected to be analyzed by Western blotting. Samples were mixed with sample buffer 3X to obtain a final concentration of 1X (62.5 mM Tris-HCl pH 6.5, 2.5% SDS, 10% glycerol, 0.01% bromophenol blue). Samples were incubated at 95°C. for 5 minutes and resolved on SDS-PAGE followed by wet-transfer to nitrocellulose membranes. Detection was done by immunoblotting using the indicated antibodies.

3.4.7 Membrane separation assay

24hrs after transfection, cells were collected in 5mM EDTA in PBS. The cells were subsequently snap frozen in liquid nitrogen and allowed to thaw at RT for 5min. The cells were resuspended in Buffer 1 (0.1 M Mes-NaOH pH 6.5, 1 mM MgAc, 0.5 mM EGTA, 200 M sodium orthovanadate, 0.2 M sucrose) and centrifuged at 10,000 g for 5 minutes at 4°C. The supernatants containing the

cytosolic proteins (S, soluble fraction) were collected. The remaining pellet was resuspended in Buffer 2 (50 mM Tris, 150 mM NaCl, 1 mM EDTA, 0.1% SDS, 1% Triton X-100) and centrifuged at 10,000 g for 5 minutes at 4°C. Samples were loaded into SDS-PAGE gels in equal volumes. Fiji was used to quantify the intensity of the bands [23]. The intensity of each fraction was calculated and divided by the total intensity to determine the distribution of proteins.

3.4.8 Cycloheximide chase

Wild-type, CLN5^{KO}, Rab7A^{KO} HeLa cells were seeded in 6-well plates the day prior to transfection. 500 ng of HA fused wild-type and mutation harbouring CLN5 were transfected into CLN5^{KO} HeLa cells. 48 hours after transfection, cells were treated with 50 μg/ml of cycloheximide in Opti-MEM. Lysates were collected at 0, 3 or 6 hour-time points and run on 10% SDS-PAGE gels. Fiji was used to quantify the intensity of the bands [23]. All protein levels were standardized to the actin loading control. Amount of remaining protein is expressed as a percentage of the 0 time point in each group.

3.4.9 Assays to determine lysosomal function

To determine the activity of cathepsin B, confluent CLN5KO, RAB7AKO and wild-type HeLa cells from 12-well plates were collected and 3×10^6 cells/ml of each cell type were transferred to 96-well plates (with black walls and a clear bottom) in triplicate. Staining was performed by adding the Magic Red substrate to PBS for 60 min at 37°C protected from light. As cells settled to the bottom, they were gently resuspended by pipetting every 10–20 min to ensure that the Magic Red was evenly dispersed among all cells. The fluorescence intensity of the Magic Red substrate was measured with a Tecan Infinite M1000 Pro plate reader (Tecan Group Ltd., Mannedorf, Switzerland) with the excitation and emission set at 592 nm and 628 nm, respectively. The average of non-stained sample fluorescence intensities was calculated for each sample and subtracted from the fluorescence reads of the Magic Red-stained samples to eliminate background fluorescence. To determine the activity of β-glucuronidase, cells were collected and lysed in TNE buffer and protein concentration was determined using the Bradford reagent. Whole cell lysate was loaded into transparent 96 well flat bottom plates as triplicates; 5 mM of methylumbelliferyl-β-D-glucuronide (MUG) (Sigma–Aldrich, Oackville, ON) was added to test the activity of β-glucuronidase. After 1 h of incubation at 37°C,

fluorescent intensities were measured Tecan Infinite M1000 Pro plate reader (Tecan Group Ltd., Mannedorf, Switzerland) with the excitation and emission set at 360 nm and 445 nm, respectively. Y-axis is calculated as (sample readings with substrate-lysis buffer with substrate)/sample readings without substrate.

3.4.10 EGFR degradation assay

Wild-type, CLN5^{KO} and Rab7A^{KO} cells were seeded in 6-well plates the day before the assay. To prevent de novo synthesis EGFR during EGF stimulation, cells were treated with 50 μg/ml cycloheximide in Opti-MEM for 1 h. Stimulation of EGF was performed with 100 ng/ml EGF in Opti-MEM containing 50 μg/ml of cycloheximide. Cell lysates were collected as indicated above and Western blotting was performed. Fiji was used to quantify the intensity of the bands (Schindelin *et al.*, 2012). All protein levels were standardized to the actin loading control. Amount of remaining protein is expressed as a percentage of the 0 time point in each group.

3.4.11 EGF-488 pulse-chase

Wild-type and CLN5^{KO} HeLa cells were seeded on coverslips the day before the experiment. Cells were serumstarved in Opti-Mem for 2 h followed by a 30-min pulse of 300 ng/ml of EGF-488. Cells were then washed with PBS, fixed in 4% paraformaldehyde at 0, 15 and 30 min and mounted onto slide using Fluoromount G (ThermoFisher Scientific). The coverslips were sealed using nail polish. Cells were imaged using a Zeiss Axio Observer fluorescence microscope using an Alpha Plan-Apo 63×/1.46 oil objective. Images were captured by a Zeiss Axiocam 506 camera controlled by Zen Pro software. The number of puncta per cell was counted using Fiji. Briefly, the images were split into their individual channels. Using the green channel, the threshold was adjusted to 0.93% in order to get signal only from the puncta. The number of puncta counted from an image was divided by the number of nuclei within that image, which gave us the number of puncta per cell. Fifty cells per condition for each time point were analyzed.

3.4.12 Acyl-RAC to isolate palmitoylated proteins

The isolation of palmitoylated protein was adapted from Modica et al., 2017. Briefly, cells were lysed in TNE (150 mM NaCl, 50 mM Tris, pH 7.5, 2 mM EDTA, 0.5% Triton X-100 and protease inhibitor cocktail) supplemented with 50mM N-Ethylmaleimide (NEM) and incubated 30 minutes in rotating wheel at 4°C.. Samples were centrifuged 10 minutes at 10000g at 4°C. and the collected supernatants were incubated 2 hours at RT on a rotating wheel. Samples were then precipitated over night with two volumes of cold acetone at -20°C to remove NEM. After washing with cold acetone, the pellets were resuspended in binding buffer (100 mM HEPES, 1 mM EDTA, 1% SDS) with 250 mM hydroxylamine (Sigma-Aldrich) (NH2OH) pH7.5 to cleave palmitate residues off of proteins. Control samples were resuspended in binding buffer containing 250mM NaCl. When the pellets were completely resuspended, water-swollen thiopropyl sepharose 6B beads (GE Healthcare Life Sciences, Mississauga, ON) were added and samples were incubated 2 hrs at RT on rotating wheel. Beads were then washed 4 times with binding buffer and captured proteins were eluted with sample buffer containing 100mM DTT.

3.4.13 Lysosomal positioning

Wild-type and CLN5KO HeLa cells were plated onto glass coverslips in 6-well plates. The following day, the cells were serum staved or not in EBSS for 120 min. The coverslips were then washed with PBS and fixed with 4% paraformaldehyde in PBS for 12 min at RT, and then washed twice with PBS. The cells were then treated with 0.1% Triton X-100 in PBS for 30 min, followed by an incubation with anti-CD63 followed by staining with DAPI to visualize the nucleus. Coverslips were mounted on cover slides with Fluoromount G (Thermo Fisher Scientific). Cells were imaged using a Zeiss Axio Observer fluorescence microscope using an Alpha Plan-Apo 63x/1.46 oil objective. Images were captured by a Zeiss Axiocam 506 camera controlled by Zen Pro software. Fluorescence intensity of CD63 in the perinuclear region and total cellular CD63 fluorescence was determined using ImageJ. After splitting the channels, the ROI was manually selected for CD63 puncta localized to the perinuclear area in wild-type cells. The same ROI was copied and used for each analyzed cell, including the CLN5KO cells. Results shown are the ratio of perinuclear intensity divided by total CD63 fluorescence per cell. Thirty cells were analyzed for each condition.

3.4.14 Autophagy assays

Cells were seeded on 6-well plates containing glass coverslips. The next day, the cells were transfected with the indicated plasmids. Forty-eight hours post-transfection, the cells were starved in EBSS for 3 h. Then, the coverslips were washed with PBS and fixed with 4% paraformaldehyde in PBS for 12 min at RT and washed twice with PBS. Fixed cells on the coverslips are mounted on cover slides with Fluoromount G (Thermo Fisher Scientific). Cells were imaged using a Zeiss Axio Observer fluorescence microscope using an Alpha Plan-Apo 63x/1.46 oil objective. Images were captured by a Zeiss Axiocam 506 camera controlled by Zen Pro software. Quantification of the fluorescence from 35 cells to analyze the colocalization of LC3 and Lamp1 was performed using Fiji software by splitting the red and green channels and manually outlining the cells to obtain the region of interest (ROI). Coloc2 was performed to determine the Pearson's coefficient. Red (LC3) in green (Lamp1) was chosen together with the bisection option for the threshold regression. For autophagic flux comparison, intensity of the red signal is divided by the green signal for each cell. Quantification of the fluorescence from 30 cells to analyze the quenching of the green signal from the mTagRFP-mWasabi-LC3 probe was performed using the Fiji software. Red and green channels were split, and the cells manually outlined to get the ROI. Red and green fluorescence total intensities coming from each selected cells are analyzed.

3.4.15 Statistics

Statistical analysis was performed using GraphPad Prism Version 7. The statistical tests used are described in the corresponding figure legends.

3.5 Supplementary figures

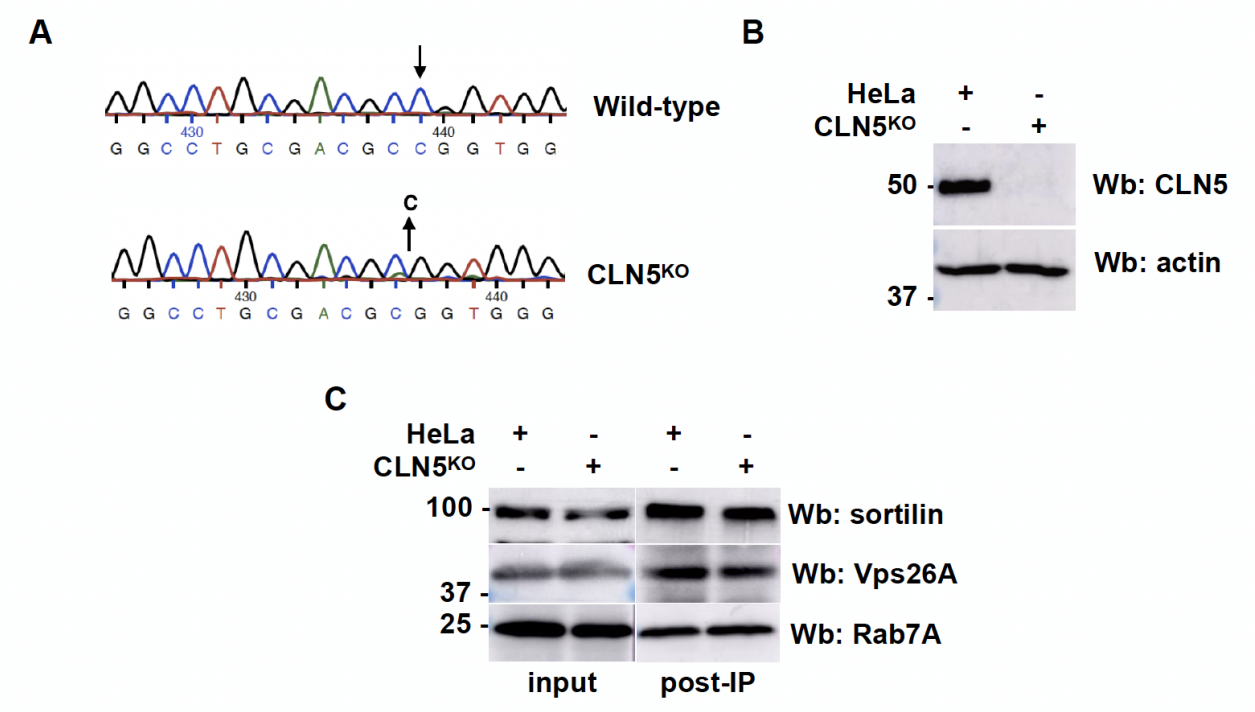

Figure 3.9

(A) DNA sequencing of genomic DNA of wild type and CLN5 knockout ($CLN5^{KO}$) HeLa cells demonstrates the deletion of 1 base pairs in the CLN5 gene. The deletion causes a frameshift, changes the encoded amino acid sequence leading to a premature stop codon after amino acid 47. Arrow indicates the position of the mutation. (B) Whole cell lysate from wild-type and $CLN5^{KO}$ HeLa cells was run on an SDS-PAGE and Western blotting (Wb) was performed using anti-CLN5 and anti-actin antibodies. (C) Retromer (Vps26A) was immunoprecipitated with anti-Vps26A antibody from wild-type and $CLN5^{KO}$ HeLa cells. Samples were run on a 12% SDS-PAGE and Western blotting (Wb) was performed with anti-sortilin, anti-Vps26A and anti-Rab7A antibodies

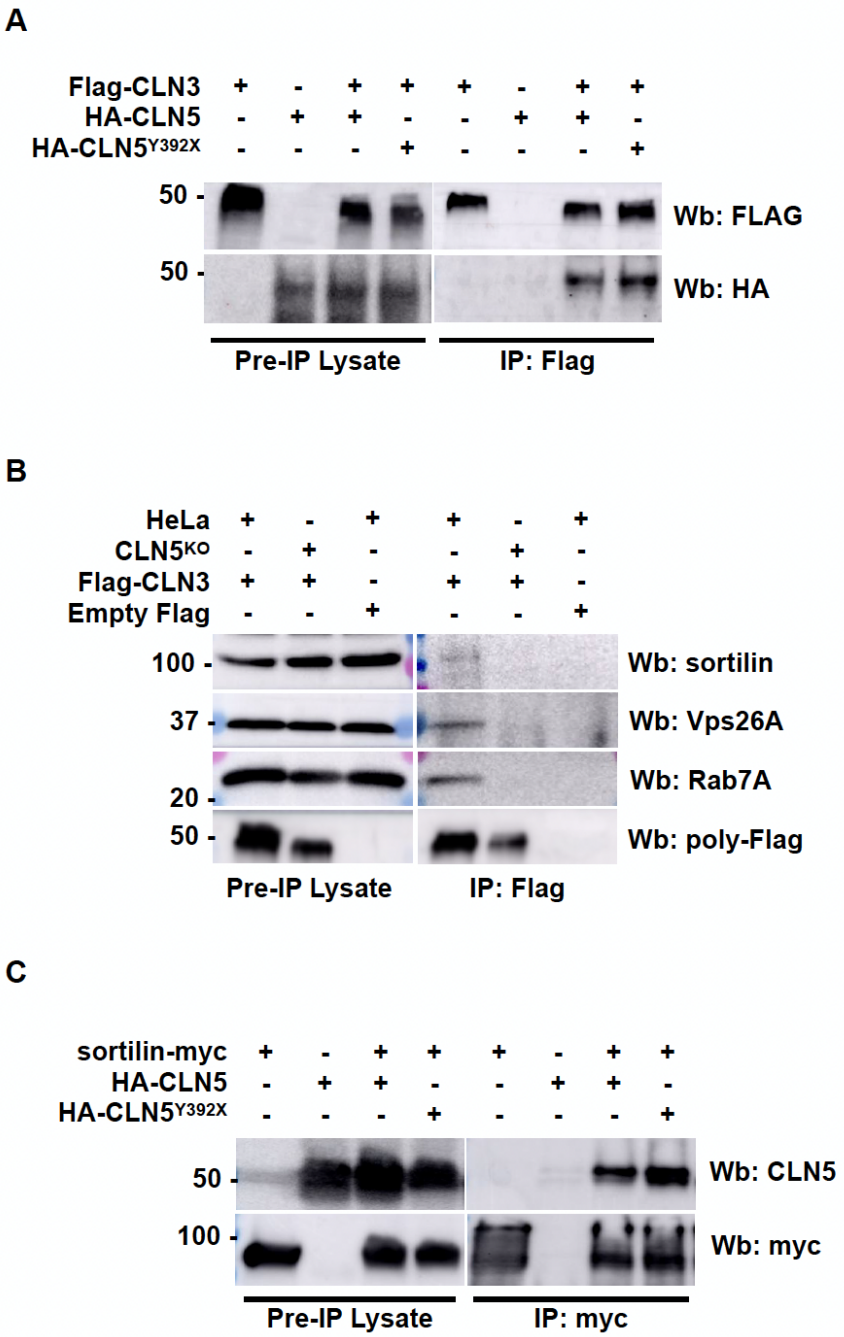

Figure 3.10: CLN5 mutations do not affect its interactions

(A) HeLa cells were co-transfected with Flag-CLN3 and wild-type HA-CLN5 or HA-CLN5^{Y392X} as indicated. Flag-CLN3 was immunoprecipitated with polyclonal anti-Flag antibody. Samples were the run on SDS-PAGE and Western blotting (Wb) was performed using monoclonal anti-Flag and anti-HA antibodies. (B) Wild-Type and CLN5^{KO} HeLa cells were transfected with Flag-CLN3 or empty plasmid as indicated. Flag-CLN3 was immunoprecipitated with monoclonal anti-Flag antibody. Samples were then run on SDS-PAGE and Western blotting (Wb) was performed using polyclonal anti- Flag, anti-Vps26A, anti-sortilin and anti-Rab7A antibodies. (C) CLN5^{KO} HeLa cells were co-transfected with sortilin-myc and wild-type HA-CLN5 or HA-CLN5^{Y392X} as indicated. Sortilin-myc was immunoprecipitated with monoclonal anti-myc antibody. Samples were the run on SDS-PAGE and Western blotting (Wb) was performed using monoclonal anti-myc and anti-CLN5 antibodies.

Part III

General Discussion and Conclusion

Chapter 4

Discussion and Conclusion

NCL is a group of rare neurodegenerative disorders caused by monogenic mutations of thirteen different genes (*CLN1-8* and *CLN10-14*). Inheritance of the mutation from both parents causes incurable NCL diseases, mostly affecting children. *CLN* gene products mostly localize to ER, endosomes, and lysosomes. While CLN5 is in the lysosomal lumen, CLN3 localizes on endolysosomal membranes (Basak *et al.*, 2021). Although the role of CLN3 and CLN5 are implicated in lysosomal homeostasis and intracellular trafficking (Metcalf *et al.*, 2008; Chandrachud *et al.*, 2015; Oetjen *et al.*, 2016; Arighi *et al.*, 2004; Adams *et al.*, 2019; Leinonen *et al.*, 2017; Huber & Mathavarajah, 2018; Best *et al.*, 2016; Leinonen *et al.*, 2017), none of their exact cellular functions have been demonstrated. Toxic material accumulation and cell death are the hallmarks of cells having a defect in CLN3 and CLN5. Understanding their molecular role and mechanism of action is crucial to generate strategies for drug development against these deadly disorders.

4.1 CLN3, CLN5 & retrograde trafficking

Previous *in vitro* studies on endocytic pathway revealed that Rab7A, the master regulator of endocytic trafficking (Feng *et al.*, 1995), interacts with CLN3 and CLN5 (Uusi-Rauva *et al.*, 2012; Mamo *et al.*, 2012), which also interact with one another (Schmiedt *et al.*, 2009). Rab7 GTPase is known to cycle between active and inactive states for its membrane binding and return to the cytosol to accomplish different cellular needs. Rab7A modulates retromer to regulate endosome-

to-TGN trafficking of proteins to prevent lysosomal degradation (Burd & Cullen, 2014). In this way, recycled receptors (sortilin, CI-MPR) can continuously carry digestive enzymes to lysosomes. The role of retromer and sortilin in cathepsin D (CTSD) sorting and processing is well established (Arighi *et al.*, 2004; Canuel *et al.*, 2008). Both CLN3 and CLN5 mutations were previously related to defects in retrograde protein sorting. In 2004, for example, Fossale *et al.* (2004) demonstrated the defects in trafficking and processing of CTSD in $CLN3^{\Delta ex7/8}$/$CLN3^{\Delta ex7/8}$ cells, yet the defective mechanisms and the effect of disease-causing point mutations in the related pathway have not been studied. On the other hand, our lab previously demonstrated the role of CLN5 for sortilin receptor stability using CLN5 knock-down ($CLN5^{KD}$) cells (Mamo *et al.*, 2012). However, using this KD system, the effects of disease-causing mutations on this trafficking pathway were never tested. Furthermore, it was not known how a soluble endolysosomal protein (CLN5) regulates protein-protein (Rab7A/retromer) interactions in the cytosol. In this current study, we generated $CLN3^{KO}$ and $CLN5^{KO}$ cells from the same parental HeLa cell line that can be rescued with wild-type or mutant CLN3 and CLN5, respectively. Using this tool, we have confirmed the previous works and expanded our understanding of the function of these proteins (Yasa *et al.*, 2020, 2021).

At first, we confirmed CLN3/Rab7A interaction using BRET in live cells. Interestingly, we showed that $CLN3^{R334H}$ and $CLN3^{V330F}$ increased this interaction. That suggests that these two mutations could retain Rab7A on endosomal membranes longer or prevent its efficient cycling. Thus, Rab7A interactions might get affected, preventing its optimal performance for different cellular functions. For example, it has shown that recruitment of Rab7A onto mitochondrial membrane is necessary for mitophagosome maturation (Yamano *et al.*, 2014). The role of retromer by binding to TBC1D5 (Rab7A GAP) has shown to control Rab7A cycle affecting mitophagic flux (Jimenez-Orgaz *et al.*, 2018). In addition, mitochondrial abnormalities have been demonstrated in the CLN3 disease model (Fossale *et al.*, 2004). All these indicate a possible role for CLN3 in regulating the GTP-GDP status of Rab7A, whose mutations might then interfere with the Rab7A cycle and mitochondrial functions. However, our FRET experiments demonstrated no differences in Rab7A GTP loading in CLN3 deficient cells. That contradicts the notion of CLN3 regulating the GTP status of Rab7A. However, not the loss of CLN3, but a site-specific mutation on CLN3 might be the cause of Rab7A membrane retention by affecting its post-translational modifications (PTMs). PTMs are known to regulate protein interaction, trafficking, stability, and membrane localization. Interestingly, CLN3 affects the palmitoylation status of proteins by regulating palmitoyl-protein Delta-9

desaturase (Narayan *et al.*, 2008). In addition, our lab has indicated that Rab7A is palmitoylated (Modica *et al.*, 2017). Thus, we checked palmitoylation of Rab7A in CLN3 deficient cells. We demonstrated that CLN3 does not have a role in the palmitoylation of Rab7A protein. However, beyond palmitoylation, Rab7 has other transient modifications like phosphorylation (Francavilla *et al.*, 2016; Lin *et al.*, 2017a; Shinde & Maddika, 2016) and ubiquitination (Sapmaz *et al.*, 2019; Wu *et al.*, 2005). Considering the interplay between these PTMs, the effect of CLN3 on Rab7A modifications should be further investigated.

When we check the membrane recruitment of Rab7A and retromer in our CLN3 and CLN5 knockout cells, we only observed a change in retromer membrane recruitment in CLN5^{KO} cells. To understand the membrane-bound Rab7A's inability to recruit retromer in CLN5^{KO} cells, we performed an acyl-rac assay to check Rab7A palmitoylation. Palmitoylation is a PTM that locates many proteins (including Rab7A, sortilin, CI-MPR) onto certain membrane subdomains (McCormick *et al.*, 2008). In this way, properly assembled proteins can then activate particular cellular pathways. For example, our lab has previously shown the importance of Rab7A palmitoylation for retromer membrane recruitment and its correct membrane localization (Modica *et al.*, 2017). Moreover, our group has shown that palmitoylation-deficient sortilin and CI-MPR fail to interact with retromer, resulting in their inability to leave the endosomes (McCormick *et al.*, 2008). Thus, palmitoylation must be the modification assuring protein interactions to promote efficient retrograde trafficking. In CLN5^{KO} cells, we observed significantly lower Rab7A palmitoylation. That explains the weakened Rab7A/retromer interaction with BRET (as measured in live cells) and the subsequent lack of retromer recruitment in CLN5^{KO} cells. Modica *et al.* (2017), have shown that palmitoylation-deficient Rab7A can still interact with retromer using co-immunoprecipitation (co-IP), where membrane compartments are destroyed. Using the same technique, we did not observe any change in the Rab7A/retromer interaction in CLN5^{KO} cells. These data suggest a role for CLN5 regulating Rab7A palmitoylation for its specific membrane localization and efficient retromer recruitment, rather than its retromer interaction *per se*. Together, complex and unique protein interactions can take place for retrograde flow. Interestingly, in our unpublished work, we found that CLN3 is also palmitoylated. In future studies, the role and the site of CLN3 palmitoylation should be investigated to reveal its mechanistic impacts on CLN3 retrograde interactions. Moreover, further effort should be given to finding palmitoyltransferase(s) responsible for CLN3, Rab7A, and sortilin palmitoylations. Targeting these enzymes might open powerful ways to cure CLN disorders.

Following its endosomal membrane recruitment, the retromer interacts with Rab7A and sortilin to start its retrograde action (Rojas *et al.*, 2008; Arighi *et al.*, 2004). Since the endosomal membrane-localized CLN3 can interact with Rab7A, we considered its role in retromer function. We found that CLN3 can interact with sortilin and retromer. While $CLN3^{E295K}$ and $CLN3^{L101P}$ weakened its sortilin interaction, only $CLN3^{L101P}$ decreased its retromer interaction. That highlights the second transmembrane helices of CLN3 as a possible site for its sortilin and retromer interactions. However, how those residues modulate these interactions are yet to be determined. Interestingly, as it is for CLN3/Rab7A, we found that V330F mutation also increases the interaction between CLN3 and retromer. That supports the possible cycling defect of Rab7A, whose speculated membrane restriction caused by $CLN3^{V330F}$ might eventually retain its retromer effector on the membrane longer; resulting in increased CLN3/retromer interaction. Therefore, all these interaction data reveal a possible cooperative work between CLN3 and CLN5 proteins in modulating retromer function.

When retromer/sortilin interaction occurs at endosomal membranes, the receptor starts its journey back to Golgi (Arighi *et al.*, 2004). The normal functioning of this pathway is necessary to maintain cellular homeostasis. Otherwise, degradation of the receptors, caused by their long stay in the acidic vesicles, will limit the transportation of newly produced enzymes from Golgi to lysosomes. That will eventually result in degradation defects followed by material accumulation and cell death, which are the hallmarks of most neurodegenerative disorders. Since the retromer complex is the main protein in the pathway and since we observed problems in its fundamental interactions at the endosome, we next investigated its leading consequences on receptor stability. We observed degradation of sortilin in both of our KO cell lines; $CLN3^{KO}$ and $CLN5^{KO}$. In addition, we also observed CI-MPR degradation in our $CLN3^{KO}$ cells. A recent work, using proteomics in CLN3-defected cells, demonstrated a decrease in CTSD and prosaposin (which are trafficked by CI-MPR and sortilin, respectively) (Schmidtke *et al.*, 2019). Thus, we aimed to determine the impact of receptor degradation in our KO cells and demonstrated both $CLN3^{KO}$ and $CLN5^{KO}$ have a defect in CTSD processing, resulting in a reduction of its mature lysosomal form in the cell. We know that lipofuscin depositions are the main pathologies seen in NCL patient cells. Lipofuscins are mainly composed of oxidized proteins and lipids such as triglycerides, free fatty acids, cholesterol, and lipoproteins. Childhood ALS (Amyotrophic Lateral Sclerosis), another metabolic disorder, has been recently defined with excessive sphingolipid biosynthesis. *SPTLC1* is the causative gene in these patients causing serine palmitoyltransferase (SPT) dysregulation (Mohassel *et al.*, 2021).

Thus, further understanding of CLN protein functions is not only essential for NCL research but might also for ALS research. Since both demonstrate problems in motor neuron functions and lipid metabolisms, the relation between SPT activity and NCL-related protein functions might reveal the cause of shared phenotypes in these neurodegenerative disorders.

While, in this work, the consequences of retromer problems in our CLN3 and CLN5 knockout models have been shown, its mutation or low expression was already related to Alzheimer's (AD) and Parkinson's (PD) diseases. Extracellular amyloid plaques and intracellular tau protein depositions are the aspects of AD. Cleavage of amyloid precursor protein (APP) results in the production of toxic Aβ. Normally, APP localizes to the plasma membrane with an unknown function. In AD patients, most of the APP stuck at TGN, where they recognized by sortilin related receptors (Haass *et al.*, 2012). Their trafficking to endosomes results in their processing if retromer-regulated Golgi turns are blocked (Small *et al.*, 2005; Small & A., 2015). Likewise, the retromer problem results in toxic α-synuclein accumulation in PD patients, caused by insufficient transportation of CTSD to lysosomes. That is because of inefficient CI-MPR retrograde trafficking limiting the amount of CTSD transportation. Thus, while my work provides a molecular explanation of CLN3 and CLN5 pathologies, it also highlights the commonly affected pathways in AD and PD. Together with our work, a better understanding of the receptor recycling pathway might reveal new therapeutic targets for all lysosomal disorders. Pharmacological chaperones to stabilize the retromer have been used against PD. Also, their efficiency to reduce APP processing has shown (Mecozzi *et al.*, 2014). Thus, the discovery of retromer upstream and downstream targets are critical to developing better drug strategies against neurodegenerative disorders.

4.2 CLN3, CLN5 & other Rab7A functions

Other than retromer function, Rab7A mediates many pathways. Endocytic cargo degradation, like EGFR, is under the control of Rab7A (Vanlandingham & Ceresa, 2009). EGF ligand induces dimerization of EGFR monomers for receptor activation. Through clathrin-mediated endocytosis, ligand-loaded EGFR is internalized and trafficked to endosomes. Until their lysosomal degradation, they can continue EGFR signaling. Mitogen-activated protein kinase (MAPK) and AKT pathways are the downstream signaling routes of EGFR activation. Their activity is known to initiate cell proliferation, growth, differentiation, and survival (Ceresa & Peterson, 2014). Thus, spatiotemporal

regulation of EGFR signaling is crucial for the prevention of oncogenic transformation. Rapid internalization and degradation of EGFR, thus EGF, hold the limiting factor in this aspect.

Both CLN3 and CLN5 knockout cells exhibited significant delays in the degradation of EGF and EGFR. Less efficient lysosomal function or decreased endocytic cargo fusion with lysosomes (both of which modulated by Rab7A) can cause delayed degradation. While the decreased lysosomal function might be related to retromer dysfunction, we wanted to investigate the fusion events to further our understanding. Rab7A regulates those pathways by its RILP and PLEKHM1 effector interactions. For fusion events to take place, RILP plays a role in vesicular positioning (Wijdeven *et al.*, 2016) and PLEKHM1 plays a role in membrane tethering (McEwan *et al.*, 2014). Our work demonstrated a significant decrease in the interactions of Rab7A/PLEKHM1 in CLN3^{KO}, and Rab7A/RILP in CLN5^{KO} cells. This finding suggests a role for these two CLN proteins on the digestive pathway, although through different Rab7A effectors. Also, we demonstrated the consequences of decreased Rab7A/RILP interaction in CLN5^{KO} cells. We found inefficient lysosomal positioning to the juxtanuclear area, must step for fusion events. We also found less autophagosome/lysosome colocalization and autophagic flux in starved CLN5 deficient cells. Together, while CLN3 regulates PLEKHM1, CLN5 regulates the RILP effector of Rab7A. Through CLN5, vesicles come close by to interact. Through CLN3, they tether for fusion. Combined with decreased lysosomal function, this could explain the significant delay in EGF and EGFR degradation in CLN3 and CLN5 deficient cells.

A question regarding the opposite degradative phenotypes of sortilin versus EGFR in our CLN3 and CLN5 knockout cells may arise. We know that they are various degradation pathways within cells. And every protein is a substrate of a different group of enzymes. In addition, we should keep in mind the degradation of sortilin must be because of its long stay in acidic vesicles, affecting its stability, resulting in its degradation. On the other hand, EGFR degradation follows EGF ligand activation and their vesicular internalization. These vesicles then ultimately fuse with lysosomes for receptor degradation. Other than TGN, sortilin is known to shuttle between endosome-to-plasma membrane. Quite recently, sortilin has been shown to regulate EGFR internalization and degradation to limit its signaling (Al-Akhrass *et al.*, 2017). Sortilin degradation in our CLN3^{KO} and CLN5^{KO} cells might also directly related to delayed EGFR degradation. Both of our knockout cells continue to produce sortilin, but their recycling is defective. So, maybe the amount of sortilin is not sufficient for EGFR internalization. Instead, they might reside on the plasma membrane and

increase EGFR signaling. Moreover, endocytic problems in CLN3 defected cells have been shown (Luiro *et al.*, 2004). That might explain the delayed degradation caused by decreased endocytosis of EGF/EGFR. Thus, it might worth investigating endocytosis of EGF/EGFR and sortilin/EGFR interaction in our CLN3 and CLN5 deficient cells.

Although CLN3 is known to interact with RILP (Uusi-Rauva *et al.*, 2012), our work demonstrated that it has nothing to do with Rab7A/RILP interaction. However, CLN3 affects the association of Hook1 (microtubule-binding protein) onto microtubules (Luiro *et al.*, 2004). We know that the long-range movement of lysosomes requires microtubule-based motors, as is in the case for autophagy induction. Together with the autophagy defects in CLN3 disease models (Lojewski *et al.*, 2014), these point out a possible complementary role for CLN3 on vesicular movement, thus autophagy. TRPML1 is required to promote Ca^{2+}- dependent centripetal transport of lysosomes (Li *et al.*, 2006). We know that mTOR (the major growth and autophagy regulator) directly targets and inactivates TRPML1 (Onyenwoke *et al.*, 2015). In this context, it would be of particular interest to test the interaction between CLN3 and TRPML1 (two of which are lysosomal transmembrane proteins) and the impact of CLN3 deficiency on TRPML1 activity.

As we have mentioned, EGFR is known to activate several signaling pathways (including Akt-mTOR (Mattoon *et al.*, 2004)). Therefore, EGFR degradation should be strictly regulated. Problems in its signaling can be the reason for upregulated Akt–mTOR pathway (Sorkin & von Zastrow, 2009) in CLN3 patient fibroblasts (FVidal-Donet *et al.*, 2013). Also, mTOR activity is known to prevent Transcription Factor EB (TFEB) nuclear translocation, thus autophagy. In line with this, we observed autophagy defects in CLN3 and CLN5 knockout cells. TFEB binds to CLEAR elements on the proximal promoter of *CLN3* and *CLN5*, which increases their protein expressions (Palmieri *et al.*, 2011). On the other hand, the anti-apoptotic activity of CLN3 and its increased expression in most of the cancer tissues have been demonstrated (Rylova *et al.*, 2002). Thus, the role of CLNs in the EGFR signaling should be further investigated to understand their function in cell survival mechanisms.

Neuronal cell death is a result of neuroinflammation. Chronic inflammation happens in almost all neurodegenerative disorders (NDs), starting with inflammasome complex activation. Upon inflammasome activation, inflammasome-related proteins are ubiquitinated and p62 associated (Shi *et al.*, 2012). That makes them a target of autophagy to prevent continuous inflammation. Addi-

tionally, Aflaki *et al.* (2015) published that inflammasome activation in microglial cells is the result of impaired autophagy. Therefore, the autophagic process for inflammasome degradation must be tightly regulated. That indicates a relation between NCL related inflammation and defects in autophagy. Retromer is involved in autophagy function (Small & A., 2015). Retromer dysfunctions in AD, PD, ALS, and FTD (Frontotemporal dementia) have been already demonstrated (Reitz, 2018). Together, our current findings on CLN3 and CLN5 regulating retromer function and autophagy indicate their possible association with the inflammasome pathway. Other than neurodegeneration, inflammation is known to cause cancer. Increased CLN3 expression in cancer tissues, such as in glioblastoma and neuroblastoma (Mirza *et al.*, 2019), suggests a common pathway between NCL- and cancer-associated inflammation. Thus, studying the role of CLNs in inflammasome activation will be an essential step to start resolving the shared inflammation problem in NCL, NDs, and cancer.

4.3 CLN3-CLN5 retrograde complex

Already commented results so far presented that CLN5 modulates Rab7A palmitoylation to regulate retromer recruitment and localization to specific membrane subdomains, while CLN3 regulates Rab7A/retromer interaction. Both CLN3 or CLN5 deficiency leads to the degradation of sortilin. In addition to these findings, we demonstrated that CLN3, which interacts with CLN5 (Vesa *et al.*, 2002), also interacts with Rab7A, retromer, and sortilin. Using BRET, we observed significantly less interaction between CLN3/Rab7A, CLN3/retromer, and CLN3/sortilin in CLN5 deficient cells, indicating CLN5 is modulating all these CLN3 downstream interactions to regulate retromer function. Therefore, our data support a model where CLN3 and CLN5 function as a complex regulating the itinerary of the lysosomal sorting receptors.

In addition to our CLN3-CLN5 complex model, Bajaj *et al.* (2020) demonstrated CLN6-CLN8 complex formation, regulating lysosomal enzyme transportation from ER to Golgi. Although the complete function of CLN proteins is not known, they seemingly have specialized cellular roles with diverged cellular localization and structural properties. However, most CLN mutations cause similar pathologies (lipofuscin depositions in the lysosomes) and symptoms. That is why it is not surprising to think of their cooperative action for lysosomal homeostasis. In our unpublished work, a specific interaction between CLN3 and CLN7 (another lysosomal transmembrane protein) was

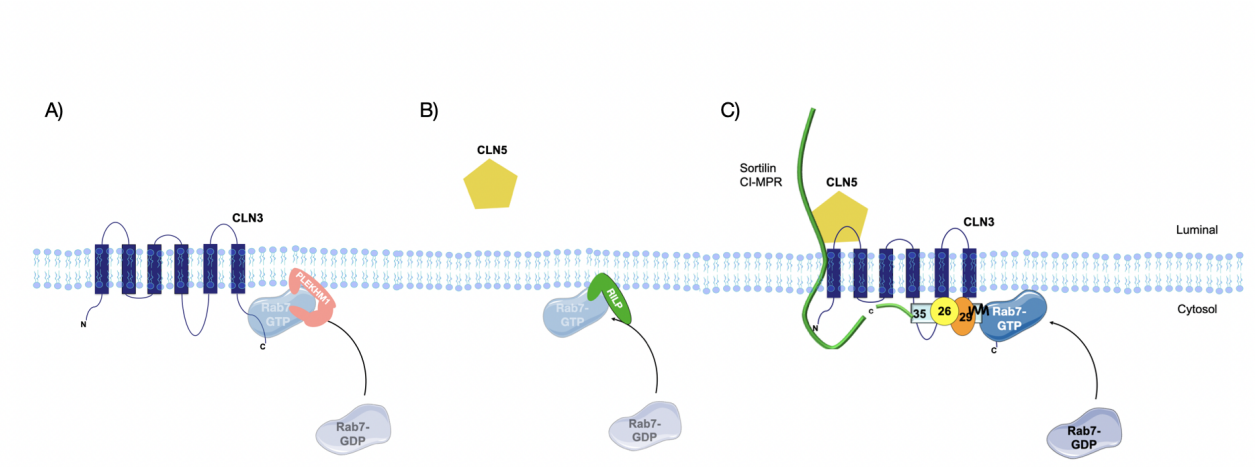

Figure 4.1: CLN3-CLN5 complex function

A) CLN3 regulates the PLEKHM1 function of Rab7A to promote vesicular membrane tethering. B) On the other hand, CLN5 regulates the RILP function of Rab7A for vesicular movement. C) And together, CLN3 and CLN5 interact to regulate retromer function. While CLN5 regulates Rab7A palmitoylation for retromer membrane localization, it also modulates the key interactions between CLN3, Rab7A, retromer, and sortilin. Therefore, CLN3 and CLN5 serve as endosomal switches regulating the itinerary of the lysosomal sorting receptors.

found, and their interaction was significantly decreased in $CLN5^{KO}$ cells. Moreover, consistent domain structures were shown between CLN3 and CLN7 proteins (Siintola *et al.*, 2007). CLN3 has been implicated in the regulation of lysosomal Ca^{2+} levels (Chandrachud *et al.*, 2015). There is no evidence supporting the idea of CLN3 as an ion transporter. Yet, it is intriguing to consider CLN7 (which is from a transporter family) as a Ca^{2+} ion transporter and to consider CLN3 as its activity regulator. These hypotheses deserve two separate investigations. CLN5 interaction with CLN1, CLN2, CLN3, CLN6, and CLN8 were demonstrated in addition to its CLN3 interaction (Schmiedt *et al.*, 2009)) (Vesa *et al.*, 2002). Furthermore, in 2007, Persaud-Sawin *et al.* (2007) showed the compensatory effects of some CLN proteins for one another. For example, while CLN1 was able to correct the defects in CLN3, CLN6, CLN8 deficient cells, the problems caused by CLN1 deficiency could not be rescued by the others. Moreover, co-IP experiments show that CLN3, CLN6, CLN8 proteins interact with each other. So, one can think that the lysosomal CLN1 protein, causing a very early NCL phenotype to most CLN diseases, might be downstream of other CLNs. Considering the shared mechanisms between CLNs, understanding their colocalization and interaction is essential. In this way, we can develop new treatment strategies against this lysosomal storage disorder.

CLN proteins and common neurodegeneration pathologies also associate with each other. For example, TDP-43 depositions, which is the pathology in ALS and FTD (Prasad *et al.*, 2019), are

observed in CLN11 patient cells (Cenik *et al.*, 2012). On the other hand, CLN3, CLN4, and CLN12 disorders demonstrate parkinsonian features in addition to NCL clinical phenotypes. Recent work also showed that AD is associated with CLN5 allelic variation (Qureshi *et al.*, 2018), resulting in the misrouting of Cathepsin D. The authors speculated that could be due to retromer dysfunction. As we have mentioned, retromer dysfunction is well known in AD (Qureshi *et al.*, 2018), and recent publications have linked mutations in the VPS35 subunit of retromer to PD (Follett *et al.*, 2014). In addition, commonly affected pathways in all neurodegenerative disorders are related to membrane trafficking. Rab GTPases are the principal proteins regulating these trafficking routes. Problems in Rab7 functions were associated with AD, PD, ALS (Kiral *et al.*, 2018). Interestingly, a study showed that Rab7 interacts with C9orf72. C9orf72 mutations are the most common cause of familial ALS and were related to downstream pathways of Rab7 (Aoki *et al.*, 2017). Notably, this thesis demonstrates the regulation of some Rab7 functions (such as retromer) by the CLN3-CLN5 complex. In conclusion, from a cell biology perspective, this work provides a greater understanding of CLN3 and CLN5 lysosomal proteins. Collectively, that knowledge can lead to an increased understanding of lysosomal disorders to target pathways implicated in Neuronal Ceroid Lipofuscinosis, Alzheimer's disease, Parkinson's disease, and Amyotrophic Lateral Sclerosis.

References

Adams, J. et al (2019). Autophagy-lysosome pathway alterations and alpha-synuclein up-regulation in the subtype of neuronal ceroid lipofuscinosis, cln5 disease. *Sci Rep.*, (9)1(151). DOI:10.1038/s41598-018-36379-z.

Aflaki, E. et al (2015). Lysosomal storage and impaired autophagy lead to inflammasome activation in gaucher macrophages. *Aging Cell*, 15(1):77–88.

Al-Akhrass, H., Naves, T. and Vincent, F. (2017). Sortilin limits egfr signaling by promoting its internalization in lung cancer. *Nat Commun*, 8(1):1182. DOI:10.1038/s41467-017-01172-5.

Andersona, G.W., H.Goebelb, H. and Simonati, A. (2013). Human pathology in ncl. *Biochimica et Biophysica Acta*, 1832(11):1807–26. DOI:10.1016/j.bbadis.2012.11.014.

Ao, X., Zou, L. and Wu, Y. (2014). Regulation of autophagy by the rab gtpase network. *Cell Death Differ*, 21(3):348–58. DOI:10.1038/cdd.2013.187.

Aoki, Y. et al (2017). C9orf72 and rab7l1 regulate vesicle trafficking in amyotrophic lateral sclerosis and frontotemporal dementia. *Acta Neuropathologica Communications*, 6(1). DOI:10.1093/brain/awx024.

Arighi, C.N. et al (2004). Role of the mammalian retromer in sorting of the cation-independent mannose 6 phosphate receptor. *J Cell Biol*, 165(1):123–33. DOI:10.1083/jcb.200312055.

Baba, T. et al (2019). Phosphatidylinositol 4,5-bisphosphate controls rab7 and plekhm1 membrane cycling during autophagosome–lysosome fusion. *The EMBO Journal*, 38. DOI:e100312https://doi.org/10.15252/embj.2018100312.

Bajaj, L. et al (2020). A cln6-cln8 complex recruits lysosomal enzymes at the er for golgi transfer. *J Clin Invest*, 130(8):4118–4132. DOI:10.1172/JCI130955.

Ballabio, A. and Bonifacino, J.S. (2020). Lysosomes as dynamic regulators of cell and organismal homeostasis. *Nature Reviews Molecular Cell Biology*, 21:101–118. DOI:10.1038/s41580-019-0185-4.

Barr, F. and Lambright, D. (2010). Rab gefs and gaps. *Curr. Opin. Cell Biol.*, 22(4):461–70. DOI:10.1016/j.ceb.2010.04.007.

Basak, I. et al (2021). A lysosomal enigma cln5 and its significance in understanding neuronal ceroid lipofuscinosis. *Cellular and Molecular Life Sciences*, 78:4735–4763. DOI:10.1007/s00018-021-03813-x.

Best, H.L. et al (2016). Characterisation of early changes in ovine cln5 and cln6 batten disease neural cultures for the rapid screening of therapeutics. *Neurobiology of Disease*, 100:62–74. DOI:10.1016/j.nbd.2017.01.001.

Birgisdottir, A.B. and Johansen, T. (2020). Autophagy and endocytosis - interconnections and interdependencies. *J Cell Sci.*, 133(10):jcs228114. DOI:10.1242/jcs.228114.

Bonifacino, J.S. (2004). The gga proteins: adaptors on the move. *Nature Reviews Molecular Cell Biology*, 5:23–32. DOI:https://doi.org/10.1038/nrm1279.

Bonifacino, J.S. and Traub, L.M. (2003). Signals for sorting of transmembrane proteins to endosomes and lysosomes. *Annual Review of Biochemistry*, 72:395–447. DOI:10.1146/annurev.biochem.72.121801.161800.

Bosch, M.E., Aldrich, A. and Fallet, R. (2016). Self-complementary aav9 gene delivery partially corrects pathology associated with juvenile neuronal ceroid lipofuscinosis (cln3). *J Neurosci.*, 36(37):9669–82. DOI:10.1523/JNEUROSCI.1635-16.2016.

Braulke, T. and S.Bonifacino, J. (2009). Sorting of lysosomal proteins. *Biochimica et Biophysica Acta (BBA) - Molecular Cell Research*, 1793(4):605–614. DOI:10.1016/j.bbamcr.2008.10.016.

Breijyeh, Z. and Karaman, R. (2020). Comprehensive review on alzheimer's disease: Causes and treatment. *MDPI*, 25(24):5789. DOI:10.3390/molecules25245789.

Burd, C. and Cullen, P. (2014). Retromer: a master conductor of endosome sorting. *Cold Spring Harb Perspect Biol.*, 6(2):a016774. DOI:10.1101/cshperspect.a016774.

Butz, E.S. et al (2019). Moving towards a new era of genomics in the neuronal ceroid lipofuscinoses. *Biochim Biophys Acta Mol Basis Dis*, 1866(9). DOI:10.1016/j.bbadis.2019.165571.

Cabukusta, B. and Neefjes, J. (2018). Mechanisms of lysosomal positioning and movement. *Traffic*, 19(10):761–769. DOI:10.1111/tra.12587.

Canuel, M. et al (2008). Sortilin mediates the lysosomal targeting of cathepsins d and h. *Biochem Biophys Res Commun*, 373(2):292–297. DOI:10.1016/j.bbrc.2008.06.021.

Cao, Q. et al (2015). Calcium release through p2x4 activates calmodulin to promote endolysosomal membrane fusion. *Journal of Cell Biology*, 209(6):879–894. DOI:10.1083/jcb.201409071.

Cao, Y. et al (2006). Autophagy is disrupted in a knock-in mouse model of juvenile neuronal ceroid lipofuscinosis. *J. Biol. Chem.*, 281(29):20483–93. DOI:10.1074/jbc.M602180200.

Carcel-Trullolsa, J., D.Kovacsa, A. and A.Pearce, D. (2015). Cell biology of the ncl proteins: What they do and don't do. *Biochimica et Biophysica Acta*, 1852(10 Pt B):2242–55. DOI:10.1016/j.bbadis.2015.04.027.

Carlo, A.S. (2013). Sortilin, a novel apoe receptor implicated in alzheimer disease. *Prion*, 7(5): 378–382. DOI:10.4161/pri.26746.

Castro-Obregon, S. (2010). The discovery of lysosomes and autophagy. *Nature Education*, 3(9)(49).

Cenik, B. et al (2012). Progranulin: A proteolytically processed protein at the crossroads of inflammation and neurodegeneration. *Journal of Biological Chemistry*, 287(39):32298–306. DOI:10.1074/jbc.R112.399170.

Centa, J.L. et al (2020). Therapeutic efficacy of antisense oligonucleotides in mouse models of cln3 batten disease. *Nature Medicine*, 26:1444–1451. DOI:10.1038/s41591-020-0986-1.

Ceresa, B.P. and Bahr, S.J. (2006). Rab7 activity affects epidermal growth factor receptor degradation by regulating endocytic trafficking from the late endosome. *J Biol Chem.*, 281(2):1099–106. DOI:10.1074/jbc.M504175200.

Ceresa, B.P. and Peterson, J.L. (2014). Cell and molecular biology of epidermal growth factor receptor. *Int. Rev. Cell Mol. Biol.*, 313:145–78. DOI:10.1016/B978-0-12-800177-6.00005-0.

Chamberlain, L.H. and Shipston, M.J. (2015). The physiology of protein s-acylation. *Physiol Rev.*, 95(2):341–376. DOI:10.1152/physrev.00032.2014.

Chandrachud, U. et al (2015). Unbiased cellbased screening in a neuronal cell model of batten disease highlights an interaction between ca2+ homeostasis, autophagy, and cln3 protein function. *J. Biol. Chem.*, 290(23):14361–14380. DOI:10.1074/jbc.M114.621706.

Chang, J.W. et al (2011). Lithium rescues the impaired autophagy process in cb-cln3(deltaex7/8/deltaex7/8) cerebellar cells and reduces neuronal vulnerability to cell death via impase inhibition. *J. Neurochem.*, 116:659–68. DOI:10.1111/j.1471-4159.2010.07158.x.

Coelho, D.and Kim, J.C. et al (2012). Mutations in abcd4 cause a new inborn error of vitamin b12 metabolism. *Nat. Genet.*, 44(10):1152–5. DOI:10.1038/ng.2386.

Cohn, Z.A. (1963). The fate of bacteria within phagocytic cells. *Journal of Experimental Medicine*, 117(1):27–42. DOI:10.1084/jem.117.1.27.

Cotman, S.L. and Staropoli, J.F. (2012). The juvenile batten disease protein, cln3, and its role in regulating anterograde and retrograde post-golgi trafficking. *Clin. Lipidol*, 7(1):79–91. DOI:10.2217/clp.11.70.

Coutinho, M.F., Prata, M.J. and Alves, S. (2012). A shortcut to the lysosome: the mannose-6-phosphate independent pathway. *Mol Genet Metab*, 107(3):257–66. DOI:10.1016/j.ymgme.2012.07.012.

Dahms, N.M. and L. J. Olson, a.P.K. (2008). Strategies for carbohydrate recognition by the mannose 6-phosphate receptors. *Glycobiology*, 18(9):664–78. DOI:10.1093/glycob/cwn061.

Danyukova, T. et al (2018). Loss of cln7 results in depletion of soluble lysosomal proteins and impaired mtor reactivation. *Hum Mol Genet*, 27(10):1711–1722. DOI:10.1093/hmg/ddy076.

de Duve, C. (2005). The lysosome turns fifty. *Nat Cell Biol*, 7:847–849. DOI:https://doi.org/10.1038/ncb0905-847.

DeTure, M.A. and Dickson, D.W. (2019). The neuropathological diagnosis of alzheimer's disease. *Molecular Neurodegeneration*, 14, 32. DOI:https://doi.org/10.1186/s13024-019-0333-5.

Doccini, S. et al (2020). Proteomic and functional analyses in disease models reveal cln5 protein involvement in mitochondrial dysfunction. *Nature-Cell Death Discovery*, 6. DOI:10.1038/s41420-020-0250-y.

Drack, A., Mullins, R. and Pfeifer, W. (2015). Immunosuppressive treatment for retinal degeneration in juvenile neuronal ceroid lipofuscinosis (juvenile batten disease). *Ophthalmic Genet.*, 36(4):359–64. DOI:10.3109/13816810.2014.886271.

Dumaresq-Doiron, K. et al (2010). The phosphatidylinositol 4-kinase pi4kiiialpha is required for the recruitment of gbf1 to golgi membranes. *J. Cell Sci.*, 123(Pt 13):2273–80. DOI:10.1242/jcs.055798.

Feng, X. et al (2018). Lysosomal potassium channels: Potential roles in lysosomal function and neurodegenerative diseases. *CNS & Neurological Disorders - Drug Targets*, 17(4):261–6. DOI:10.2174/1871527317666180202110717.

Feng, Y., Press, B. and Ness, A.W. (1995). Rab 7: an important regulator of late endocytic membrane traffic. *J Cell Biology*, 131(6 Pt 1):1435–52. DOI:10.1083/jcb.131.6.1435.

Finan, G.M., Okada, H. and Kim, T.W. (2011). Bace1 retrograde trafficking is uniquely regulated by the cytoplasmic domain of sortilin. *J Biol Chem*, 286(14):12602–16. DOI:10.1074/jbc.M110.170217.

First-Person (2020). *First Person interview*. https://jcs.biologists.org/content/133/6/jcs244913.

Follett, J. et al (2014). The vps35 d620n mutation linked to parkinson's disease disrupts the cargo sorting function of retromer. *Traffic*, 15(2):230–44.

Forgac, M. (2007). Vacuolar atpases: rotary proton pumps in physiology and pathophysiology. *Nature Reviews Molecular Cell Biology*, 8:917–929. DOI:10.1038/nrm2272.

Fossale, E. et al (2004). Membrane trafficking and mitochondrial abnormalities precede subunit c deposition in a cerebellar cell model of juvenile neuronal ceroid lipofuscinosis. *BMC Neurosci.*, 5. DOI:10.1186/1471-2202-5-57.

Francavilla, C. et al (2016). Multilayered proteomics reveals molecular switches dictating ligand-dependent egfr trafficking. *Nat Struct Mol Biol.*, 23:608–618. DOI:10.1038/nsmb.3218.

FVidal-Donet, J.M. et al (2013). Alterations in ros activity and lysosomal ph account for distinct patterns of macroautophagy in lincl and jncl fibroblasts. *PLoS ONE*, 8(2):e55526. DOI:10.1371/journal.pone.0055526.

Gall, L.L. et al (2020). Molecular and cellular mechanisms affected in als. *J Pers Med.*, 10(3):101. DOI:10.3390/jpm10030101.

Ganley, I.G. et al (2011). Distinct autophagosomal-lysosomal fusion mechanism revealed by thapsigargininduced autophagy arrest. *Mol. Cell*, 42(6):731–43. DOI:10.1016/j.molcel.2011.04.024.

Ghosh, P., Dahms, N.M. and Kornfeld, S. (2003). Mannose 6-phosphate receptors: new twists in the tale. *Nature Reviews Molecular Cell Biology*, 4:pages202–213. DOI:10.1038/nrm1050.

Gieselmann, V. (1995). Lysosomal storage diseases. *Biochim Biophys Acta*, 1270:103–136. DOI:10.1016/0925-4439(94)00075-2.

Glickman, J. and Kornfeld., S. (1993). Mannose 6-phosphate-independent targeting of lysosomal enzymes in i-cell disease b lymphoblasts. *J Cell Biol.*, 123(1):99–108. DOI:10.1083/jcb.123.1.99.

Greiner-Tollersrud, O.K. and Berg, T. (2000-2013). Lysosomal storage disorders. *Madame Curie Bioscience Database, Landes Bioscience*. DOI:10.1007/0-387-28957-7-6.

Grosshans, B., Ortiz, D. and Novick, P. (2006). Rabs and their effectors; achieving specificity in membrane traffic. *Proc. Natl. Acad. Sci.*, 103(32):11821–11827. DOI:10.1073/pnas.0601617103.

Gómez-Benito, M. et al (2020). Modeling parkinson's disease with the alpha-synuclein protein. *Front Pharmacol.*, 11:356. DOI:10.3389/fphar.2020.00356.

Haass, C. et al (2012). Trafficking and proteolytic processing of app. *Cold Spring Harb Perspect Med.*, 2(5):a006270. DOI:10.1101/cshperspect.a006270.

Halling, D.B. et al (2016). Conserved properties of individual ca2+-binding sites in calmodulin. *PNAS*, 113(9):E1216–25. DOI:10.1073/pnas.1600385113.

Hanafusa, H. et al (2019). Lrrk1 phosphorylation of rab7 at s72 links trafficking of egfr-containing endosomes to its effector rilp. *Journal of Cell Science*, 132(11):jcs228809. DOI:10.1242/jcs.228809.

Hansen, M., Rubinsztein, D.C. and Walker, D.W. (2018). Autophagy as a promoter of longevity: insights from model organisms. *Nature Reviews Molecular Cell Biology*, 19:579–593. DOI:10.1038/s41580-018-0033-y.

Haskell, R. et al (2000). Batten disease: evaluation of cln3 mutations on protein localization and function. *Hum Mol Genet*, 9(5):735–44. DOI:10.1093/hmg/9.5.735. PMID: 10749980.

Heo, J. et al (2018). Rab7a phosphorylation by tbk1 promotes mitophagy via the pink-parkin pathway. *Science Advances*, 4(11):eaav0443. DOI:10.1126/sciadv.aav0443.

Hiesberger, T. et al (1998). Cellular uptake of saposin (sap) precursor and lysosomal delivery by the low density lipoprotein receptor-related protein (lrp). *EMBO J*, 17(16):4617–25. DOI:10.1093/emboj/17.16.4617.

Homma, Y., Hiragi, S. and Fukuda, M. (2020). Rab family of small gtpases: an updated view on their regulation and functions. *The FEBS Journal*, 288(1):36–55. DOI:10.1111/febs.15453.

H.R.Nelvagala et al (2020). Pathomechanisms in the neuronal ceroid lipofuscinoses. *Biochimica et Biophysica Acta*, 1866(9). DOI:10.1016/j.bbadis.2019.165570.

Huber, R.J. and Mathavarajah, S. (2018). Cln5 is secreted and functions as a glycoside hydrolase in dictyostelium. *Cellular Signalling*, 42:236–248. DOI:10.1016/j.cellsig.2017.11.001.

Hutagalung, A. and Novick, P. (2011). Role of rab gtpases in membrane traffic and cell physiology. *Physiol Rev.*, 91(1):119–49. DOI:10.1152/physrev.00059.2009.

Jalankoa, A., Tyynelab, J. and Peltonen, L. (2006). From genes to systems: New global strategies for the characterization of ncl biology. *Biochimica et Biophysica Acta (BBA) - Molecular Basis of Disease*, 1762(10):934–944. DOI:10.1016/j.bbadis.2006.09.001.

J.Bonangelino, C., Chavez, E.M. and Bonifacino, J.S. (2002). Genomic screen for vacuolar protein sorting genes in saccharomyces cerevisiae. *MBoC*, 13(7):2486–2501. DOI:10.1091/mbc.02-01-0005.

Jimenez-Orgaz, A. et al (2018). Control of rab7 activity and localization through the retromer-tbc1d5 complex enables rab7-dependent mitophagy. *EMBO J.*, 37(2):235–254. DOI:10.15252/embj.201797128.

Johansson, M. et al (2007). Activation of endosomal dynein motors by stepwise assembly of rab7-rilp-p150glued, orp1l, and the receptor betalll spectrin. *J Cell Biol.*, 176(4):459–71. DOI:10.1083/jcb.200606077.

Johnson, D. et al (2016). The position of lysosomes within the cell determines their luminal ph. *Journal of Cell Biology*, 212 (6):677–692. DOI:10.1083/jcb.201507112.

Jules, F. et al (2017). Cln5 is cleaved by members of the spp/sppl family to produce a mature soluble protein. *Exp Cell Res*, 357(1):40–50. DOI:10.1016/j.yexcr.2017.04.024.

Khandia, R. et al (2019). A comprehensive review of autophagy and its various roles in infectious, non-infectious, and lifestyle diseases: Current knowledge and prospects for disease prevention, novel drug design, and therapy. *MDPI cells*, 8(7)(674). DOI:10.3390/cells8070674.

Kinchen, J.M. and Ravichandran, K.S. (2010). Identification of two evolutionarily conserved genes regulating processing of engulfed apoptotic cells. *Nature*, 464:778–782. DOI:10.1038/nature08853.

Kiral, F.R. et al (2018). Rab gtpases and membrane trafficking in neurodegeneration. *Curr Biol*, 28(8):R471–R486.

Kobayashi, H. et al (2009). Functional rescue of beta-adrenoceptor dimerization and trafficking by pharmacological chaperones. *Traffic*, 10(8):1019–33. DOI:10.1111/j.1600-0854.2009.00932.x.

Koch, S. et al (2011). Morphologic and functional correlates of synaptic pathology in the cathepsin d knockout mouse model of congenital neuronal ceroid lipofuscinosis. *J Neuropathol Exp Neurol*, 70(12):1089–96. DOI:10.1097/NEN.0b013e318238fc28.

Kolset, S.O. et al (1996). Serglycin-binding proteins in activated macrophages and platelets. *Leukoc Biol*, 59(4):545–54. DOI:10.1002/jlb.59.4.545.

Kumsal, T. and Maria, C.A. (2017). Chaperone-mediated autophagy and endosomal microautophagy: joint by a chaperone. *Journal of Biological Chemistry*, 5414–5424 pages.

Laurent-Matha, V. et al (2006). Processing of human cathepsin d is independent of its catalytic function and autoactivation: involvement of cathepsins. *J Biochem.*, 139(3):363–71. DOI:10.1093/jb/mvj037.

Law, F. and Rocheleau, C.E. (2017). Vps34 and the armus/tbc-2 rab gaps: Putting the brakes on the endosomal rab5 and rab7 gtpases. *Cell Logist*, 7(4):e1403530. DOI:10.1080/21592799.2017.1403530.

Lee, J.H. et al (2015). Presenilin 1 maintains lysosomal ca(2+) homeostasis via trpml1 by regulating vatpase-mediated lysosome acidification. *Cell Reports*, 12(9):1430–44. DOI:10.1016/j.celrep.2015.07.050.

Lefrancois, S. et al (2003). The lysosomal trafficking of sphingolipid activator proteins (saps) is mediated by sortilin. *Embo J*, 22(24):6430–6437. DOI:10.1093/emboj/cdg629.

Leinonen, H. et al (2017). Retinal degeneration in a mouse model of cln5 disease is associated with compromised autophagy. *Sci Rep.*, 7. DOI:10.1038/s41598-017-01716-1.

Li, F. and Zhang, H. (2019). Lysosomal acid lipase in lipid metabolism and beyond. *Arterioscler Thromb Vasc Biol.*, 39(5):850–856. DOI:10.1161/ATVBAHA.119.312136.

Li, P., Gu, M. and Xu, H. (2019). Lysosomal ion channels as decoders of cellular signals). *Trends in Biochemical Sciences*, 44(2):110–124. DOI:10.1016/j.tibs.2018.10.006.

Li, X. et al (2006). A molecular mechanism to regulate lysosome motility for lysosome positioning and tubulation. *Nat Cell Biol*, 18:404–417. DOI:10.1038/ncb3324.

Lin, X. et al (2014). Rilp interacts with hops complex via vps41 subunit to regulate endocytic trafficking. *Scientific Reports*, 4:7282. DOI:10.1038/srep07282.

Lin, X. et al (2017a). Tyrosine phosphorylation of rab7 by src kinase. *Cell Signalling*, 35:84–94. DOI:10.1016/j.cellsig.2017.03.006.

Lin, X. et al (2017b). Tyrosine phosphorylation of rab7 by src kinase. *Cell Signal.*, 35. DOI:10.1016/j.cellsig.2017.03.006.

Linder, M.E. and Deschenes, R.J. (2007). Palmitoylation: policing protein stability and traffic. *Nat Rev Mol Cell Biol*, 8:74–84. DOI:10.1038/nrm2084.

Lojewski, X. et al (2014). Human ipsc models of neuronal ceroid lipofuscinosis capture distinct effects of tpp1 and cln3 mutations on the endocytic pathway. *Hum. Mol. Genet.*, 23(8):2005–22. DOI:10.1093/hmg/ddt596.

Lu, J.Y., Verkruyse, L.A. and Hofmann, S.L. (1996). Lipid thioesters derived from acylated proteins accumulate in infantile neuronal ceroid lipofuscinosis: correction of the defect in lymphoblasts by recombinant palmitoyl-protein thioesterase. *Proc. Natl. Acad. Sci.*, 93:10046–10050. DOI:10.1073/pnas.93.19.10046.

Lubke, T., Lobel, P. and Sleat, D.E. (2009). Proteomics of the lysosome. *Biochimica et Biophysica Acta*, 1793(4):625–635. DOI:10.1016/j.bbamcr.2008.09.018.

Luiro, K. et al (2004). Interconnections of cln3, hook1 and rab proteins link batten disease to defects in the endocytic pathway. *Hum Mol Genet*, 13:3017–3027. DOI:10.1093/hmg/ddh321.

Malik, A.R. and Willnow, T.E. (2020). Vps10p domain receptors: Sorting out brain health and disease. *Trends in Neurosciences*, 43(11):870–885. DOI:10.1016/j.tins.2020.08.003.

Mamo, A. et al (2012). The role of ceroid lipofuscinosis neuronal protein 5 (cln5) in endosomal sorting. *Mol Cell Biol*, 32(10):1855–66. DOI:10.1128/MCB.06726-11.

Marwaha, R. et al (2017). The rab7 effector plekhm1 binds arl8b to promote cargo traffic to lysosomes. *J. Cell Biol.*, 216(4):1051–1070. DOI:10.1083/jcb.201607085.

Masten, M.C., Mink, J.W. and Augustine, E.F. (2020). Batten disease: an expert update on agents in preclinical and clinical trials. *Expert Opinion on Investigational Drugs*, 29(12):1317–1322. DOI:10.1080/13543784.2020.1837110.

Mattoon, D.R. et al (2004). The docking protein gab1 is the primary mediator of egf-stimulated activation of the pi-3k/akt cell survival pathway. *BMC Biol*, 2. DOI:10.1186/1741-7007-2-24.

McCormick, P.J. et al (2008). Palmitoylation controls recycling in lysosomal sorting and trafficking. *Traffic*, 9(11):1984–97. DOI:10.1111/j.1600-0854.2008.00814.x.

McEwan, D.G. et al (2014). Plekhm1 regulates autophagosome-lysosome fusion through hops complex and lc3/gabarap proteins. *Cell*, 57(1):39–54. DOI:10.1016/j.molcel.2014.11.006.

Mecozzi, V. et al (2014). Pharmacological chaperones stabilize retromer to limit app processing. *Nat Chem Biol.*, 10:443–449. DOI:10.1038/nchembio.1508.

Mercier, J.F. et al (2002). Quantitative assessment of beta 1- and beta 2-adrenergic receptor homo- and heterodimerization by bioluminescence resonance energy transfer. *J Biol Chem.*, 277(47):44925–31. DOI:10.1074/jbc.M205767200.

Mertins, P. et al (2013). Integrated proteomic analysis of post-translational modifications by serial enrichment. *Nature Methods*, 10:634–637. DOI:10.1038/nmeth.2518.

Metcalf, D.J. et al (2008). Loss of the batten disease gene cln3 prevents exit from the tgn of the mannose 6-phosphate receptor. *Traffic*, 9(11):1905–14. DOI:10.1111/j.1600-0854.2008.00807.x.

Meyers, R.A. (2006). Structure and function of lysosomes. *Encyclopedia of Molecular Cell Biology and Molecular Medicine*.

Mink, J.W. et al (2013). Classification and natural history of the neuronal ceroid lipofuscinoses. *J Child Neurol.*, 28(9):1101–1105. DOI:10.1177/0883073813494268.

Mirza, M. et al (2019). The cln3 gene and protein: What we know. *Mol. Genet. Genomic Med.*, 7(12):e859. DOI:10.1002/mgg3.859.

Mitchell, D.A. et al (2006). Protein palmitoylation by a family of dhhc protein s-acyltransferases. *J Lipid Res*, 47(6):1118–27. DOI:10.1194/jlr.R600007-JLR200.

Mitchell, N., Russell, K. and Wellby, M. (2018). Longitudinal in vivo monitoring of the cns demonstrates the efficacy of gene therapy in a sheep model of cln5 batten disease. *Mol. Ther.*, 26(10):2366–2378. DOI:10.1016/j.ymthe.2018.07.015.

Modica, G. et al (2017). Rab7 palmitoylation is required for efficient endosome-to-tgn trafficking. *Journal of Cell Science*, 130(15):2579–2590. DOI:10.1242/jcs.199729.

Moharir, A. et al (2013). The role of n-glycosylation in folding, trafficking, and functionality of lysosomal protein cln5. *Plos One*, 8(9):e74299. DOI:10.1371/journal.pone.0074299.

Mohassel, P. et al (2021). Childhood amyotrophic lateral sclerosis caused by excess sphingolipid synthesis. *Nature medicine*. DOI:10.1038/s41591-021-01346-1.

Mole, S. and Cotman, S. (2015). Genetics of the neuronal ceroid lipofuscinoses (batten disease). *Biochim Biophys Acta*, (10 Pt B):2237–41. DOI:10.1016/j.bbadis.2015.05.011.

Moremen, K.W., Tiemeyer, M. and Nairn, A.V. (2012). Vertebrate protein glycosylation: diversity, synthesis and function). *Nat Rev Mol Cell Biol*, 13(7):448–462. DOI:10.1038/nrm3383.

Morgan, D.O. et al (1987). Insulin-like growth factor ii receptor as a multifunctional binding protein. *Nature*, 329:301–307. DOI:10.1038/329301a0.

Motyka, B. et al (2000). Mannose 6-phosphate / insulin-like growth factor ii receptor is a death receptor for granzyme b during cytotoxic t cell induced apoptosis. *Cell*, 103(3):491–500. DOI:10.1016/S0092-8674(00)00140-9.

Mullock, B. et al (2000). Syntaxin 7 is localized to late endosome compartments, associates with vamp 8, and is required for late endosome-lysosome fusion. *Mol Biol Cell.*, 11(9). DOI:10.1091/mbc.11.9.3137.

Nakamura, S. and Yoshimori, T. (2017). New insights into autophagosome-lysosome fusion. *J Cell Sci.*, 130(7):1209–1216. DOI:10.1242/jcs.196352.

Narayan, S.B., Tan, L.U. and Bennett, M.J. (2008). Intermediate levels of neuronal palmitoyl-protein delta-9 desaturase in heterozygotes for murine batten disease. *Molecular Genetics and Metabolism*, 93(1):89–91. DOI:10.1016/j.ymgme.2007.09.005.

NCL Resource, S.M. (2017). https://www.ucl.ac.uk/ncl/CLN3mutationtable.htm. 2021-03-16.

Ni, X. and Morales, C.R. (2006). The lysosomal trafficking of acid sphingomyelinase is mediated by sortilin and mannose 6-phosphate receptor. *Traffic*, 7(7):889–902. DOI:10.1111/j.1600-0854.2006.00429.x.

Nordmann, M. et al (2010). The mon1-ccz1 complex is the gef of the late endosomal rab7 homolog ypt7. *Curr Biol*, 20(18):1654–9. DOI:10.1016/j.cub.2010.08.002.

Nordmann, M., Urgenmann, C. and Cabrera, M. (2012). Role of rab7/ypt7 in organizing membrane trafficking at the late endosome. *Rab GTPases and Membrane Trafficking, Chapter 10*, pages 132–143. DOI:10.2174/978160805365011201010132.

Noskova, L. et al (2011). Mutations in dnajc5, encoding cysteine-string protein alpha, cause autosomal-dominant adult-onset neuronal ceroid lipofuscinosis. *Am. J. Hum. Genet*, 89(2):241–52. DOI:10.1016/j.ajhg.2011.07.003.

Nykjaer, A. and Willnow, T.E. (2012). Sortilin: a receptor to regulate neuronal viability and function. *Cell*, 35(4):261–70. DOI:10.1016/j.tins.2012.01.003.

Oetjen, S., Khul, D. and Hermey, G. (2016). Revisiting the neuronal localization and trafficking of cln3 in juvenile neuronal lipofuscinosis. *J Neurochem.*, 139(3):456–470. DOI:10.1111/jnc.13744.

Onyenwoke, R.U. et al (2015). The mucolipidosis iv ca2+ channel trpml1 (mcoln1) is regulated by the tor kinase. *Biochem J*, 470(3):331–42. DOI:10.1042/BJ20150219.

Palmieri, M. et al (2011). Characterization of the clear network reveals an integrated control of cellular clearance pathways. *Human Molecular Genetics*, 20(19):3852–66. DOI:10.1093/hmg/ddr306.

Palmieri, M., Pal, R. and Nelvagal, H. (2017). Mtorc1-independent tfeb activation via akt inhibition promotes cellular clearance in neurodegenerative storage diseases. *Nat. Commun.*, 8, 14338. DOI:https://doi.org/10.1038/ncomms14338.

Pankiv, S. et al (2010). Fyco1 is a rab7 effector that binds to lc3 and pi3p to mediate microtubule plus end–directed vesicle transport. *J. Cell Biol.*, 188(2):253–69. DOI:10.1083/jcb.200907015.

Parlati, F. et al (2002). Distinct snare complexes mediating membrane fusion in golgi transport based on combinatorial specificity. *PNAS*, 99(8):5424–9. DOI:10.1073/pnas.082100899.

Perdigao, C. et al (2020). Intracellular trafficking mechanisms of synaptic dysfunction in alzheimer's disease. *Front Cell Neurosci.*, 14:72. DOI:10.3389/fncel.2020.00072.

Persaud-Sawin, D.A. et al (2007). Neuronal ceroid lipofuscinosis: A common pathway? *Pediatric Research*, 61:146–152. DOI:10.1203/pdr.0b013e31802d8a4a.

Petersen, C. et al (1999). Propeptide cleavage conditions sortilin/neurotensin receptor-3 for ligand binding. *EMBO J*, 18(3):595–604. DOI:10.1093/emboj/18.3.595.

Pfeffer, S. and Aivazian, D. (2004). Targetting rab gtpases to distinct membrane compartments. *Nat. Rev. Mol. Cell Biol.*, 5:886–896. DOI:10.1038/nrm1500.

Pfeffer, S.R. (2019). Npc intracellular cholesterol transporter 1 (npc1)-mediated cholesterol export from lysosomes). *Journal of Biological Chemistry*, 294(5):1706–1709. DOI:10.1074/jbc.TM118.004165.

Platt, F.M. et al (2018). Lysosomal storage diseases. *Nature Reviews Disease Primers*, 4(1):27. DOI:10.1038/s41572-018-0025-4.

Poteryaev, D. et al (2010). Identification of the switch in early-to-late endosome transition. *Cell*, 141(3):497–508. DOI:10.1016/j.cell.2010.03.011.

Prasad, A. et al (2019). Molecular mechanisms of tdp-43 misfolding and pathology in amyotrophic lateral sclerosis. *Front. Mol. Neurosci*, 12:25. DOI:10.3389/fnmol.2019.00025.

Prause, J. et al (2013). Altered localization, abnormal modification and loss of function of sigma receptor-1 in amyotrophic lateral sclerosis. *Hum. Mol. Genet.*, 22(8):1581–600. DOI:10.1093/hmg/ddt008.

Progida, C. et al (2007). Rilp is required for the proper morphology and function of late endosomes. *J. Cell Sci.*, 120(Pt 21):3729–37. DOI:10.1242/jcs.017301.

Qian, M. et al (2007). Proteomics analysis of serum from mutant mice reveals lysosomal proteins selectively transported by each of the two mannose 6-phosphate receptors. *Molecular & Cellular Proteomics*, 7(1):58–70. DOI:10.1074/mcp.M700217-MCP200.

Qureshi, Y. et al (2018). An alzheimer's disease-linked loss-of-function cln5 variant impairs cathepsin d maturation, consistent with a retromer trafficking defect. *Mol Cell Biol.*, 38(20):e00011–18. DOI:10.1128/MCB.00011-18.

Rak, A. et al (2004). Structure of the rab7:rep-1 complex. *Cell*, 117(6):749–60. DOI:10.1016/j.cell.2004.05.017.

Ratajczak, E. et al (2014). Fret-assisted determination of cln3 membrane topology. *PLOS ONE*. DOI:10.1371/journal.pone.0102593.

Reczek, D. et al (2007). Limp-2 is a receptor for lysosomal mannose-6-phosphate-independent targeting of glucocerebrosidase. *Cell*, 131(4):770–783. DOI:10.1016/j.cell.2007.10.018.

Reitz, C. (2018). Retromer dysfunction and neurodegenerative disease. *Curr Genomics*, 19(4):279–288.

Rocha, N. et al (2009). Cholesterol sensor orp1l contacts the er protein vap to control rab7-rilp-p150 glued and late endosome positioning. *J Cell Biol*, 185(7):1209–25. DOI:10.1083/jcb.200811005.

Rojas, R. et al (2008). Regulation of retromer recruitment to endosomes by sequential action of rab5 and rab7. *J Cell Biol.*, 183(3):513–526. DOI:10.1083/jcb.200804048.

Ronza, A. et al (2018). Cln8 is an er cargo receptor that regulates lysosome biogenesis. *Nature Cell Biology*, 20(12):1370–1377. DOI:10.1038/s41556-018-0228-7.

Rosenberg, J.B. et al (2019). Advances in the treatment of neuronal ceroid lipofuscinosis. *Expert Opinion in Orphan Drugs*, 7(11). DOI:10.1080/21678707.2019.1684258.

Rylova, S.N. et al (2002). The cln3 gene is a novel molecular target for cancer drug discovery. *Cancer Research*, 62(3):801–8.

Sanger, A. et al (2019). Adaptor protein complexes and disease at a glance. *Journal of Cell Science*, 132(20). DOI:10.1242/jcs.222992.

Sapmaz, A. et al (2019). Usp32 regulates late endosomal transport and recycling through deubiquitylation of rab7. *Nature Communications*, 10:1454. DOI:10.1038/s41467-019-09437-x.

Sardiello, M. (2016). Transcription factor eb: from master coordinatorof lysosomal pathways to candidate therapeutictarget in degenerative storage diseases. *Annals of the New York Academy of Science*, 1371(1):3–14. DOI:10.1111/nyas.13131.

Sauvageau, E. and Lefrancois, S. (2019). A beginner's guide to bioluminescence resonance energy transfer (bret). *Biochem*, 41 (6):36–40. DOI:https://doi.org/10.1042/BIO04106036.

Schindelin, J. et al (2012). Fiji: an open-source platform for biological-image analysis. *Nat. Methods*, 9:676–682. DOI:https://doi.org/10.1038/nmeth.2019.

Schmidtke, C. et al (2019). Lysosomal proteome analysis reveals that cln3-defective cells have multiple enzyme deficiencies associated with changes in intracellular trafficking. *Journal of Biological Chemistry*, 294(24):9592–9604. DOI:10.1074/jbc.RA119.008852.

Schmiedt, M.L. et al (2009). The neuronal ceroid lipofuscinosis protein cln5:new insights into cellular maturation, transport,and consequences of mutations. *WILEY-Human Mutation*, 31(3):356–65. DOI:10.1002/humu.21195.

Schwake, M., Schroder, B. and Saftig, P. (2013). Lysosomal membrane proteins and their central role in physiology). *Traffic*, 14(7):739–48. DOI:10.1111/tra.12056.

Seaman, M.N. (2009). Endosome-to-golgi retrieval. *Cell*, 139. DOI:10.1016/j.cell.2009.11.040.

Seaman, M.N. et al (1997). Endosome to golgi retrieval of the vacuolar protein sorting receptor, vps10p, requires the function of the vps29, vps30, and vps35 gene products. *Journal of Cell Biology*, 137(1):79–92. DOI:10.1083/jcb.137.1.79.

Seaman, M.N.J. (2004). Cargo-selective endosomal sorting for retrieval to the golgi requires retromer. *J. Cell Biol.*, 165(1):111–122. DOI:10.1083/jcb.200312034.

Seaman, M.N.J. et al (2009). Membrane recruitment of the cargo-selective retromer subcomplex is catalysed by the small gtpase rab7 and inhibited by the rab-gap tbc1d5. *J Cell Science*, 122(Pt 14):2371–82. DOI:10.1242/jcs.048686.

Seranova, E. et al (2017). Dysregulation of autophagy as a common mechanism in lysosomal storage diseases. *Essays Biochem*, 61(6):733–749. DOI:10.1042/EBC20170055.

Sharma, K. et al (2014). Ultradeep human phosphoproteome reveals a distinct regulatory nature of tyr and ser/thr-based signaling. *Cell Reports*, 8(5):1583–1594. DOI:10.1016/j.celrep.2014.07.036.

Shi, C. et al (2012). Activation of autophagy by inflammatory signals limits il1 beta production by targeting ubiquitinated inflammasomes for destruction. *Nature Immunology*, 13(3):255–263.

Shi, G.P. et al (2000). Role for cathepsin f in invariant chain processing and major histocompatibility complex class ii peptide loading by macrophages. *J Exp Med*, 191(7):1177–1186. DOI:10.1084/jem.191.7.1177.

Shinde, S.R. and Maddika, S. (2016). Pten modulates egfr late endocytic trafficking and degradation by dephosphorylating rab7. *Nature Communications*, 7. DOI:10.1038/ncomms10689.

Siintola, E. et al (2007). The novel neuronal ceroid lipofuscinosis gene mfsd8 encodes a putative lysosomal transporter. *Am J Hum Genet.*, 81(1):136–146. DOI:10.1086/518902.

Singh, P.K. and Muqit, M.M. (2020). Parkinson's: A disease of aberrant vesicle trafficking. *Annual Review of Cell and Developmental Biology*, 36:1:237–264.

Small, S. and A., P.G. (2015). Retromer in alzheimer disease, parkinson disease and other neurological disorders. *Nat Rev Neurosci.*, 16(3):126–32. DOI:10.1038/nrn3896.

Small, S. et al (2005). Model-guided microarray implicates the retromer complex in alzheimer's disease. *Ann Neurol.*, 58(6):909–19. DOI:10.1002/ana.20667.

Small, S.A. and Petsko, G.A. (2015). Retromer in alzheimer disease, parkinson disease and other neurological disorders. *Nature Reviews Neurosciences*, 16(3):126–32. DOI:10.1038/nrn3896.

Solé-Domènech, S. et al (2018). Lysosomal enzyme tripeptidyl peptidase 1 destabilizes fibrillar aβ by multiple endoproteolytic cleavages within the β-sheet domain. *Proc. Natl. Acad. Sci.*, 115(7):1493–1498. DOI:10.1073/pnas.1719808115.

Song, P. et al (2016). Parkin modulates endosomal organization and function of the endo-lysosomal pathway. *J Neurosci*, 36(8):2425–37. DOI:10.1523/JNEUROSCI.2569-15.2016.

Sorkin, A. and von Zastrow, M. (2009). Endocytosis and signalling: intertwining molecular networks. *Nat. Rev. Mol. Cell Biol.*, 10:609–622. DOI:10.1038/nrm2748.

Steenhuis, P. et al (2010). Lysosomal targeting of the cln7 membrane glycoprotein and transport via the plasma membrane require a dileucine motif. *Traffic*, 11(7):987–1000. DOI:10.1111/j.1600-0854.2010.01073.x.

Steinberg, B.E. et al (2010). A cation counter flux supports lysosomal acidification. *Journal of Cell Biology*, 189(7):1171–1186. DOI:10.1083/jcb.200911083.

Stenmark, H. (2009). Rab gtpases as coordinators of vesicle traffic. *Nature Reviews Molecular Cell Biology*, 10:513–525. DOI:10.1038/nrm2728.

Stick, R.V. and Williams, S.J. (2009). Glycoproteins and proteoglycans. *Carbohydrates: The Essential Molecules of Life (Second Edition)*. DOI:10.1016/B978-0-240-52118-3.X0001-4.

Stoka, V., Turk, V. and Turk, B. (2016). Lysosomal cathepsins and their regulation in aging and neurodegeneration. *Ageing Research Reviews*, 32:22–37. DOI:10.1016/j.arr.2016.04.010.

Storch, S., Pohl, S. and Braulke, T. (2004). A dileucine motif and a cluster of acidic amino acids in the second cytoplasmic domain of the batten disease-related cln3 protein are required for efficient lysosomal targeting. *Journal of Biological Chemistry*, 279(51):53625–34. DOI:10.1074/jbc.M410930200.

Straus, W. (1954). Isolation and biochemical properties of droplets from the cells of rat kidney. *Journal of Biological Chemistry*, 207(2)(745-55).

Supplementary-figures (2020). *CLN3 regulates endosomal function by modulating Rab7-effector interactions*. http://jcs.biologists.org/lookup/doi/10.1242/jcs.234047.supplemental.

Tong, P.Y. and Kornfeld, S. (1989). Ligand interactions of the cation-dependent mannose-6 phosphate receptor. *J Biol Chem*, 264(14):7970–5.

Trivedi, P.C., Bartlett, J.J. and Pulinilkunnil, T. (2020). Lysosomal biology and function: Modern view of cellular debris bin. *Cells*, 9(5). DOI:10.3390/cells9051131.

Tropak, M. et al (2004). Pharmacological enhancement of beta-hexosaminidase activity in fibroblasts from adult tay-sachs and sandhoff patients. *J. Biol. Chem*, 279:13478–13487. DOI:https://doi.org/10.1074/jbc.M308523200.

Tu, Y. et al (2020). Endosome-to-tgn trafficking: Organelle-vesicle and organelle-organelle interactions. *Front. Cell Dev. Biol.*, 8:163. DOI:10.3389/fcell.2020.00163.

Uusi-Rauva, K. et al (2012). Neuronal ceroid lipofuscinosis protein cln3 interacts with motor proteins and modifies location of late endosomal compartments. *Cell Mol Life Science*, 69(12):2075–89. DOI:10.1007/s00018-011-0913-1.

van der Kant, R. et al (2013). Late endosomal transport and tethering are coupled processes controlled by rilp and the cholesterol sensor orp1l. *Journal of Cell Science*, 126(Pt 15):3462–74. DOI:10.1242/jcs.129270.

van Weering, J.R.T. et al (2012). Molecular basis for snx-bar-mediated assembly of distinct endosomal sorting tubules. *EMBO J*, 31(23):4466–80. DOI:10.1038/emboj.2012.283.

Vanlandingham, P. and Ceresa, P. (2009). Rab7 regulates late endocytic trafficking downstream of multivesicular body biogenesis and cargo sequestration. *J Biol Chem.*, 284(18):12110–24. DOI:10.1074/jbc.M809277200.

Vesa, J. et al (2002). Neuronal ceroid lipofuscinoses are connected at molecular level: Interaction of cln5 protein with cln2 and cln3. *MBoC*, 13(7):2410–2420. DOI:10.1091/mbc.E02-01-0031.

Vlieta, C. et al (2003). Intracellular sorting and transport of proteins. *Progress in Biophysics and Molecular Biology*, 83(1):1–45. DOI:10.1016/s0079-6107(03)00019-1.

Wagner, S.A. et al (2011). A proteome-wide, quantitative survey of in vivo ubiquitylation sites reveals widespread regulatory roles. *Mol Cell Proteomics*, 10(10):M111.013284. DOI:10.1074/mcp.M111.013284.

Walter, P. and Blobel, G. (1981). Translocation of proteins across the endoplasmic reticulum. *Journal of Cell Biology*, 91(2 Pt 1):545–50. DOI:10.1083/jcb.91.2.545.

Weber, R.A. et al (2020). Maintaining iron homeostasis is the key role of lysosomal acidity for cell proliferation. *Molecular Cell*, 77(3):645–655.e7. DOI:10.1016/j.molcel.2020.01.003.

Wijdeven, R.H. et al (2016). Cholesterol and orp1l-mediated er contact sites control autophagosome transport and fusion with the endocytic pathway. *Nat Commun.*, 7. DOI:10.1038/ncomms11808.

Wu, M. et al (2005). Structural basis for recruitment of rilp by small gtpase rab7. *EMBO J*, 24(8):1491–1501. DOI:10.1038/sj.emboj.7600643.

Yamano, K. et al (2014). Mitochondrial rab gaps govern autophagosome biogenesis during mitophagy. *Elife*, 3:e01612. DOI:10.7554/eLife.01612.

Yasa, S. et al (2020). Cln3 regulates endosomal function by modulating rab7a–effector interactions. *Journal of Cell Science*, 133(6):jcs234047. DOI:10.1242/jcs.234047.

Yasa, S. et al (2021). Cln5 and cln3 function as a complex to regulate endolysosome function. *Biochemical Journal*, 478. DOI:10.1038/nsmb.3218.

Yasuda, S. et al (2016). Mon1-ccz1 activates rab7 only on late endosomes and dissociates from the lysosome in mammalian cells. *J. Cell Sci.*, 129 (2):329–340. DOI:10.1242/jcs.178095.

York, S.J. et al (1999). The rate of internalization of the mannose 6-phosphate/insulin-like growth factor ii receptor is enhanced by multivalent ligand binding. *J Biol Chem*, 274(2):1164–71. DOI:10.1074/jbc.274.2.1164.

Zaffagnini, G. and Martens, S. (2016). Mechanisms of selective autophagy. *J Mol Biol.*, 428(9 Pt A):1714–1724. DOI:10.1016/j.jmb.2016.02.004.

Zerial, M. and McBride, H. (2001). Rab proteins as membrane organizers. *Nature Rev Mol Cell Biol*, 2:107–117. DOI:10.1038/35052055.

Zhao, Y.G. and Zhang, H. (2018). Autophagosome maturation: An epic journey from the er to lysosomes. *Journal of Cell Biology*, 218(3):757–770. DOI:10.1083/jcb.201810099.

Zhou, C. et al (2012). Monitoring autophagic flux by an improved tandem fluorescent-tagged lc3 (mtagrfp-mwasabi-lc3) reveals that high-dose rapamycin impairs autophagic flux in cancer cells. *Autophagy*, 8(8):1215–26. DOI:10.4161/auto.20284.